Gamma-Ray Bursts

Contents

1 Topics

- GRB classification
- GRB empirical correlations
- "Genuine short" GRBs: Possible identifications and selection effects
- A modified spectral energy distribution for highly energetic GRBs
- The observed spectra of the P-GRBs
- GRB prompt emission spectra below 5 keV: challenges for future missions
- Interpretation of the ultra high energy emission from GRBs observed by Fermi and AGILE
- Analysis of different families of progenitors for GRBs with different energetics
- GRBs at redshift $z > 6$
- GRBs originating from a multiple collapse
- Prompt emission and X-ray flares: the clumpiness of CBM
- Microphysical description of the interaction between the fireshell and the CBM
- Theoretical interpretation of the "plateau" phase in the X-ray afterglow
- Emission from newly born neutron stars, or "neo neutron stars".
- Induced Gravitational Collapse process for GRBs associated with supernovae.
- Redshift estimators for GRBs with no measured redshift.
- Binary Driven Hypernovae (BdHNe) as progenitor of GRBs via Induced Gravitational Collapse.

- GRB light curves as composed of four different episodes.
- Different kinds of binary systems as GRB progenitors.
- “Cosmic Matrix” for GRBs.

2 Participants

2.1 ICRANet participants

- David Arnett
- Carlo Luciano Bianco
- Massimo Della Valle
- Luca Izzo
- Marco Muccino
- Giovanni Battista Pisani
- Jorge Armando Rueda Hernandez
- Remo Ruffini
- Gregory Vereshchagin
- She-Sheng Xue

2.2 Past collaborators

- Andrey Baranov
- Maria Grazia Bernardini (OAB, Italy)
- Joao Braga (INPE, Brazil)
- Sabrina Casanova (MPIK, Germany)
- Letizia Caito
- Pascal Chardonnet (Université de Savoie, France)
- Guido Chincarini (Universit di Milano "Bicocca", Italy)
- Demetrios Christodoulou (ETH Zurich, Switzerland)

- Alessandra Corsi (INAF-IASF Roma, Italy)
- Valeri Chechetkin
- Maria Giovanna Dainotti
- Thibault Damour (IHES, France)
- Walter Ferrara
- Federico Fraschetti (CEA Saclay, France)
- Roberto Guida
- Vahe Gurzadyan (Yerevan Physics Institute, Armenia)
- Wen-Biao Han
- Massimiliano Lattanzi (Oxford Astrophysics, UK)
- Vincenzo Liccardo
- Nino Panagia
- Barbara Patricelli (Pisa University, Italy)
- Elena Pian
- Giuliano Preparata (Università di Milano, Italy)
- Jay D. Salmonson (Livermore Lab, USA)
- Vineeth Valsan
- Jim Wilson (Livermore Lab, USA)

2.3 Ongoing collaborations

- Alexey Aksenov (ITEP, Russia)
- Lorenzo Amati (INAF-IASF Bologna, Italy)
- Ulisses Barres de Almeida (CBPF, Brazil)
- Riccardo Belvedere (ICRANet-Rio, Brazil)
- Sandip Kumar Chakrabarti (S.N. Bose National Centre and Indian Centre for Space Physics, India)

- Christian Cherubini (Universit Campus Biomedico, Italy)
- Alessandro Chieffi (INAF-IASF Roma, Italy)
- Stefano Covino (OAB, Italy)
- Gustavo de Barros (UFRJ, Brazil)
- Simonetta Filippi (Universit Campus Biomedico, Italy)
- Filippo Frontera (Universit di Ferrara, Italy)
- Chris Fryer (Los Alamos National Laboratories, USA).
- Dafne Guetta (OAR, Italy)
- Cristiano Guidorzi (OAB, Italy)
- Stanislav Kelner (MEPhI, Russia, and MPIK, Germany)
- Marco Limongi (OAR, Italy)
- Vanessa Mangano (INAF-IASF Palermo, Italy)
- Ana Virginia Penacchioni (INPE, Brazil)
- Luis Juracy Rangel Lemos (Fundao Universidade Federal do Tocantins, Brazil)
- Soroush Shakeri (Isfahan University of Technology, Iran)
- Ivan Siutsou (ICRANet-Rio, Brazil)
- Susanna Vergani (Dunsink Observatory, Ireland)
- Francesco Vissani (INFN, Italy)
- Elena Zaninoni (ICRANet-Rio, Brazil)

2.4 Students

- Yerlan Aimuratov (IRAP PhD, Kazakhstan)
- Cristina Barbarino (IRAP PhD, Italy)
- Laura Marcela Becerra Bayona (IRAP PhD, Colombia)
- Maxime Enderli (IRAP PhD, France)

- Davide Gizzi (Undergraduate, Sapienza University, Italy)
- Fernanda Gomes De Oliveira (IRAP PhD, Brazil)
- Milos Kovacevic (IRAP PhD, Serbia)
- Hendrik Ludwig (IRAP PhD, Germany)
- Rahim Moradi (IRAP PhD, Iran)
- Jose Fernando Rodriguez Ruiz (IRAP PhD, Colombia)
- Yu Wang (IRAP PhD, China)

3 Brief summary of recent progresses

Major progresses have been accomplished this year in the following aspects:

- In establishing that all GRBs originate in binary systems.
- In defining a new GRB classification, leading to 7 different families of events with 7 different progenitor binary systems.
- In reanalyzing, in view of the new classification, the event GRB 090510 and, more specifically, the problematic of the traditionally called "short GRBs".
- In obtaining, for the first time, a complete theoretical simulation of all the phases of an Induced Graitational Collapse (IGC) event, leading to a new interpretation of both Binary Driven Hypernovae (BdHNe) and X-ray flashes (XRFs).
- In identifying a collimation in the late time X-ray emission associated to BdHNe.

4 Selected publications before 2005

4.1 Refereed journals

1. D. Christodoulou, R. Ruffini; "Reversible Transformations of a Charged Black Hole"; Physical Review D, 4, 3552 (1971).

   A formula is derived for the mass of a black hole as a function of its "irreducible mass", its angular momentum, and its charge. It is shown that 50% of the mass of an extreme charged black hole can be converted into energy as contrasted with 29% for an extreme rotating black hole.

2. T. Damour, R. Ruffini; "Quantum electrodynamical effects in Kerr-Newman geometries"; Physical Review Letters, 35, 463 (1975).

   Following the classical approach of Sauter, of Heisenberg and Euler and of Schwinger the process of vacuum polarization in the field of a "bare" Kerr-Newman geometry is studied. The value of the critical strength of the electromagnetic fields is given together with an analysis of the feedback of the discharge on the geometry. The relevance of this analysis for current astrophysical observations is mentioned.

3. G. Preparata, R. Ruffini, S.-S. Xue; "The dyadosphere of black holes and gamma-ray bursts"; Astronomy & Astrophysics, 338, L87 (1999).

   The "dyadosphere" has been defined as the region outside the horizon of a black hole endowed with an electromagnetic field (abbreviated to EMBH for "electromagnetic black hole") where the electromagnetic field exceeds the critical value, predicted by Heisenberg & Euler for $e^{\pm}$ pair production. In a very short time ($\sim O(\hbar/mc^2)$) a very large number of pairs is created there. We here give limits on the EMBH parameters leading to a Dyadosphere for $10M_{\odot}$ and $10^5 M_{\odot}$ EMBH's, and give as well the pair densities as functions of the radial coordinate. We here assume that the pairs reach thermodynamic equilibrium with a photon gas and estimate the average energy per pair as a function of the EMBH mass. These data give the initial conditions for the analysis of an enormous pair-electromagnetic-pulse or "P.E.M. pulse" which naturally leads to relativistic expansion. Basic energy requirements for gamma ray bursts (GRB),

including GRB971214 recently observed at z=3.4, can be accounted for by processes occurring in the dyadosphere. In this letter we do not address the problem of forming either the EMBH or the dyadosphere: we establish some inequalities which must be satisfied during their formation process.

4. R. Ruffini, J.D. Salmonson, J.R. Wilson, S.-S. Xue; "On the pair electromagnetic pulse of a black hole with electromagnetic structure"; Astronomy & Astrophysics, 350, 334 (1999).

   We study the relativistically expanding electron-positron pair plasma formed by the process of vacuum polarization around an electromagnetic black hole (EMBH). Such processes can occur for EMBH's with mass all the way up to $6 \times 10^5 M_\odot$. Beginning with a idealized model of a Reissner-Nordstrom EMBH with charge to mass ratio $\xi = 0.1$, numerical hydrodynamic calculations are made to model the expansion of the pair-electromagnetic pulse (PEM pulse) to the point that the system is transparent to photons. Three idealized special relativistic models have been compared and contrasted with the results of the numerically integrated general relativistic hydrodynamic equations. One of the three models has been validated: a PEM pulse of constant thickness in the laboratory frame is shown to be in excellent agreement with results of the general relativistic hydrodynamic code. It is remarkable that this precise model, starting from the fundamental parameters of the EMBH, leads uniquely to the explicit evaluation of the parameters of the PEM pulse, including the energy spectrum and the astrophysically unprecedented large Lorentz factors (up to 6×10^3 for a $10^3 M_\odot$ EMBH). The observed photon energy at the peak of the photon spectrum at the moment of photon decoupling is shown to range from 0.1 MeV to 4 MeV as a function of the EMBH mass. Correspondingly the total energy in photons is in the range of 10^{52} to 10^{54} ergs, consistent with observed gamma-ray bursts. In these computations we neglect the presence of baryonic matter which will be the subject of forthcoming publications.

5. R. Ruffini, J.D. Salmonson, J.R. Wilson, S.-S. Xue; "On the pair-electro magnetic pulse from an electromagnetic black hole surrounded by a baryonic remnant"; Astronomy & Astrophysics, 359, 855 (2000).

   The interaction of an expanding Pair-Electromagnetic pulse (PEM pulse) with a shell of baryonic matter surrounding a Black Hole with electromagnetic structure (EMBH) is analyzed for selected values of the baryonic mass at selected distances well outside the dyadosphere of an EMBH. The dyadosphere, the region in which a super critical field exists for the creation of e+e- pairs, is here considered in the special case of a Reissner-Nordstrom geometry. The interaction of the PEM pulse with the baryonic matter is described using a simplified model of a slab of constant thickness in the laboratory frame (constant-thickness approximation) as well as performing the integration of the general

relativistic hydrodynamical equations. Te validation of the constant-thickness approximation, already presented in a previous paper Ruffini et al. (1999) for a PEM pulse in vacuum, is here generalized to the presence of baryonic matter. It is found that for a baryonic shell of mass-energy less than 1% of the total energy of the dyadosphere, the constant-thickness approximation is in excellent agreement with full general relativistic computations. The approximation breaks down for larger values of the baryonic shell mass, however such cases are of less interest for observed Gamma Ray Bursts (GRBs). On the basis of numerical computations of the slab model for PEM pulses, we describe (i) the properties of relativistic evolution of a PEM pulse colliding with a baryonic shell; (ii) the details of the expected emission energy and observed temperature of the associated GRBs for a given value of the EMBH mass; $10^3 M_\odot$, and for baryonic mass-energies in the range 10^{-8} to 10^{-2} the total energy of the dyadosphere.

6. C.L. Bianco, R. Ruffini, S.-S. Xue; "The elementary spike produced by a pure e+e- pair-electromagnetic pulse from a Black Hole: The PEM Pulse"; Astronomy & Astrophysics, 368, 377 (2001).

   In the framework of the model that uses black holes endowed with electromagnetic structure (EMBH) as the energy source, we study how an elementary spike appears to the detectors. We consider the simplest possible case of a pulse produced by a pure e^+e^- pair-electro-magnetic plasma, the PEM pulse, in the absence of any baryonic matter. The resulting time profiles show a *Fast-Rise-Exponential-Decay* shape, followed by a power-law tail. This is obtained without any special fitting procedure, but only by fixing the energetics of the process taking place in a given EMBH of selected mass, varying in the range from 10 to 10^3 $M_\odot$ and considering the relativistic effects to be expected in an electron-positron plasma gradually reaching transparency. Special attention is given to the contributions from all regimes with Lorentz γ factor varying from $\gamma = 1$ to $\gamma = 10^4$ in a few hundreds of the PEM pulse travel time. Although the main goal of this paper is to obtain the elementary spike intensity as a function of the arrival time, and its observed duration, some qualitative considerations are also presented regarding the expected spectrum and on its departure from the thermal one. The results of this paper will be comparable, when data will become available, with a subfamily of particularly short GRBs not followed by any afterglow. They can also be propedeutical to the study of longer bursts in presence of baryonic matter currently observed in GRBs.

7. R. Ruffini, C.L. Bianco, P. Chardonnet, F. Fraschetti, S.-S. Xue; "Relative spacetime transformations in Gamma-Ray Bursts"; The Astrophysical Journal, 555, L107 (2001).

   The GRB 991216 and its relevant data acquired from the BATSE experiment

and RXTE and Chandra satellites are used as a prototypical case to test the theory linking the origin of gamma ray bursts (GRBs) to the process of vacuum polarization occurring during the formation phase of a black hole endowed with electromagnetic structure (EMBH). The relative space-time transformation paradigm (RSTT paradigm) is presented. It relates the observed signals of GRBs to their past light cones, defining the events on the worldline of the source essential for the interpretation of the data. Since GRBs present regimes with unprecedently large Lorentz γ factor, also sharply varying with time, particular attention is given to the constitutive equations relating the four time variables: the comoving time, the laboratory time, the arrival time at the detector, duly corrected by the cosmological effects. This paradigm is at the very foundation of any possible interpretation of the data of GRBs.

8. R. Ruffini, C.L. Bianco, P. Chardonnet, F. Fraschetti, S.-S. Xue; "On the interpretation of the burst structure of Gamma-Ray Bursts"; The Astrophysical Journal, 555, L113 (2001).

   Given the very accurate data from the BATSE experiment and RXTE and Chandra satellites, we use the GRB 991216 as a prototypical case to test the EMBH theory linking the origin of the energy of GRBs to the electromagnetic energy of black holes. The fit of the afterglow fixes the only two free parameters of the model and leads to a new paradigm for the interpretation of the burst structure, the IBS paradigm. It leads as well to a reconsideration of the relative roles of the afterglow and burst in GRBs by defining two new phases in this complex phenomenon: a) the injector phase, giving rise to the proper-GRB (P-GRB), and b) the beam-target phase, giving rise to the extended afterglow peak emission (E-APE) and to the afterglow. Such differentiation leads to a natural possible explanation of the bimodal distribution of GRBs observed by BATSE. The agreement with the observational data in regions extending from the horizon of the EMBH all the way out to the distant observer confirms the uniqueness of the model.

9. R. Ruffini, C.L. Bianco, P. Chardonnet, F. Fraschetti, S.-S. Xue; "On a possible Gamma-Ray Burst-Supernova time sequence"; The Astrophysical Journal, 555, L117 (2001).

   The data from the Chandra satellite on the iron emission lines in the afterglow of GRB 991216 are used to give further support for the EMBH theory, which links the origin of the energy of GRBs to the extractable energy of electromagnetic black holes (EMBHs), leading to an interpretation of the GRB-supernova correlation. Following the relative space-time transformation (RSTT) paradigm and the interpretation of the burst structure (IBS) paradigm, we introduce a paradigm for the correlation between GRBs and supernovae. The following sequence of events is shown as kinematically possible and consistent with the

available data: a) the GRB-progenitor star P_1 first collapses to an EMBH, b) the proper GRB (P-GRB) and the peak of the afterglow (E-APE) propagate in interstellar space until the impact on a supernova-progenitor star P_2 at a distance $\leq 2.69 \times 10^{17}$ cm, and they induce the supernova explosion, c) the accelerated baryonic matter (ABM) pulse, originating the afterglow, reaches the supernova remnants 18.5 hours after the supernova explosion and gives rise to the iron emission lines. Some considerations on the dynamical implementation of the paradigm are presented. The concept of induced supernova explosion introduced here specifically for the GRB-supernova correlation may have more general application in relativistic astrophysics.

10. R. Ruffini, C.L. Bianco, P. Chardonnet, F. Fraschetti, S.-S. Xue; "On the physical processes which lie at the bases of time variability of GRBs"; Il Nuovo Cimento B, 116, 99 (2001).

    The relative-space-time-transformation (RSTT) paradigm and the interpretation of the burst-structure (IBS) paradigm are applied to probe the origin of the time variability of GRBs. Again GRB 991216 is used as a prototypical case, thanks to the precise data from the CGRO, RXTE and Chandra satellites. It is found that with the exception of the relatively inconspicuous but scientifically very important signal originating from the initial "proper gamma ray burst" (P-GRB), all the other spikes and time variabilities can be explained by the interaction of the accelerated-baryonic-matter pulse with inhomogeneities in the interstellar matter. This can be demonstrated by using the RSTT paradigm as well as the IBS paradigm, to trace a typical spike observed in arrival time back to the corresponding one in the laboratory time. Using these paradigms, the identification of the physical nature of the time variablity of the GRBs can be made most convincingly. It is made explicit the dependence of a) the intensities of the afterglow, b) the spikes amplitude and c) the actual time structure on the Lorentz gamma factor of the accelerated-baryonic-matter pulse. In principle it is possible to read off from the spike structure the detailed density contrast of the interstellar medium in the host galaxy, even at very high redshift.

11. R. Ruffini, C.L. Bianco, P. Chardonnet, F. Fraschetti, S.-S. Xue; "On the structures in the afterglow peak emission of gamma ray bursts"; The Astrophysical Journal, 581, L19 (2002).

    Using GRB 991216 as a prototype, it is shown that the intensity substructures observed in what is generally called the "prompt emission" in gamma ray bursts (GRBs) do originate in the collision between the accelerated baryonic matter (ABM) pulse with inhomogeneities in the interstellar medium (ISM). The initial phase of such process occurs at a Lorentz factor $\gamma \sim 310$. The crossing of ISM inhomogeneities of sizes $\Delta R \sim 10^{15}$ cm occurs in a detector arrival time interval of ~ 0.4 s implying an apparent superluminal behavior of $\sim 10^5 c$.

The long lasting debate between the validity of the external shock model vs. the internal shock model for GRBs is solved in favor of the first.

12. R. Ruffini, C.L. Bianco, P. Chardonnet, F. Fraschetti, S.-S. Xue; "On the structure of the burst and afterglow of Gamma-Ray Bursts I: the radial approximation"; International Journal of Modern Physics D, 12, 173 (2003).

    We have recently proposed three paradigms for the theoretical interpretation of gamma-ray bursts (GRBs). (1) The relative space-time transformation (RSTT) paradigm emphasizes how the knowledge of the entire world-line of the source from the moment of gravitational collapse is a necessary condition in order to interpret GRB data. (2) The interpretation of the burst structure (IBS) paradigm differentiates in all GRBs between an injector phase and a beam-target phase. (3) The GRB-supernova time sequence (GSTS) paradigm introduces the concept of *induced supernova explosion* in the supernovae-GRB association. In the introduction the RSTT and IBS paradigms are enunciated and illustrated using our theory based on the vacuum polarization process occurring around an electromagnetic black hole (EMBH theory). The results are summarized using figures, diagrams and a complete table with the space-time grid, the fundamental parameters and the corresponding values of the Lorentz gamma factor for GRB 991216 used as a prototype. In the following sections the detailed treatment of the EMBH theory needed to understand the results of the three above letters is presented. We start from the considerations on the dyadosphere formation. We then review the basic hydrodynamic and rate equations, the equations leading to the relative space-time transformations as well as the adopted numerical integration techniques. We then illustrate the five fundamental eras of the EMBH theory: the self acceleration of the e^+e^- pair-electromagnetic plasma (PEM pulse), its interaction with the baryonic remnant of the progenitor star, the further self acceleration of the e^+e^- pair-electroma-gnetic radiation and baryon plasma (PEMB pulse). We then study the approach of the PEMB pulse to transparency, the emission of the proper GRB (P-GRB) and its relation to the "short GRBs". Particular attention is given to the free parameters of the theory and to the values of the thermodynamical quantities at transparency. Finally the three different regimes of the afterglow are described within the fully radiative and radial approximations: the ultrarelativistic, the relativistic and the nonrelativistic regimes. The best fit of the theory leads to an unequivocal identification of the "long GRBs" as extended emission occurring at the afterglow peak (E-APE). The relative intensities, the time separation and the hardness ratio of the P-GRB and the E-APE are used as distinctive observational test of the EMBH theory and the excellent agreement between our theoretical predictions and the observations are documented. The afterglow power-law indexes in the EMBH theory are compared

and contrasted with the ones in the literature, and no beaming process is found for GRB 991216. Finally, some preliminary results relating the observed time variability of the E-APE to the inhomogeneities in the interstellar medium are presented, as well as some general considerations on the EMBH formation. The issue of the GSTS paradigm will be the object of a forthcoming publication and the relevance of the iron-lines observed in GRB 991216 is shortly reviewed. The general conclusions are then presented based on the three fundamental parameters of the EMBH theory: the dyadosphere energy, the baryonic mass of the remnant, the interstellar medium density. An in depth discussion and comparison of the EMBH theory with alternative theories is presented as well as indications of further developments beyond the radial approximation, which will be the subject of paper II in this series. Future needs for specific GRB observations are outlined.

13. R. Ruffini, C.L. Bianco, P. Chardonnet, F. Fraschetti, V. Gurzadyan, S.-S. Xue; "On the instantaneous spectrum of gamma ray bursts"; International Journal of Modern Physics D, 13, 843 (2004).

    A theoretical attempt to identify the physical process responsible for the afterglow emission of Gamma-Ray Bursts (GRBs) is presented, leading to the occurrence of thermal emission in the comoving frame of the shock wave giving rise to the bursts. The determination of the luminosities and spectra involves integration over an infinite number of Planckian spectra, weighted by appropriate relativistic transformations, each one corresponding to a different viewing angle in the past light cone of the observer. The relativistic transformations have been computed using the equations of motion of GRBs within our theory, giving special attention to the determination of the equitemporal surfaces. The only free parameter of the present theory is the "effective emitting area" in the shock wave front. A self consistent model for the observed hard-to-soft transition in GRBs is also presented. When applied to GRB 991216 a precise fit $\left(\chi^2 \simeq 1.078\right)$ of the observed luminosity in the 2–10 keV band is obtained. Similarly, detailed estimates of the observed luminosity in the 50–300 keV and in the 10–50 keV bands are obtained.

4.2 Conference proceedings

1. R. Ruffini; "Beyond the critical mass: The dyadosphere of black holes"; in "Black Holes and High Energy Astrophysics", H. sato, N. Sugiyama, Editors; p. 167; Universal Academy Press (Tokyo, Japan, 1998).

    The "dyadosphere" (from the Greek word "duas-duados" for pairs) is here defined as the region outside the horizon of a black hole endowed with an electromagnetic field (abbreviated to EMBH for "electromagnetic black hole")

where the electromagnetic field exceeds the critical value, predicted by Heisenberg and Euler for e^+e^- pair production. In a very short time ($\sim O(\hbar/mc^2)$), a very large number of pairs is created there. I give limits on the EMBH parameters leading to a Dyadosphere for $10M_\odot$ and $10^5M_\odot$ EMBH's, and give as well the pair densities as functions of the radial coordinate. These data give the initial conditions for the analysis of an enormous pair-electromagnetic-pulse or "PEM-pulse" which naturally leads to relativistic expansion. Basic energy requirements for gamma ray bursts (GRB), including GRB971214 recently observed at $z = 3.4$, can be accounted for by processes occurring in the dyadosphere.

2. R. Ruffini, C.L. Bianco, P. Chardonnet, F. Fraschetti, L. Vitagliano, S.-S. Xue; "New perspectives in physics and astrophysics from the theoretical understanding of Gamma-Ray Bursts"; in "COSMOLOGY AND GRAVITATION: Xth Brazilian School of Cosmology and Gravitation; 25th Anniversary (1977-2002)", Proceedings of the Xth Brazilian School on Cosmology and Gravitation, Mangaratiba, Rio de Janeiro (Brazil), July - August 2002, M. Novello, S.E. Perez Bergliaffa, Editors; AIP Conference Proceedings, 668, 16 (2003).

   If due attention is given in formulating the basic equations for the Gamma-Ray Burst (GRB) phenomenon and in performing the corresponding quantitative analysis, GRBs open a main avenue of inquiring on totally new physical and astrophysical regimes. This program is very likely one of the greatest computational efforts in physics and astrophysics and cannot be actuated using shortcuts. A systematic approach is needed which has been highlighted in three basic new paradigms: the relative space-time transformation (RSTT) paradigm, the interpretation of the burst structure (IBS) paradigm, the GRB-supernova time sequence (GSTS) paradigm. From the point of view of fundamental physics new regimes are explored: (1) the process of energy extraction from black holes; (2) the quantum and general relativistic effects of matter-antimatter creation near the black hole horizon; (3) the physics of ultrarelativisitc shock waves with Lorentz gamma factor $\gamma > 100$. From the point of view of astronomy and astrophysics also new regimes are explored: (i) the occurrence of gravitational collapse to a black hole from a critical mass core of mass $M \gtrsim 10M_\odot$, which clearly differs from the values of the critical mass encountered in the study of stars "catalyzed at the endpoint of thermonuclear evolution" (white dwarfs and neutron stars); (ii) the extremely high efficiency of the spherical collapse to a black hole, where almost 99.99% of the core mass collapses leaving negligible remnant; (iii) the necessity of developing a fine tuning in the final phases of thermonuclear evolution of the stars, both for the star collapsing to the black hole and the surrounding ones, in order to explain the possible occurrence of the "induced gravitational collapse". New regimes

are as well encountered from the point of view of nature of GRBs: (I) the basic structure of GRBs is uniquely composed by a proper-GRB (P-GRB) and the afterglow; (II) the long bursts are then simply explained as the peak of the afterglow (the E-APE) and their observed time variability is explained in terms of inhomogeneities in the interstellar medium (ISM); (III) the short bursts are identified with the P-GRBs and the crucial information on general relativistic and vacuum polarization effects are encoded in their spectra and intensity time variability. A new class of space missions to acquire information on such extreme new regimes are urgently needed.

3. R. Ruffini, C.L. Bianco, P. Chardonnet, F. Fraschetti, S.-S. Xue; "The EMBH Model in GRB 991216 and GRB 980425"; in Proceedings of "Third Rome Workshop on Gamma-Ray Burst in the Afterglow Era", 17-20 September 2002; M. Feroci, F. Frontera, N. Masetti, L. Piro, Editors; ASP Conference Series, 312, 349 (2004).

   This is a summary of the two talks presented at the Rome GRB meeting by C.L. Bianco and R. Ruffini. It is shown that by respecting the Relative Space-Time Transformation (RSTT) paradigm and the Interpretation of the Burst Structure (IBS) paradigm, important inferences are possible: a) in the new physics occurring in the energy sources of GRBs, b) on the structure of the bursts and c) on the composition of the interstellar matter surrounding the source.

4. M.G. Bernardini, C.L. Bianco, P. Chardonnet, F. Fraschetti, R. Ruffini, S.-S. Xue; "A New Astrophysical 'Triptych': GRB030329/SN2003dh/ URCA-2"; in "GAMMA-RAY BURSTS: 30 YEARS OF DISCOVERY", Proceedings of the Los Alamos "Gamma Ray Burst Symposium", Santa Fe, New Mexico, 8 12 September 2003, E.E. Fenimore, M. Galassi, Editors; AIP Conference Proceedings, 727, 312 (2004).

   We analyze the data of the Gamma-Ray Burst/Supernova GRB030329/ SN2003dh system obtained by HETE-2, R-XTE, XMM and VLT within our theory for GRB030329. By fitting the only three free parameters of the EMBH theory, we obtain the luminosity in fixed energy bands for the prompt emission and the afterglow. Since the Gamma-Ray Burst (GRB) analysis is consistent with a spherically symmetric expansion, the energy of GRB030329 is $E = 2.1 \times 10^{52}$ erg, namely $\sim 2 \times 10^3$ times larger than the Supernova energy. We conclude that either the GRB is triggering an induced-supernova event or both the GRB and the Supernova are triggered by the same relativistic process. In no way the GRB can be originated from the supernova. We also evidence that the XMM observations, much like in the system GRB980425/SN1998bw, are not part of the GRB afterglow, as interpreted in the literature, but are associated to the Supernova phenomenon. A dedicated campaign of observations

is needed to confirm the nature of this XMM source as a newly born neutron star cooling by generalized URCA processes.

5. F. Fraschetti, M.G. Bernardini, C.L. Bianco, P. Chardonnet, R. Ruffini, S.-S. Xue; "The GRB980425-SN1998bw Association in the EMBH Model"; in "GAMMA-RAY BURSTS: 30 YEARS OF DISCOVERY", Proceedings of the Los Alamos "Gamma Ray Burst Symposium", Santa Fe, New Mexico, 8 12 September 2003, E.E. Fenimore, M. Galassi, Editors; AIP Conference Proceedings, 727, 424 (2004).

   Our GRB theory, previously developed using GRB 991216 as a prototype, is here applied to GRB 980425. We fit the luminosity observed in the 40–700 keV, 2–26 keV and 2–10 keV bands by the BeppoSAX satellite. In addition the supernova SN1998bw is the outcome of an "induced gravitational collapse" triggered by GRB 980425, in agreement with the GRB-Supernova Time Sequence (GSTS) paradigm. A further outcome of this astrophysically exceptional sequence of events is the formation of a young neutron star generated by the SN1998bw event. A coordinated observational activity is recommended to further enlighten the underlying scenario of this most unique astrophysical system.

6. A. Corsi, M.G. Bernardini, C.L. Bianco, P. Chardonnet, F. Fraschetti, R. Ruffini, S.-S. Xue; "GRB 970228 Within the EMBH Model"; in "GAMMA-RAY BURSTS: 30 YEARS OF DISCOVERY", Proceedings of the Los Alamos "Gamma Ray Burst Symposium", Santa Fe, New Mexico, 8 12 September 2003, E.E. Fenimore, M. Galassi, Editors; AIP Conference Proceedings, 727, 428 (2004).

   We consider the gamma-ray burst of 1997 February 28 (GRB 970228) within the ElectroMagnetic Black Hole (EMBH) model. We first determine the value of the two free parameters that characterize energetically the GRB phenomenon in the EMBH model, that is to say the dyadosphere energy, $E_{dya} = 5.1 \times 10^{52}$ ergs, and the baryonic remnant mass M_B in units of E_{dya}, $B = M_B c^2 / E_{dya} = 3.0 \times 10^{-3}$. Having in this way estimated the energy emitted during the beam-target phase, we evaluate the role of the InterStellar Medium (ISM) number density (n_{ISM}) and of the ratio $\mathcal{R}$ between the effective emitting area and the total surface area of the GRB source, in reproducing the observed profiles of the GRB 970228 prompt emission and X-ray (2-10 keV energy band) afterglow. The importance of the ISM distribution three-dimensional treatment around the central black hole is also stressed in this analysis.

5 Publications (2005–2016)

5.1 Refereed journals

1. R. Ruffini, C.L. Bianco, P. Chardonnet, F. Fraschetti, V. Gurzadyan, S.-S. Xue; "Emergence of a filamentary structure in the fireball from GRB spectra"; International Journal of Modern Physics D, 14, 97 (2005).

   It is shown that the concept of a fireball with a definite filamentary structure naturally emerges from the analysis of the spectra of Gamma-Ray Bursts (GRBs). These results, made possible by the recently obtained analytic expressions of the equitemporal surfaces in the GRB afterglow, depend crucially on the single parameter R describing the effective area of the fireball emitting the X-ray and gamma-ray radiation. The X-ray and gamma-ray components of the afterglow radiation are shown to have a thermal spectrum in the comoving frame of the fireball and originate from a stable shock front described self-consistently by the Rankine-Hugoniot equations. Precise predictions are presented on a correlation between spectral changes and intensity variations in the prompt radiation verifiable, e.g., by the Swift and future missions. The highly variable optical and radio emission depends instead on the parameters of the surrounding medium. The GRB 991216 is used as a prototype for this model.

2. R. Ruffini, M.G. Bernardini, C.L. Bianco, P. Chardonnet, F. Fraschetti, V. Gurzadyan, M. Lattanzi, L. Vitagliano, S.-S. Xue; "Extracting energy from black holes: 'long' and 'short' GRBs and their astrophysical settings"; Il Nuovo Cimento C, 28, 589 (2005).

   The introduction of the three interpretational paradigms for Gamma-Ray Bursts (GRBs) and recent progress in understanding the X- and gamma-ray luminosity in the afterglow allow us to make assessments about the astrophysical settings of GRBs. In particular, we evidence the distinct possibility that some GRBs occur in a binary system. This subclass of GRBs manifests itself in a "tryptich": one component formed by the collapse of a massive star to a black hole, which originates the GRB; a second component by a supernova and a third one by a young neutron star born in the supernova event. Similarly, the understanding of the physics of quantum relativistic processes during the

gravitational collapse makes possible precise predictions about the structure of short GRBs.

3. M.G. Bernardini, C.L. Bianco, P. Chardonnet, F. Fraschetti, R. Ruffini, S.-S. Xue; "Theoretical interpretation of luminosity and spectral properties of GRB 031203"; The Astrophysical Journal, 634, L29 (2005).

   The X-ray and gamma-ray observations of the source GRB 031203 by INTEGRAL are interpreted within our theoretical model. In addition to a complete spacetime parameterization of the GRB, we specifically assume that the afterglow emission originates from a thermal spectrum in the comoving frame of the expanding baryonic matter shell. By determining the two free parameters of the model and estimating the density and filamentary structure of the ISM, we reproduce the observed luminosity in the 20-200 keV energy band. As in previous sources, the prompt radiation is shown to coincide with the peak of the afterglow, and the luminosity substructure is shown to originate in the filamentary structure of the ISM. We predict a clear hard-to-soft behavior in the instantaneous spectra. The time-integrated spectrum over 20 s observed by INTEGRAL is well fitted. Despite the fact that this source has been considered "unusual", it appears to us to be a normal low-energy GRB.

4. R. Ruffini, M.G. Bernardini, C.L. Bianco, P. Chardonnet, F. Fraschetti, S.-S. Xue; Evidence for isotropic emission in GRB991216; Advances in Space Research, 38, 1291 (2006).

   The issue of the possible presence or absence of jets in GRBs is here re-examined for GRB991216. We compare and contrast our theoretically predicted afterglow luminosity in the 2–10 keV band for spherically symmetric versus jetted emission. At these wavelengths the jetted emission can be excluded and data analysis confirms spherical symmetry. These theoretical fits are expected to be improved by the forthcoming data of the Swift mission.

5. R. Ruffini, M.G. Bernardini, C.L. Bianco, P. Chardonnet, F. Fraschetti, R. Guida, S.-S. Xue; "GRB 050315: A step toward understanding the uniqueness of the overall GRB structure"; The Astrophysical Journal, 645, L109 (2006).

   Using the Swift data of GRB 050315, we are making progress toward understanding the uniqueness of our theoretically predicted gamma-ray burst (GRB) structure, which is composed of a proper GRB (P-GRB), emitted at the transparency of an electron-positron plasma with suitable baryon loading, and an afterglow comprising the so-called prompt emission due to external shocks. Thanks to the Swift observations, the P-GRB is identified, and for the first time we can theoretically fit detailed light curves for selected energy bands on a

continuous timescale ranging over 106 s. The theoretically predicted instantaneous spectral distribution over the entire afterglow is presented, confirming a clear hard-to-soft behavior encompassing, continuously, the "prompt emission" all the way to the latest phases of the afterglow.

6. C.L. Bianco, L. Caito, R. Ruffini; "Theoretical interpretation of GRB 011121"; Il Nuovo Cimento B, 121, 1441 (2006).

   GRB011121 is analyzed as a prototype to understand the "flares" recently observed by Swift in the afterglow of many GRB sources. Detailed theoretical computation of the GRB011121 light curves in selected energy bands are presented and compared and contrasted with observational BeppoSAX data.

7. R. Ruffini, M.G. Bernardini, C.L. Bianco, P. Chardonnet, F. Fraschetti, R. Guida, S.-S. Xue; "GRB 050315: A step toward the uniqueness of the overall GRB structure"; Il Nuovo Cimento B, 121, 1367 (2006).

   Using the *Swift* data of GRB 050315, we progress on the uniqueness of our theoretically predicted Gamma-Ray Burst (GRB) structure as composed by a proper-GRB (P-GRB), emitted at the transparency of an electron-positron plasma with suitable baryon loading, and an afterglow comprising the so called "prompt emission" as due to external shocks. Thanks to the *Swift* observations, we can theoretically fit detailed light curves for selected energy bands on a continuous time scale ranging over 10^6 seconds. The theoretically predicted instantaneous spectral distribution over the entire afterglow confirms a clear hard-to-soft behavior encompassing, continuously, the "prompt emission" all the way to the latest phases of the afterglow. Consequences of the instrumental threshold on the definition of "short" and "long" GRBs are discussed.

8. M.G. Bernardini, C.L. Bianco, L. Caito, P. Chardonnet, A. Corsi, M.G. Dainotti, F. Fraschetti, R. Guida, R. Ruffini, S.-S. Xue; GRB970228 as a prototype for short GRBs with afterglow; Il Nuovo Cimento B, 121, 1439 (2006).

   GRB970228 is analyzed as a prototype to understand the relative role of short GRBs and their associated afterglows, recently observed by Swift and HETE-II. Detailed theoretical computation of the GRB970228 light curves in selected energy bands are presented and compared with observational BeppoSAX data.

9. M.G. Dainotti, M.G. Bernardini, C.L. Bianco, L. Caito, R. Guida, R. Ruffini; "GRB060218 and GRBs associated with Supernovae Ib/c"; Astronomy & Astrophysics, 471, L29 (2007).

   Context: The *Swift* satellite has given continuous data in the range 0.3–150 keV from 0 s to 10^6 s for GRB060218 associated with SN2006aj. This Gamma-Ray Burst (GRB) which has an unusually long duration ($T_{90} \sim 2100$ s) fulfills the

Amati relation. These data offer the opportunity to probe theoretical models for GRBs connected with Supernovae (SNe).
Aims: We plan to fit the complete γ- and X-ray light curves of this long duration GRB, including the prompt emission, in order to clarify the nature of the progenitors and the astrophysical scenario of the class of GRBs associated with SNe Ib/c.
Methods: We apply our "fireshell" model based on the formation of a black hole, giving the relevant references. It is characterized by the precise equations of motion and equitemporal surfaces and by the role of thermal emission.
Results: The initial total energy of the electron-positron plasma $E_{e^\pm}^{tot} = 2.32 \times 10^{50}$ erg has a particularly low value, similar to the other GRBs associated with SNe. For the first time, we observe a baryon loading $B = 10^{-2}$ which coincides with the upper limit for the dynamical stability of the fireshell. The effective CircumBurst Medium (CBM) density shows a radial dependence $n_{cbm} \propto r^{-\alpha}$ with $1.0 \lesssim \alpha \lesssim 1.7$ and monotonically decreases from 1 to 10^{-6} particles/cm^3. This behavior is interpreted as being due to a fragmentation in the fireshell. Analogies with the fragmented density and filling factor characterizing Novae are outlined. The fit presented is particularly significant in view of the complete data set available for GRB060218 and of the fact that it fulfills the Amati relation.
Conclusions: We fit GRB060218, usually considered as an X-Ray Flash (XRF), as a "canonical GRB" within our theoretical model. The smallest possible black hole, formed by the gravitational collapse of a neutron star in a binary system, is consistent with the especially low energetics of the class of GRBs associated with SNe Ib/c. We provide the first evidence for a fragmentation in the fireshell. This fragmentation is crucial in explaining both the unusually large T_{90} and the consequently inferred abnormally low value of the CBM effective density.

10. M.G. Bernardini, C.L. Bianco, L. Caito, M.G. Dainotti, R. Guida, R. Ruffini; "GRB970228 and a class of GRBs with an initial spikelike emission"; Astronomy & Astrophysics, 474, L13 (2007).

Context: The discovery by *Swift* and HETE-2 of an afterglow emission associated possibly with short GRBs opened the new problematic of their nature and classification. This issue has been further enhanced by the observation of GRB060614 and by a new analysis of the BATSE catalog which led to the identification of a new class of GRBs with "an occasional softer extended emission lasting tenths of seconds after an initial spikelike emission".
Aims: We plan a twofold task: a) to fit this new class of "hybrid" sources within our "canonical GRB" scenario, where all GRBs are generated by a "common engine" (i.e. the gravitational collapse to a black hole); b) to propose GRB970228 as the prototype of the above mentioned class, since it shares the

same morphology and observational features.
Methods: We analyze *Beppo*SAX data on GRB970228 within the "fireshell" model and we determine the parameters describing the source and the CircumBurst Medium (CBM) needed to reproduce its light curves in the 40–700 keV and 2–26 keV energy bands.
Results: We find that GRB970228 is a "canonical GRB", like e.g. GRB050315, with the main peculiarity of a particularly low average density of the CBM $\langle n_{cbm}\rangle \sim 10^{-3}$ particles/cm^3. We also simulate the light curve corresponding to a rescaled CBM density profile with $\langle n_{cbm}\rangle = 1$ particle/cm^3. From such a comparison it follows that the total time-integrated luminosity is a faithful indicator of the nature of GRBs, contrary to the peak luminosity which is merely a function of the CBM density.
Conclusions: We call attention on discriminating the short GRBs between the "genuine" and the "fake" ones. The "genuine" ones are intrinsically short, with baryon loading $B \lesssim 10^{-5}$, as stated in our original classification. The "fake" ones, characterized by an initial spikelike emission followed by an extended emission lasting tenths of seconds, have a baryon loading $10^{-4} \lesssim B \leq 10^{-2}$. They are observed as such only due to an underdense CBM consistent with a galactic halo environment which deflates the afterglow intensity.

11. R. Guida, M.G. Bernardini, C.L. Bianco, L. Caito, M.G. Dainotti, R. Ruffini; "The Amati relation in the "fireshell" model"; Astronomy & Astrophysics, 487, L37 (2008).

Context: The cosmological origin of gamma-ray bursts (GRBs) has been firmly established, with redshifts up to $z = 6.29$. They are possible candidates for use as "distance indicators" for testing cosmological models in a redshift range hardly achievable by other cosmological probes. Asserting the validity of the empirical relations among GRB observables is now crucial for their calibration.
Aims: Motivated by the relation proposed by Amati and collaborators, we look within the "fireshell" model for a relation between the peak energy E_p of the νF_ν total time-integrated spectrum of the afterglow and the total energy of the afterglow E_{aft}, which in our model encompasses and extends the prompt emission.
Methods: The fit within the fireshell model, as for the "canonical" GRB050315, uses the complete arrival time coverage given by the Swift satellite. It is performed simultaneously, self-consistently, and recursively in the four BAT energy bands (15–25 keV, 25–50 keV, 50–100 keV, and 100-150 keV), as well as in the XRT one (0.2–10 keV). It uniquely determines the two free parameters characterizing the GRB source, the total energy $E_{tot}^{e^\pm}$ of the $e^\pm$ plasma and its baryon loading B, as well as the effective CircumBurst Medium (CBM) distribution. We can then build two sets of "gedanken" GRBs varying the total energy of the electron-positron plasma $E_{tot}^{e^\pm}$ and keeping the same baryon loading

B of GRB050315. The first set assumes the one obtained in the fit of GRB050315 for the effective CBM density. The second set assumes instead a constant CBM density equal to the average value of the GRB050315 prompt phase.
Results: For the first set of "gedanken" GRBs we find a relation $E_p \propto (E_{aft})^a$, with $a = 0.45 \pm 0.01$, whose slope strictly agrees with the Amati one. Such a relation, in the limit $B \to 10^{-2}$, coincides with the Amati one. Instead, no correlation is found in the second set of "gedanken" GRBs.
Conclusions: Our analysis excludes the proper GRB (P-GRB) from the prompt emission, extends all the way to the latest afterglow phases, and is independent of the assumed cosmological model, since all "gedanken" GRBs are at the same redshift. The Amati relation, on the other hand, includes the P-GRB, focuses only on the prompt emission, being therefore influenced by the instrumental threshold that fixes the end of the prompt emission, and depends on the assumed cosmology. This might explain the intrinsic scatter observed in the Amati relation.

12. L. Caito, M.G. Bernardini, C.L. Bianco, M.G. Dainotti, R. Guida, R. Ruffini; "GRB060614: a "fake" short GRB from a merging binary system"; Astronomy & Astrophysics, 489, 501 (2009).

Context: GRB060614 observations by VLT and by Swift have infringed the traditionally accepted gamma-ray burst (GRB) collapsar scenario that purports the origin of all long duration GRBs from supernovae (SN). GRB060614 is the first nearby long duration GRB clearly not associated with a bright Ib/c SN. Moreover, its duration ($T_{90} \sim 100$ s) makes it hardly classifiable as a short GRB. It presents strong similarities with GRB970228, the prototype of a new class of "fake" short GRBs that appear to originate from the coalescence of binary neutron stars or white dwarfs spiraled out into the galactic halo. *Aims*: Within the "canonical" GRB scenario based on the "fireshell" model, we test if GRB060614 can be a "fake" or "disguised" short GRB. We model the traditionally termed "prompt emission" and discriminate the signal originating from the gravitational collapse leading to the GRB from the process occurring in the circumburst medium (CBM). *Methods*: We fit GRB060614 light curves in Swift's BAT ($15 - 150$ keV) and XRT ($0.2 - 10$ keV) energy bands. Within the fireshell model, light curves are formed by two well defined and different components: the proper-GRB (P-GRB), emitted when the fireshell becomes transparent, and the extended afterglow, due to the interaction between the leftover accelerated baryonic and leptonic shell and the CBM. *Results*: We determine the two free parameters describing the GRB source within the fireshell model: the total $e^{\pm}$ plasma energy ($E^{e^{\pm}}_{tot} = 2.94 \times 10^{51}$erg) and baryon loading ($B = 2.8 \times 10^{-3}$). A small average CBM density $\sim 10^{-3}$ particles/cm^3 is inferred, typical of galactic halos. The first spikelike emission is identified with the P-GRB and the following prolonged emission with the extended afterglow peak. We obtain very

good agreement in the BAT ($15-150$ keV) energy band, in what is traditionally called "prompt emission", and in the XRT ($0.2-10$ keV) one. *Conclusions*: The *anomalous* GRB060614 finds a natural interpretation within our canonical GRB scenario: it is a "disguised" short GRB. The total time-integrated extended afterglow luminosity is greater than the P-GRB one, but its peak luminosity is smaller since it is deflated by the peculiarly low average CBM density of galactic halos. This result points to an old binary system, likely formed by a white dwarf and a neutron star, as the progenitor of GRB060614 and well justifies the absence of an associated SN Ib/c. Particularly important for further studies of the final merging process are the temporal structures in the P-GRB down to 0.1 s.

13. M.G. Bernardini, C.L. Bianco, L. Caito, M.G. Dainotti, R. Guida, R. Ruffini; "GRB970228 in the "canonical GRB" scenario"; Journal of the Korean Physical Society, 56, 1575 (2010).

    Within the "fireshell" model, we define a "canonical GRB" light curve with two sharply different components: the proper-GRB (P-GRB), emitted when the optically thick fireshell of an electron-positron plasma originating from the phenomenon reaches transparency, and the afterglow, emitted due to the collision between the remaining optically thin fireshell and the circumburst medium (CBM). On the basis of the recent understanding of GRB970228 as the prototype for a new class of GRBs with "an occasional softer extended emission lasting tenths of seconds after an initial spikelike emission", we outline our "canonical GRB" scenario, originating from the gravitational collapse to a black hole, with special emphasis on the discrimination between "genuine" and "fake" short GRBs. Furthermore, we investigate how the GRB970228 analysis provides a theoretical explanation for the apparent absence of such a correlation for the GRBs belonging to this new class.

14. L. Caito, M.G. Bernardini, C.L. Bianco, M.G. Dainotti, R. Guida, R. Ruffini; "GRB060614: a preliminary result"; Journal of the Korean Physical Society, 56, 1579 (2010).

    The explosion of GRB 060614 produced a deep break in the GRB scenario and opened new horizons of investigation because it can't be traced back to any traditional scheme of classification. In fact, it manifests peculiarities both of long bursts and of short bursts, and above all, it is the first case of a long-duration near GRB without any bright Ib/c associated Supernova. We will show that, in our canonical GRB scenario, this "anomalous" situation finds a natural interpretation and allows us to discuss a possible variation in the traditional classification scheme, introducing a distinction between "genuine" and "fake" short bursts.

15. M.G. Dainotti, M.G. Bernardini, C.L. Bianco, L. Caito, R. Guida, R. Ruffini; "The astrophysical trypthic: GRB, SN and URCA can be extended to GRB060218?"; Journal of the Korean Physical Society, 56, 1588 (2010).

    The *Swift* satellite has given continuous data in the range 0.3–150 keV from 0 s to 10^6 s for GRB060218 associated with SN2006aj. This GRB is the fourth GRB spectroscopically associated with SNe after the cases of GRB980425-SN1998bw, GRB031203-SN2003lw, GRB 030329-SN2003dh. It has an unusually long duration ($T_{90} \sim 2100$ s). These data offer the opportunity to probe theoretical models for Gamma-Ray Bursts (GRBs) connected with Supernovae (SNe). We plan to fit the complete γ- and X-ray light curves of this long duration GRB, including the prompt emission, in order to clarify the nature of the progenitors and the astrophysical scenario of the class of GRBs associated to SNe Ib/c. We apply our "fireshell" model based on the formation of a black hole, giving the relevant references. The initial total energy of the electron-positron plasma $E^{tot}_{e^\pm} = 2.32 \times 10^{50}$ erg has a particularly low value similarly to the other GRBs associated with SNe. For the first time we observe a baryon loading $B = 10^{-2}$ which coincides with the upper limit for the dynamical stability of the fireshell. The effective CircumBurst Medium (CBM) density shows a radial dependence $n_{cbm} \propto r^{-\alpha}$ with $1.0 \lesssim \alpha \lesssim 1.7$ and monotonically decreases from 1 to 10^{-6} particles/cm^3. Such a behavior is interpreted as due to a fragmentation in the fireshell. Such a fragmentation is crucial in explaining both the unusually large T_{90} and the consequently inferred abnormal low value of the CBM effective density. We fit GRB060218, usually considered as an X-Ray Flash (XRF), as a "canonical GRB" within our theoretical model. The smallest possible black hole, formed by the gravitational collapse of a neutron star in a binary system, is consistent with the especially low energetics of the class of GRBs associated with SNe Ib/c. We present the URCA process and the connection between the GRBs associated with SNe extended also to the case of GRB060218.

16. L. Izzo, M.G. Bernardini, C.L. Bianco, L. Caito, B. Patricelli, R. Ruffini; "GRB 090423 at Redshift 8.1: a Theoretical Interpretation"; Journal of the Korean Physical Society, 57, 551 (2010).

    GRB 090423 is the farthest gamma ray burst ever observed, with a redshift of about 8.1. We present within the fireshell scenario a complete analysis of this GRB. We model the prompt emission and the first rapid flux decay of the afterglow emission as being to the canonical emission of the interaction in the interval $0 \leq t \leq 440$ s by using accelerated baryonic matter with the circumburst medium. After the data reduction of the Swift data in the BAT (15 - 150 keV) and XRT (0.2 - 10 keV) energy bands, we interpret the light curves and the spectral distribution in the context of the fireshell scenario. We also confirm in this source the existence of a second component, a plateau phase,

as being responsible for the late emission in the X-ray light curve. This extra component originates from the fact that the ejecta have a range of the bulk Lorentz Γ factor, which starts to interact each other ejecta at the start of the plateau phase.

17. L. Caito, L. Amati, M.G. Bernardini, C.L. Bianco, G. De Barros, L. Izzo, B. Patricelli, R. Ruffini; "GRB 071227: an additional case of a disguised short burst"; Astronomy & Astrophysics, 521, A80 (2010).

    Context: Observations of gamma-ray bursts (GRBs) have shown an hybridization between the two classes of long and short bursts. In the context of the fireshell model, the GRB light curves are formed by two different components: the *proper* GRB (P-GRB) and the extended afterglow. Their relative intensity is linked to the fireshell baryon loading B. The GRBs with P-GRB predominance are the short ones, the remainders are long. A new family of *disguised* short bursts has been identified: long bursts with a protracted low instantaneous luminosity due to a low density CircumBurst Medium (CBM). In the 15–150 keV energy band GRB 071227 exhibits a short duration (about 1.8s) spike-like emission followed by a very soft extended tail up to one hundred seconds after the trigger. It is a faint ($E_{iso} = 5.8 \times 10^{50}$) nearby GRB ($z = 0.383$) that does not have an associated type Ib/c bright supernova (SN). For these reasons, GRB 071227 has been classified as a short burst not fulfilling the Amati relation holding for long burst. *Aims:* We check the classification of GRB 071227 provided by the fireshell model. In particular, we test whether this burst is another example of a *disguised* short burst, after GRB 970228 and GRB 060614, and, for this reason, whether it fulfills the Amati relation. *Methods:* We simulate GRB 071227 light curves in the *Swift* BAT 15–50 keV bandpass and in the XRT (0.3–10 keV) energy band within the fireshell model. *Results:* We perform simulations of the tail in the 15–50 keV bandpass, as well as of the first part of the X-ray afterglow. This infers that: $E_{tot}^{e^{\pm}} = 5.04 \times 10^{51}$ erg, $B = 2.0 \times 10^{-4}$, $E_{P-GRB}/E_{aft} \sim 0.25$, and $\langle n_{cbm} \rangle = 3.33$ particles/cm^3. These values are consistent with those of "long duration" GRBs. We interpret the observed energy of the first hard emission by identifying it with the P-GRB emission. The remaining long soft tail indeed fulfills the Amati relation. *Conclusions:* Previously classified as a short burst, GRB 071227 on the basis of our analysis performed in the context of the fireshell scenario represents another example of a *disguised* short burst, after GRB 970228 and GRB 060614. Further confirmation of this result is that the soft tail of GRB 071227 fulfills the Amati relation.

18. M.G. Bernardini, C.L. Bianco, L. Caito, L. Izzo, B. Patricelli, R. Ruffini; "Analysis of GRB060607A within the fireshell model: prompt emission, X-ray flares and late afterglow phase"; Astronomy & Astrophysics, submitted to.

Context: GRB060607A is a very distant ($z = 3.082$) and energetic event ($E_{iso} \sim 10^{53}$ erg). Its main peculiarity is that the peak of the near-infrared (NIR) afterglow has been observed with the REM robotic telescope. This NIR peak has been interpreted as the afterglow onset within the fireball forward shock model, and the initial Lorentz gamma factor of the emitting system has been inferred. *Aims*: We analyze GRB060607A within the fireshell model. We emphasize the central role of the prompt emission in determining the initial Lorentz gamma factor of the extended afterglow and we interpret the X-ray flares as produced by the interaction of the optically thin fireshell with overdense CircumBurst Medium (CBM) clumps. *Methods*: We deal only with the Swift BAT and XRT observations, that are the basic contribution to the GRB emission and that are neglected in the treatment adopted in the current literature. The numerical modeling of the fireshell dynamics allows to calculate all its characteristic quantities, in particular the exact value of the Lorentz gamma factor at the transparency. *Results*: We show that the theoretically computed prompt emission light curves are in good agreement with the observations in all the *Swift* BAT energy bands as well as the spectra integrated over different time intervals. The flares observed in the decaying phase of the X-ray afterglow are also reproduced by the same mechanism, but in a region in which the typical dimensions of the clumps are smaller than the visible area of the fireshell and most energy lies in the X-ray band due to the hard-to-soft evolution. *Conclusions*: We show that it is possible to obtain flares with $\Delta t/t$ compatible with the observations when the three-dimensional structure of the CBM clumps is duly taken into account. We stop our analysis at the beginning of the X-ray plateau phase, since we suppose this originates from the instabilities developed in the collision between different subshells within a structured fireshell.

19. G. de Barros, M. G. Bernardini, C.L. Bianco, L. Caito, L. Izzo, B. Patricelli, R. Ruffini; "On the nature of GRB 050509b: a disguised short GRB"; Astronomy & Astrophyscs, 529, A130 (2011)

Context: GRB 050509b, detected by the *Swift* satellite, is the first case where an X-ray afterglow has been observed associated with a short gamma-ray burst (GRB). Within the fireshell model, the canonical GRB light curve presents two different components: the proper-GRB (P-GRB) and the extended afterglow. Their relative intensity is a function of the fireshell baryon loading parameter B and of the CircumBurst Medium (CBM) density (n_{CBM}). In particular, the traditionally called short GRBs can be either "genuine" short GRBs (with $B \lesssim 10^{-5}$, where the P-GRB is energetically predominant) or "disguised" short GRBs (with $B \gtrsim 3.0 \times 10^{-4}$ and $n_{CBM} \ll 1$, where the extended afterglow is energetically predominant). *Aims*: We verify whether GRB 050509b can be classified as a "genuine" short or a "disguised" short GRB, in the fireshell model. *Methods*: We investigate two alternative scenarios. In the first, we start from

the assumption that this GRB is a "genuine" short burst. In the second attempt, we assume that this GRB is a "disguised" burst. *Results*: If GRB 050509b were a genuine short GRB, there should initially be very hard emission which is ruled out by the observations. The analysis that assumes that this is a disguised short GRB is compatible with the observations. The theoretical model predicts a value of the extended afterglow energy peak that is consistent with the Amati relation. *Conclusions*: GRB 050509b cannot be classified as a "genuine" short GRB. The observational data are consistent with a "disguised" short GRB classification, i.e., a long burst with a weak extended afterglow "deflated" by the low density of the CBM. We expect that all short GRBs with measured redshifts are disguised short GRBs because of a selection effect: if there is enough energy in the afterglow to measure the redshift, then the proper GRB must be less energetic than the afterglow. The Amati relation is found to be fulfilled only by the extended afterglow excluding the P-GRB.

20. L. Caito, M.G. Bernardini, C.L. Bianco, L. Izzo, B. Patricelli, R. Ruffini; "GRB 071227: another disguised short burst"; International Journal of Modern Physics D, 20, 1931 (2011).

    Observations of Gamma-ray Bursts (GRBs) put forward in the recent years have revealed, with increasing evidence, that the historical classification between long and short bursts has to be revised. Within the Fireshell scenario, both short and long bursts are canonical bursts, consisting of two different phases. First, a Proper-GRB (P-GRB), that is the emission of photons at the transparency of the fireshell. Then, the Extended Afterglow, multiwavelength emission due to the interacion of the baryonic remnants of the fireshell with the CircumBurst Medium (CBM). We discriminate between long and short bursts by the amount of energy stored in the first phase with respect to the second one. Within the Fireshell scenario, we have introduced a third intermediate class: the disguised GRBs. They appear like short bursts, because their morphology is characterized by a first, short, hard episode and a following deflated tail, but this last part — coincident with the peak of the afterglow — is energetically predominant. The origin of this peculiar kind of sources is inferred to a very low average density of the environment (of the order of 10^{-3}). After GRB 970228 and GRB 060614, we find in GRB 071227 a third example of disguised burst.

21. L. Izzo, M.G. Bernardini, C.L. Bianco, L. Caito, B. Patricelli, L.J. Rangel Lemos, R. Ruffini; "GRB 080916C and the high-energy emission in the fireshell scenario"; International Journal of Modern Physics D, 20, 1949 (2011).

    In this paper we discuss a possible explanation for the high energy emission (up to $\sim$ GeV) seen in GRB 080916C. We propose that the GeV emission is

originated by the collision between relativistic baryons in the fireshell after the transparency and the nucleons located in molecular clouds near the burst site. This collision should give rise pion production, whose immediate decay provides high energy photons, neutrinos and leptons. Using a public code (SYBILL) we simulate these relativistic collisions in their simple form, so that we can draw our preliminar results in this paper. We will present moreover our hypothesis that the delayed onset of this emission identifies in a complete way the P-GRB emission.

22. B. Patricelli, M.G. Bernardini, C.L. Bianco, L. Caito, L. Izzo, R. Ruffini, G. Vereshchagin; "A new spectral energy distribution of photons in the fireshell model of GRBs"; International Journal of Modern Physics D, 20, 1983 (2011).

    The analysis of various Gamma-Ray Bursts (GRBs) having a low energetics (an isotropic energy $E_{iso} \lesssim 10^{53}$ ergs) within the fireshell model has shown how the $N(E)$ spectrum of their prompt emission can be reproduced in a satisfactory way by a convolution of thermal spectra. Nevertheless, from the study of very energetic bursts ($E_{iso} \lesssim 10^{54}$ ergs) such as, for example, GRB 080319B, some discrepancies between the numerical simulations and the observational data have been observed. We investigate a different spectrum of photons in the comoving frame of the fireshell in order to better reproduce the spectral properties of GRB prompt emission within the fireshell model. We introduce a phenomenologically modified thermal spectrum: a thermal spectrum characterized by a different asymptotic power-law index in the low energy region. Such an index depends on a free parameter α, so that the pure thermal spectrum corresponds to the case $\alpha = 0$. We test this spectrum by comparing the numerical simulations with the observed prompt emission spectra of various GRBs. From this analysis it has emerged that the observational data can be correctly reproduced by assuming a modified thermal spectrum with $\alpha = -1.8$.

23. A.V. Penacchioni, R. Ruffini, L. Izzo, M. Muccino, C.L. Bianco, L. Caito, B. Patricelli, L. Amati; "Evidence for a proto-black hole and a double astrophysical component in GRB 101023"; Astronomy & Astrophysics, 538, A58 (2012).

    Context: It has been recently shown that GRB 090618, observed by AGILE, Coronas Photon, Fermi, Konus, Suzaku and Swift, is composed of two very different components: episode 1, lasting 50 s, shows a thermal plus power-law spectrum with a characteristic temperature evolving in time as a power law; episode 2 (the remaining 100 s) is a canonical long GRB. We have associated episode 1 to the progenitor of a collapsing bare core leading to the formation of a black hole: what was defined as a "proto black hole". *Aims*: In precise analogy with GRB 090618 we aim to analyze the 89s of the emission of GRB

101023, observed by Fermi, Gemini, Konus and Swift, to see if there are two different episodes: the first one presenting a characteristic black-body temperature evolving in time as a broken power law, and the second one consistent with a canonical GRB. *Methods*: To obtain information on the spectra, we analyzed the data provided by the GBM detector onboard the Fermi satellite, and we used the heasoft package XSPEC and RMFIT to obtain their spectral distribution. We also used the numerical code GRBsim to simulate the emission in the context of the fireshell scenario for episode 2. *Results*: We confirm that the first episode can be well fit by a black body plus power-law spectral model. The temperature changes with time following a broken power law, and the photon index of the power-law component presents a soft-to-hard evolution. We estimate that the radius of this source increases with time with a velocity of $1.5 \times 10^4 km/s$. The second episode appears to be a canonical GRB. By using the Amati and the Atteia relations, we determined the cosmological redshift, $z \sim 0.9 \pm 0.084(stat.) \pm 0.2(sys.)$. The results of GRB 090618 are compared and contrasted with the results of GRB 101023. Particularly striking is the scaling law of the soft X-ray component of the afterglow. *Conclusions*: We identify GRB 090618 and GRB 101023 with a new family of GRBs related to a single core collapse and presenting two astrophysical components: a first one related to the proto-black hole prior to the process of gravitational collapse (episode 1), and a second one, which is the canonical GRB (episode 2) emitted during the formation of the black hole. For the first time we are witnessing the process of a black hole formation from the instants preceding the gravitational collapse up to the GRB emission. This analysis indicates progress towards developing a GRB distance indicator based on understanding the P-GRB and the prompt emission, as well as the soft X-ray behavior of the late afterglow.

24. R. Negreiros, R. Ruffini, C. L. Bianco, J. A. Rueda; "Cooling of young neutron stars in GRB associated to supernovae"; Astronomy & Astrophysics, 540, A12 (2012).

Context: The traditional study of neutron star cooling has been generally applied to quite old objects such as the Crab Pulsar (957 years) or the central compact object in Cassiopeia A (330 years) with an observed surface temperature $\sim 10^6$ K. However, recent observations of the late ($t = 10^8$–10^9 s) emission of the supernovae (SNe) associated to GRBs (GRB-SN) show a distinctive emission in the X-ray regime consistent with temperatures $\sim 10^7$–10^8 K. Similar features have been also observed in two Type Ic SNe SN 2002ap and SN 1994I that are not associated to GRBs. *Aims*: We advance the possibility that the late X-ray emission observed in GRB-SN and in isolated SN is associated to a hot neutron star just formed in the SN event, here defined as a neo-neutron star. *Methods*: We discuss the thermal evolution of neo-neutron stars in the age regime that spans from ~ 1 minute (just after the proto-neutron

star phase) all the way up to ages $<$ 10–100 yr. We examine critically the key factor governing the neo-neutron star cooling with special emphasis on the neutrino emission. We introduce a phenomenological heating source, as well as new boundary conditions, in order to mimic the high temperature of the atmosphere for young neutron stars. In this way we match the neo-neutron star luminosity to the observed late X-ray emission of the GRB-SN events: URCA-1 in GRB980425-SN1998bw, URCA-2 in GRB030329-SN2003dh, and URCA-3 in GRB031203-SN2003lw. *Results*: We identify the major role played by the neutrino emissivity in the thermal evolution of neo-neutron stars. By calibrating our additional heating source at early times to $\sim 10^{12}$–10^{15} erg/g/s, we find a striking agreement of the luminosity obtained from the cooling of a neo-neutron stars with the prolonged ($t = 10^8$–10^9 s) X-ray emission observed in GRB associated with SN. It is therefore appropriate a revision of the boundary conditions usually used in the thermal cooling theory of neutron stars, to match the proper conditions of the atmosphere at young ages. The traditional thermal processes taking place in the crust might be enhanced by the extreme high-temperature conditions of a neo-neutron star. Additional heating processes that are still not studied within this context, such as e^+e^- pair creation by overcritical fields, nuclear fusion, and fission energy release, might also take place under such conditions and deserve further analysis. *Conclusions*: Observation of GRB-SN has shown the possibility of witnessing the thermal evolution of neo-neutron stars. A new campaign of dedicated observations is recommended both of GRB-SN and of isolated Type Ic SN.

25. L. Izzo, R. Ruffini, A.V. Penacchioni, C.L. Bianco, L. Caito, S.K. Chakrabarti, J.A. Rueda, A. Nandi, B. Patricelli; "A double component in GRB 090618: a proto-black hole and a genuinely long gamma-ray burst"; Astronomy & Astrophysics, 543, A10 (2012).

Context: The joint X-ray and gamma-ray observations of GRB 090618 by very many satellites offer an unprecedented possibility of testing crucial aspects of theoretical models. In particular, they allow us to test (a) in the process of gravitational collapse, the formation of an optically thick e+e.-baryon plasma self-accelerating to Lorentz factors in the range $200 < \Gamma < 3000$; (b) its transparency condition with the emission of a component of 10^{53-54} baryons in the TeV region and (c) the collision of these baryons with the circumburst medium (CBM) clouds, characterized by dimensions of 10^{15-16} cm. In addition, these observations offer the possibility of testing a new understanding of the thermal and power-law components in the early phase of this GRB. *Aims*: We test the fireshell model of GRBs in one of the closest ($z = 0.54$) and most energetic ($E_{iso} = 2.90 \times 10^{53}$ erg) GRBs, namely GRB 090618. It was observed at ideal conditions by several satellites, namely *Fermi*, *Swift*, Konus-WIND, AGILE, RT-2, and Suzaku, as well as from on-ground optical observatories.

Methods: We analyzed the emission from GRB 090618 using several spectral models, with special attention to the thermal and power-law components. We determined the fundamental parameters of a canonical GRB within the context of the fireshell model, including the identification of the total energy of the e^+e^- plasma, $E_{tot}^{e^+e^-}$, the proper GRB (P-GRB), the baryon load, the density and structure of the CBM. *Results*: We find evidence of the existence of two different episodes in GRB 090618. The first episode lasts 50 s and is characterized by a spectrum consisting of a thermal component, which evolves between $kT = 54$ keV and $kT = 12$ keV, and a power law with an average index $\gamma = 1.75 \pm 0.04$. The second episode, which lasts for ~ 100 s, behaves as a canonical long GRB with a Lorentz gamma factor at transparency of $\Gamma = 495$, a temperature at transparency of 29.22 keV and with a characteristic size of the surrounding clouds of $R_{cl} \sim 10^{15-16}$ cm and masses of $\sim 10^{22-24}$ g. *Conclusions*: We support the recently proposed two-component nature of GRB 090618, namely, episode 1 and episode 2, with a specific theoretical analysis.We furthermore illustrate that episode 1 cannot be considered to be either a GRB or a part of a GRB event, but it appears to be related to the progenitor of the collapsing bare core, leading to the formation of the black hole, which we call a "proto-black hole". Thus, for the first time, we are witnessing the process of formation of a black hole from the phases just preceding the gravitational collapse all the way up to the GRB emission.

26. B. Patricelli, M.G. Bernardini, C.L. Bianco, L. Caito, G. De Barros, L. Izzo, R. Ruffini, G.V. Vereshchagin; "Analysis of GRB 080319B and GRB 050904 within the Fireshell Model: Evidence for a Broader Spectral Energy Distribution"; The Astrophysical Journal, 756, 16 (2012).

The observation of GRB 080319B, with an isotropic energy $E_{iso} = 1.32 \times 10^{54}$ erg, and GRB 050904, with $E_{iso} = 1.04 \times 10^{54}$ erg, offers the possibility of studying the spectral properties of the prompt radiation of two of the most energetic Gamma Ray Bursts (GRBs). This allows us to probe the validity of the fireshell model for GRBs beyond 10^{54} erg, well outside the energy range where it has been successfully tested up to now (10^{49}–10^{53} erg). We find that in the low energy region, the prompt emission spectra observed by *Swift* BAT reveals more power than theoretically predicted. The opportunities offered by these observations to improve the fireshell model are outlined in this paper. One of the distinguishing features of the fireshell model is that it relates the observed GRB spectra to the spectrum in the comoving frame of the fireshell. Originally, a fully radiative condition and a comoving thermal spectrum were adopted. An additional power-law in the comoving thermal spectrum is required due to the discrepancy of the theoretical and observed light curves and spectra in the fireshell model for GRBs 080319B and 050904. A new phenomenological parameter α is correspondingly introduced in the model. We perform numerical

simulations of the prompt emission in the *Swift* BAT bandpass by assuming different values of α within the fireshell model. We compare them with the GRB 080319B and GRB 050904 observed time-resolved spectra, as well as with their time-integrated spectra and light curves. Although GRB 080319B and GRB 050904 are at very different redshifts (z=0.937 and z=6.29 respectively), a value of $\alpha = -1.8$ leads for both of them to a good agreement between the numerical simulations and the observed BAT light curves, time-resolved and time-integrated spectra. Such a modified spectrum is also consistent with the observations of previously analyzed less energetic GRBs and reasons for this additional agreement are given. Perspectives for future low energy missions are outlined.

27. M. Muccino, R. Ruffini, C.L. Bianco, L. Izzo, A.V. Penacchioni; "GRB 090227B: The missing link between the genuine short and long GRBs"; The Astrophysical Journal, 763, 125 (2013).

The time-resolved spectral analysis of GRB 090227B, made possible by the *Fermi*-GBM data, allows to identify in this source the missing link between the genuine short and long GRBs. Within the Fireshell model of the Gamma-Ray Bursts (GRBs) we predict genuine short GRBs: bursts with the same inner engine of the long bursts but endowed with a severely low value of the Baryon load, $B \lesssim 5 \times 10^{-5}$. A first energetically predominant emission occurs at the transparency of the e^+e^- plasma, the Proper-GRB (P-GRB), followed by a softer emission, the extended afterglow. The typical separation between the two emissions is expected to be of the order of 10^{-3} – 10^{-2} s. We identify the P-GRB of GRB 090227B in the first 96 ms of emission, where a thermal component with the temperature $kT = (517 \pm 28)$ keV and a flux comparable with the non thermal part of the spectrum is observed. This non thermal component as well as the subsequent emission, where there is no evidence for a thermal spectrum, is identified with the extended afterglow. We deduce a theoretical cosmological redshift $z = 1.61 \pm 0.14$. We then derive the total energy $E^{tot}_{e^+e^-} = (2.83 \pm 0.15) \times 10^{53}$ ergs, the Baryon load $B = (4.13 \pm 0.05) \times 10^{-5}$, the Lorentz Γ factor at transparency $\Gamma_{tr} = (1.44 \pm 0.01) \times 10^4$, and the intrinsic duration $\Delta t' \sim 0.35$ s. We also determine the average density of the CircumBurst Medium (CBM), $\langle n_{CBM} \rangle = (1.90 \pm 0.20) \times 10^{-5}$ particles/cm^3. There is no evidence of beaming in the system. In view of the energetics and of the Baryon load of the source, as well as of the low interstellar medium and of the intrinsic time scale of the signal, we identify the GRB progenitor as a binary neutron star. From the recent progress in the theory of neutron stars, we obtain masses of the stars $m_1 = m_2 = 1.34 M_\odot$ and their corresponding radii $R_1 = R_2 = 12.24$ km and thickness of their crusts ~ 0.47 km, consistent with the above values of the Baryon load, of the energetics and of the time duration of the event.

28. A.V. Penacchioni, R. Ruffini, C.L. Bianco, L. Izzo, M. Muccino, G.B. Pisani, J.A. Rueda; "GRB 110709B in the induced gravitational collapse paradigm"; Astronomy & Astrophysics, 551, A133 (2013).

Context: GRB 110709B is the first source for which *Swift* BAT triggered twice, with a time separation of ~ 10 minutes. The first emission (called here Episode 1) goes from 40 s before the first trigger up to 60 s after it. The second emission (hereafter Episode 2) goes from 35 s before the second trigger to 100 s after it. These features reproduce the ones of GRB 090618, which has been recently interpreted within the Induced Gravitational Collapse paradigm (IGC). In line with this paradigm we assume the progenitor to be a close binary system composed of a core of an evolved star and a Neutron Star (NS). The evolved star explodes as a Supernova (SN) and ejects material that is partially accreted by the NS. We identify this process with Episode 1. The accretion process brings the NS over its critical mass, thus gravitationally collapsing to a BH. This process leads to the GRB emission, Episode 2. The double trigger has given for the first time the possibility to have a coverage of the X-ray emission observed by XRT both prior to and during the prompt phase of GRB 110709B. *Aims*: We analyze the spectra and time variability of Episode 1 and 2 and compute the relevant parameters of the binary progenitor, as well as the astrophysical parameters both in the SN and the GRB phase in the IGC paradigm. *Methods*: We perform a time-resolved spectral analysis of Episode 1 by fitting the spectrum with a blackbody (BB) plus a power-law (PL) spectral model. From the BB fluxes and temperatures of Episode 1 and the luminosity distance d_L, we evaluate the evolution with time of the radius of the BB emitter, associated here to the evolution of the SN ejecta. We analyze Episode 2 within the Fireshell model, identifying the Proper-GRB (P-GRB) and simulating the light curve and spectrum. We establish the redshift to be $z = 0.75$, following the phenomenological methods by Amati, by Yonetoku and by Grupe, and our analysis of the late X-ray afterglow. It is most remarkable that the determination of the cosmological redshift on the ground of the scaling of the late X-ray afterglow, already verified in GRB 090618 and GRB 101023, is again verified by this analysis. *Results*: We find for Episode 1 a temperature of the BB component that evolves with time following a broken PL, with the slope of the PL at early times $\alpha = 0$ (constant function) and the slope of the PL at late times $\beta = -4 \pm 2$. The break occurs at $t = 41.21$ s. The total energy of Episode 1 is $E_{iso}^{(1)} = 1.42 \times 10^{53}$ erg. The total energy of Episode 2 is $E_{iso}^{(2)} = 2.43 \times 10^{52}$ erg. We find at transparency a Lorentz factor $\Gamma \sim 1.73 \times 10^2$, laboratory radius of 6.04×10^{13} cm, P-GRB observed temperature $kT_{P-GRB} = 12.36$ keV, baryon load $B = 5.7 \times 10^{-3}$ and P-GRB energy of $E_{P-GRB} = 3.44 \times 10^{50}$ erg. We find a remarkable coincidence of the cosmological redshift by the scaling of the XRT data and with three other phenomenological methods. *Conclusions*: We inter-

pret GRB 110709B as a member of the IGC sources, together with GRB 970828, GRB 090618 and GRB 101023. The existence of the XRT data during the prompt phase of the emission of GRB 110709B (Episode 2) offers an unprecedented tool for improving the diagnostic of GRBs emission.

29. G.B. Pisani, L. Izzo, R. Ruffini, C.L. Bianco, M. Muccino, A.V. Penacchioni, J.A. Rueda, Y. Wang; "Novel distance indicator for gamma-ray bursts associated with supernovae"; Astronomy & Astrophysics, 552, L5 (2013).

    Context: In recent years it has been proposed that the temporal coincidence of a Gamma Ray Burst (GRB) and a type Ib/c supernova (SN) can be explained by the concept of Induced Gravitational Collapse (IGC) of a Neutron Star (NS) to a Black Hole (BH) by accretion of matter ejected by a SN Ib/c. This scenario reveals a possible common behavior in the late time X-ray emission of this subclass of GRBs. *Aims*: We want to test if such a common behavior can actually be present in the sources belonging to this GRB sub-class and if this may lead to a redshift estimator for these sources. *Methods*: We build a sample of GRBs belonging to this sub-class, and we rescale the X-ray light curves of all of them both in time and in flux to a common cosmological redshift. *Results*: We found that the X-ray light curves of all the GRBs of the sample with a measured redshift present a common late time behavior when rescaled to a common redshift $z = 1$. We then use this result to estimate the redshift of the GRBs of the sample with no measured redshift. *Conclusions*: The common behavior in the late decay of the X-ray light curves of the GRBs of the sample points to a common physical mechanism in this particular phase of the GRB emission, possibly related to the SN process. This scenario may represent an invaluable tool to estimate the redshift of GRBs belonging to this sub-class of events. More GRBs are therefore needed in order to enlarge the subclass and to make more stringent constraints on the redshift estimates performed with this method for GRBs pertaining to this class.

30. C.L. Bianco, M. G. Bernardini, L. Caito, G. De Barros, L. Izzo, M. Muccino, B. Patricelli, A.V. Penacchioni, G.B. Pisani, R. Ruffini; "The canonical GRB scenario"; Il Nuovo Cimento C, 36 s01, 21 (2013).

    The canonical GRB scenario implied by the fireshell model is briefly summarized.

31. A.V. Penacchioni, R. Ruffini, L. Izzo, M. Muccino, C.L. Bianco, L. Caito, B. Patricelli; "Evidences for a double component in the emission of GRB 101023"; Il Nuovo Cimento C, 36 s01, 117 (2013).

    In this work we present the results of the analysis of GRB 101023 in the fireshell scenario. Its redshift is not known, so we attempted to infer it from the Am-

ati Relation, obtaining $z = 0.9$. Its light curve presents a double emission, which makes it very similar to the already studied GRB 090618. We called each part Episode 1 and Episode 2. We performed a time-resolved spectral analysis with RMFIT using different spectral models, and fitted the light curve with a numerical code integrating the fireshell equations of motion. We used Fermi GBM data to build the light curve, in particular the second NaI detector, in the range (8.5–1000 keV). We considered different hypotheses regarding which part of the light curve could be the GRB and performed the analysis of all of them. We noticed a great variation of the temperature with time in the first episode, as well as almost no variation of the progenitor radius. We found that the first emission does not match the requirements for a GRB, while the second part perfectly agrees with being a canonical GRB, with a P-GRB lasting 4 s.

32. M. Muccino, R. Ruffini, C.L. Bianco, L. Izzo, A.V. Penacchioni, G.B. Pisani; "GRB 090510: A Disguised Short Gamma-Ray Burst with the Highest Lorentz Factor and Circumburst Medium"; The Astrophysical Journal, 772, 62 (2013).

GRB 090510, observed both by Fermi and AGILE satellites, is the first bright short-hard Gamma-Ray Burst (GRB) with an emission from the keV up to the GeV energy range. Within the Fireshell model, we interpret the faint precursor in the light curve as the emission at the transparency of the expanding e^+e^- plasma: the Proper-GRB (P-GRB). From the observed isotropic energy we assume a total plasma energy $E^{tot}_{e^+e^-} = (1.10 \pm 0.06) \times 10^{53}$erg and derive a Baryon load $B = (1.45 \pm 0.28) \times 10^{-3}$ and a Lorentz factor at transparency $\Gamma_{tr} = (6.7 \pm 1.6) \times 10^2$. The main emission $\sim$ 0.4s after the initial spike is interpreted as the extended afterglow, due to the interaction of the ultrarelativistic baryons with the CircumBurst Medium (CBM). Using the condition of fully radiative regime, we infer a CBM average spherically symmetric density of $\langle n_{CBM} \rangle = (1.85 \pm 0.14) \times 10^3$ particles/cm^3, one of the highest found in the Fireshell model. The value of the filling factor, $1.5 \times 10^{-10} \leq \mathcal{R} \leq 3.8 \times 10^{-8}$, leads to the estimate of filaments with densities $n_{fil} = n_{CBM}/\mathcal{R} \approx (10^6 - 10^{14})$ particles/cm^3. The sub-MeV and the MeV emissions are well reproduced. When compared to the canonical GRBs with $\langle n_{CBM} \rangle \approx 1$ particles/cm^3 and to the disguised short GRBs with $\langle n_{CBM} \rangle \approx 10^{-3}$ particles/cm^3, the case of GRB 090510 leads to the existence of a new family of bursts exploding in an over-dense galactic region with $\langle n_{CBM} \rangle \approx 10^3$ particles/cm^3. The joint effect of the high Γ_{tr} and the high density compresses in time and "inflates" in intensity the extended afterglow, making it appear as a short burst, which we here define as "disguised short GRB by excess". The determination of the above parameters values may represent an important step towards the explanation of the GeV emission.

33. R. Ruffini, M. Muccino, C.L. Bianco, M. Enderli, L. Izzo, M. Kovacevic, A.V. Penacchioni, G.B. Pisani, J.A. Rueda, Y. Wang; "On Binary Driven Hypernovae and their nested late X-ray emission"; Astronomy & Astrophysics, 565, L10 (2014).

Context: The induced gravitational collapse (IGC) paradigm addresses the very energetic (10^{52}–10^{54} erg) long gamma-ray bursts (GRBs) associated to supernovae (SNe). Unlike the traditional "collapsar" model, an evolved FeCO core with a companion neutron star (NS) in a tight binary system is considered as the progenitor. This special class of sources, here named "binary driven hypernovae" (BdHNe), presents a composite sequence composed of four different episodes with precise spectral and luminosity features.
Aims: We first compare and contrast the steep decay, the plateau, and the power-law decay of the X-ray luminosities of three selected BdHNe (GRB 060729, GRB 061121, and GRB 130427A). Second, to explain the different sizes and Lorentz factors of the emitting regions of the four episodes, for definiteness, we use the most complete set of data of GRB 090618. Finally, we show the possible role of r-process, which originates in the binary system of the progenitor.
Methods: We compare and contrast the late X-ray luminosity of the above three BdHNe. We examine correlations between the time at the starting point of the constant late power-law decay t_a^*, the average prompt luminosity $\langle L_{iso} \rangle$, and the luminosity at the end of the plateau L_a. We analyze a thermal emission ($\sim$ 0.97–0.29 keV), observed during the X-ray steep decay phase of GRB 090618.
Results: The late X-ray luminosities of the three BdHNe, in the rest-frame energy band 0.3–10 keV, show a precisely constrained "nested" structure. In a space-time diagram, we illustrate the different sizes and Lorentz factors of the emitting regions of the three episodes. For GRB 090618, we infer an initial dimension of the thermal emitter of $\sim 7 \times 10^{12}$ cm, expanding at $\Gamma \approx 2$. We find tighter correlations than the Dainotti-Willingale ones.
Conclusions: We confirm a constant slope power-law behavior for the late X-ray luminosity in the source rest frame, which may lead to a new distance indicator for BdHNe. These results, as well as the emitter size and Lorentz factor, appear to be inconsistent with the traditional afterglow model based on synchrotron emission from an ultra-relativistic ($\Gamma \sim 10^2$–10^3) collimated jet outflow. We argue, instead, for the possible role of r-process, originating in the binary system, to power the mildly relativistic X-ray source.

34. R. Ruffini, L. Izzo, M. Muccino, G.B. Pisani, J.A. Rueda, Y. Wang, C. Barbarino, C.L. Bianco, M. Enderli, M. Kovacevic; "Induced gravitational collapse at extreme cosmological distances: the case of GRB 090423"; Astronomy & Astrophysics, 569, A39 (2014).

Context: The induced gravitational collapse (IGC) scenario has been introduced in order to explain the most energetic gamma ray bursts (GRBs), $E_{iso} = 10^{52} - 10^{54}$ erg, associated with type Ib/c supernovae (SNe). It has led to the concept of binary-driven hypernovae (BdHNe) originating in a tight binary system composed by a FeCO core on the verge of a SN explosion and a companion neutron star (NS). Their evolution is characterized by a rapid sequence of events: 1) The SN explodes, giving birth to a new NS (νNS). The accretion of SN ejecta onto the companion NS increases its mass up to the critical value; 2) The consequent gravitational collapse is triggered, leading to the formation of a black hole (BH) with GRB emission; 3) A novel feature responsible for the emission in the GeV, X-ray, and optical energy range occurs and is characterized by specific power-law behavior in their luminosity evolution and total spectrum; 4) The optical observations of the SN then occurs.
Aims: We investigate whether GRB 090423, one of the farthest observed GRB at $z = 8.2$, is a member of the BdHN family.
Methods: We compare and contrast the spectra, the luminosity evolution, and the detectability in the observations by *Swift* of GRB 090423 with the corresponding ones of the best known BdHN case, GRB 090618.
Results: Identification of constant slope power-law behavior in the late X-ray emission of GRB 090423 and its overlapping with the corresponding one in GRB 090618, measured in a common rest frame, represents the main result of this article. This result represents a very significant step on the way to using the scaling law properties, proven in Episode 3 of this BdHN family, as a cosmological standard candle.
Conclusions: Having identified GRB 090423 as a member of the BdHN family, we can conclude that SN events, leading to NS formation, can already occur already at $z = 8.2$, namely at 650 Myr after the Big Bang. It is then possible that these BdHNe originate stem from 40-60 $M_\odot$ binaries. They are probing the Population II stars after the completion and possible disappearance of Population III stars.

35. M. Muccino, C.L. Bianco, L. Izzo, Y. Wang, M. Enderli, M. Kovacevic, G.B. Pisani, A.V. Penacchioni, R. Ruffini; "The Genuine Short GRB 090227B and the Disguised by Excess GRB 090510"; Gravitation and Cosmology, 20, 197 (2014).

GRB 090227B and GRB 090510, traditionally classified as short gamma-ray Bursts (GRBs), indeed originate from different systems. For GRB 090227B we inferred a total energy of the e^+e^- plasma $E^{tot}_{e^+e^-} = (2.83 \pm 0.15) \times 10^{53}$ erg, a baryon load of $B = (4.1 \pm 0.05) \times 10^{-5}$, and a CircumBurst Medium (CBM) average density $\langle n_{CBM} \rangle = (1.90 \pm 0.20) \times 10^{-5}$ cm^{-3}. From these results we have assumed the progenitor of this burst to be a symmetric neutron stars (NSs) merger with masses $m = 1.34 M_\odot$, radii $R = 12.24$ km. GRB 090510,

instead, has $E^{tot}_{e^+e^-} = (1.10 \pm 0.06) \times 10^{53}$ erg, $B = (1.45 \pm 0.28) \times 10^{-3}$, implying a Lorentz factor at transparency of $\Gamma = (6.7 \pm 1.7) \times 10^2$, which are characteristic of the long GRB class, and a very high CBM density, $\langle n_{CBM} \rangle = (1.85 \pm 0.14) \times 10^3$ cm^{-3}. The joint effect of the high values of Γ and of $\langle n_{CBM} \rangle$ compresses in time and "inflates" in intensity in an extended afterglow, making appear GRB 090510 as a short burst, which we here define as "disguised short GRB by excess" occurring an overdense region with 10^3 cm^{-3}.

36. M. Muccino, C.L. Bianco, L. Izzo, Y. Wang, M. Enderli, G.B. Pisani, A.V. Penacchioni, R. Ruffini; "Two short bursts originating from different astrophysical systems: The genuine short GRB 090227B and the disguised short GRB 090510 by excess"; Journal of the Korean Physical Society, 65, 865 (2014).

    GRB 090227B and GRB 090510 are two gamma-ray bursts (GRBs) traditionally classified as short bursts. The major outcome of our analysis is that they indeed originate from different systems. In the case of GRB 090227B, from the inferred values of the total energy of the e^+e^- plasma, $E^{tot}_{e^+e^-} = (2.83 \pm 0.15) \times 10^{53}$ erg, the engulfed baryonic mass M_B, expressed as $B = M_B c^2 / E^{tot}_{e^+e^-} = (4.1 \pm 0.05) \times 10^{-5}$, and the circumburst medium (CBM) average density, $\langle n_{CBM} \rangle = (1.90 \pm 0.20) \times 10^{-5}$ cm^{-3}, we have assumed the progenitor of this burst to be a symmetric neutron star (NS) merger with masses $m = 1.34 M_\odot$, radii $R = 12.24$ km, and crustal thicknesses of ~ 0.47 km. In the case of GRB 090510, we have derived the total plasma energy, $E^{tot}_{e^+e^-} = (1.10 \pm 0.06) \times 10^{53}$ erg, the Baryon load, $B = (1.45 \pm 0.28) \times 10^{-3}$, and the Lorentz factor at transparency, $\Gamma = (6.7 \pm 1.7) \times 10^2$, which are characteristic of the long GRB class, as well as a very high CBM density, $\langle n_{CBM} \rangle = (1.85 \pm 0.14) \times 10^3$ cm^{-3}. The joint effect of the high values of Γ and $\langle n_{CBM} \rangle$ compresses in time and "inflates" in intensity the extended afterglow, making GRB 090510 appear to be a short burst, which we here define as a "disguised short GRB by excess", occurring in an overdense region with 10^3 cm^{-3}.

37. R. Ruffini, Y. Wang, M. Kovacevic, C.L. Bianco, M. Enderli, M. Muccino, A.V. Penacchioni, G.B. Pisani, J. Rueda; "GRB 130427A and SN 2013cq: A Multi-wavelength Analysis of An Induced Gravitational Collapse Event"; The Astrophysical Journal, 798, 10 (2015).

    We have performed our data analysis of the observations by *Swift*, *NuStar* and *Fermi* satellites in order to probe the induced gravitational collapse (IGC) paradigm for GRBs associated with supernovae (SNe), in the "terra incognita" of GRB 130427A. We compare and contrast our data analysis with those in the literature. We have verified that the GRB 130427A conforms to the IGC paradigm by examining the power law behavior of the luminosity in the early 10^4 s of the XRT observations. This has led to the identification of the four

different episodes of the "binary driven hypernovae" (BdHNe) and to the prediction, on May 2, 2013, of the occurrence of SN 2013cq, duly observed in the optical band on May 13, 2013. The exceptional quality of the data has allowed the identification of novel features in *Episode 3* including: a) the confirmation and the extension of the existence of the recently discovered "nested structure" in the late X-ray luminosity in GRB 130427A, as well as the identification of a spiky structure at 10^2 s in the cosmological rest-frame of the source; b) a power law emission of the GeV luminosity light curve and its onset at the end of *Episode 2*; c) different Lorentz Γ factors for the emitting regions of the X-ray and GeV emissions in this *Episode 3*. These results make it possible to test the details of the physical and astrophysical regimes at work in the BdHNe: 1) a newly born neutron star and the supernova ejecta, originating in *Episode 1*, 2) a newly formed black hole originating in *Episode 2*, and 3) the possible interaction among these components, observable in the standard features of *Episode 3*.

38. M. Muccino, R. Ruffini, C.L. Bianco, M. Enderli, M. Kovacevic, L. Izzo, A.V. Penacchioni, G.B. Pisani, J.A. Rueda, Y. Wang; "On binary driven hypernovae and their nested late X-ray emission"; Astronomy Reports, 59, 581 (2015).

    The induced gravitational collapse (IGC) paradigm addresses energetic (10^{52}–10^{54} erg), long gamma-ray bursts (GRBs) associated to supernovae (SNe) and proposes as their progenitors tight binary systems composed of an evolved FeCO core and a companion neutron star (NS). Their emission is characterized by four specific episodes: Episode 1, corresponding to the on-set of the FeCO SN explosion and the accretion of the ejecta onto the companion NS; Episode 2, related the collapse of the companion NS to a black hole (BH) and to the emission of a long GRB; Episode 3, observed in X-rays and characterized by a steep decay, a plateau phase and a late power-law decay; Episode 4, corresponding to the optical SN emission due to the ^{56}Ni decay. We focus on Episode 3 and we show that, from the thermal component observed during the steep decay of the prototype GRB 090618, the emission region has a typical dimension of $\sim 10^{13}$ cm, which is inconsistent with the typical size of the emitting region of GRBs, e.g., $\sim 10^{16}$ cm. We propose, therefore, that the X-ray afterglow emission originates from a spherically symmetric SN ejecta expanding at $\Gamma \sim 2$ or, possibly, from the accretion onto the newly formed black hole, and we name these systems "binary driven hypernovae" (BdHNe). This interpretation is alternative to the traditional afterglow model based on the GRB synchrotron emission from a collimated jet outflow, expanding at ultra-relativistic Lorentz factor of $\Gamma \sim 10^2 - 10^3$ and originating from the collapse of a single object. We show then that the rest-frame energy band 0.3–10 keV X-ray luminosities of three selected BdHNe, GRB 060729, GRB 061121, and GRB 130427A, evidence

a precisely constrained "nested" structure and satisfy precise scaling laws between the average prompt luminosity, $< L_{iso} >$, and the luminosity at the end of the plateau, L_a, as functions of the time at the end of the plateau. All these features extend the applicability of the "cosmic candle" nature of Episode 3. The relevance of r-process in fulfilling the demanding scaling laws and the nested structure are indicated.

39. R. Ruffini, J.A. Rueda, C. Barbarino, C. L. Bianco, H. Dereli, M. Enderli, L. Izzo, M. Muccino, A.V. Penacchioni, G.B. Pisani, Y. Wang; "Induced Gravitational Collapse in the BATSE era: the case of GRB 970828"; Astronomy Reports, 59, 626 (2015).

    Following the recently established "Binary-driven HyperNova" (BdHN) paradigm, we here interpret GRB 970828 in terms of the four episodes typical of such a model. The "Episode 1", up to 40 s after the trigger time t_0, with a time varying thermal emission and a total energy of $E_{iso,1st} = 2.60 \times 10^{53}$ erg, is interpreted as due to the onset of an hyper-critical accretion process onto a companion neutron star, triggered by the companion star, an FeCO core approaching a SN explosion. The "Episode 2", observed up t_0+90 s, is interpreted as a canonical gamma ray burst, with an energy of $E_{tot}^{e^+e^-} = 1.60 \times 10^{53}$ erg, a baryon load of $B = 7 \times 10^{-3}$ and a bulk Lorentz factor at transparency of $\Gamma = 142.5$. From this Episode 2, we infer that the GRB exploded in an environment with a large average particle density $\langle n \rangle \approx 10^3$ particles/cm^3 and dense clouds characterized by typical dimensions of $(4 \div 8) \times 10^{14}$ cm and $\delta n/n \sim 10$. The "Episode 3" is identified from t_0+90 s all the way up to 10^{5-6} s: despite the paucity of the early X-ray data, typical in the BATSE, pre-Swift era, we find extremely significant data points in the late X-ray afterglow emission of GRB 970828, which corresponds to the ones observed in all BdHNe sources. The "Episode 4", related to the Supernova emission, does not appear to be observable in this source, due to the presence of darkening from the large density of the GRB environment, also inferred from the analysis of the Episode 2.

40. Y. Wang, R. Ruffini, M. Kovacevic, C.L. Bianco, M. Enderli, M. Muccino, A.V. Penacchioni, G.B. Pisani, J.A. Rueda; "Predicting supernova associated to gamma-ray burst 130427a"; Astronomy Reports, 59, 667 (2015).

    Binary systems constituted by a neutron star and a massive star are not rare in the universe. The Induced Gravitational Gamma-ray Burst (IGC) paradigm interprets Gamma-ray bursts as the outcome of a neutron star that collapses into a black hole due to the accretion of the ejecta coming from its companion massive star that underwent a supernova event. GRB 130427A is one of the most luminous GRBs ever observed, of which isotropic energy exceeds 10^{54} erg. And it is within one of the few GRBs obtained optical, X-ray and GeV

spectra simultaneously for hundreds of seconds, which provides an unique opportunity so far to understand the multi-wavelength observation within the IGC paradigm, our data analysis found low Lorentz factor blackbody emission in the Episode 3 and its X-ray light curve overlaps typical IGC Golden Sample, which comply to the IGC mechanisms. We consider these findings as clues of GRB 130427A belonging to the IGC GRBs. We predicted on GCN the emergence of a supernova on May 2, 2013, which was later successfully detected on May 13, 2013.

41. R. Ruffini, M. Muccino, M. Kovacevic, F.G. Oliveira, J.A. Rueda, C.L. Bianco, M. Enderli, A.V. Penacchioni, G.B. Pisani, Y. Wang, E. Zaninoni; "GRB 140619B: a short GRB from a binary neutron star merger leading to black hole formation"; The Astrophysical Journal, 808, 190 (2015).

We show the existence of two families of short GRBs, both originating from the merger of binary neutron stars (NSs): family-1 with $E_{iso} < 10^{52}$ erg, leading to a massive NS as the merged core, and family-2 with $E_{iso} > 10^{52}$ erg, leading to a black hole (BH). Following the identification of the prototype GRB 090227B, we present the details of a new example of family-2 short burst: GRB 140619B. From the spectral analysis of the early ~ 0.2 s, we infer an observed temperature $kT = (324 \pm 33)$ keV of the e^+e^--plasma at transparency (P-GRB), a theoretically derived redshift $z = 2.67 \pm 0.37$, a total burst energy $E^{tot}_{e^+e^-} = (6.03 \pm 0.79) \times 10^{52}$ erg, a rest-frame peak energy $E_{p,i} = 4.7$ MeV, and a baryon load $B = (5.52 \pm 0.73) \times 10^{-5}$. We also estimate the corresponding emission of gravitational waves. Two additional examples of family-2 short bursts are identified: GRB 081024B and GRB 090510, remarkable for its well determined cosmological distance. We show that marked differences exist in the nature of the afterglows of these two families of short bursts: family-2 bursts, leading to BH formation, consistently exhibit high energy emission following the P-GRB emission; family-1 bursts, leading to the formation of a massive NS, should never exhibit high energy emission. We also show that both the families fulfill an $E_{p,i}$–E_{iso} relation with slope $\gamma = 0.59 \pm 0.07$ and a normalization constant incompatible with the one for long GRBs. The observed rate of such family-2 events is $\rho_0 = \left(2.1^{+2.8}_{-1.4}\right) \times 10^{-4}\mathrm{Gpc}^{-3}\mathrm{yr}^{-1}$.

42. R. Ruffini, Y. Aimuratov, C.L. Bianco, M. Enderli, M. Kovacevic, R. Moradi, M. Muccino, A.V. Penacchioni, G.B. Pisani, J.A. Rueda, Y. Wang; "Induced gravitational collapse in FeCO Core-Neutron star binaries and Neutron star-Neutron star binary mergers"; International Journal of Modern Physics A, 30, 1545023 (2015).

We review the recent progress in understanding the nature of gamma-ray bursts (GRBs). The occurrence of GRB is explained by the Induced Gravitational Collapse (IGC) in FeCO Core-Neutron star binaries and Neutron star-Neutron star

binary mergers, both processes occur within binary system progenitors. Making use of this most unexpected new paradigm, with the fundamental implications by the neutron star (NS) critical mass, we find that different initial configurations of binary systems lead to different GRB families with specific new physical predictions confirmed by observations.

43. R. Ruffini, M. Muccino, Y. Aimuratov, C.L. Bianco, C. Cherubini, M. Enderli, M. Kovacevic, R. Moradi, A.V. Penacchioni, G.B. Pisani, J.A. Rueda, Y. Wang; "GRB 090510: A genuine short-GRB from a binary neutron star coalescing into a Kerr-Newman black hole"; The Astrophysical Journal, 831, 178 (2016).

    In a new classification of merging binary neutron stars (NSs) we separate short gamma-ray bursts (GRBs) in two sub-classes. The ones with $E_{\rm iso} \lesssim 10^{52}$ erg coalesce to form a massive NS and are indicated as short gamma-ray flashes (S-GRFs). The hardest, with $E_{\rm iso} \gtrsim 10^{52}$ erg, coalesce to form a black hole (BH) and are indicated as genuine short-GRBs (S-GRBs). Within the fireshell model, S-GRBs exhibit three different components: the P-GRB emission, observed at the transparency of a self-accelerating baryon-e^+e^- plasma; the prompt emission, originating from the interaction of the accelerated baryons with the circumburst medium; the high-energy (GeV) emission, observed after the P-GRB and indicating the formation of a BH. GRB 090510 gives the first evidence for the formation of a Kerr BH or, possibly, a Kerr-Newman BH. Its P-GRB spectrum can be fitted by a convolution of thermal spectra whose origin can be traced back to an axially symmetric dyadotorus. A large value of the angular momentum of the newborn BH is consistent with the large energetics of this S-GRB, which reach in the 1–10000 keV range $E_{\rm iso} = (3.95 \pm 0.21) \times 10^{52}$ erg and in the 0.1–100 GeV range $E_{\rm LAT} = (5.78 \pm 0.60) \times 10^{52}$ erg, the most energetic GeV emission ever observed in S-GRBs. The theoretical redshift $z_{\rm th} = 0.75 \pm 0.17$ that we derive from the fireshell theory is consistent with the spectroscopic measurement $z = 0.903 \pm 0.003$, showing the self-consistency of the theoretical approach. All S-GRBs exhibit GeV emission, when inside the *Fermi*-LAT field of view, unlike S-GRFs, which never evidence it. The GeV emission appears to be the discriminant for the formation of a BH in GRBs, confirmed by their observed overall energetics.

44. Ruffini, R.; Rueda, J. A.; Muccino, M.; Aimuratov, Y.; Becerra, L. M.; Bianco, C. L.; Kovacevic, M.; Moradi, R.; Oliveira, F. G.; Pisani, G. B.; Wang, Y.; On the classification of GRBs and their occurrence rates; The Astrophysical Journal, 832, 136 (2016).

    There is mounting evidence for the binary nature of the progenitors of gamma-ray bursts (GRBs). For a long GRB, the induced gravitational collapse (IGC)

paradigm proposes as progenitor, or "in-state", a tight binary system composed of a carbon-oxygen core (CO_{core}) undergoing a supernova (SN) explosion which triggers hypercritical accretion onto a neutron star (NS) companion. For a short GRB, a NS-NS merger is traditionally adopted as the progenitor. We divide long and short GRBs into two sub-classes, depending on whether or not a black hole (BH) is formed in the merger or in the hypercritical accretion process exceeding the NS critical mass. For long bursts, when no BH is formed we have the sub-class of X-ray flashes (XRFs), with isotropic energy $E_{iso} \lesssim 10^{52}$ erg and rest-frame spectral peak energy $E_{p,i} \lesssim 200$ keV. When a BH is formed we have the sub-class of binary-driven hypernovae (BdHNe), with $E_{iso} \gtrsim 10^{52}$ erg and $E_{p,i} \gtrsim 200$ keV. In analogy, short bursts are similarly divided into two sub-classes. When no BH is formed, short gamma-ray flashes (S-GRFs) occur, with $E_{iso} \lesssim 10^{52}$ erg and $E_{p,i} \lesssim 2$ MeV. When a BH is formed, the authentic short GRBs (S-GRBs) occur, with $E_{iso} \gtrsim 10^{52}$ erg and $E_{p,i} \gtrsim 2$ MeV. We give examples and observational signatures of these four sub-classes and their rate of occurrence. From their respective rates it is possible that "in-states" of S-GRFs and S-GRBs originate from the "out-states" of XRFs. We indicate two additional progenitor systems: white dwarf-NS and BH-NS. These systems have hybrid features between long and short bursts. In the case of S-GRBs and BdHNe evidence is given of the coincidence of the onset of the high energy GeV emission with the birth of a Kerr BH.

45. Becerra, L.; Bianco, C. L.; Fryer, C. L.; Rueda, J. A.; Ruffini, R.; On the induced gravitational collapse scenario of gamma-ray bursts associated with supernovae; The Astrophysical Journal, 833, 107 (2016).

    Following the induced gravitational collapse (IGC) paradigm of gamma-ray bursts (GRBs) associated with type Ib/c supernovae, we present numerical simulations of the explosion of a carbon-oxygen (CO) core in a binary system with a neutron-star (NS) companion. The supernova ejecta trigger a *hypercritical* accretion process onto the NS thanks to a copious neutrino emission and the trapping of photons within the accretion flow. We show that temperatures 1–10 MeV develop near the NS surface, hence electron-positron annihilation into neutrinos becomes the main cooling channel leading to accretion rates 10^{-9}–10^{-1} $M_\odot$ s^{-1} and neutrino luminosities 10^{43}–10^{52} erg s^{-1} (the shorter the orbital period the higher the accretion rate). We estimate the maximum orbital period, $P_{\rm max}$, as a function of the NS initial mass, up to which the NS companion can reach by hypercritical accretion the critical mass for gravitational collapse leading to black-hole (BH) formation. We then estimate the effects of the accreting and orbiting NS companion onto a novel geometry of the supernova ejecta density profile. We present the results of a 1.4×10^7 particle simulation which show that the NS induces accentuated asymmetries in the ejecta density around the orbital plane. We elaborate on the observables associated with the

above features of the IGC process. We apply this framework to specific GRBs: we find that X-ray flashes (XRFs) and binary-driven hypernovae (BdHNe) are produced in binaries with $P > P_{\rm max}$ and $P < P_{\rm max}$, respectively. We analyze in detail the case of XRF 060218.

46. Pisani, G. B.; Ruffini, R.; Aimuratov, Y.; Bianco, C. L.; Kovacevic, M.; Moradi, R.; Muccino, M.; Penacchioni, A. V.; Rueda, J. A.; Shakeri, S.; Wang, Y.; On the universal late X-ray emission of binary-driven hypernovae and its possible collimation; The Astrophysical Journal, 833, 159 (2016).

    It has been previously discovered a universal power-law behaviour of the late X-ray emission (LXRE) of a "golden sample" (GS) of six long energetic GRBs, when observed in the rest-frame of the source. This remarkable feature, independent on the different isotropic energy (E_{iso}) of each GRB, has been used to estimate the cosmological redshift of some long GRBs. This analysis is here extended to a new class of 161 long GRBs, all with $E_{iso} > 10^{52}$ erg. These GRBs are indicated as binary-driven hypernovae (BdHNe) in view of their progenitors: a tight binary systems composed of a carbon-oxigen core ($CO_{\rm core}$) and a neutron star (NS) undergoing an induced gravitational collapse (IGC) to a black hole (BH) triggered by the $CO_{\rm core}$ explosion as a supernova (SN). We confirm the universal behaviour of the LXRE for the "enlarged sample" (ES) of 161 BdHNe observed up to the end of 2015, assuming a double-cone emitting region. We obtain a distribution of half-opening angles peaking at $\theta = 17.62^\circ$, with mean value 30.05°, and a standard deviation 19.65°. This, in turn, leads to the possible establishment of a new cosmological candle. Within the IGC model, such universal LXRE behaviour is only indirectly related to the GRB and originates from the SN ejecta, of a standard constant mass, being shocked by the GRB emission. The fulfillment of the universal relation in the LXRE and its independence of the prompt emission, further confirmed in this article, establishes a crucial test for any viable GRB model.

5.2 Conference proceedings

1. R. Ruffini, M.G. Bernardini, C.L. Bianco, P. Chardonnet, F. Fraschetti, V. Gurzadyan, L. Vitagliano, S.-S. Xue; "The Blackholic energy: long and short Gamma-Ray Bursts (New perspectives in physics and astrophysics from the theoretical understanding of Gamma-Ray Bursts, II)"; in Proceedings of the XIth Brazilian School on Cosmology and Gravitation, Mangaratiba, Rio de Janeiro (Brazil), July August 2004, M. Novello, S.E. Perez Bergliaffa, Editors; AIP Conference Proceedings, 782, 42 (2005).

We outline the confluence of three novel theoretical fields in our modeling of Gamma-Ray Bursts (GRBs): 1) the ultrarelativistic regime of a shock front expanding with a Lorentz gamma factor ~ 300; 2) the quantum vacuum polarization process leading to an electron-positron plasma originating the shock front; and 3) the general relativistic process of energy extraction from a black hole originating the vacuum polarization process. There are two different classes of GRBs: the long GRBs and the short GRBs. We here address the issue of the long GRBs. The theoretical understanding of the long GRBs has led to the detailed description of their luminosities in fixed energy bands, of their spectral features and made also possible to probe the astrophysical scenario in which they originate. We are specially interested, in this report, to a subclass of long GRBs which appear to be accompanied by a supernova explosion. We are considering two specific examples: GRB980425/SN1998bw and GRB030329/SN2003dh. While these supernovae appear to have a standard energetics of 10^{49} ergs, the GRBs are highly variable and can have energetics 10^4 – 10^5 times larger than the ones of the supernovae. Moreover, many long GRBs occurs without the presence of a supernova. It is concluded that in no way a GRB can originate from a supernova. The precise theoretical understanding of the GRB luminosity we present evidence, in both these systems, the existence of an independent component in the X-ray emission, usually interpreted in the current literature as part of the GRB afterglow. This component has been observed by Chandra and XMM to have a strong decay on scale of months. We have named here these two sources respectively URCA-1 and URCA-2, in honor of the work that George Gamow and Mario Shoenberg did in 1939 in this town of Urca identifying the basic mechanism, the Urca processes, leading to the process of gravitational collapse and the formation of a neutron star and a supernova. The further hypothesis is considered to relate this X-ray source to a neutron star, newly born in the Supernova. This hypothesis should be submitted to further theoretical and observational investigation. Some theoretical developments to clarify the astrophysical origin of this new scenario are outlined. We turn then to the theoretical developments in the short GRBs: we first report some progress in the understanding the dynamical phase of collapse, the mass-energy formula and the extraction of blackholic energy which have been motivated by the analysis of the short GRBs. In this context progress has also been accomplished on establishing an absolute lower limit to the irreducible mass of the black hole as well as on some critical considerations about the relations of general relativity and the second law of thermodynamics. We recall how this last issue has been one of the most debated in theoretical physics in the past thirty years due to the work of Bekenstein and Hawking. Following these conceptual progresses we analyze the vacuum polarization process around an overcritical collapsing shell. We evidence the existence of a separatrix and a dyadosphere trapping surface in

the dynamics of the electron-positron plasma generated during the process of gravitational collapse. We then analyze, using recent progress in the solution of the Vlasov-Boltzmann-Maxwell system, the oscillation regime in the created electron-positron plasma and their rapid convergence to a thermalized spectrum. We conclude by making precise predictions for the spectra, the energy fluxes and characteristic time-scales of the radiation for short-bursts. If the precise luminosity variation and spectral hardening of the radiation we have predicted will be confirmed by observations of short-bursts, these systems will play a major role as standard candles in cosmology. These considerations will also be relevant for the analysis of the long-bursts when the baryonic matter contribution will be taken into account.

2. R. Ruffini, M.G. Bernardini, C.L. Bianco, P. Chardonnet, F. Fraschetti, V. Gurzadyan, L. Vitagliano, S.-S. Xue; "Black hole physics and astrophysics: The GRB-Supernova connection and URCA-1 URCA-2"; in Proceedings of the Tenth Marcel Grossmann Meeting on General Relativity, Rio de Janeiro, Brazil, July 2003, M. Novello, S.E. Perez-Bergliaffa, Editors; p. 369; World Scientific, (Singapore, 2006).

   We outline the confluence of three novel theoretical fields in our modeling of Gamma-Ray Bursts (GRBs): 1) the ultrarelativistic regime of a shock front expanding with a Lorentz gamma factor $\sim$ 300; 2) the quantum vacuum polarization process leading to an electron-positron plasma originating the shock front; and 3) the general relativistic process of energy extraction from a black hole originating the vacuum polarization process. There are two different classes of GRBs: the long GRBs and the short GRBs. We here address the issue of the long GRBs. The theoretical understanding of the long GRBs has led to the detailed description of their luminosities in fixed energy bands, of their spectral features and made also possible to probe the astrophysical scenario in which they originate. We are specially interested, in this report, to a subclass of long GRBs which appear to be accompanied by a supernova explosion. We are considering two specific examples: GRB980425/SN1998bw and GRB030329/SN2003dh. While these supernovae appear to have a standard energetics of 10^{49} ergs, the GRBs are highly variable and can have energetics 10^4 – 10^5 times larger than the ones of the supernovae. Moreover, many long GRBs occurs without the presence of a supernova. It is concluded that in no way a GRB can originate from a supernova. The precise theoretical understanding of the GRB luminosity we present evidence, in both these systems, the existence of an independent component in the X-ray emission, usually interpreted in the current literature as part of the GRB afterglow. This component has been observed by Chandra and XMM to have a strong decay on scale of months. We have named here these two sources respectively URCA-1 and URCA-2, in honor of the work that George Gamow and Mario Shoenberg did in 1939 in

this town of Urca identifying the basic mechanism, the Urca processes, leading to the process of gravitational collapse and the formation of a neutron star and a supernova. The further hypothesis is considered to relate this X-ray source to a neutron star, newly born in the Supernova. This hypothesis should be submitted to further theoretical and observational investigation. Some theoretical developments to clarify the astrophysical origin of this new scenario are outlined.

3. M.G. Bernardini, C.L. Bianco, P. Chardonnet, F. Fraschetti, R. Ruffini, S.-S. Xue; "General features of GRB 030329 in the EMBH model"; in Proceedings of the Tenth Marcel Grossmann Meeting on General Relativity, Rio de Janeiro, Brazil, July 2003, M. Novello, S.E. Perez-Bergliaffa, Editors; p. 2459; World Scientific, (Singapore, 2006).

   GRB 030329 is considered within the EMBH model. We determine the three free parameters and deduce its luminosity in given energy bands comparing it with the observations. The observed substructures are compared with the predictions of the model: by applying the result that substructures observed in the extended afterglow peak emission (E-APE) do indeed originate in the collision of the accelerated baryonic matter (ABM) pulse with the inhomogeneities in the interstellar medium around the black-hole, masks of density inhomogeneities are considered in order to reproduce the observed temporal substructures. The induced supernova concept is applied to this system and the general consequences that we are witnessing are the formation of a cosmological thriptych of a black hole originating the GRB 030329, the supernova SN2003dh and a young neutron star. Analogies to the system GRB 980425–SN1998bw are outlined.

4. R. Ruffini, M.G. Bernardini, C.L. Bianco, P. Chardonnet, A. Corsi, F. Fraschetti, S.-S. Xue; "GRB 970228 and its associated Supernova in the EMBH model"; in Proceedings of the Tenth Marcel Grossmann Meeting on General Relativity, Rio de Janeiro, Brazil, July 2003, M. Novello, S.E. Perez-Bergliaffa, Editors; p. 2465; World Scientific, (Singapore, 2006).

   The γ-ray burst of 1997 February 28 is analyzed within the Electromagnetic Black Hole model. We first estimate the value of the total energy deposited in the dyadosphere, E_{dya}, and the amount of baryonic matter left over by the EMBH progenitor star, $B = M_B c^2 / E_{dya}$. We then consider the role of the interstellar medium number density n_{ISM} and of the ratio R between the effective emitting area and the total surface area of the γ-ray burst source, in reproducing the prompt emission and the X-ray afterglow of this burst. Some considerations are also done concerning the possibility of explaining, within the theory, the observed evidence for a supernova in the optical afterglow.

5. F. Fraschetti, M.G. Bernardini, C.L. Bianco, P. Chardonnet, R. Ruffini, S.-S. Xue; "Inferences on the ISM structure around GRB980425 and GRB980425-SN1998bw association in the EMBH Model"; in Proceedings of the Tenth Marcel Grossmann Meeting on General Relativity, Rio de Janeiro, Brazil, July 2003, M. Novello, S.E. Perez-Bergliaffa, Editors; p. 2451; World Scientific, (Singapore, 2006).

   We determine the four free parameters within the EMBH model for GRB 980425 and deduce its luminosity in given energy bands, its spectra and its time variability in the prompt radiation. We compute the basic kinematical parameters of GRB 980425. In the extended afterglow peak emission the Lorentz γ factor is lower than the critical value 150 which has been found in Ruffini et al. (2002) to be necessary in order to perform the tomography of the ISM surrounding the GRB as suggested by Dermer & Mitman (1999). The detailed structure of the density inhomogeneities as well as the effects of radial apparent superluminal effects are evaluated within the EMBH model. Under the assumption that the energy distribution of emitted radiation is thermal in the comoving frame, time integrated spectra of EMBH model for prompt emission are computed. The induced supernova concept is applied to this system and general consequences on the astrophysical and cosmological scenario are derived.

6. R. Ruffini, M.G. Bernardini, C.L. Bianco, P. Chardonnet, F. Fraschetti, R. Guida, S.-S. Xue; "GRB 050315: A step in the proof of the uniqueness of the overall GRB structure"; in "GAMMA-RAY BURSTS IN THE SWIFT ERA: Sixteenth Maryland Astrophysics Conference", Washington, DC, USA, November 29th December 2nd 2005, Stephen S. Holt, Neil Gehrels, John A. Nousek, Editors; AIP Conference Proceedings, 836, 103 (2006).

   Using the Swift data of GRB 050315, we progress in proving the uniqueness of our theoretically predicted Gamma-Ray Burst (GRB) structure as composed by a proper-GRB, emitted at the transparency of an electron-positron plasma with suitable baryon loading, and an afterglow comprising the "prompt radiation" as due to external shocks. Detailed light curves for selected energy bands are theoretically fitted in the entire temporal region of the Swift observations ranging over 10^6 seconds.

7. R. Ruffini, M.G. Bernardini, C.L. Bianco, P. Chardonnet, F. Fraschetti, S.-S. Xue; "Theoretical Interpretation of GRB 031203 and URCA-3"; in "Relativistic Astrophysics and Cosmology - Einsteins Legacy", B. Aschenbach, V. Burwitz, G. Hasinger, B. Leibundgut, Editors; Springer-Verlag (2007).

8. R. Ruffini, M.G. Bernardini, C.L. Bianco, L. Caito, P. Chardonnet, M.G.

Dainotti, F. Fraschetti, R. Guida, M. Rotondo, G. Vereshchagin, L. Vita-gliano, S.-S. Xue; "The Blackholic energy and the canonical Gamma-Ray Burst"; in Proceedings of the XIIth Brazilian School on Cosmology and Gravitation, Mangaratiba, Rio de Janeiro (Brazil), September 2006, M. Novello, S.E. Perez Bergliaffa, Editors; AIP Conference Proceedings, 910, 55 (2007).

Gamma-Ray Bursts (GRBs) represent very likely "the" most extensive computational, theoretical and observational effort ever carried out successfully in physics and astrophysics. The extensive campaign of observation from space based X-ray and γ-ray observatory, such as the *Vela*, CGRO, BeppoSAX, HETE-II, INTEGRAL, *Swift*, R-XTE, *Chandra*, XMM satellites, have been matched by complementary observations in the radio wavelength (e.g. by the VLA) and in the optical band (e.g. by VLT, Keck, ROSAT). The net result is unprecedented accuracy in the received data allowing the determination of the energetics, the time variability and the spectral properties of these GRB sources. The very fortunate situation occurs that these data can be confronted with a mature theoretical development. Theoretical interpretation of the above data allows progress in three different frontiers of knowledge: **a)** the ultrarelativistic regimes of a macroscopic source moving at Lorentz gamma factors up to ~ 400; **b)** the occurrence of vacuum polarization process verifying some of the yet untested regimes of ultrarelativistic quantum field theories; and **c)** the first evidence for extracting, during the process of gravitational collapse leading to the formation of a black hole, amounts of energies up to 10^{55} ergs of blackholic energy — a new form of energy in physics and astrophysics. We outline how this progress leads to the confirmation of three interpretation paradigms for GRBs proposed in July 2001. Thanks mainly to the observations by *Swift* and the optical observations by VLT, the outcome of this analysis points to the existence of a "canonical" GRB, originating from a variety of different initial astrophysical scenarios. The communality of these GRBs appears to be that they all are emitted in the process of formation of a black hole with a negligible value of its angular momentum. The following sequence of events appears to be canonical: the vacuum polarization process in the dyadosphere with the creation of the optically thick self accelerating electron-positron plasma; the engulfment of baryonic mass during the plasma expansion; adiabatic expansion of the optically thick "fireshell" of electron-positron-baryon plasma up to the transparency; the interaction of the accelerated baryonic matter with the interstellar medium (ISM). This leads to the canonical GRB composed of a proper GRB (P-GRB), emitted at the moment of transparency, followed by an extended afterglow. The sole parameters in this scenario are the total energy of the dyadosphere E_{dya}, the fireshell baryon loading M_B defined by the dimensionless parameter $B \equiv M_B c^2 / E_{dya}$, and the ISM filamentary distribution

around the source. In the limit $B \to 0$ the total energy is radiated in the P-GRB with a vanishing contribution in the afterglow. In this limit, the canonical GRBs explain as well the short GRBs. In these lecture notes we systematically outline the main results of our model comparing and contrasting them with the ones in the current literature. In both cases, we have limited ourselves to review already published results in refereed publications. We emphasize as well the role of GRBs in testing yet unexplored grounds in the foundations of general relativity and relativistic field theories.

9. R. Ruffini, M.G. Bernardini, C.L. Bianco, L. Caito, P. Chardonnet, M.G. Dainotti, F. Fraschetti, R. Guida, G. Vereshchagin, S.-S. Xue; "The role of GRB 031203 in clarifying the astrophysical GRB scenario"; in Proceedings of the 6^{th} Integral Workshop - The Obscured Universe, Moscow, (Russia), July 2006, S. Grebenev, R. Sunyaev, C. Winkler, A. Parmar, L. Ouwehand, Editors; ESA Special Publication, SP-622, 561 (2007).

   The luminosity and the spectral distribution of the afterglow of GRB 031203 have been presented within our theoretical framework, which envisages the GRB structure as composed by a proper-GRB, emitted at the transparency of an electron-positron plasma with suitable baryon loading, and an afterglow comprising the "prompt emission" as due to external shocks. In addition to the GRB emission, there appears to be a prolonged soft X-Ray emission lasting for 10^6–10^7 seconds followed by an exponential decay. This additional source has been called by us URCA-3. It is urgent to establish if this component is related to the GRB or to the Supernova (SN). In this second case, there are two possibilities: either the interaction of the SN ejecta with the interstellar medium or, possibly, the cooling of a young neutron star formed in the SN 2003lw process. The analogies and the differences between this triptych GRB 031203 / SN 2003lw / URCA-3 and the corresponding ones GRB 980425 / SN 1998bw / URCA-1 and GRB 030329 / SN 2003dh / URCA-2, as well as GRB 060218 / SN 2006aj are discussed.

10. M.G. Bernardini, C.L. Bianco, L. Caito, M.G. Dainotti, R. Guida, R. Ruffini; "GRB970228 and the class of GRBs with an initial spikelike emission: do they follow the Amati relation?"; in Relativistic Astrophysics Proceedings of the 4^{th} Italian-Sino Workshop, Pescara (Italy), July 2007, C.L. Bianco, S.-S. Xue, Editors; AIP Conference Proceedings, 966, 7 (2008).

    On the basis of the recent understanding of GRB050315 and GRB060218, we return to GRB970228, the first Gamma-Ray Burst (GRB) with detected afterglow. We proposed it as the prototype for a new class of GRBs with "an occasional softer extended emission lasting tenths of seconds after an initial spikelike emission". Detailed theoretical computation of the GRB970228 light curves in selected energy bands for the prompt emission are presented and

compared with observational *Beppo*SAX data. From our analysis we conclude that GRB970228 and likely the ones of the above mentioned new class of GRBs are "canonical GRBs" have only one peculiarity: they exploded in a galactic environment, possibly the halo, with a very low value of CBM density. Here we investigate how GRB970228 unveils another peculiarity of this class of GRBs: they do not fulfill the "Amati relation". We provide a theoretical explanation within the fireshell model for the apparent absence of such correlation for the GRBs belonging to this new class.

11. C.L. Bianco, M.G. Bernardini, L. Caito, M.G. Dainotti, R. Guida, R. Ruffini; "The "Fireshell" Model and the "Canonical" GRB Scenario; in Relativistic Astrophysics Proceedings of the 4^{th} Italian-Sino Workshop, Pescara (Italy), July 2007, C.L. Bianco, S.-S. Xue, Editors; AIP Conference Proceedings, 966, 12 (2008).

    In the "fireshell" model we define a "canonical GRB" light curve with two sharply different components: the Proper-GRB (P-GRB), emitted when the optically thick fireshell of electron-positron plasma originating the phenomenon reaches transparency, and the afterglow, emitted due to the collision between the remaining optically thin fireshell and the CircumBurst Medium (CBM). We outline our "canonical GRB" scenario, originating from the gravitational collapse to a black hole, with a special emphasis on the discrimination between "genuine" and "fake" short GRBs.

12. L. Caito, M.G. Bernardini, C.L. Bianco, M.G. Dainotti, R. Guida, R. Ruffini; "GRB 060614: A Progress Report"; in Relativistic Astrophysics Proceedings of the 4^{th} Italian-Sino Workshop, Pescara (Italy), July 2007, C.L. Bianco, S.-S. Xue, Editors; AIP Conference Proceedings, 966, 16 (2008).

    The explosion of GRB 060614, detected by the Swift satellite, produced a deep break in the GRB scenario opening new horizons of investigation, because it can't be traced back to any traditional scheme of classification. In fact, it manifests peculiarities both of long bursts and of short bursts. Above all, it is the first case of long duration near GRB without any bright Ib/c associated Supernova. We will show that, in our canonical GRB scenario, this "anomalous" situation finds a natural interpretation and allows us to discuss a possible variation to the traditional classification scheme, introducing the distinction between "genuine" and "fake" short bursts.

13. M.G. Dainotti, M.G. Bernardini, C.L. Bianco, L. Caito, R. Guida, R. Ruffini; "GRB 060218 and the Binaries as Progenitors of GRB-SN Systems"; in Relativistic Astrophysics Proceedings of the 4^{th} Italian-Sino Workshop, Pescara (Italy), July 2007, C.L. Bianco, S.-S. Xue, Editors; AIP Conference Proceedings, 966, 25 (2008).

We study the Gamma-Ray Burst (GRB) 060218: a particularly close source at $z = 0.033$ with an extremely long duration, namely $T_{90} \sim 2000$ s, related to SN 2006aj. This source appears to be a very soft burst, with a peak in the spectrum at 4.9 keV, therefore interpreted as an X-Ray Flash (XRF). It fullfills the Amati relation. I present the fitting procedure, which is time consuming. In order to show its sensitivity I also present two examples of fits with the same value of B and different value of $E^{tot}_{e^\pm}$. We fit the X- and γ-ray observations by *Swift* of GRB 060218 in the 0.1–150 keV energy band during the entire time of observations from 0 all the way to 10^6 s within a unified theoretical model. The free parameters of our theory are only three, namely the total energy $E^{tot}_{e^\pm}$ of the $e^\pm$ plasma, its baryon loading $B \equiv M_B c^2 / E^{tot}_{e^\pm}$, as well as the CircumBurst Medium (CBM) distribution. We justify the extremely long duration of this GRB by a total energy $E^{tot}_{e^\pm} = 2.32 \times 10^{50}$ erg, a very high value of the baryon loading $B = 1.0 \times 10^{-2}$ and the effective CircumBurst Medium (CBM) density which shows a radial dependence $n_{cbm} \propto r^{-\alpha}$ with $1.0 \leq \alpha \leq 1.7$ and monotonically decreases from 1 to 10^{-6} particles/cm^3. We recall that this value of the B parameter is the highest among the sources we have analyzed and it is very close to its absolute upper limit expected. By our fit we show that there is no basic differences between XRFs and more general GRBs. They all originate from the collapse process to a black hole and their difference is due to the variability of the three basic parameters within the range of full applicability of the theory. We also think that the smallest possible black hole, formed by the gravitational collapse of a neutron star in a binary system, is consistent with the especially low energetics of the class of GRBs associated with SNe Ib/c.

14. R. Guida, M.G. Bernardini, C.L. Bianco, L. Caito, M.G. Dainotti, R. Ruffini; "The Amati Relation within the Fireshell Model"; in Relativistic Astrophysics Proceedings of the 4^{th} Italian-Sino Workshop, Pescara (Italy), July 2007, C.L. Bianco, S.-S. Xue, Editors; AIP Conference Proceedings, 966, 46 (2008).

    In this work we show the existence of a spectral-energy correlation within our "fireshell" model for GRBs. The free parameters of the model are the total energy $E^{e\pm}_{tot}$ of the $e^\pm$ plasma and its baryon loading $B \equiv M_B\, c^2 / E^{e\pm}_{tot}$, characterizing the source, and the parameters describing the effective CircumBurst medium (CBM) distribution, namely its particle number density ρ and its effective emitting area R. We build a sample of pseudo-GRBs, i.e. a set of theoretically simulated light curves, varying the total energy of the electron-positron plasma $E^{e\pm}_{tot}$ and keeping the same baryon loading; the parametrization used to describe the distribution of the CircumBurst medium is the same as well for all the pseudo-GRBs. The values of these parameters (B, ρ and R) used in this work are equal to the ones assumed to fit GRB050315, a *Swift* burst representing a good example of what in the literature has been addressed as "canoni-

cal light curve". For each GRB of the sample we calculate the νF_ν spectrum integrating the theoretically computed light curve over the total time, namely from our T_0, the end of the Proper-GRB (P-GRB), up to the end of our afterglow phase, when the fireshell Lorentz gamma factor is close to unity; we exclude the P-GRB from this spectral computation because, following our "canonical" GRB scenario, this component of the GRB emission is physically different from the other component, that is our afterglow component, so one should take care in no mixing them. We find that the maximum of this spectrum, that is the observed peak energy $E_{p,tot}$, correlates with the initial electron-positron plasma energy $E_{tot}^{e\pm}$ in a way very similar to the Amati one: $E_{p,tot} \propto (E_{tot}^{e\pm})^{0.5}$.

15. R. Guida, M.G. Bernardini, C.L. Bianco, L. Caito, M.G. Dainotti, R. Ruffini; "Theoretical interpretation of the Amati relation within the fireshell model"; in GAMMA-RAY BURSTS 2007: Proceedings of the Santa Fe Conference, Santa Fe (NM, USA), November 2007, M. Galassi, D. Palmer, E. Fenimore, Editors; AIP Conference Proceedings, 1000, 60 (2008).

    We discuss within our theoretical "fireshell" model for Gamma-Ray Bursts (GRBs) the theoretical interpretation of the phenomenological correlation between the isotropic-equivalent radiated energy of the prompt emission E_{iso} and the cosmological rest-frame νF_ν spectrum peak energy E_p observed by Amati and collaborators. Possible reasons for some of the outliers of this relation are given.

16. L. Caito, M.G. Bernardini, C.L. Bianco, M.G. Dainotti, R. Guida, R. Ruffini; "GRB 060614: a Fake Short Gamma-Ray Burst"; in GAMMA-RAY BURSTS 2007: Proceedings of the Santa Fe Conference, Santa Fe (NM, USA), November 2007, M. Galassi, D. Palmer, E. Fenimore, Editors; AIP Conference Proceedings, 1000, 301 (2008).

    The explosion of GRB 060614 produced a deep break in the GRB scenario and opened new horizons of investigation because it can't be traced back to any traditional scheme of classification. In fact, it manifests peculiarities both of long bursts and of short bursts and, above all, it is the first case of long duration near GRB without any bright Ib/c associated Supernova. We will show that, in our canonical GRB scenario, this "anomalous" situation finds a natural interpretation and allows us to discuss a possible variation to the traditional classification scheme, introducing the distinction between "genuine" and "fake" short bursts.

17. C.L. Bianco, M.G. Bernardini, L. Caito, M.G. Dainotti, R. Guida, R. Ruffini; "Short and canonical GRBs"; in GAMMA-RAY BURSTS 2007: Proceedings of the Santa Fe Conference, Santa Fe (NM, USA), November 2007,

M. Galassi, D. Palmer, E. Fenimore, Editors; AIP Conference Proceedings, 1000, 305 (2008).

Within the "fireshell" model for the Gamma-Ray Bursts (GRBs) we define a "canonical GRB" light curve with two sharply different components: the Proper-GRB (P-GRB), emitted when the optically thick fireshell of electron-positron plasma originating the phenomenon reaches transparency, and the afterglow, emitted due to the collision between the remaining optically thin fireshell and the CircumBurst Medium (CBM). We outline our "canonical GRB" scenario, with a special emphasis on the discrimination between "genuine" and "fake" short GRBs.

18. C.L. Bianco, M.G. Bernardini, L. Caito, M.G. Dainotti, R. Guida, R. Ruffini, G. Vereshchagin, S.-S. Xue; "The Equations of motion of the "fireshell""; in OBSERVATIONAL EVIDENCE FOR BLACK HOLES IN THE UNIVERSE: Proceedings of the 2^{nd} Kolkata Conference, Kolkata (India), February 2008, S.K. Chakrabarti, A.S. Majumdar, Editors; AIP Conference Proceedings, 1053, 259 (2008).

    The Fireshell originating a Gamma-Ray Burst (GRB) encompasses an optically thick regime followed by an optically thin one. In the first one the fireshell self-accelerates from a Lorentz gamma factor equal to 1 all the way to 200-300. The physics of this system is based on the continuous annihilation of electron-positron pairs in an optically thick e^+e^- plasma with a small baryon loading. In the following regime, the optically thin fireshell, composed by the baryons left over after the transparency point, ballistically expands into the Circum-Burst Medium (CBM). The dynamics of the fireshell during both regimes will be analyzed. In particular we will re-examine the validity of the constant-index power-law relation between the fireshell Lorentz gamma factor and its radial coordinate, usually adopted in the current literature on the grounds of an "ultrarelativistic" approximation. Such expressions are found to be mathematically correct but only approximately valid in a very limited range of the physical and astrophysical parameters and in an asymptotic regime which is reached only for a very short time, if any.

19. M.G. Bernardini, C.L. Bianco, L. Caito, M.G. Dainotti, R. Guida, R. Ruffini; "The "Canonical" GRBs within the fireshell model"; in OBSERVATIONAL EVIDENCE FOR BLACK HOLES IN THE UNIVERSE: Proceedings of the 2^{nd} Kolkata Conference, Kolkata (India), February 2008, S.K. Chakrabarti, A.S. Majumdar, Editors; AIP Conference Proceedings, 1053, 267 (2008).

    Within the fireshell model we define a "canonical" GRB light curve with two sharply different components: the Proper-GRB (P-GRB), emitted when the optically thick fireshell of electron-positron plasma originating the phenomenon

reaches transparency, and the afterglow, emitted due to the collision between the remaining optically thin fireshell and the CircumBurst Medium (CBM). On the basis of the recent understanding of GRB970228 as the prototype for a new class of GRBs with "an occasional softer extended emission lasting tenths of seconds after an initial spikelike emission" we outline our "canonical" GRB scenario, originating from the gravitational collapse to a black hole, with a special emphasis on the discrimination between short GRBs and the ones appearing as such due to their peculiar astrophysical setting.

20. M.G. Dainotti, M.G. Bernardini, C.L. Bianco, L. Caito, R. Guida, R. Ruffini; "GRB 060218: the density mask and its peculiarity compared to the other sources"; in OBSERVATIONAL EVIDENCE FOR BLACK HOLES IN THE UNIVERSE: Proceedings of the 2^{nd} Kolkata Conference, Kolkata (India), February 2008, S.K. Chakrabarti, A.S. Majumdar, Editors; AIP Conference Proceedings, 1053, 283 (2008).

    The Swift satellite has given continuous data in the range 0.3150 keV from 0 s to 106 s for GRB060218 associated with SN2006aj. It has an unusually long duration ($T_{90} \sim 2100$ s). We plan to fit the complete γ- and X-ray light curves of this long duration GRB, including the prompt emission and we give peculiar attention to the afterglow lightcurve in order to better constrain the density mask. We apply our "fireshell" model based on the formation of a black hole, giving the relevant references. The initial total energy of the electron-positron plasma $E^{tot}_{e^{\pm}} == 2.32 \times 10^{50}$ erg has a particularly low value similarly to the other GRBs associated with SNe. For the first time we observe a baryon loading $B = 10^{-2}$ which coincides with the upper limit for the dynamical stability of the fireshell. The effective CircumBurst Medium (CBM) density shows a radial dependence $n_{cbm} \propto r^{-a}$ with $1.0 \leq a \leq 1.7$ and monotonically decreases from 1 to 10^{-6} particles/cm^3. Such a behavior is interpreted as due to a fragmentation in the fireshell. Such a fragmentation is crucial in explaining both the unusually large T_{90} and the consequently inferred abnormal low value of the CBM effective density. We present the comparison between the density mask of this source and the ones of a normal GRB 050315 and a fake short, GRB 970228, making some assumptions on the CBM behaviour in the surrounding of the Black hole.

21. L. Caito, M.G. Bernardini, C.L. Bianco, M.G. Dainotti, R. Guida, R. Ruffini; "GRB 060614 in the canonical fireshell model"; in OBSERVATIONAL EVIDENCE FOR BLACK HOLES IN THE UNIVERSE: Proceedings of the 2^{nd} Kolkata Conference, Kolkata (India), February 2008, S.K. Chakrabarti, A.S. Majumdar, Editors; AIP Conference Proceedings, 1053, 291 (2008).

    Gamma-Ray Burst (GRB) 060614 is the first nearby long duration GRB clearly not associated to any bright Ib/c Supernova. The explosion of this burst un-

dermines one of the fundamental assumptions of the standard scenario and opens new horizons and hints of investigation. GRB 060614, hardly classifiable as a short GRB, is not either a "typical" long GRB since it occurs in a low star forming region. Moreover, it presents deep similarities with GRB 970228, which is the prototype of the "fake" short bursts, or better canonical GRBs disguised as short ones. Within the "fireshell" model, we test if this "anomalous" source can be a disguised short GRB.

22. L.J. Rangel Lemos, S. Casanova, R. Ruffini, S.S. Xue; "Fermis approach to the study of pp interactions"; in OBSERVATIONAL EVIDENCE FOR BLACK HOLES IN THE UNIVERSE: Proceedings of the 2^{nd} Kolkata Conference, Kolkata (India), February 2008, S.K. Chakrabarti, A.S. Majumdar, Editors; AIP Conference Proceedings, 1053, 275 (2008).

    The physics of hadronic interactions found much difficulties for explain the experimental data. In this work we study the approach of Fermi (1950) about the multiplicity of pions emitted in pp interactions and in follow we compare with the modern approach

23. R. Ruffini, A.G. Aksenov, M.G. Bernardini, C.L. Bianco, L. Caito, M.G. Dainotti, G. De Barros, R. Guida, G.V. Vereshchagin, S.-S. Xue; "The canonical Gamma-Ray Bursts and their 'precursors"'; in 2008 NANJING GAMMA-RAY BURST CONFERENCE, Proceedings of the 2008 Nanjing Gamma-Ray Burst Conference, Nanjing (China), June 2008, Y.-F. Huang, Z.-G. Dai, B. Zhang, Editors; AIP Conference Proceedings, 1065, 219 (2008).

    The fireshell model for Gamma-Ray Bursts (GRBs) naturally leads to a canonical GRB composed of a proper-GRB (P-GRB) and an afterglow. P-GRBs, introduced by us in 2001, are sometimes considered "precursors" of the main GRB event in the current literature. We show in this paper how the fireshell model leads to the understanding of the structure of GRBs, with precise estimates of the time sequence and intensities of the P-GRB and the of the afterglow. It leads as well to a natural classification of the canonical GRBs which overcomes the traditional one in short and long GRBs.

24. M.G. Bernardini, C.L. Bianco, L. Caito, M.G. Dainotti, R. Guida, R. Ruffini; "Preliminary analysis of GRB060607A within the fireshell model"; in 2008 NANJING GAMMA-RAY BURST CONFERENCE; Proceedings of the 2008 Nanjing Gamma-Ray Burst Conference, Nanjing (China), June 2008, Y.-F. Huang, Z.-G. Dai, B. Zhang, Editors; AIP Conference Proceedings, 1065, 227 (2008).

    GRB060607A is a very distant ($z = 3.082$) and energetic event ($E_{iso} \sim 10^{53}$ erg). Its main peculiarity is that the peak of the near-infrared afterglow has

been observed with the REM robotic telescope, allowing to infer the initial Lorentz gamma factor of the emitting system. We present a preliminary analysis of the spectra and light curves of GRB060607A prompt emission within the fireshell model. We show that the N(E) spectrum of the prompt emission, whose behavior is usually described as "simple power-law", can also be fitted in a satisfactory way by a convolution of thermal spectra as predicted by the model we applied. The theoretical time-integrated spectrum of the prompt emission as well as the light curves in the BAT and XRT energy band are in good agreement with the observations, enforcing the plausibility of our approach. Furthermore, the initial value of Lorentz gamma factor we predict is compatible with the one deduced from the REM observations.

25. C.L. Bianco, M.G. Bernardini, L. Caito, M.G. Dainotti, R. Guida, R. Ruffini; "The "fireshell" model and the "canonical GRB" scenario"; in 2008 NANJING GAMMA-RAY BURST CONFERENCE; Proceedings of the 2008 Nanjing Gamma-Ray Burst Conference, Nanjing (China), June 2008, Y.-F. Huang, Z.-G. Dai, B. Zhang, Editors; AIP Conference Proceedings, 1065, 223 (2008).

    The Swift observation of GRB 060614, as well as the catalog analysis by Norris & Bonnell (2006), opened the door "on a new Gamma-Ray Bursts (GRBs) classification scheme that straddles both long and short bursts" (Gehrels et al. 2006). Within the "fireshell" model for the Gamma-Ray Bursts (GRBs) we define a "canonical GRB" light curve with two sharply different components: the Proper-GRB (P-GRB), emitted when the optically thick fireshell of electron-positron plasma originating the phenomenon reaches transparency, and the afterglow, emitted due to the collision between the remaining optically thin fireshell and the CircumBurst Medium (CBM). We here outline our "canonical GRB" scenario, which implies three different GRB classes: the "genuine" short GRBs, the "fake" or "disguised" short GRBs and the other (so-called "long") GRBs. We also outline some implications for the theoretical interpretation of the Amati relation.

26. G. De Barros, M.G. Bernardini, C.L. Bianco, L. Caito, M.G. Dainotti, R. Guida, R. Ruffini; "Is GRB 050509b a genuine short GRB?"; in 2008 NANJING GAMMA-RAY BURST CONFERENCE; Proceedings of the 2008 Nanjing Gamma-Ray Burst Conference, Nanjing (China), June 2008, Y.-F. Huang, Z.-G. Dai, B. Zhang, Editors; AIP Conference Proceedings, 1065, 231 (2008).

    Within our "fireshell" model we introduced a "canonical" GRB scenario which differentiates physically the "proper GRB" (P-GRB) emission when photons decouple, and the afterglow emission due to interaction of the accelerated baryons with the CircumBurst Medium (CBM). The ratio between energetics

of the two components is ruled by the baryon loading of the fireshell. We here analyse the possibility that GRB050509b is the first case of a "genuine" short GRB the ones with smaller baryon loading. In such a case, the GRB050509b "prompt emission" would be dominated by the "proper GRB" and, moreover, the P-GRB total energy would be greater than the afterglow one. Our fit of the afterglow data and of the P-GRB energetics indicates that this source present the smallest baryon loading we ever encountered so far, being on the order of 10^{-4}.

27. G. De Barros, A.G. Aksenov, C.L. Bianco, R. Ruffini, G.V. Vereshchagin; "Fireshell versus Fireball scenarios"; in 2008 NANJING GAMMA-RAY BURST CONFERENCE; Proceedings of the 2008 Nanjing Gamma-Ray Burst Conference, Nanjing (China), June 2008, Y.-F. Huang, Z.-G. Dai, B. Zhang, Editors; AIP Conference Proceedings, 1065, 234 (2008).

    We revisit Cavallo and Rees classification based on the analysis of initial conditions in electron-positron-photon plasma which appears suddenly around compact astrophysical objects and gives origin to GRBs. These initial conditions were recently studied in [1,2] by numerical integration of relativistic Boltzmann equations with collision integrals, including binary and triple interactions between particles. The main conclusion is that the pair plasma in GRB sources quickly reaches thermal equilibrium well before its expansion starts. In light of this work we comment on each of the four scenarios proposed by Cavallo and Rees and discuss their applicability to describe evolution of GRB sources.

28. M.G. Bernardini, C.L. Bianco, L. Caito, M.G. Dainotti, R. Guida, R. Ruffini; "GRB970228 as a prototype for the class of GRBs with an initial spikelike emission"; in Proceedings of the Eleventh Marcel Grossmann Meeting on General Relativity, Berlin, Germany, July 2006, H. Kleinert, R.T. Jantzen, Editors; World Scientific, (Singapore, 2008).

    We interpret GRB970228 prompt emission within our "canonical" GRB scenario, identifying the initial spikelike emission with the Proper-GRB (P-GRB) and the following bumps with the afterglow peak emission. Furthermore, we emphasize the necessity to consider the "canonical" GRB as a whole due to the highly non-linear nature of the model we applied.

29. M.G. Bernardini, C.L. Bianco, L. Caito, M.G. Dainotti, R. Guida, R. Ruffini; "GRB980425 and the puzzling URCA1 emission"; in Proceedings of the Eleventh Marcel Grossmann Meeting on General Relativity, Berlin, Germany, July 2006, H. Kleinert, R.T. Jantzen, Editors; World Scientific, (Singapore, 2008).

We applied our "fireshell" model to GRB980425 observational data, reproducing very satisfactory its prompt emission. We use the results of our analysis to provide a possible interpretation for the X-ray emission of the source S1. The effect on the GRB analysis of the lack of data in the pre-Swift observations is also outlined.

30. C.L. Bianco, M.G. Bernardini, L. Caito, P. Chardonnet, M.G. Dainotti, F. Fraschetti, R. Guida, R. Ruffini, S.-S. Xue; "Theoretical interpretation of 'long' and 'short' GRBs"; in Proceedings of the Eleventh Marcel Grossmann Meeting on General Relativity, Berlin, Germany, July 2006, H. Kleinert, R.T. Jantzen, Editors; World Scientific, (Singapore, 2008).

    Within the "fireshell" model we define a "canonical GRB" light curve with two sharply different components: the Proper-GRB (P-GRB), emitted when the optically thick fireshell of electron-positron plasma originating the phenomenon reaches transparency, and the afterglow, emitted due to the collision between the remaining optically thin fireshell and the CircumBurst Medium (CBM). We here present the consequences of such a scenario on the theoretical interpretation of the nature of "long" and "short" GRBs.

31. C.L. Bianco, M.G. Bernardini, P. Chardonnet, F. Fraschetti, R. Ruffini, S.-S. Xue; "Theoretical interpretation of luminosity and spectral properties of GRB 031203"; in Proceedings of the Eleventh Marcel Grossmann Meeting on General Relativity, Berlin, Germany, July 2006, H. Kleinert, R.T. Jantzen, Editors; World Scientific, (Singapore, 2008).

    We show how an emission endowed with an instantaneous thermal spectrum in the co-moving frame of the expanding fireshell can reproduce the time-integrated GRB observed non-thermal spectrum. An explicit example in the case of GRB 031203 is presented.

32. C.L. Bianco, R. Ruffini; "The 'Fireshell' model in the Swift era"; in Proceedings of the Eleventh Marcel Grossmann Meeting on General Relativity, Berlin, Germany, July 2006, H. Kleinert, R.T. Jantzen, Editors; World Scientific, (Singapore, 2008).

    We here re-examine the validity of the constant-index power-law relation between the fireshell Lorentz gamma factor and its radial coordinate, usually adopted in the current Gamma-Ray Burst (GRB) literature on the grounds of an "ultrarelativistic" approximation. Such expressions are found to be mathematically correct but only approximately valid in a very limited range of the physical and astrophysical parameters and in an asymptotic regime which is reached only for a very short time, if any.

33. L. Caito, M.G. Bernardini, C.L. Bianco, M.G. Dainotti, R. Guida, R. Ruffini; "Theoretical interpretation of GRB011121"; in Proceedings of the Eleventh Marcel Grossmann Meeting on General Relativity, Berlin, Germany, July 2006, H. Kleinert, R.T. Jantzen, Editors; World Scientific, (Singapore, 2008).

    GRB 011121, detected by the BeppoSAX satellite, is studied as a prototype to understand the presence of flares observed by Swift in the afterglow of many GRB sources. Detailed theoretical analysis of the GRB 011121 light curves in selected energy bands are presented and compared with observational data. An interpretation of the flare of this source is provided by the introduction of the three-dimensional structure of the CircumBurst Medium(CBM).

34. M.G. Dainotti, M.G. Bernardini, C.L. Bianco, L. Caito, R. Guida, R. Ruffini; "On GRB 060218 and the GRBs related to Supernovae Ib/c"; in Proceedings of the Eleventh Marcel Grossmann Meeting on General Relativity, Berlin, Germany, July 2006, H. Kleinert, R.T. Jantzen, Editors; World Scientific, (Singapore, 2008).

    We study the Gamma-Ray Burst (GRB) 060218: a particularly close source at $z = 0.033$ with an extremely long duration, namely $T_{90} \sim 2000$ s, related to SN 2006aj. This source appears to be a very soft burst, with a peak in the spectrum at 4.9 keV, therefore interpreted as an X-Ray Flash (XRF) and it obeys to the Amati relation. We fit the X- and γ-ray observations by Swift of GRB 060218 in the 0.1150 keV energy band during the entire time of observations from 0 all the way to 106 s within a unified theoretical model. The details of our theoretical analysis have been recently published in a series of articles. The free parameters of the theory are only three, namely the total energy $E^{tot}_{e^\pm}$ of the $e^\pm$ plasma, its baryon loading $B = M_B c^2 / E^{tot}_{e^\pm}$, as well as the CircumBurst Medium (CBM) distribution. We fit the entire light curve, including the prompt emission as an essential part of the afterglow. We recall that this value of the B parameter is the highest among the sources we have analyzed and it is very close to its absolute upper limit expected. We successfully make definite predictions about the spectral distribution in the early part of the light curve, exactly we derive the instantaneous photon number spectrum N(E) and we show that although the spectrum in the co-moving frame of the expanding pulse is thermal, the shape of the final spectrum in the laboratory frame is clearly non thermal. In fact each single instantaneous spectrum is the result of an integration of thousands of thermal spectra over the corresponding EQuiTemporal Surfaces (EQTS). By our fit we show that there is no basic differences between XRFs and more general GRBs. They all originate from the collapse process to a black hole and their difference is due to the variability of the three basic parameters within the range of full applicability of the theory.

35. R. Guida, M.G. Bernardini, C.L. Bianco, L. Caito, M.G. Dainotti, R. Ruffini; "Theoretical interpretation of GRB060124"; in Proceedings of the Eleventh Marcel Grossmann Meeting on General Relativity, Berlin, Germany, July 2006, H. Kleinert, R.T. Jantzen, Editors; World Scientific, (Singapore, 2008).

    We show the preliminary results of the application of our "fireshell" model to GRB060124. This source is very peculiar because it is the first event for which both the prompt and the afterglow emission were observed simultaneously by the three Swift instruments: BAT (15 - 350 keV), XRT (0,2 - 10 keV) and UVOT (170 - 650 nm), due to the presence of a precursor $\sim$ 570 s before the main burst. We analyze GRB060124 within our "canonical" GRB scenario, identifying the precursor with the P-GRB and the prompt emission with the afterglow peak emission. In this way we reproduce correctly the energetics of both these two components. We reproduce also the observed time delay between the precursor (P-GRB) and the main burst. The effect of such a time delay in our model will be discussed.

36. R. Ruffini, M.G. Bernardini, C.L. Bianco, L. Caito, P. Chardonnet, C. Cherubini, M.G. Dainotti, F. fraschetti, A. Geralico, R. Guida, B. Patricelli, M. Rotondo, J. Rueda Hernandez, G. Vereshchagin, S.-S. Xue; "Gamma-Ray Bursts"; in Proceedings of the Eleventh Marcel Grossmann Meeting on General Relativity, Berlin, Germany, July 2006, H. Kleinert, R.T. Jantzen, Editors; World Scientific, (Singapore, 2008).

    We show by example how the uncoding of Gamma-Ray Bursts (GRBs) offers unprecedented possibilities to foster new knowledge in fundamental physics and in astrophysics. After recalling some of the classic work on vacuum polarization in uniform electric fields by Klein, Sauter, Heisenberg, Euler and Schwinger, we summarize some of the efforts to observe these effects in heavy ions and high energy ion collisions. We then turn to the theory of vacuum polarization around a Kerr-Newman black hole, leading to the extraction of the blackholic energy, to the concept of dyadosphere and dyadotorus, and to the creation of an electron-positron-photon plasma. We then present a new theoretical approach encompassing the physics of neutron stars and heavy nuclei. It is shown that configurations of nuclear matter in bulk with global charge neutrality can exist on macroscopic scales and with electric fields close to the critical value near their surfaces. These configurations may represent an initial condition for the process of gravitational collapse, leading to the creation of an electron-positron-photon plasma: the basic self-accelerating system explaining both the energetics and the high energy Lorentz factor observed in GRBs. We then turn to recall the two basic interpretational paradigms of our GRB model: 1) the Relative Space-Time Transformation (RSTT) paradigm and

2) the Interpretation of the Burst Structure (IBS) paradigm. These paradigms lead to a "canonical" GRB light curve formed from two different components: a Proper-GRB (P-GRB) and an extended afterglow comprising a raising part, a peak, and a decaying tail. When the P-GRB is energetically predominant we have a "genuine" short GRB, while when the afterglow is energetically predominant we have a so-called long GRB or a "fake" short GRB. We compare and contrast the description of the relativistic expansion of the electron-positron plasma within our approach and within the other ones in the current literature. We then turn to the special role of the baryon loading in discriminating between "genuine" short and long or "fake" short GRBs and to the special role of GRB 991216 to illustrate for the first time the "canonical" GRB bolometric light curve. We then propose a spectral analysis of GRBs, and proceed to some applications: GRB 031203, the first spectral analysis, GRB 050315, the first complete light curve fitting, GRB 060218, the first evidence for a critical value of the baryon loading, GRB 970228, the appearance of "fake" short GRBs. We finally turn to the GRB-Supernova Time Sequence (GSTS) paradigm: the concept of induced gravitational collapse. We illustrate this paradigm by the systems GRB 980425 / SN 1998bw, GRB 030329 / SN 2003dh, GRB 031203 / SN 2003lw, GRB 060218 / SN 2006aj, and we present the enigma of the URCA sources. We then present some general conclusions.

37. R. Ruffini, A.G. Aksenov, M.G. Bernardini, C.L. Bianco, L. Caito, M.G. Dainotti, G. De Barros, R. Guida, G. Vereshchagin, S.-S. Xue; "The canonical Gamma-Ray Bursts: long, 'fake'-'disguised' and 'genuine' short bursts; in PROBING STELLAR POPULATIONS OUT TO THE DISTANT UNIVERSE: CEFALU 2008, Proceedings of the International Conference; Cefal (Italy), September 2008, G. Giobbi, A. Tornambe, G. Raimondo, M. Limongi, L. A. Antonelli, N. Menci, E. Brocato, Editors; AIP Conference Proceedings, 1111, 325 (2009).

The Gamma-Ray Bursts (GRBs) offer the unprecedented opportunity to observe for the first time the blackholic energy extracted by the vacuum polarization during the process of gravitational collapse to a black hole leading to the formation of an electron-positron plasma. The uniqueness of the Kerr-Newman black hole implies that very different processes originating from the gravitational collapse a) of a single star in a binary system induced by the companion, or b) of two neutron stars, or c) of a neutron star and a white dwarf, do lead to the same structure for the observed GRB. The recent progress of the numerical integration of the relativistic Boltzmann equations with collision integrals including 2-body and 3-body interactions between the particles offer a powerful conceptual tool in order to differentiate the traditional "fireball" picture, an expanding hot cavity considered by Cavallo and Rees, as opposed to the "fireshell" model, composed of an internally cold shell of relativistically

expanding electron-positron-baryon plasma. The analysis of the fireshell naturally leads to a canonical GRB composed of a proper-GRB and an extended afterglow. By recalling the three interpretational paradigms for GRBs we show how the fireshell model leads to an understanding of the GRB structure and to an alternative classification of short and long GRBs.

38. M.G. Bernardini, M.G. Dainotti, C.L. Bianco, L. Caito, R. Guida, R. Ruffini; "Prompt emission and X-ray flares: the case of GRB 060607 A"; in PROBING STELLAR POPULATIONS OUT TO THE DISTANT UNIVERSE: CEFALU 2008, Proceedings of the International Conference; Cefal (Italy), September 2008, G. Giobbi, A. Tornambe, G. Raimondo, M. Limongi, L. A. Antonelli, N. Menci, E. Brocato, Editors; AIP Conference Proceedings, 1111, 383 (2009).

    GRB 060607A is a very distant and energetic event. Its main peculiarity is that the peak of the near-infrared (NIR) afterglow has been observed with the REM robotic telescope, allowing to estimate the initial Lorentz gamma factor within the fireball forward shock model. We analyze GRB 060607A within the fireshell model. The initial Lorentz gamma factor of the fireshell can be obtained adopting the exact solutions of its equations of motion, dealing only with the BAT and XRT observations, that are the basic contribution to the afterglow emission, up to a distance from the progenitor $r \sim 10^{18}$ cm. According to the "canonical GRB" scenario we interpret the whole prompt emission as the peak of the afterglow emission, and we show that the observed temporal variability of the prompt emission can be produced by the interaction of the fireshell with overdense CircumBurst Medium (CBM) clumps. This is indeed the case also of the X-ray flares which are present in the early phases of the afterglow light curve.

39. C.L. Bianco, M.G. Bernardini, L. Caito, M.G. Dainotti, R. Guida, R. Ruffini; "The 'fireshell' model and the 'canonical GRB' scenario. Implications for the Amati relation"; in PROBING STELLAR POPULATIONS OUT TO THE DISTANT UNIVERSE: CEFALU 2008, Proceedings of the International Conference; Cefal (Italy), September 2008, G. Giobbi, A. Tornambe, G. Raimondo, M. Limongi, L. A. Antonelli, N. Menci, E. Brocato, Editors; AIP Conference Proceedings, 1111, 587 (2009).

    Within the "fireshell" model for GRBs we define a "canonical GRB" light curve with two sharply different components: the Proper-GRB (P-GRB), emitted when the optically thick fireshell reaches transparency, and the extended afterglow, emitted due to the collision between the remaining optically thin fireshell and the CircumBurst Medium (CBM). We here outline our "canonical GRB" scenario, which implies three different GRB classes: the "genuine" short GRBs, the "fake" or "disguised" short GRBs and the other (so-called "long") GRBs.

We will also outline the corresponding implications for the Amati relation, which are opening its use for cosmology.

40. R. Ruffini, A.G. Aksenov, M.G. Bernardini, C.L. Bianco, L. Caito, P. Chardonnet, M.G. Dainotti, G. De Barros, R. Guida, L. Izzo, B. Patricelli, L.J. Rangel Lemos, M. Rotondo, J.A. Rueda Hernandez, G. Vereshchagin, S.-S. Xue; "The Blackholic energy and the canonical Gamma-Ray Burst IV: the 'long', 'genuine short' and 'fake disguised short' GRBs"; in Proceedings of the XIIIth Brazilian School on Cosmology and Gravitation, Mangaratiba, Rio de Janeiro (Brazil), July-August 2008, M. Novello, S.E. Perez Bergliaffa, Editors; AIP Conference Proceedings, 1132, 199 (2009).

    We report some recent developments in the understanding of GRBs based on the theoretical framework of the "fireshell" model, already presented in the last three editions of the "Brazilian School of Cosmology and Gravitation". After recalling the basic features of the "fireshell model", we emphasize the following novel results: 1) the interpretation of the X-ray flares in GRB afterglows as due to the interaction of the optically thin fireshell with isolated clouds in the CircumBurst Medium (CBM); 2) an interpretation as "fake - disguised" short GRBs of the GRBs belonging to the class identified by Norris & Bonnell; we present two prototypes, GRB 970228 and GRB 060614; both these cases are consistent with an origin from the final coalescence of a binary system in the halo of their host galaxies with particularly low CBM density $n_{cbm} \sim 10^{-3}$ particles/cm^3; 3) the first attempt to study a genuine short GRB with the analysis of GRB 050509B, that reveals indeed still an open question; 4) the interpretation of the GRB-SN association in the case of GRB 060218 via the "induced gravitational collapse" process; 5) a first attempt to understand the nature of the "Amati relation", a phenomenological correlation between the isotropic-equivalent radiated energy of the prompt emission E_{iso} with the cosmological rest-frame νF_ν spectrum peak energy $E_{p,i}$. In addition, recent progress on the thermalization of the electron-positron plasma close to their formation phase, as well as the structure of the electrodynamics of Kerr-Newman Black Holes are presented. An outlook for possible explanation of high-energy phenomena in GRBs to be expected from the AGILE and the Fermi satellites are discussed. As an example of high energy process, the work by Enrico Fermi dealing with ultrarelativistic collisions is examined. It is clear that all the GRB physics points to the existence of overcritical electrodynamical fields. In this sense we present some progresses on a unified approach to heavy nuclei and neutron stars cores, which leads to the existence of overcritical fields under the neutron star crust.

41. A.G. Aksenov, M.G. Bernardini, C.L. Bianco, L. Caito, C. Cherubini,

G. De Barros, A. Geralico, L. Izzo, F.A. Massucci, B. Patricelli, M. Rotondo, J.A. Rueda Hernandez, R. Ruffini, G. Vereshchagin, S.-S. Xue; "The fireshell model for Gamma-Ray Bursts"; in The Shocking Universe, Proceedings of the conference held in Venice (Italy), September 2009, G. Chincarini, P. DAvanzo, R. Margutti, R. Salvaterra, Editors; SIF Conference Proceedings, 102, 451 (2010).

The fireshell model for GRBs is briefly outlined, and the currently ongoing developments are summarized.

42. M.G. Bernardini, C.L. Bianco, L. Caito, L. Izzo, B. Patricelli, R. Ruffini; "The end of the prompt emission within the fireshell model"; in The Shocking Universe, Proceedings of the conference held in Venice (Italy), September 2009, G. Chincarini, P. DAvanzo, R. Margutti, R. Salvaterra, Editors; SIF Conference Proceedings, 102, 489 (2010)

    The shallow decay emission, revealed by the Swift satellite in the X-ray afterglow of a good sample of bursts, is a puzzle. Within the fireshell model it has been recently proposed an alternative explanation: if we assume that after the prompt phase the system has a range of Lorentz factors, the plateau phase is simply the product of the injection of slower material into the fireshell. This injection produces a modification both in the dynamics of the fireshell and in the spectrum of the emitted radiation. We postulate that this spread in the fireshell Lorentz factor occurs when the fireshell becomes transparent and do not depend on a prolonged activity of the central engine. The aim of this paper is to characterize dynamically the system in order to understand the nature of that material.

43. L. Izzo, M.G. Bernardini, C.L. Bianco, L. Caito, B. Patricelli, R. Ruffini; "GRB 090423 in the fireshell scenario"; in The Shocking Universe, Proceedings of the conference held in Venice (Italy), September 2009, G. Chincarini, P. DAvanzo, R. Margutti, R. Salvaterra, Editors; SIF Conference Proceedings, 102, 537 (2010).

44. B. Patricelli, M.G. Bernardini, C.L. Bianco, L. Caito, L. Izzo, R. Ruffini, G. Vereshchagin; "A new spectral energy distribution of photons in the fireshell model of GRBs"; in The Shocking Universe, Proceedings of the conference held in Venice (Italy), September 2009, G. Chincarini, P. DAvanzo, R. Margutti, R. Salvaterra, Editors; SIF Conference Proceedings, 102, 559 (2010).

    The fireshell model of Gamma Ray Bursts (GRBs) postulates that the emission process is thermal in the comoving frame of the fireshell, but this is just a first approximation. We investigate a different spectrum of photons in the comoving frame in order to better reproduce the observed spectral properties of

GRB prompt emission. We introduce a modified thermal spectrum whose low energy slope depends on an index α, left as a free parameter. We test it by comparing the numerical simulations with observed BAT spectra integrated over different intervals of time. We find that the observational data can be correctly reproduced by assuming $\alpha = -1.8$.

45. C.L. Bianco, M.G. Bernardini, L. Caito, G. De Barros, L. Izzo, B. Patricelli, R. Ruffini; "Disguised Short Bursts and the Amati Relation"; in Deciphering the ancient universe with Gamma-Ray Bursts, Proceedings of the conference held in Kyoto (Japan), April 2010, N. Kawai, S. Nagataki, Editors; AIP Conference Proceedings, 1279, 299 (2010).

    The class of "Disguised short" GRBs implied by the fireshell scenario is presented, with special emphasis on the implications for the Amati relation.

46. L. Izzo, M.G. Bernardini, C.L. Bianco, L. Caito, B. Patricelli, L.J. Rangel Lemos, R. Ruffini; "On GRB 080916C and GRB 090902B observed by the Fermi satellite"; in Deciphering the ancient universe with Gamma-Ray Bursts, Proceedings of the conference held in Kyoto (Japan), April 2010, N. Kawai, S. Nagataki, Editors; AIP Conference Proceedings, 1279, 343 (2010).

    We propose a possible explanation, in the context of the Fireshell scenario, for the high-energy emission observed in GRB 080916C and GRB 090902B. The physical process underlying this emission consists mainly in the interaction of the baryon in the Fireshell with some high-density region around the burst site. Moreover we associate the observed delay of the onset of the high-energy emission as due to the P-GRB emission.

47. B. Patricelli, M.G. Bernardini, C.L. Bianco, L. Caito, G. De Barros, L. Izzo, R. Ruffini; "Black Holes in Gamma Ray Bursts"; in Deciphering the ancient universe with Gamma-Ray Bursts, Proceedings of the conference held in Kyoto (Japan), April 2010, N. Kawai, S. Nagataki, Editors; AIP Conference Proceedings, 1279, 406 (2010).

    Within the fireshell model, Gamma Ray Bursts (GRBs) originate from an optically thick $e^{\pm}$ plasma created by vacuum polarization process during the formation of a Black Hole (BH). Here we briefly recall the basic features of this model, then we show how it is possible to interpret GRB observational properties within it. In particular we present, as a specific example, the analysis of GRB 050904 observations of the prompt emission light curve and spectrum in the Swift BAT energy band (15-150 keV).

48. M.G. Bernardini, C.L. Bianco, L. Caito, M.G. Dainotti, R. Guida, R. Ruffini; "The GRB classification within the "fireshell" model: short, long and

"fake" short GRBs"; in Proceedings of the 3rd Stueckelberg Workshop on Relativistic Field Theories, Pescara, Italy, July 2008, N. Carlevaro, R. Ruffini, G.V. Vereshchagin, Editors; Cambridge Scientific Publishers, (UK, 2011).

49. C.L. Bianco, M.G. Bernardini, L. Caito, M.G. Dainotti, R. Guida, R. Ruffini, G.V. Vereshchagin, S.-S. Xue; "Equations of motion of the "fireshell""; in Proceedings of the 3rd Stueckelberg Workshop on Relativistic Field Theories, Pescara, Italy, July 2008, N. Carlevaro, R. Ruffini, G.V. Vereshchagin, Editors; Cambridge Scientific Publishers, (UK, 2011).

50. L. Caito, M.G. Bernardini, C.L. Bianco, M.G. Dainotti, R. Guida, R. Ruffini; "GRB 060614: another example of "fake" short burst from a merging binary system"; in Proceedings of the 3rd Stueckelberg Workshop on Relativistic Field Theories, Pescara, Italy, July 2008, N. Carlevaro, R. Ruffini, G.V. Vereshchagin, Editors; Cambridge Scientific Publishers, (UK, 2011).

51. G. De Barros, M.G. Bernardini, C.L. Bianco, L. Caito, R. Guida, R. Ruffini; "Analysis of GRB 050509b"; in Proceedings of the 3rd Stueckelberg Workshop on Relativistic Field Theories, Pescara, Italy, July 2008, N. Carlevaro, R. Ruffini, G.V. Vereshchagin, Editors; Cambridge Scientific Publishers, (UK, 2011).

52. R. Ruffini, L. Izzo, A.V. Penacchioni, C.L. Bianco, L. Caito, S.K. Chakrabarti, A. Nandi; "GRB 090618: a possible case of multiple GRB?"; in Proceedings of the 25th Texas Symposium on Relativistic Astrophysics, held in Heidelberg (Germany), December 2010, F.M. Rieger, C. van Eldik, W. Hofmann, Editors; PoS(Texas2010), 101.

53. L.J. Rangel Lemos, C.L. Bianco, H.J. Mosquera Cuesta, J.A. Rueda, R. Ruffini; "Luminosity function of BATSE GRBs dominated by extended afterglow"; in Proceedings of the 25th Texas Symposium on Relativistic Astrophysics, held in Heidelberg (Germany), December 2010, F.M. Rieger, C. van Eldik, W. Hofmann, Editors; PoS(Texas2010), 204.

54. R. Ruffini, A.G. Aksenov, M.G. Bernardini, C.L. Bianco, L. Caito, P. Chardonnet, M.G. Dainotti, G. De Barros, R. Guida, L. Izzo, B. Patricelli, L.J. Rangel Lemos, M. Rotondo, J.A. Rueda Hernandez, G. Vereshchagin, She-Sheng Xue; "Black Holes Energetics and GRBs"; in The Sun, the Stars, the Universe and General Relativity: Proceedings of Sobral 2009; S.E. Perez Bergliaffa, M. Novello , R. Ruffini, Editors; Cambridge Scientific Publishers (UK, 2011).

55. C.L. Bianco, L. Amati, M.G. Bernardini, L. Caito, G. De Barros, L. Izzo, B. Patricelli, R. Ruffini; "The class of 'disguised' short GRBs and its implications for the Amati relation"; in GRBs as probes - from the progenitors environment to the high redshift Universe, Proceedings of the conference held in Como (Italy), May 2011, S. Campana, P. DAvanzo, A. Melandri, Editors; Mem. S.A.It. Suppl., 21, 139 (2012).

56. A.V. Penacchioni, R. Ruffini, L. Izzo, M. Muccino, C.L. Bianco, L. Caito, B. Patricelli; "Evidences for a double component in the emission of GRB 101023"; in GRBs as probes - from the progenitors environment to the high redshift Universe, Proceedings of the conference held in Como (Italy), May 2011, S. Campana, P. DAvanzo, A. Melandri, Editors; Mem. S.A.It. Suppl., 21, 230 (2012).

57. M.G. Bernardini, C.L. Bianco, L. Caito, L. Izzo, B. Patricelli, R. Ruffini; "The X-Ray Flares of GRB 060607A within the Fireshell Model"; in Proceedings of the Twelfth Marcel Grossmann Meeting on General Relativity, Paris, France, July 2009, T. Damour, R.T. Jantzen, R. Ruffini, Editors; World Scientific, (Singapore, 2012).

58. L. Izzo, M.G. Bernardini, C.L. Bianco, L. Caito, B. Patricelli, R. Ruffini; "GRB 090423 in the Fireshell Scenario: A Canonical GRB at Redshift 8.2"; in Proceedings of the Twelfth Marcel Grossmann Meeting on General Relativity, Paris, France, July 2009, T. Damour, R.T. Jantzen, R. Ruffini, Editors; World Scientific, (Singapore, 2012).

59. B. Patricelli, M.G. Bernardini, C.L. Bianco, L. Caito, L. Izzo, R. Ruffini, G.V. Vereshchagin; "A New Spectral Energy Distribution of Photons in the Fireshell Model of GRBs"; in Proceedings of the Twelfth Marcel Grossmann Meeting on General Relativity, Paris, France, July 2009, T. Damour, R.T. Jantzen, R. Ruffini, Editors; World Scientific, (Singapore, 2012).

60. C.L. Bianco, M.G. Bernardini, L. Caito, G. De Barros, L. Izzo, M. Muccino, B. Patricelli, A.V. Penacchioni, G.B. Pisani, R. Ruffini; "Needs for a new GRB classification following the fireshell model: genuine short, disguised short and long GRBs"; in Proceedings of the Gamma-Ray Bursts 2012 Conference, held in Munich (Germany), May 2012, A. Rau, J. Greiner, Editors; PoS(GRB 2012), 043.

61. A.V. Penacchioni, G.B. Pisani, R. Ruffini, C.L. Bianco, L. Izzo, M. Muccino; "The proto-black hole concept in GRB 101023 and its possible extension to GRB 110709B"; in Proceedings of the Gamma-Ray Bursts 2012

Conference, held in Munich (Germany), May 2012, A. Rau, J. Greiner, Editors; PoS(GRB 2012), 042.

62. B. Patricelli, M.G. Bernardini, C.L. Bianco, L. Caito, L. Izzo, R. Ruffini; "GRB 050904: The study of a high redshift GRB within the Fireshell Model"; in Proceedings of the Twelfth Marcel Grossmann Meeting on General Relativity, Paris, France, July 2009, T. Damour, R.T. Jantzen, R. Ruffini, Editors; World Scientific, (Singapore, 2012).

63. L. Izzo, G.B. Pisani, M. Muccino, J.A. Rueda, Y.Wang, C.L. Bianco, A.V. Penacchioni, R. Ruffini; "A common behavior in the late X-ray afterglow of energetic GRB-SN systems"; EAS Publications Series, Volume 61, 595-597 (2013).

64. R. Ruffini; "Black Holes, Supernovae and Gamma Ray Bursts"; in Proceedings of the Thirteenth Marcel Grossmann Meeting on General Relativity, Stockholm, Sweden, July 2012, R.T. Jantzen, K. Rosquist, R. Ruffini, Editors; World Scientific, (Singapore, 2015).

65. M. Muccino, R. Ruffini, C.L. Bianco, L. Izzo, A.V. Penacchioni, G.B. Pisani; "GRB 090227B: The missing link between the genuine short and long GRBs"; in Proceedings of the Thirteenth Marcel Grossmann Meeting on General Relativity, Stockholm, Sweden, July 2012, R.T. Jantzen, K. Rosquist, R. Ruffini, Editors; World Scientific, (Singapore, 2015).

66. A.V. Penacchioni, R. Ruffini, C.L. Bianco, L. Izzo, M. Muccino, G.B. Pisani, J.A. Rueda; "The family of the Induced Gravitational Collapse scenario: The case of GRB 110709B"; in Proceedings of the Thirteenth Marcel Grossmann Meeting on General Relativity, Stockholm, Sweden, July 2012, R.T. Jantzen, K. Rosquist, R. Ruffini, Editors; World Scientific, (Singapore, 2015).

67. A.V. Penacchioni, R. Ruffini, C.L. Bianco, L. Izzo, M. Muccino, G.B. Pisani; "GRB 111228, analysis within the Induced Gravitational Collapse scenario and association with a supernova"; in Proceedings of the Thirteenth Marcel Grossmann Meeting on General Relativity, Stockholm, Sweden, July 2012, R.T. Jantzen, K. Rosquist, R. Ruffini, Editors; World Scientific, (Singapore, 2015).

68. G.B. Pisani, L. Izzo, R. Ruffini, C.L. Bianco, M. Muccino, A.V. Penacchioni, J.A. Rueda, Y. Wang; "On a novel distance indicator for Gamma-Ray Bursts associated with supernovae"; in Proceedings of the Thirteenth Marcel Grossmann Meeting on General Relativity, Stockholm,

Sweden, July 2012, R.T. Jantzen, K. Rosquist, R. Ruffini, Editors; World Scientific, (Singapore, 2015).

69. M. Muccino, R. Ruffini, C.L. Bianco, L. Izzo, A.V. Penacchioni, G.B. Pisani; "GRB 090510, explosion of a GRB in the highest circumburst medium even inferred: a disguised short GRB"; in Proceedings of the Thirteenth Marcel Grossmann Meeting on General Relativity, Stockholm, Sweden, July 2012, R.T. Jantzen, K. Rosquist, R. Ruffini, Editors; World Scientific, (Singapore, 2015).

70. L. Izzo, G.B. Pisani, M. Muccino, R. Ruffini, C.L. Bianco, M. Enderli, Y. Wang; "Hints for a physically based GRB distance indicator"; in Proceedings of the Thirteenth Marcel Grossmann Meeting on General Relativity, Stockholm, Sweden, July 2012, R.T. Jantzen, K. Rosquist, R. Ruffini, Editors; World Scientific, (Singapore, 2015).

The Astrophysical Journal, 831:178 (17pp), 2016 November 10 doi:10.3847/0004-637X/831/2/178

GRB 090510: A GENUINE SHORT GRB FROM A BINARY NEUTRON STAR COALESCING INTO A KERR–NEWMAN BLACK HOLE

R. Ruffini[1,2,3,4], M. Muccino[1,2], Y. Aimuratov[1,3], C. L. Bianco[1,2], C. Cherubini[5], M. Enderli[1,3], M. Kovacevic[1,3], R. Moradi[1,2], A. V. Penacchioni[6,7], G. B. Pisani[1,2], J. A. Rueda[1,2,4], and Y. Wang[1,2]
[1] Dipartimento di Fisica, Sapienza Università di Roma and ICRA, Piazzale Aldo Moro 5, I-00185 Roma, Italy
[2] ICRANet, Piazza della Repubblica 10, I-65122 Pescara, Italy
[3] Université de Nice Sophia-Antipolis, Grand Château Parc Valrose, Nice, CEDEX 2, France
[4] ICRANet-Rio, Centro Brasileiro de Pesquisas Fisicas, Rua Dr. Xavier Sigaud 150, Rio de Janeiro, RJ, 22290-180, Brazil
[5] ICRA and Unit of Nonlinear Physics and Mathematical Modeling, Department of Engineering, Università Campus Bio-Medico di Roma, Via Alvaro del Portillo 21, I-00128, Rome, Italy
[6] University of Siena, Department of Physical Sciences, Earth and Environment, Via Roma 56, I-53100 Siena, Italy
[7] ASI Science Data Center, via del Politecnico s.n.c., I-00133 Rome Italy
Received 2015 October 9; revised 2016 September 1; accepted 2016 September 3; published 2016 November 7

ABSTRACT

In a new classification of merging binary neutron stars (NSs) we separate short gamma-ray bursts (GRBs) into two subclasses. The ones with $E_{\rm iso} \lesssim 10^{52}$ erg coalesce to form a massive NS and are indicated as short gamma-ray flashes (S-GRFs). The hardest, with $E_{\rm iso} \gtrsim 10^{52}$ erg, coalesce to form a black hole (BH) and are indicated as genuine short GRBs (S-GRBs). Within the fireshell model, S-GRBs exhibit three different components: the proper GRB (P-GRB) emission, observed at the transparency of a self-accelerating baryon-e^+e^- plasma; the prompt emission, originating from the interaction of the accelerated baryons with the circumburst medium; and the high-energy (GeV) emission, observed after the P-GRB and indicating the formation of a BH. GRB 090510 gives the first evidence for the formation of a Kerr BH or, possibly, a Kerr–Newman BH. Its P-GRB spectrum can be fitted by a convolution of thermal spectra whose origin can be traced back to an axially symmetric dyadotorus. A large value of the angular momentum of the newborn BH is consistent with the large energetics of this S-GRB, which reach in the 1–10,000 keV range $E_{\rm iso} = (3.95 \pm 0.21) \times 10^{52}$ erg and in the 0.1–100 GeV range $E_{\rm LAT} = (5.78 \pm 0.60) \times 10^{52}$ erg, the most energetic GeV emission ever observed in S-GRBs. The theoretical redshift $z_{\rm th} = 0.75 \pm 0.17$ that we derive from the fireshell theory is consistent with the spectroscopic measurement $z = 0.903 \pm 0.003$, showing the self-consistency of the theoretical approach. All S-GRBs exhibit GeV emission, when inside the *Fermi*-LAT field of view, unlike S-GRFs, which never evidence it. The GeV emission appears to be the discriminant for the formation of a BH in GRBs, confirmed by their observed overall energetics.

Key words: gamma-ray burst: general – gamma-ray burst: individual (GRB 090510)

1. INTRODUCTION

Thanks to a fortunate coincidence of observations by *AGILE*, *Fermi*, and *Swift* satellites, together with the optical observations by the Very Large Telescope (VLT)/FORS2 and the Nordic Optical Telescope, it has been possible to obtain an unprecedented set of data, extending from the optical–UV, through the X-rays, all the way up to the high-energy (GeV) emission, which allowed detailed temporal/spectral analyses of GRB 090510 (De Pasquale et al. 2010).

In contrast with this outstanding campaign of observations, a theoretical analysis of the broadband emission of GRB 090510 has been advanced within the synchrotron/self-synchrotron Compton and traditional afterglow models (see, e.g., Sections 5.2.1 and 5.2.2 in Ackermann et al. 2010). Paradoxically, this same methodology has been applied in the description of markedly different types of sources: e.g., Soderberg et al. (2006b) for the low energetic long gamma-ray burst (GRB) 060218, Perley et al. (2014) for the high energetic long GRB 130427A, and Soderberg et al. (2006a) for the short gamma-ray flash (S-GRF) 051221A (see also Curran et al. 2008, and references therein).

In the meantime, it has become evident that GRBs can be subdivided into a variety of classes and subclasses (Ruffini et al. 2015b, 2015c, 2016), each of them characterized by specific different progenitors, which deserve specific theoretical treatments and understanding. In addition, every subclass shows different episodes corresponding to specifically different astrophysical processes, which can be identified thanks to specific theoretical treatments and data analysis. In this article, we take GRB 090510 as a prototype for S-GRBs and perform a new time-resoved spectral analysis, in excellent agreement with the above temporal and spectral analysis performed by, e.g., the *Fermi* team. Now this analysis, guided by a theoretical approach successfully tested in this new family of short GRBs (S-GRBs; Muccino et al. 2013a; Ruffini et al. 2015b), is directed to identify a precise sequence of different events made possible by the exceptional quality of the data of GRB 090510. This includes a new structure in the thermal emission of the proper GRB (P-GRB) emission, followed by the onset of the GeV emission linked to the black hole (BH) formation, allowing us, as well, to derive the structure of the circumburst medium (CBM) from the spiky structure of the prompt emission. This sequence, for the first time, illustrates the formation process of a BH.

Already in 1974 February, soon after the public announcement of the GRB discovery (Strong et al. 1975), Damour & Ruffini (1975) presented the possible relation of GRBs to the vacuum polarization process around a Kerr–Newman BH. There, evidence was given for (a) the formation of a vast amount of e^+e^--baryon plasma; (b) the energetics of GRBs to be of the order of $E_{\rm max} \approx 10^{54} M_{\rm BH}/M_\odot$ erg, where $M_{\rm BH}$ is the

BH mass; and (c) additional ultra-high-energy cosmic rays with energy up to $\sim 10^{20}$ eV originating from such extreme processes. A few years later, the role of an e^+e^- plasma of comparable energetics for the origin of GRBs was considered by Cavallo & Rees (1978), and it took almost 30 yr to clarify some of the analogies and differences between these two processes, leading, respectively, to the alternative concepts of "fireball" and "fireshell" (Aksenov et al. 2007, 2009). In this article we give the first evidence for the formation of a Kerr–Newman BH, in GRB 090510, from the merger of two massive neutron stars (NSs) in a binary system.

GRBs are usually separated into two categories, based on their duration properties (e.g., Mazets et al. 1981; Dezalay et al. 1992; Klebesadel 1992, pp. 161–68; Kouveliotou et al. 1993; Tavani 1998). S-GRBs have a duration $T_{90} \lesssim 2$ s, while the remaining ones with $T_{90} \gtrsim 2$ s are traditionally classified as long GRBs.

S-GRBs are often associated with NS–NS mergers (see, e.g., Goodman 1986; Paczynski 1986; Eichler et al. 1989; Narayan et al. 1991; Meszaros & Rees 1997, Rosswog et al. 2003; Lee et al. 2004; Nakar 2007; Endrizzi et al. 2016; Ruiz et al. 2016; see also Berger 2014 for a recent review): their host galaxies are of both early and late type, their localization with respect to the host galaxy often indicates a large offset (Sahu et al. 1997; van Paradijs et al. 1997; Bloom et al. 2006; Troja et al. 2008; Fong et al. 2010; Berger 2011; Kopač et al. 2012) or a location of minimal star-forming activity with typical CBM densities of $\sim 10^{-5}$–10^{-4} cm^{-3}, and no supernovae (SNe) have ever been associated with them.

The progenitors of long GRBs, on the other hand, have been related to massive stars (Woosley & Bloom 2006). However, in spite of the fact that most massive stars are found in binary systems (Smith 2014), that most Type Ib/c SNe occur in binary systems (Smith et al. 2011), and that SNe associated with long GRBs are indeed of Type Ib/c (Della Valle 2011), the effects of binarity on long GRBs have been for a long time largely ignored in the literature. Indeed, until recently, long GRBs have been interpreted as single events in the jetted *collapsar* fireball model (see, e.g., Rees & Meszaros 1992; Woosley 1993; Kobayashi et al. 1997; Piran 2005; Gehrels et al. 2009; Kumar & Zhang 2015 and references therein).

Multiple components evidencing the presence of a precise sequence of different astrophysical processes have been found in several long GRBs (e.g., Izzo et al. 2012; Penacchioni et al. 2012). Following this discovery, further results led to the introduction of a new paradigm explicating the role of binary sources as progenitors of the long GRB–SN connection. New developments have led to the formulation of the induced gravitational collapse (IGC) paradigm (Ruffini et al. 2001a, 2007, 2015c; Rueda & Ruffini 2012). The IGC paradigm explains the GRB-SN connection in terms of the interactions between an evolved carbon–oxygen core (CO_{core}) undergoing an SN explosion and its hypercritical accretion on a binary NS companion (Ruffini 2015). A large majority of long bursts are related to SNe and are spatially correlated with bright star-forming regions in their host galaxies (Fruchter et al. 2006; Svensson et al. 2010), with a typical CBM density of ~ 1 cm^{-3} (Izzo et al. 2012; Penacchioni et al. 2012).

A new situation has occurred with the observation of the high-energy GeV emission by the *Fermi*-LAT instrument and its correlation with both long and short bursts with isotropic energy $E_{iso} \gtrsim 10^{52}$ erg, which has been evidenced in Ruffini et al. (2015b, 2015c), respectively. On the basis of this correlation, the occurrence of such prolonged GeV emission has been identified with the onset of the formation of a BH (Ruffini et al. 2015b, 2015c).

As recalled above, the long GRBs associated with SNe have been linked to the hypercritical accretion process occurring in a tight binary system when the ejecta of an exploding CO_{core} accrete onto an NS binary companion (see, e.g., Rueda & Ruffini 2012; Fryer et al. 2014; Becerra et al. 2015). When the hypercritical accretion occurs in a widely separated system with an orbital separation $>10^{11}$ cm (Becerra et al. 2015), the accretion is not sufficient to form a BH. For these softer systems with rest-frame spectral peak energy $E_{peak} < 200$ keV the upper limit of their observed energy is $E_{iso} \approx 10^{52}$ erg, which corresponds to the maximum energy attainable in the accretion onto an NS (Ruffini et al. 2015c). Such a long burst corresponds to an X-ray flash (XRF). The associated X-ray afterglow is also explainable in terms of the interaction of the prompt emission with the SN ejecta (C. L. Fryer et al. 2016, in preparation). In these systems no GeV emission is expected in our theory and, indeed, is not observed. Interestingly, pioneering evidence for such an XRF had already been given in a different context by Heise (2003), Amati et al. (2004), and Soderberg et al. (2006b). For tighter binaries ($<10^{11}$ cm; Becerra et al. 2015), the hypercritical accretion onto the companion NS leads to the formation of a BH. For these harder systems with $E_{peak} > 200$ keV the lower limit of their observed energy is $E_{iso} \approx 10^{52}$ erg, which necessarily needs the accretion process into a BH. An associated prolonged GeV emission occurs after the P-GRB emission and at the beginning of the prompt emission and originates at the onset of the BH formation (Ruffini et al. 2015c). These more energetic events are referred to as binary-driven hypernovae (BdHNe). Specific constant power-law behaviors are observed in their high-energy GeV, X-rays, and optical luminosity light curves (Pisani et al. 2013; Ruffini et al. 2014, 2015c).

In total analogy, the formation of a BH can occur in short bursts, depending on the mass of the merged core of the binary system. When the two NS masses are large enough, the merged core can exceed the NS critical mass and BH formation is possible. In the opposite case, a massive NS (MNS) is created, possibly, with some additional orbiting material to guarantee the angular momentum conservation. We then naturally expect the existence of two short-burst subclasses: authentic S-GRBs, characterized by the formation of a BH (Ruffini et al. 2015b), with $E_{iso} \gtrsim 10^{52}$ erg, a harder spectrum (see Section 5.2), and associated with a prolonged GeV emission (see Section 6.5); and S-GRFs, producing an MNS (Ruffini et al. 2015b), with $E_{iso} \lesssim 10^{52}$ erg. In this second subclass, of course, the GeV emission should not occur and, indeed, is never observed.

Following the discovery of the first prototype of this S-GRB class, namely, GRB 090227B (Muccino et al. 2013a), the first detailed analysis of such a genuine S-GRB originating from a binary NS merger leading to a BH was done for GRB 140619B by Ruffini et al. (2015b), determining as well the estimated emission of gravitational waves. The latter has been estimated following the method applied by Oliveira et al. (2014) for GRB 090227B. From the spectral analysis of the early ~ 0.2 s, they inferred an observed temperature $kT = (324 \pm 33)$ keV of the e^+e^- plasma at transparency (P-GRB), a theoretically derived redshift $z = 2.67 \pm 0.37$, a total burst energy $E^{tot}_{e^+e^-} = (6.03 \pm 0.79) \times 10^{52}$ erg, a rest-frame peak energy

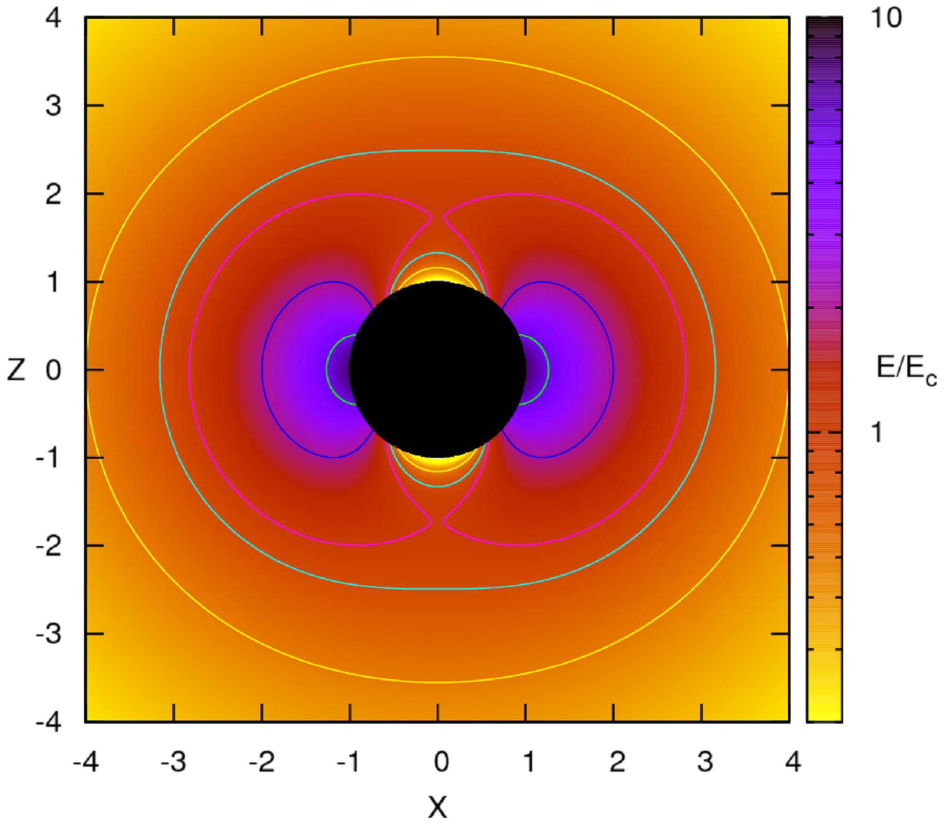

Figure 1. Projection of the dyadotorus of a Kerr–Newman BH corresponding to selected values of the ratio E/E_c, where E_c is the critical value for vacuum polarization and E is the electric field strength. The plot assumes a black hole mass energy $\mu = M_{\rm BH}/M_\odot = 10$. This figure is reproduced from Cherubini et al. (2009), with their kind permission.

$E_{p,i} = 4.7$ MeV, a baryon load $B = (5.52 \pm 0.73) \times 10^{-5}$, and an average CBM density $n_{\rm CBM} = (4.7 \pm 1.2) \times 10^{-5}$ cm^{-3}.

We turn in this article to the most interesting case of GRB 090510, which has, in addition to very similar properties of the members of this new class of S-GRB sources, a spectroscopically determined value of redshift and represents one of the most energetic sources of this family both in the γ-ray and in the GeV ranges. Actually, a first attempt to analyze GRB 090510 was made by interpreting this source as a long GRB (Muccino et al. 2013b). An unusually large value of the CBM density was needed in order to fit the data: this interpretation was soon abandoned when it was noticed that GRB 090510 did not fulfill the nesting conditions of the late X-ray emission typical of long GRBs (Ruffini et al. 2014); see also Section 5.1 and Figure 5.

In light of the recent progress in the understanding of the fireshell theory, we address the interpretation of GRB 090510 as the merging of a binary NS. We give clear evidence for the validity of this interpretation. In view of the good quality of the data both in γ-rays and in the GeV range, we have performed a more accurate description of the P-GRB, best fitted by a convolution of thermal spectra. This novel feature gives the first indication for the existence of an axially symmetric configuration of the dyadotorus emitting the e^+e^- plasma, which had been previously theoretically considered and attentively searched for. This gives the first indication that indeed the angular momentum plays a role and a dyadotorus is formed, as theoretically predicted in a series of papers (see Cherubini et al. 2009; Ruffini 2009; see also Figure 1). This naturally leads to the evidence for the formation of a rotating BH as the outcome of the gravitational collapse. We turn then to the main new feature of GRB 090510, which is the high-energy 0.1–100 GeV emission (see Figure 10). The direct comparison of the GeV emission in this source and in the BdHN 130427A shows the remarkable similarities of these two GeV components (see Figure 10). The fact that the S-GRB 090510 originates from a binary NS merger and the BdHN 130427A originates from the IGC of an SN hypercritical accretion process onto a companion NS clearly points to the BH as originating this GeV emission, the reason being that these two astrophysical systems are different in their progenitors and physical processes and have in the formation of a BH their unique commonality.

This paper is structured as follows: in Section 2 we summarize the relevant aspects of the fireshell theory and compare and contrast it with alternative approaches. In Section 3 we discuss the recent progress on the NS equilibrium configuration relevant for S-GRBs and BdHNe. In Section 4 we move on to describe the observations of GRB 090510 and their analysis. The S-GRB nature of GRB 090510 is justified in Section 5, and we offer an interpretation of our results in Section 6. Section 7 concludes this work.

A standard flat ΛCDM cosmological model with $\Omega_m = 0.27$ and $H_0 = 71$ km s^{-1} Mpc^{-1} is adopted throughout the paper.

2. SUMMARY OF THE FIRESHELL MODEL

The fireshell scenario (Ruffini et al. 2001a, 2001b, 2001c) has been initially introduced to describe a GRB originating in a gravitational collapse leading to the formation of a

Kerr–Newman BH. A distinct sequence of physical and astrophysical events are taken into account:

(1) An optically thick pair plasma—the fireshell of total energy $E^{\rm tot}_{e^+e^-}$—is considered. As a result, it starts to expand and accelerate under its own internal pressure (Ruffini et al. 1999). The baryonic remnant of the collapsed object is engulfed by the fireshell—the baryonic contamination is quantified by the baryon load $B = M_B c^2/E^{\rm tot}_{e^+e^-}$, where M_B is the mass of the baryonic remnant (Ruffini et al. 2000; Aksenov et al. 2007, 2009).
(2) After the engulfment, the fireshell is still optically thick and continues to self-accelerate until it becomes transparent. When the fireshell reaches transparency, a flash of thermal radiation termed proper-GRB (P-GRB) is emitted (Ruffini et al. 1999, 2000).
(3) In GRBs, the e^+e^--baryon plasma expands with ultrarelativistic velocities from the ultrarelativistic region near the BH to large distances. To describe such a dynamics that deals with unprecedentedly large Lorentz factors and also regimes sharply varying with time, Ruffini et al. (2001c) introduced the appropriate relative spacetime transformation paradigm. This paradigm gives particular attention to the constitutive equations relating four time variables: the comoving time, the laboratory time, the arrival time, and the arrival time at the detector corrected by the cosmological effects. This paradigm is essential for the interpretation of the GRB data: the absence of adopting such a relativistic paradigm in some current works has led to a serious misinterpretation of the GRB phenomenon.
(4) In compliance with the previous paradigm, the interactions between the ultrarelativistic shell of accelerated baryons left over after transparency and the CBM have been considered. They lead to a modified blackbody spectrum in the comoving frame (Patricelli et al. 2012). The observed spectrum is, however, nonthermal in general; this is due to the fact that, once the constant arrival time effect is taken into account in the equitemporal surfaces (EQTSs; see Bianco & Ruffini 2005a, 2005b), the observed spectral shape results from the convolution of a large number of modified thermal spectra with different Lorentz factors and temperatures.
(5) All the above relativistic effects, after the P-GRB emission, are necessary for the description of the prompt emission of GRBs, as outlined in Ruffini et al. (2001b). The prompt emission originates in the collisions of the accelerated baryons, moving at Lorentz factor $\gamma \approx 100$–1000, with interstellar clouds of CBM with masses of $\sim 10^{22}$–10^{24} g, densities of ~ 0.1–1 cm^{-3}, and size of $\sim 10^{15}$–10^{16} cm, at typical distances from the BH of $\sim 10^{16}$–10^{17} cm (see, e.g., Izzo et al. 2012 for long bursts). Our approach differs from alternative treatments purporting late activities from the central engine (see, e.g., the collapsar model in Woosley 1993; Popham et al. 1999; Woosley & Bloom 2006, and references therein; and the magnetar model in Zhang & Mészáros 2001; Dai et al. 2006; Metzger et al. 2011; Bucciantini et al. 2012; Lü & Zhang 2014, and references therein).
(6) $E^{\rm tot}_{e^+e^-}$ and B are the only two parameters that are needed in a spherically symmetric fireshell model to determine the physics of the fireshell evolution until the transparency condition is fulfilled. Three additional parameters, all related to the properties of the CBM, are needed to reproduce a GRB light curve and its spectrum: the CBM density profile $n_{\rm CBM}$, the filling factor $\mathcal{R}$ that accounts for the size of the effective emitting area, and an index α that accounts for the modification of the low-energy part of the thermal spectrum (Patricelli et al. 2012). They are obtained by running a trial-and-error simulation of the observed light curves and spectra that starts at the fireshell transparency.
(7) A more detailed analysis of the pair creation process around a Kerr–Newman BH has led to the concept of dyadotorus (Cherubini et al. 2009). There, the axially symmetric configuration with a specific distribution of the e^+e^-, as well as its electromagnetic field, has been presented as a function of the polar angle. The total spectrum at the transparency of the e^+e^- plasma is a convolution of thermal spectra at different angles.

This formalism describing the evolution of a baryon-loaded pair plasma is describable in terms of only three intrinsic parameters: the e^+e^- plasma energy $E^{\rm tot}_{e^+e^-}$, the baryon load B, and the specific angular momentum a of the incipient newly formed BH. It is, therefore, independent of the way the pair plasma is created.

In addition to the specific case, developed for the sake of example, of the dyadotorus created by a vacuum polarization process in an already-formed Kerr–Newman BH, more possibilities have been envisaged in the meantime:

(a) The concept of dyadotorus can be applied as well in the case of a pair plasma created via the $\bar{\nu} \leftrightarrow e^+e^-$ mechanism in an NS merger as described in Narayan et al. (1992), Salmonson & Wilson (2002), Rosswog et al. (2003), and Zalamea & Beloborodov (2011), assuming that the created pair plasma is optically thick. The relative role of neutrino and weak interactions vs. the electromagnetic interactions in building the dyadotorus is currently topic of intense research.
(b) Equally important is the relativistic magnetohydrodynamical process leading to a dyadotorus, indicated in the general treatment of Ruffini & Wilson (1975), and leading to the birth of a Kerr–Newman BH, surrounded by an opposite-charged magnetosphere in a system endowed with global charge neutrality. Active research is ongoing.
(c) Progress in understanding the NS equilibrium configuration imposing the global charge neutrality condition, as opposed to the local charge neutrality usually assumed (Rotondo et al. 2011a, 2011b; Rueda et al. 2011, 2014; Rueda & Ruffini 2013). A critical mass for a nonrotating NS of $M^{\rm NS}_{\rm crit} \approx 2.67 M_\odot$ has been found for the NL3 nuclear equation of state (Belvedere et al. 2012). The effects of rotation and of the nuclear equation of state on the critical mass are presented in Belvedere et al. (2014, 2015) and Cipolletta et al. (2015). The existence of electromagnetic fields close to the critical value has been evidenced in the interface between the core and the crust in the above global neutrality model, as well as very different density distributions in the crust and in the core, which could play an important role during the NS–NS mergers (see Figure 2 and Oliveira et al. 2014).

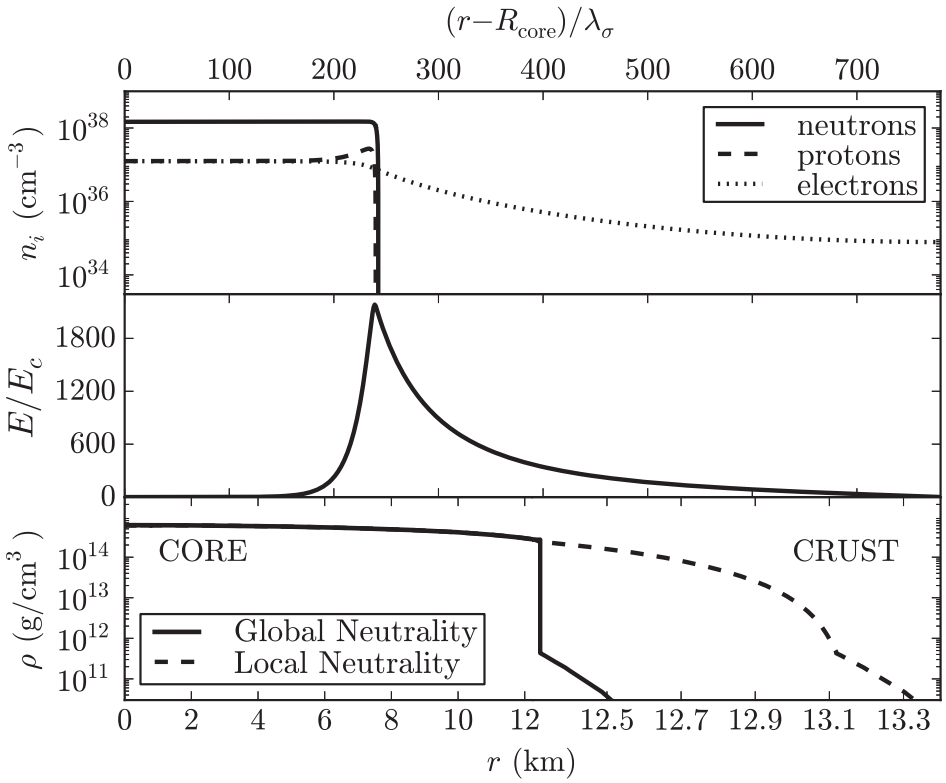

Figure 2. Particle density profiles (top panel) and the electric field in units of E_c (middle panel) in the core-crust transition layer normalized to the σ-meson Compton wavelength $\lambda_\sigma = \hbar/(m_\sigma c) \sim 0.4$ fm. Bottom panel: density profile inside an NS star with central density $\rho \sim 5\rho_{\rm nuc}$, where $\rho_{\rm nuc}$ is the nuclear density, from the solution of the Tolman–Oppenheimer–Volkoff (TOV) equations (locally neutral case) and the globally neutral solution presented in Belvedere et al. (2012). The density at the edge of the crust is the neutron drip density $\rho_{\rm drip} = 4.3 \times 10^{11}$ g cm^3. This figure is reproduced from Belvedere et al. (2012), with their kind permission.

The above three possibilities have been developed in recent years, but they do not have to be considered exaustive for the formation of a dyadotorus endowed by the above three parameters.

In conclusion, the evolution in the understanding of the GRB phenomenon, occurring under very different initial conditions, has evidenced the possibility of using the dyadotorus concept for describing sources of an optically thick baryon-loaded e^+e^- plasma within the fireshell treatment in total generality.

3. ON THE ROLE OF THE $\approx 10^{52}$ ERG LIMIT FOR S-GRBs AND BdHNe

The key role of neutrino emission in the hypercritical accretion process onto an NS has been already examined in the literature (see, e.g., Zel'dovich et al. 1972; Ruffini & Wilson 1973). The problem of hypercritical accretion in a binary system composed of a CO$_{\rm core}$ and a companion NS has been studied in Becerra et al. (2015, 2016) (see also references therein). The energy released during the process, in the form of neutrinos and photons, is given by the gain of gravitational potential energy of the matter being accreted by the NS and depends also on the change of binding energy of the NS while accreting matter and on the angular momentum carried by the accreting material (see, e.g., Becerra et al. 2016 and Ruffini et al. 2016). For a typical NS mass of ≈ 1.4 $M_\odot$, a value observed in galactic NS binaries (Zhang et al. 2011; Antoniadis 2015), and an NS critical mass $M_{\rm crit}^{\rm NS}$ in the range from 2.2 $M_\odot$ up to 3.4 $M_\odot$ depending on the equations of state and angular momentum (see Becerra et al. 2015, 2016; Cipolletta et al. 2015, for details), the accretion luminosity can be as high as $L_{\rm acc} \sim 0.1 \dot{M}_b c^2 \sim 10^{47}$–$10^{51}$ erg s^{-1} for accretion rates $\dot{M}_b \sim 10^{-6}$–10^{-2} $M_\odot$ s^{-1} (see Becerra et al. 2015, 2016, for details). For binary systems with a separation of $\sim 10^{10}$ cm ($P \sim 5$ minutes), our numerical simulations indicate that (a) the accretion process duration lasts $\Delta t_{\rm acc} \sim 10^2$ s (see, e.g., Becerra et al. 2015, 2016), (b) the NS collapses to a BH, and (c) a total energy larger than $\approx 10^{52}$ erg is released during the hypercritical accretion process. These systems correspond to the BdHNe (Becerra et al. 2016). For systems with larger separations the hypercritical accretion is not sufficient to induce the collapse of the NS into a BH and the value of $\approx 10^{52}$ erg represents a theoretical estimate of the upper limit to the energy emitted by the norm in the hypercritical accretion process. This subclass of sources corresponds to the XRFs (Becerra et al. 2016).

The same energetic considerations do apply in the analysis of the hypercritical accretion occurring in a close binary NS system undergoing merging (Ruffini 2015). Therefore, in total generality, we can conclude that the energy emitted during an NS–NS merger leading to the formation of a BH should be larger than $\approx 10^{52}$ erg (see Figure 3).

The limit of $\approx 10^{52}$ erg clearly depends on the initial NS mass undergoing accretion, by norm assumed to be ≈ 1.4 $M_\odot$, and on the yet-unknown value of $M_{\rm crit}^{\rm NS}$, for which only an absolute upper limit of 3.2 $M_\odot$ has been established for the nonrotating case (Rhoades & Ruffini 1974). As already pointed out in Ruffini (2015), for NS–NS mergers, the direct determination of the energy threshold of $\approx 10^{52}$ erg dividing S-GRFs and S-GRBs, as well as XRFs and BdHNe, provides fundamental information for the determination of the actual value of $M_{\rm crit}^{\rm NS}$, for the minimum mass of the newly born BH, and for the mass of the accreting NS.

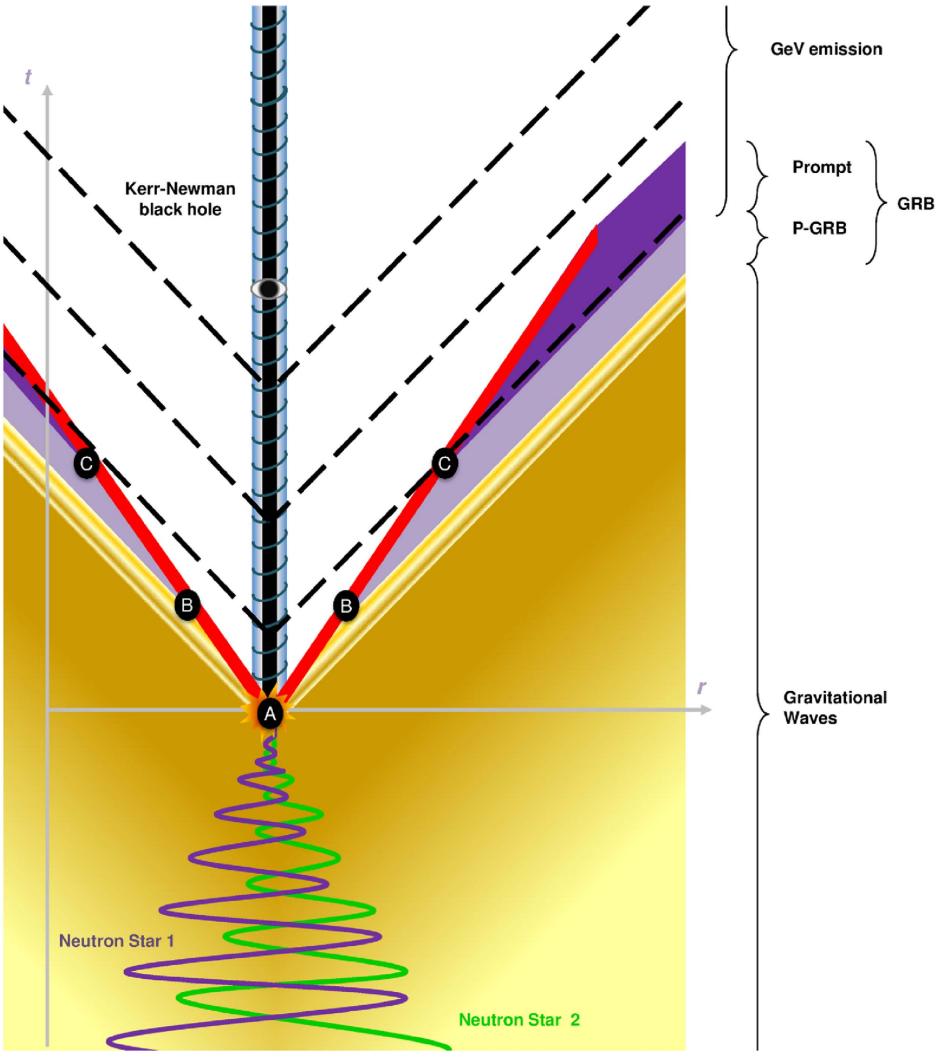

Figure 3. Spacetime diagram of an S-GRB, a binary NS merger leading to BH formation (taken from Enderli et al. 2015, with their kind permission). The binary orbit gradually shrinks due to energy loss through gravitational-wave emission (yellow–brown). At point A, the merger occurs: the fireshell (in red) is created and starts its expansion. It reaches transparency at point B, emitting the P-GRB (light purple). The prompt emission (deep purple) then follows at point C. The dashed lines represent the GeV emission (delayed relative to the start of the GRB) originating in the newly born BH. This spacetime diagram well illustrates how the GeV emission originates in the newly born BH and follows a different spacetime path from the prompt emission, contrary to what is stated in Ackermann et al. (2010). The prompt emission originates from the interactions of the baryons, accelerated to ultrarelativistic Lorentz factors during the pair-baryon electromagnetic pulse, with the clumpy CBM (see Section 2). The analysis of the spiky structure of the prompt emission allows us to infer the structure of the CBM (see Figure 9). There is the distinct possibility that the GeV emission prior to 0.6 s in the arrival time may interact with the prompt emission. In this sense the work by Zou et al. (2011) may become of interest.

4. ANALYSIS OF GRB 090510

In this section, we summarize the observations of GRB 090510, as well as the data analysis. We used *Fermi* (GBM and LAT) and *Swift*/XRT data for the purposes of this work.

4.1. Observations

The *Fermi*/GBM instrument (Meegan et al. 2009) was triggered at T_0 = 00:22:59.97 UT on 2009 May 10 by the short and bright burst GRB 090510 (Guiriec et al. 2009, trigger 263607781/090510016). The trigger was set off by a precursor emission of duration 30 ms, followed ∼0.4 s later by a hard episode lasting ∼1 s. This GRB was also detected by *Swift* (Hoversten et al. 2009), *Fermi*/LAT (Ohno & Pelassa 2009), *AGILE* (Longo et al. 2009), Konus-*Wind* (Golenetskii et al. 2009), and *Suzaku*-WAM (Ohmori et al. 2009). The position given by the GBM is consistent with that deduced from *Swift* and LAT observations.

During the first second after LAT trigger at 00:23:01.22 UT, *Fermi*/LAT detected over 50 (over 10) events with an energy above 100 MeV (1 GeV) up to the GeV range, and more than 150 (20) within the first minute (Omodei et al. 2009). This makes GRB 090510 the first bright S-GRB with an emission detected from the keV to the GeV range.

Observations of the host galaxy of GRB 090510, located by VLT/FORS2, provided a measurement of spectral emission lines. This led to the determination of a redshift $z = 0.903 \pm 0.003$ (Rau et al. 2009). The refined position of GRB 090510 obtained from the Nordic Optical Telescope (Olofsson et al. 2009) is offset by $0\farcs7$ relative to the center of the host galaxy in the VLT/FORS2 image. At $z = 0.903$, this corresponds to a projected distance of 5.5 kpc. The identified host galaxy is a late-type galaxy

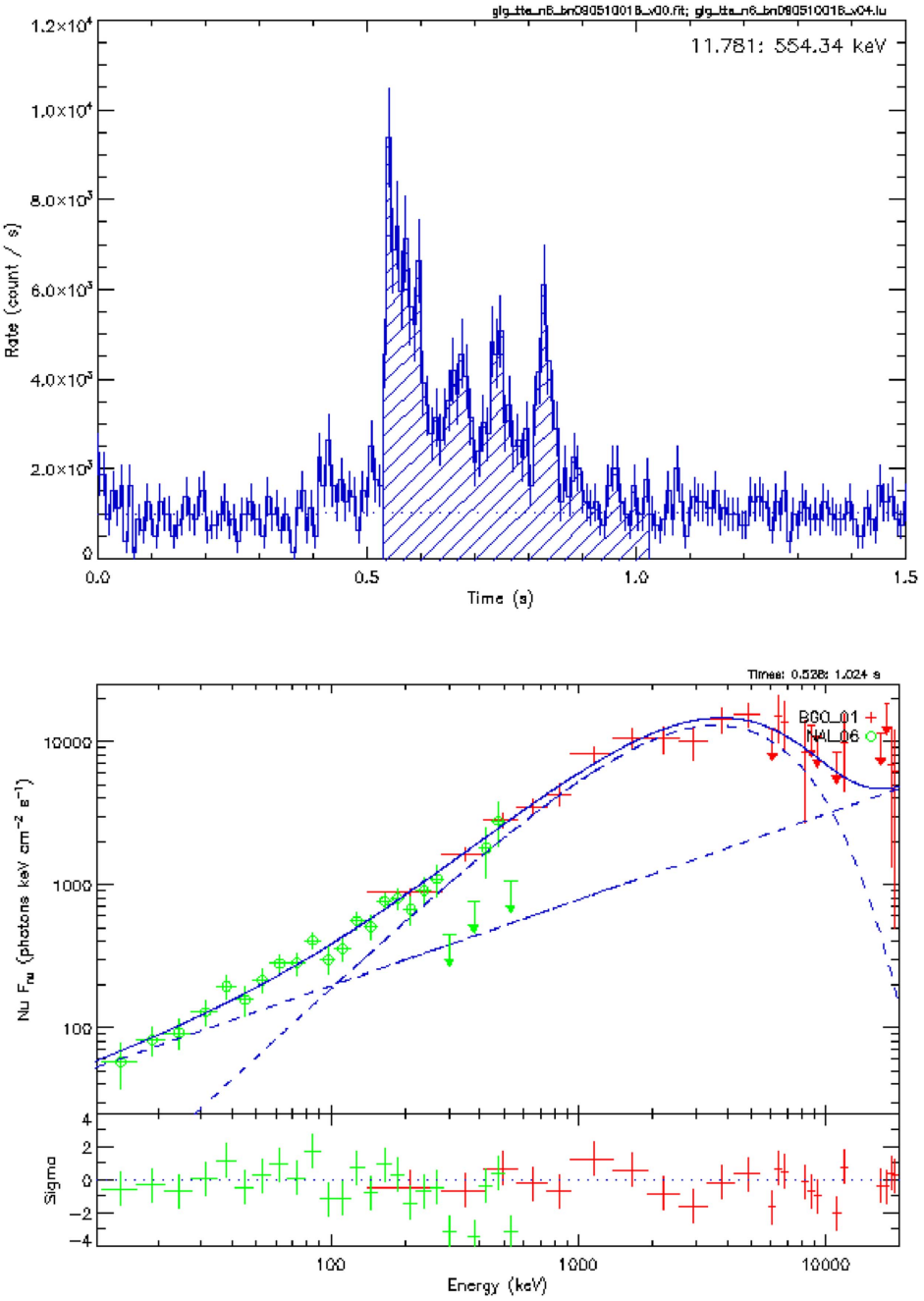

Figure 4. Top panel: GBM NaI-n6 light curve of GRB 090510 and interval considered to compute $E_{\rm iso}$. Bottom panel: Comptonized+power-law best fit of the corresponding spectrum (from $T_0 + 0.528$ to $T_0 + 1.024$ s).

of stellar mass $5 \times 10^9\ M_\odot$, with a rather low star formation rate SFR $= 0.3\ M_\odot\ {\rm yr}^{-1}$ (Berger 2014, and references therein).

4.2. Data Analysis

Our analysis focused on *Fermi* (GBM and LAT) and *Swift*/XRT data. The *Fermi*/GBM signal is the most luminous in the NaI-n6 (8–900 keV, dropping the overflow high-energy channels and cutting out the K edge between ~30 and ~40 keV) and BGO-b1 (260 keV–40 MeV, again dropping the overflow high-energy channels) detectors. We additionally considered *Fermi*/LAT data in the 100 MeV–100 GeV energy range. We made use of standard software in our analysis: GBM time-tagged data—suitable in particular for S-GRBs—were analyzed with the rmfit package[8]; LAT data were analyzed with the *Fermi* Science tools.[9] The data were retrieved from the *Fermi* science support center.[10] *Swift*/XRT data were retrieved from the UK *Swift* Data Centre at the University of Leicester,[11] and they have been reduced and analyzed using XSPEC.

Using GBM time-tagged event data binned in 16 ms intervals, the best fit in the interval $T_0 + 0.528$ s to $T_0 + 1.024$ s is a Comptonized+power-law model (see

[8] http://fermi.gsfc.nasa.gov/ssc/data/analysis//rmfit/vc_rmfit_tutorial.pdf
[9] http://fermi.gsfc.nasa.gov/ssc/data/analysis//documentation/Cicerone/
[10] http://fermi.gsfc.nasa.gov/ssc/data/access/
[11] http://www.swift.ac.uk/archive/index.php

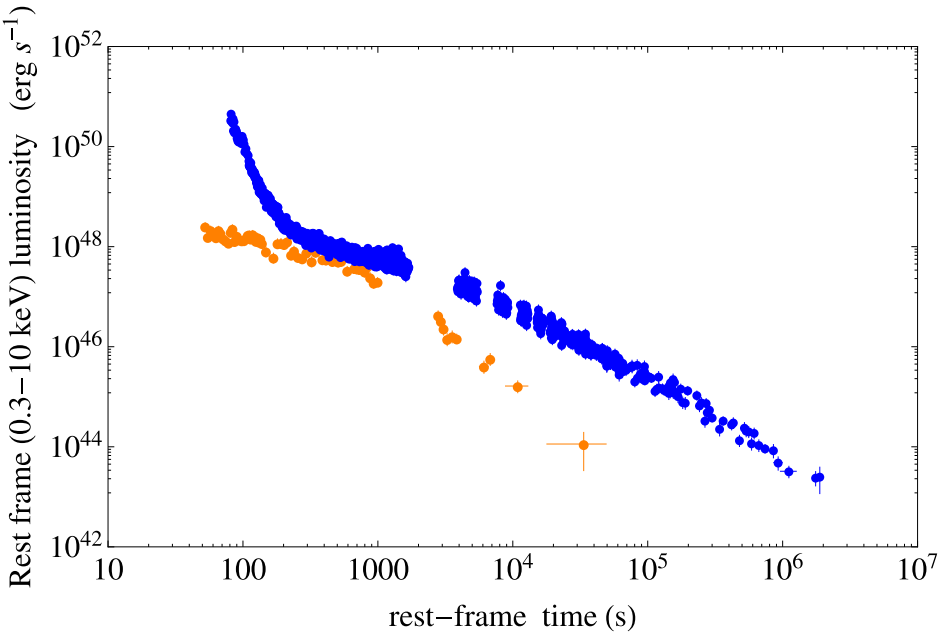

Figure 5. Rest-frame 0.3–10 keV luminosity light curves of GRB 090510 (in orange) and GRB 090618 (in blue), the prototypical IGC source. An overlapping pattern has been observed in IGC sources (Pisani et al. 2013), as well as a nesting behavior (Ruffini et al. 2014); it is clear from the deviation between the two light curves that GRB 090510 does not follow this characteristic pattern, thereby confirming its non-IGC nature.

Table 1
Spectral Analysis of the P-GRB of GRB 090510 in the Time Interval $T_0 + 0.528$ s to $T_0 + 0.640$ s.

Model	$C - \mathrm{STAT/dof}$	E_{peak} (keV)	α	β	γ	kT (keV)
Band	221.46/237	2987 ± 343	-0.64 ± 0.05	-3.13 ± 0.42	⋯	⋯
Comp	392.65/238	3020 ± 246	-0.64 ± 0.05	⋯	⋯	⋯
Comp+PL	209.26/236	2552 ± 233	-0.26 ± 0.14	⋯	-1.45 ± 0.07	⋯
PL	492.83/239	⋯	⋯	⋯	-1.20 ± 0.02	⋯
BB+PL	250.09/237	⋯	⋯	⋯	-1.38 ± 0.04	477.5 ± 24.9

Note. The Columns List the Model, its C-STAT Over the Number of Degrees of Freedom (dof), the Peak Energy E_{peak} is the Peak Energy of the Comp or Band Component, the Low-energy Index α of the Comp or Band Component, the High-energy Index β of the Band Component, the Power-law Index γ, and the Temperature kT of the Blackbody Component.

Figure 4). Using this spectral model, we find an isotropic energy $E_{\mathrm{iso}} = (3.95 \pm 0.21) \times 10^{52}$ erg. The observed peak energy of the best-fit Band model of the time-integrated GBM data is 4.1 ± 0.4 MeV, which corresponds to a rest-frame value of 7.89 ± 0.76 MeV.

The best-fit model during the first pulse (from $T_0 + 0.528$ s to $T_0 + 0.640$ s) in the 8 keV–40 MeV range is also a Comptonized+power-law model, preferred over a power law (PL, $\Delta C - \mathrm{STAT} = 100$), a blackbody plus PL (BB + PL, $\Delta C - \mathrm{STAT} = 41$), or a Band model ($\Delta C - \mathrm{STAT} = 12$). The fitting statistics are summarized in Table 1. The peak energy E_{peak} of the Comptonized component is 2.6 MeV. The total isotropic energy contained in this time interval is $\sim 1.77 \times 10^{52}$ erg, while the isotropic energy contained in the Comptonized part reaches $\sim 1.66 \times 10^{52}$ erg.

5. GRB 090510 AS AN S-GRB

We here justify the interpretation of GRB 090510 as an S-GRB event. In addition to the duration and hardness properties that are similar to other GRBs interpreted as binary NS mergers, the pattern of the late X-ray emission and the position of GRB 090510 in the E_{peak}–E_{iso} plane favor this interpretation.

5.1. Late X-Ray Emission (Episode 3)

An important feature of BdHNe is the existence of a pattern in the behavior of their 0.3–10 keV late X-ray luminosity light curves, which we refer to as Episode 3 (see, e.g., Ruffini et al. 2015c). This emission is observationally characterized by the overlapping of the common late power-law behavior (Pisani et al. 2013), as well as by the nesting, namely, an inverse (direct) proportionality relation between the duration (the luminosity) of the plateau phase and the energy of the GRB emission: the more energetic the source, the smaller (higher) the duration (the luminosity) of the plateau (Ruffini et al. 2014).

If GRB 090510 were to be an IGC event exploding in a high-density environment, this characteristic Episode 3 would be expected and should be seen. Thanks to adequate coverage by the *Swift*/XRT instrument, the late X-ray (0.3–10 keV) emission of GRB 090510 has been well sampled. We computed its rest-frame 0.3–10 keV luminosity light curve, using a simple power-law

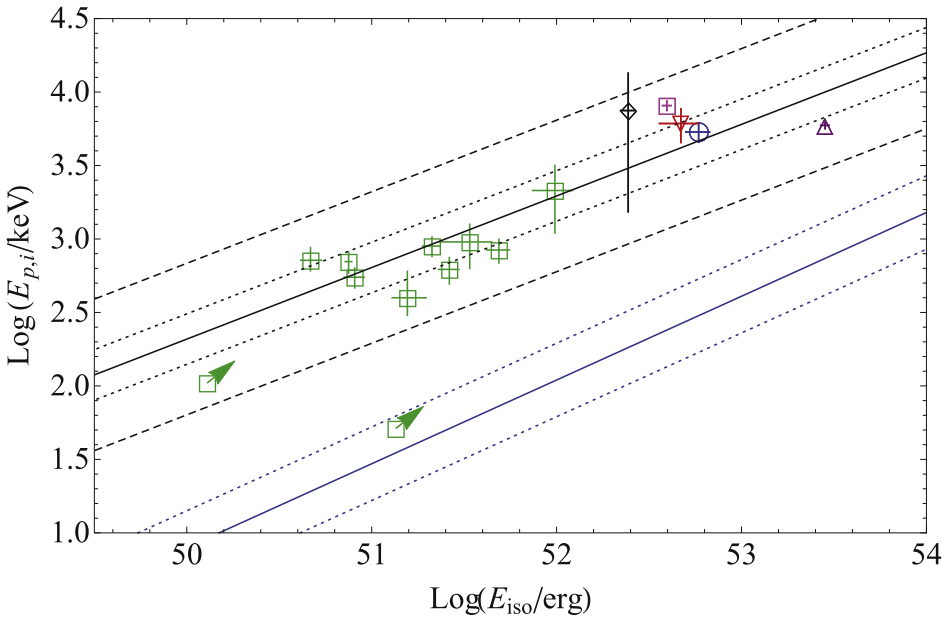

Figure 6. E_{peak}–E_{iso} plot of all short bursts with redshift. The black line marks the relation for S-GRBs (which includes the theoretical redshifts we obtained for four GRBs). This relation takes the form $\log E_{peak} = A + \gamma(\log E_{iso})$, where $A = -22.0 \pm 3.2$, $\gamma = 0.49 \pm 0.06$, and E_{peak} and E_{iso} are respectively given in keV and erg. The dotted and dashed lines represent the 1σ and 3σ scatter of the relation, respectively ($\sigma_{sc} = 0.17 \pm 0.04$ dex). Green boxes indicate S-GRFs with a measured redshift; only lower limits are available for the two S-GRFs singled out by an arrow. GRB 090510 is marked by the pink square. The other four symbols indicate S-GRBs with a redshift derived from the fireshell analysis. The black diamond indicates GRB 081024B, the red inverted triangle GRB 140402A, the blue square GRB 140619B, and the purple triangle GRB 090227B. For comparison, the blue line marks the relation for long GRBs given in Calderone et al. (2015), $\log E_{peak} = A + \gamma(\log E_{iso} - B)$, where $A = 2.73$, $B = 53.21$, and $\gamma = 0.57 \pm 0.06$. The dotted lines represent the 1σ scatter of the relation ($\sigma_{sc} = 0.25$ dex).

spectral fit and taking care of the *K*-correction as follows:

$$L_{rf} = 4\pi d_l^2(z) f_{obs} \frac{\int_{0.3/(1+z)\ \mathrm{keV}}^{10/(1+z)\ \mathrm{keV}} E^{-\gamma} dE}{\int_{0.3\ \mathrm{keV}}^{10\ \mathrm{keV}} E^{-\gamma} dE}, \quad (1)$$

where f_{obs} is the XRT flux (in erg s^{-1} cm^{-2}) in the observed 0.3–10 keV range, d_l is the luminosity distance, γ is the photon index of the XRT spectrum, and $E^{-\gamma}$ is the spectral model (here, a simple power law) fitting the observed XRT flux.

The rest-frame 0.3–10 keV luminosity light curve is plotted in Figure 5: the comparison with the prototypical IGC source GRB 090618 shows a clear deviation from the overlapping and nesting patterns. Indeed, the late X-ray emission of GRB 090510 is much weaker than that of typical IGC sources and does not follow the typical power-law behavior as a function of time, which has a slope $-1.7 \leqslant \alpha_X \leqslant -1.3$. As a consequence, this result is inconsistent with the hypothesis of GRB 090510 being a BdHN disguised as a short burst. Instead, the interpretation as an S-GRB is in full agreement with the theory and the data (see below).

5.2. E_{peak}–E_{iso} Relation

Although the sample of short bursts with a measured redshift and an estimate of E_{peak} is of modest size in comparison to that of long GRBs, it has been noted that a relation similar to the Amati one (Amati et al. 2002; Amati & Della Valle 2013) exists for short bursts (see, e.g., Zhang et al. 2012; Calderone et al. 2015). Plotted in Figure 6, this E_{peak}–E_{iso} relation has almost the same slope as the Amati relation, but they drastically differ in their amplitudes.

While Zhang et al. (2012) extended this analysis to the above-defined S-GRFs, we have recently added four S-GRBs in this E_{peak}–E_{iso} relation, which we have called the MuRuWaZha relation (Ruffini et al. 2015a).

With the parameters $E_{peak} = (7.89 \pm 0.76)$ MeV and $E_{iso} = (3.95 \pm 0.21) \times 10^{52}$ erg obtained in the previous sections, GRB 090510 falls right on the relation fulfilled by S-GRBs, and far from that of long GRBs (see Figure 6). This point further strengthens the identification of GRB 090510 as an S-GRB.

5.3. The Offset from the Host Galaxy

Long bursts are known to trace star formation (e.g., Bloom et al. 2002). They explode mainly in low-mass galaxies with high specific star formation rates. On the other hand, short bursts occur in a wider range of host galaxies, including old, elliptical galaxies with little star formation and young galaxies. Their median projected offset from the center of their host, about 5 kpc, is also known to be four times larger than that of long bursts (Bloom et al. 2002). With a projected offset of 5.5 kpc, as detailed previously, GRB 090510 falls in the typical short-burst range. Its host galaxy is a late-type one.

The results of the fireshell analysis summarized in the next section also support this conclusion. The average CBM density of GRB 090510 is indeed evaluated at $\langle n_{CBM} \rangle = 8.7 \times 10^{-6}$ cm^{-3} (see next section), a low value that is typical of galactic halos.

6. INTERPRETATION

GRB 090510 exhibits several peculiar features: the spectrum of the P-GRB is not purely thermal, a weak precursor emission is clearly seen, and a GeV emission is observed—which never occurs in S-GRFs but appears to be a general property of the S-GRBs. This section is devoted to the analysis and interpretation of these features.

Ruffini et al. (2015b) establish theoretical predictions concerning S-GRBs that originate in a binary NS merger, with and without BH formation. We find that these predictions are fulfilled and that

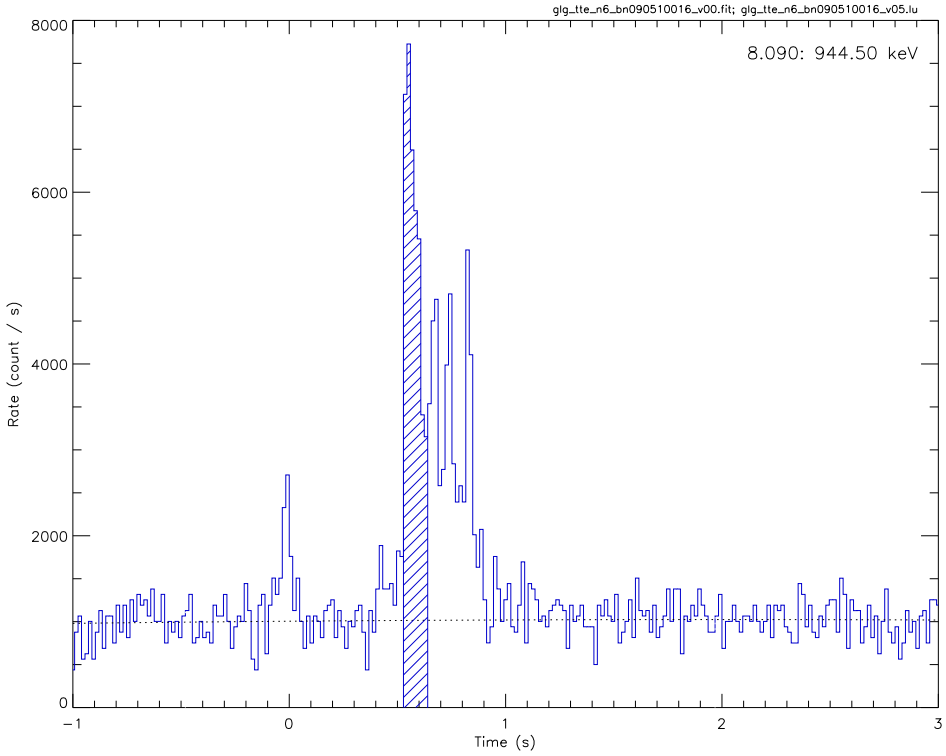

Figure 7. Counts light curve of GRB 090510 as seen by the NaI-n6 detector of *Fermi*/GBM with a 16 ms binning. The dashed area represents the interval in which the P-GRB is identified.

all features are consistent with GRB 090510 resulting from an NS merger, leading to the formation of a Kerr–Newman BH.

6.1. P-GRB

The identification of the P-GRB is especially relevant to the fireshell analysis, since it marks the reaching of the transparency of the fireshell. The P-GRB is followed by the prompt emission (Ruffini et al. 2001a). It is suggested in Ruffini et al. (2015b) that the GeV emission is produced by the newborn BH and starts only after the P-GRB is emitted, at the beginning of the prompt emission. Here, the bulk of the GeV emission is detected after the first main spike is over. Therefore, we identify the first main spike (from $T_0 + 0.528$ to $T_0 + 0.644$ s; see Figure 7) with the P-GRB. The results of the analysis within the fireshell theory (presented hereafter) also offer an a posteriori confirmation of this identification of the P-GRB.

The best-fit model of the P-GRB spectrum consists of a Comptonized+power-law model. We note that a Comptonized component may be viewed as a convolution of blackbodies (see Figure 8 and Table 2, for details).

The geometry of the fireshell is dictated by the geometry of the pair-creation region. It is in general assumed to be a spherically symmetric dyadosphere, which leads to a P-GRB spectrum generally described by a single thermal component in good agreement with the spectral data. Cherubini et al. (2009) found that the region of pair creation in a Kerr–Newman geometry becomes axially symmetric, thus effectively becoming a dyadotorus. Qualitatively, one expects a pure thermal spectrum resulting from the dyadosphere, while a convolution of thermal spectra of different temperatures is expected for a dyadotorus (see Figure 1).

In the present case of GRB 090510, also in view of the good quality of the γ-ray data, the P-GRB is best fitted by a convolution of thermal spectra. The theoretically expected temperatures of the thermal components in the dyadotorus are a function of the polar angle. Knowing that the final spectrum at the transparency condition is a convolution of such thermal spectra at different angles, we adopted for simplicity a discrete number of thermal components (see Table 2). The number of such thermal components, leading in principle to a continuum, is a function of the quality of the data. This provides the first indication that indeed the angular momentum plays a role in the merging of the two NSs and that the dyadotorus is formed as theoretically predicted in a series of papers (Cherubini et al. 2009; Ruffini 2009). This opens a new area of research that is not going to be addressed in the present article. Previous identifications of pure thermal components in the P-GRB of other GRBs (e.g., Izzo et al. 2012; Ruffini et al. 2015b) nevertheless evidence that the angular momentum of the BH formed by GRB 090510 must be substantially large in order to affect the P-GRB spectrum.

Finally, the extra power-law component observed in the P-GRB spectrum is very likely related to a mildly jetted component necessary to fulfill the conservation of the energy and angular momentum of the system.

6.2. Prompt Emission

In order to simulate the light curve and spectrum of the prompt emission of GRB 090510, we assume that the initial fireshell energy $E^{\rm tot}_{e^+e^-}$ is equal to $E_{\rm iso}$. Since the P-GRB spectrum is not purely thermal, we derive an effective blackbody temperature from the peak energy of the Comptonized component. We obtain a temperature $kT_{\rm obs} = (633 \pm 62)$ keV.

The fireshell theory allows the determination of all essential quantities of the model from the total pair plasma energy $E^{\rm tot}_{e^+e^-}$

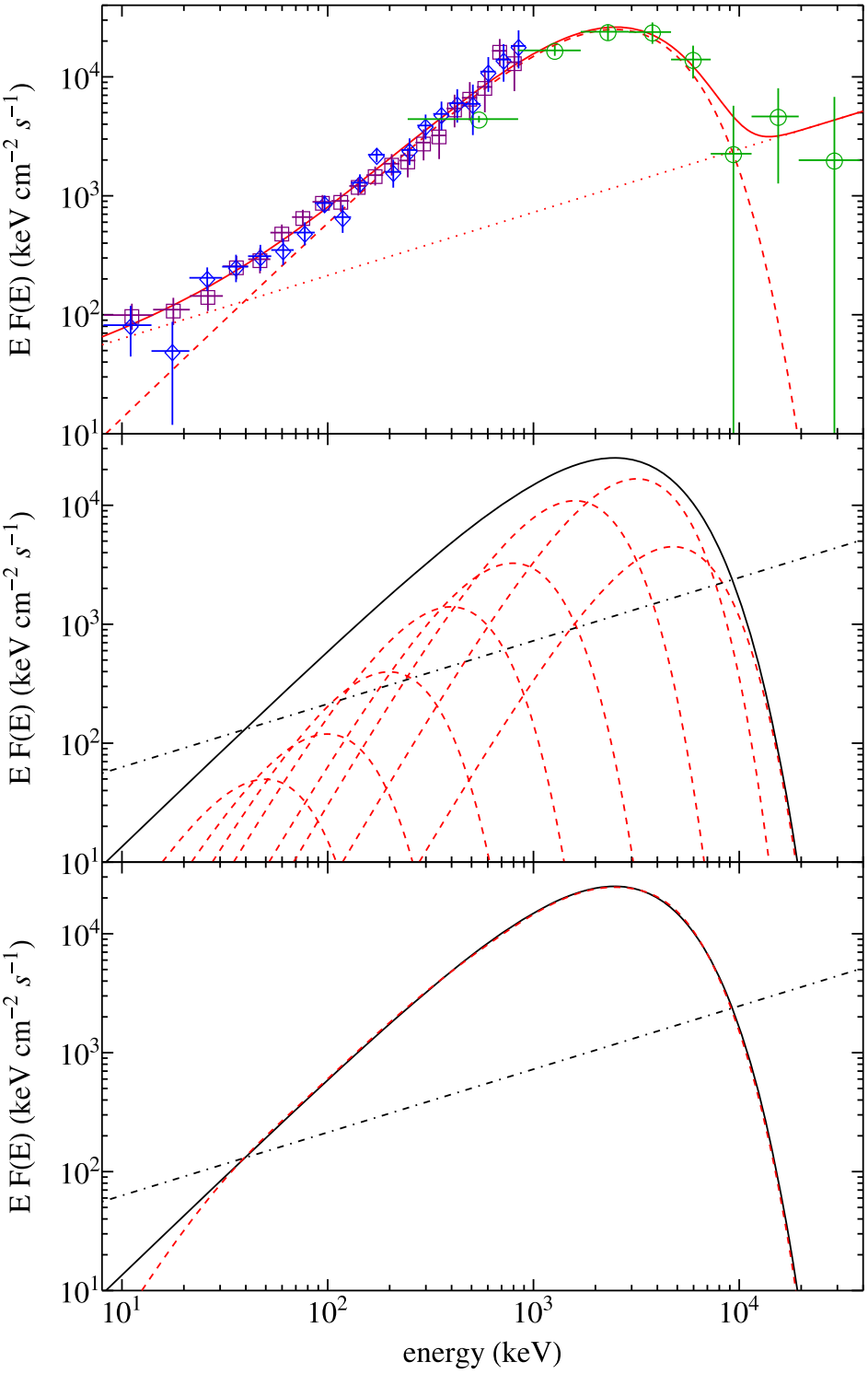

Figure 8. Top panel: P-GRB spectrum of GRB 090510 from the *Fermi*-GBM NaI-n6 (purple squares) and n7 (blue diamonds) and the BGO-b1 (green circles) detectors, in the time interval from $T_0 + 0.528$ to $T_0 + 0.644$ s. The best fit (solid red line) is composed of a power-law model (dotted red line) and a Comptonized model (dashed red curve). Middle panel: above Comptonized model (here the solid black line), viewed as a convolution of thermal components (dashed red curves). The convolution of blackbodies produces the result plotted in the bottom panel, namely, a dashed red curve reproducing the Comptonized model. The power-law component (dot-dashed black line in the middle and bottom panels) is very likely related to a mildly jetted component necessary to fulfill the conservation of the energy and angular momentum of the system.

and from the ratio of the energy contained in the P-GRB to $E^{\rm tot}_{e^+e^-}$. This ratio directly leads to the baryon load B, which, in conjunction with $E^{\rm tot}_{e^+e^-}$ and the relation between the predicted and observed temperatures, gives the Lorentz factor at transparency, the temperature of the fireshell at transparency, and the radius at transparency.

Given $E_{\rm iso} = 3.95 \times 10^{52}$ erg and $E_{\rm P\text{-}GRB} = (42.1 \pm 3.8)\%$ $E^{\rm tot}_{e^+e^-}$, we deduce a baryon load $B = 5.54 \times 10^{-5}$, a Lorentz

Table 2
The Parameters of the Blackbody (BB) Spectra Used in the Convolution Shown in Figure 8

BB	kT (keV)	$E_{\rm BB}/E_{\rm P\text{-}GRB}$ (%)
1	1216	8.8
2	811	43.6
3	405	31.8
4	203	9.6
5	101	4.4
6	51	1.2
7	25	0.4
8	13	0.2

Note. The columns list the number of BBs, their temperatures, and their energy content with respect to the P-GRB energy computed from the Comptonized model.

Table 3
Parameters Derived from the Fireshell Analysis of GRB 090510

Parameter	Value
B	$(5.54 \pm 0.70) \times 10^{-5}$
$\gamma_{\rm tr}$	$(1.04 \pm 0.07) \times 10^{4}$
$r_{\rm tr}$	$(7.60 \pm 0.50) \times 10^{12}$ cm
$E^{\rm tot}_{e^+e^-}$	$(3.95 \pm 0.21) \times 10^{52}$ erg
$kT_{\rm blue}$	$(1.20 \pm 0.11) \times 10^{3}$ keV
$\langle n \rangle$	$(8.7 \pm 2.1) \times 10^{-6}$ cm^{-3}

Note. Shown in the table are the baryon load B, the Lorentz factor at transparency $\gamma_{\rm tr}$, the fireshell radius at transparency $r_{\rm tr}$, the total energy of the electron-pair plasma $E^{\rm tot}_{e^+e^-}$, the blueshifted temperature of the fireshell at transparency $kT_{\rm blue}$, and the CBM average density $\langle n \rangle$

factor $\gamma = 1.04 \times 10^4$, a temperature at transparency $kT = 1.2$ MeV, and a radius at transparency $r_{\rm tr} = 7.60 \times 10^{12}$ cm (see Table 3).

In order to determine the profile of the CBM, a simulation of the prompt emission following the P-GRB has been performed. The simulation starts at the transparency of the fireshell with the parameters that we determined above. A trial-and-error procedure is undertaken, guided by the necessity to fit the light curve of GRB 090510. The results of this simulation (reproduction of the light curve and spectrum, in the time interval from $T_0 + 0.644$ to $T_0 + 0.864$ s, and CBM profile) are shown in Figure 9. The average CBM density is found to be $\langle n_{\rm CBM} \rangle = 8.7 \times 10^{-6}$ cm^{-3}. This low value, typical of galactic halo environments, is consistent with the large offset from the center of the host and further justifies the interpretation of GRB 090510 as an S-GRB originating in a binary NS merger.

Our theoretical fit of the prompt emission (see red line in the middle panel of Figure 9) predicts a cutoff at ∼10 MeV. The spectrum at energy $\gtrsim$10 MeV could be affected by the onset of the high-energy power-law component manifested both in the data of the Mini-Calorimeter on board *AGILE* (see top panel of Figure 4 in Giuliani et al. 2010) and in the data points from the *Fermi*-GBM BGO-b1 detector.

6.3. Precursor Emission

There is a weak precursor emission about 0.4 s before the P-GRB (or ∼0.21 s in the cosmological rest frame). Two GeV photons have been detected during the precursor emission. Precursors are commonly seen in long bursts: Lazzati (2005) found that ∼20% of them show evidence of an emission preceding the main emission by tens of seconds. Short bursts are less frequently associated with precursors.

No significant emission from the GRB itself is expected prior to the P-GRB—since it marks the transparency of the fireshell

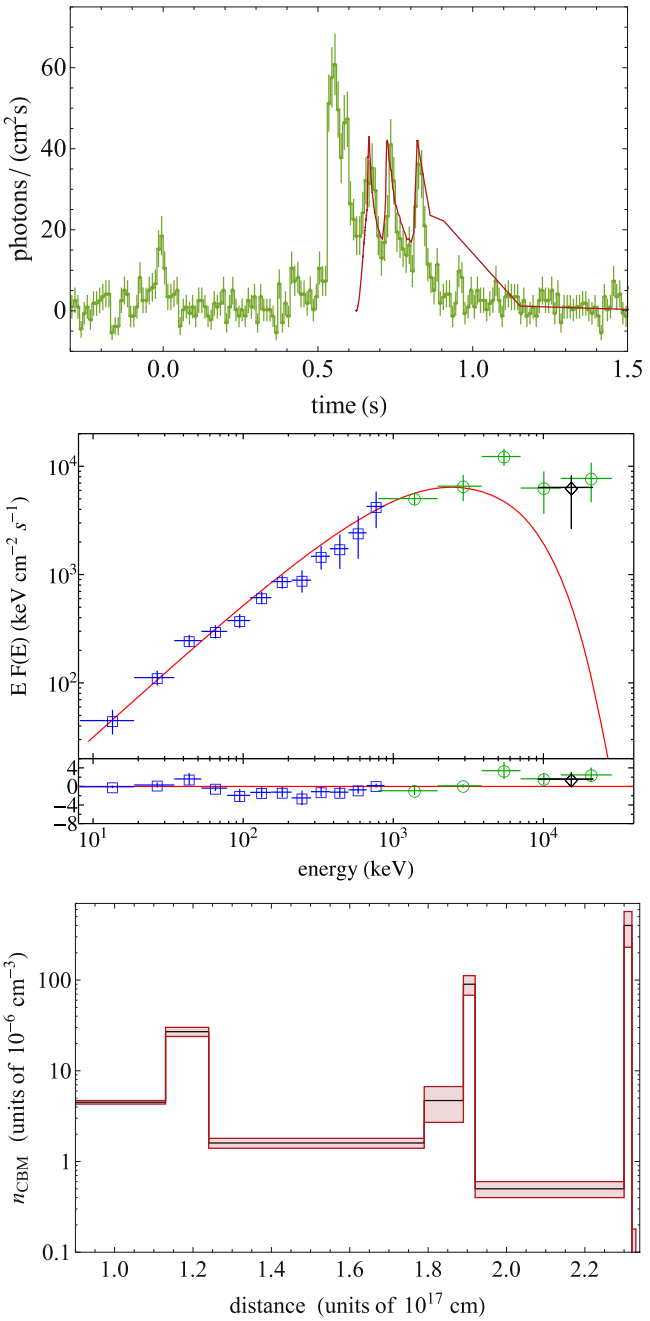

Figure 9. Results of the fireshell simulation of GRB 090510. Top panel: fit of the prompt emission *Fermi*-GBM NaI-n6 light curve. Middle panel: fit of the corresponding spectrum including the *Fermi*-NaI-6 (blue squares) and BGO-b1 (green circles) data in the time interval from $T_0 + 0.644$ to $T_0 + 0.864$ s. A single data point obtained from the Mini-Calorimeter on board *AGILE*, in the range 10–20 MeV and in the first 0.2 s of the *AGILE* light curve (from $T_0 + 0.5$ to $T_0 + 0.7$ s in the *Fermi* light curve), is shown for comparison (reproduced from Figure 4 in Giuliani et al. 2010). Bottom panel: density profile of the CBM inferred from the simulation of CBM clouds of $\sim 10^{22}$ g.

—but the precursor may be explainable in the context of a binary NS merger by invoking the effects of the interaction between the two NSs just prior to merger. Indeed, it has been suggested that precursor emission in short bursts may be caused by resonant fragmentation of the crusts (Tsang et al. 2012) or by the interaction of the NS magnetospheres (Hansen & Lyutikov 2001).

The timescale (∼0.21 s between the precursor and the P-GRB) is consistent with a pre-merger origin of the precursor emission. From its formation to its transparency, the fireshell undergoes a swift evolution. The thermalization of the pair plasma is achieved almost instantaneously ($\sim 10^{-13}$ s; Aksenov et al. 2007), and the e^+e^- plasma of GRB 090510 reaches the ultrarelativistic regime (i.e., a Lorentz factor $\gamma > 10$) in a matter of 4.2×10^{-2} s, according to the numerical simulation. The radius of the fireshell at transparency, $r_{\rm tr} = 7.60 \times 10^{12}$ cm, corresponds to more than 100 lt-s; however, relativistic motion in the direction of the observer squeezes the light curve by a factor of $\sim 2\gamma^2$, which makes the fireshell capable of traveling that distance under the observed timescale.

The spectral analysis of this precursor is limited by the low number of counts. Muccino et al. (2013b) interpreted the spectrum with a blackbody plus power-law model. This leads to a blackbody temperature of 34.2 ± 7.5 keV. The isotropic energy contained in the precursor amounts to $(2.28 \pm 0.39) \times 10^{51}$ erg.

6.4. Redshift Estimate

An interesting feature of the fireshell model is the possibility to infer a theoretical redshift from the observations of the P-GRB and the prompt emission. In the case of GRB 090510, a comparison is therefore possible between the measured redshift $z = 0.903 \pm 0.003$ and its theoretical derivation. An agreement between the two values would in particular strengthen the validity of our P-GRB choice, which would in turn strengthen our results obtained with this P-GRB.

The feature of the redshift estimate stems from the relations, engraved in the fireshell theory, between different quantities computed at the transparency point: the radius in the laboratory frame, the comoving frame and blueshifted temperatures of the plasma, the Lorentz factor, and the fraction of energy radiated in the P-GRB and in the prompt emission as functions of B (see Figure 4 in Ruffini et al. 2015b). Thus, the ratio $E_{\rm P\text{-}GRB}/E^{\rm tot}_{e^+e^-}$ implies a finite range for the coupled parameters $E^{\rm tot}_{e^+e^-}$ and B (last panel of Figure 4 in Ruffini et al. 2015b). Assuming $E^{\rm tot}_{e^+e^-} = E_{\rm iso}$, this ratio is known since it is equal to the ratio between the observed fluences of the respective quantities:

$$\frac{E_{\rm P\text{-}GRB}}{E^{\rm tot}_{e^+e^-}} \approx \frac{4\pi S_{\rm P\text{-}GRB} d_l^2(z)/(1+z)}{4\pi S^{\rm tot}_{e^+e^-} d_l^2(z)/(1+z)} = \frac{S_{\rm P\text{-}GRB}}{S^{\rm tot}_{e^+e^-}}. \quad (2)$$

With the measured values $S_{\rm P\text{-}GRB} = (9.31 \pm 0.76) \times 10^{-6}$ erg cm^{-2} and $S^{\rm tot}_{e^+e^-} = (2.19 \pm 0.18) \times 10^{-5}$ erg cm^{-2}, we find $E_{\rm P\text{-}GRB}/E^{\rm tot}_{e^+e^-} = (42.1 \pm 3.8)\%$.

In addition, knowing the couple $[E^{\rm tot}_{e^+e^-}, B]$ gives the (blueshifted toward the observer) temperature of the fireshell at transparency $kT_{\rm blue}$ (Figure 4 in Ruffini et al. 2015b, second panel). But we also have the following relation between $kT_{\rm blue}$ and the observed temperature at transparency $kT_{\rm obs}$, linking their ratio to the redshift:

$$\frac{kT_{\rm blue}}{kT_{\rm obs}} = 1 + z. \quad (3)$$

Finally, since we assume that $E^{\rm tot}_{e^+e^-} = E_{\rm iso}$, we also have an expression of $E^{\rm tot}_{e^+e^-}$ as a function of z using the formula of the K-corrected isotropic energy:

$$E_{\rm iso} = 4\pi d_l^2(z) \frac{S_{\rm tot}}{1+z} \frac{\int_{1/(1+z)\ \rm keV}^{10000/(1+z)\ \rm keV} EN(E)dE}{\int_{8\ \rm keV}^{40000\ \rm keV} EN(E)dE} \quad (4)$$

where $N(E)$ is the photon spectrum of the GRB and the fluence $S_{\rm tot}$ is obtained in the full GBM energy range 8–40,000 keV.

The use of all these relations allows a redshift to be determined by an iterative procedure, testing at every step the value of the parameters $E^{\rm tot}_{e^+e^-}(z)$ and $kT_{\rm blue}$. The procedure successfully ends when both values are consistent according to the relations described above. In the case of GRB 090510, we find $z = 0.75 \pm 0.17$, which provides a satisfactory agreement with the measured value $z = 0.903 \pm 0.003$.

6.5. GeV Emission

GRB 090510 is associated with a high-energy emission, consistently with all other observed S-GRBs, i.e., energetic events with $E_{\rm iso} \gtrsim 10^{52}$ erg. The only case of an S-GRB without GeV emission, namely, GRB 090227B, has been explained by the absence of alignment between the LAT and the source at the time of the GRB emission. Nevertheless, evidence of some GeV emission in this source has been recently obtained (R. Ruffini et al. 2016, in preparation).

The GeV light curve of GRB 090510 is plotted in Figure 10, together with other S-GRB light curves and showing a common power-law behavior, which goes as $t^{-1.32}$, similar to the clustering of the GeV light curves found by Nava et al. (2014). These S-GRBs are compared with that of the BdHN 130427A, which shares a similar behavior. Ruffini et al. (2015b) suggest and argue that the GeV emission is related to the presence of a BH and its activity. This view is supported by the fact that the GeV emission is delayed with respect to the γ-ray emission: it starts only after the P-GRB is over.

The GeV emission of GRB 090510 is particularly intense, reaching $E_{\rm LAT} = (5.78 \pm 0.60) \times 10^{52}$ erg. Such a large value, one of the largest observed among S-GRBs, is consistent with the large angular momentum of the newborn BH. This energetic cannot be explained in terms of NSs in view of the lower value of the gravitational binding energy.

The absence of GeV emission in S-GRFs is also confirmed from the strong upper limit to the GeV emission for S-GRBs imposed by the *Fermi*-LAT sensitivity. We assume for a moment that the GeV emission of an S-GRF is similar to that of S-GRBs. We then compute the observed GeV flux light curve of S-GRB 090510 at different redshifts, e.g., $z = 2.67$ and 5.52, which correspond to the redshifts of the S-GRB 081024B and of the S-GRB 140402A, respectively (Y. Aimuratov et al. 2016, in preparation). The result is that if we compare these computed flux light curves with the *Fermi*-LAT sensitivity of the Pass 8 Release 2 Version 6 Instrument Response Functions,[12] which is approximately 10^{-11} erg cm^{-2} s^{-1}, all

[12] http://www.slac.stanford.edu/exp/glast/groups/canda/lat_Performance_files/broadband_flux_sensitivity_p8r2_source_v6_all_10yr_zmax100_n03.0_e1.50_ts25.png

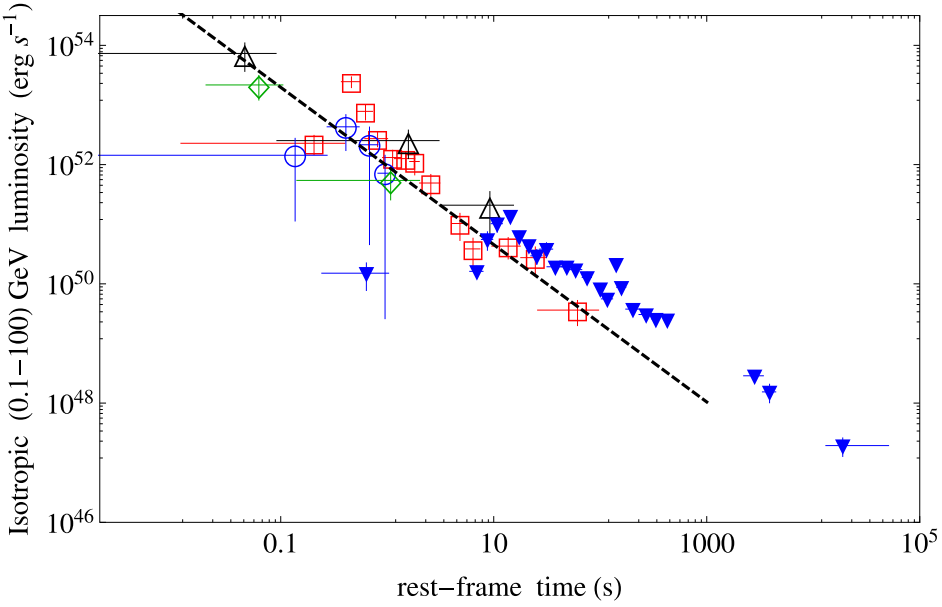

Figure 10. Isotropic rest-frame 0.1–100 GeV luminosity light curves of the S-GRBs 090510 (red squares), 081024B (green diamonds), 140402A (black triangles), and 140619B (blue circles) compared to that of the BdHN 130427A (blue downward-pointing triangles). The dashed black line marks the common behavior of all the S-GRB light curves, which goes as $t^{-1.32}$. In our approach this communality follows straightforwardly from the equality of the masses of the emerging extreme BH.

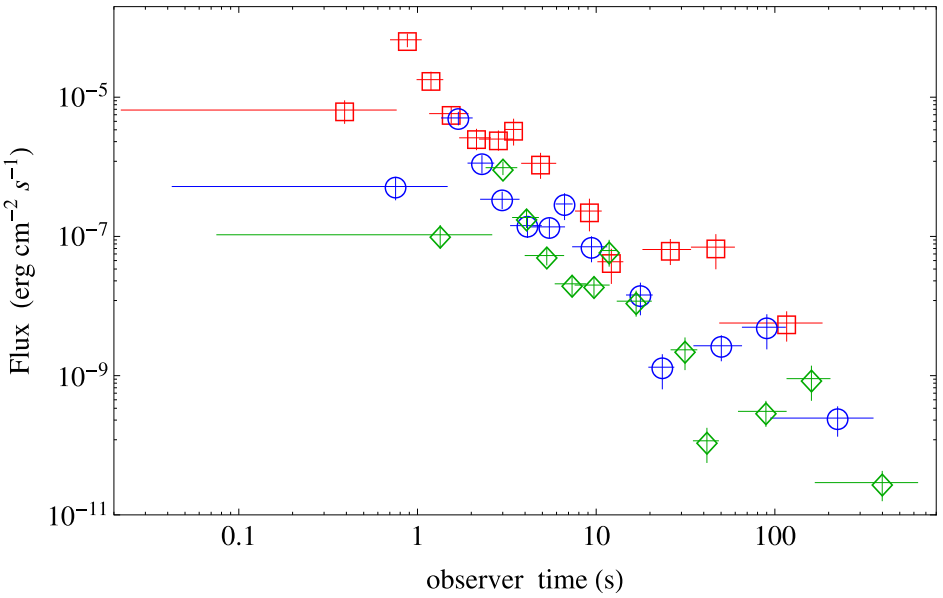

Figure 11. Observed 0.1–100 GeV flux light curve of the S-GRB 090510 (red squares) and the corresponding ones obtained by translating this S-GRB at $z = 2.67$ (blue circles) and at $z = 5.52$ (green diamonds).

of them are always well above the LAT broadband sensitivity by a factor of $\sim 10^5$ (see Figure 11). This result does not depend on the choice of the source. In their rest frame all the S-GRB GeV light curves follow a similar behavior. Therefore, the GeV emission of S-GRB 090510 is always above $\sim 10^5$ times the LAT sensitivity, even at higher redshifts. If we now assume that S-GRFs do conform to the same behavior of S-GRBs, the absence of detection of GeV emission implies that the S-GRFs necessarily have fluxes at least 10^5–10^6 times smaller than those of S-GRBs.

6.6. On the Energy Requirement of the GeV Emission

In order to estimate the energy requirement of the 0.1–100 GeV emission of Figure 10, we consider the accretion of mass $M_{\rm acc}$ onto a Kerr–Newman BH, dominated by its angular momentum and endowed with electromagnetic fields not influencing the geometry, which remains approximately that of a Kerr BH. We recall that if the infalling accreted material is in an orbit co-rotating with the BH spin, up to $\eta_+ = 42.3\%$ of the initial mass is converted into radiation, for a maximally rotating Kerr BH, while this efficiency drops to

$\eta_- = 3.8\%$ when the infalling material is on a counter-rotating orbit (see Ruffini & Wheeler 1969, in problem 2 of Section 104 in Landau & Lifshitz 2003). Therefore, the GeV emission can be expressed as

$$E_{\rm LAT} = f_b^{-1}\eta_{\pm} M_{\rm acc} c^2, \quad (5)$$

and depends not only on the efficiency $\eta_{\pm}$ in the accretion process of matter $M_{\rm acc}$ but also on the geometry of the emission described by the beaming factor $f_b \equiv 1 - \cos\theta$ (here θ is the half-opening angle of jet-like emission).

Depending on the assumptions we introduce in Equation (5), we can give constraints on the amount of accreted matter or on the geometry of the system.

For an isotropic emission, $f_b \equiv 1$, the accretion of $M_{\rm acc} \gtrsim 0.08\ M_\odot$, for the co-rotating case, and of $M_{\rm acc} \gtrsim 0.86\ M_\odot$, for the counter-rotating case, is required.

Alternatively, we can assume that the accreted matter comes from the crustal material from a $1.6 + 1.6\ M_\odot$ NS–NS binary progenitor. The crustal mass from the NL3 nuclear model for each of these NSs is $M_c = 4.30 \times 10^{-5}\ M_\odot$ (see, e.g., Belvedere et al. 2012, and Figure 2). Assuming that crustal material accounts also for the baryon load mass, e.g., $M_B \equiv E^{\rm tot}_{e^+e^-B}/c^2 = 1.22 \times 10^{-6}\ M_\odot$, the total available mass for accretion is $M_{\rm acc} \equiv 2M_c - M_B = 8.48 \times 10^{-5}\ M_\odot$. Then, the presence of a beaming is necessary: from Equation (5), a half-opening beaming angle $\theta \gtrsim 2\overset{\circ}{.}70$, for the co-rotating case, and $\theta \gtrsim 0\overset{\circ}{.}81$, for the counter-rotating case, would be required.

The above considerations are clearly independent from the relativistic beaming angle $\theta_r = \gamma_{\rm LAT}^{-1} \approx 0\overset{\circ}{.}1$, where the lower limit on the Lorentz factor $\gamma_{\rm LAT} \approx 550$ has been derived, in a different context, by Lithwick & Sari (2001) to the GeV luminosity light curve (see Figure 10).

Further consequences on these results for the estimate of the rate of these S-GRBs will be presented elsewhere (R. Ruffini et al. 2016, in preparation).

7. CONCLUSIONS

It is interesting to recall some of the main novelties introduced in this paper with respect to previous works on GRB 090510. Particularly noteworthy are the differences from the previous review of short bursts by Nakar (2007), made possible by the discovery of the high-energy emission by the *Fermi* team in this specific source (Ackermann et al. 2010). A new family of short bursts characterized by the presence of a BH and associated high-energy emission with LAT data now available comprises GRBs 081024B, 090227B, 090510, 140402A, and 140619B (see, e.g., Figure 10). The excellent data obtained by the *Fermi* team and interpreted within the fireshell model have allowed us to relate in this paper the starting point of the high-energy emission to the birth of a BH.

Our fireshell analysis assumes that the γ-ray and the GeV components originate from different physical processes. First, the interpretation of the prompt emission differs from the standard synchrotron model: we model the collisions of the baryon accelerated by the GRB outflow with the ambient medium following a fully relativistic approach (see Section 2). Second, we assume that the GeV emission originates from the matter accretion onto the newly born BH, and we show that indeed the energy requirement is fulfilled. This approach explains also the delayed onset of the GeV emission, i.e., it is observable only after the transparency condition, namely, after the P-GRB emission.

The joint utilization of the excellent data from the *Fermi*-GBM NaI-n6 and n7 and the BGO-b1 detectors and from the Mini-Calorimeter on board *AGILE* (Giuliani et al. 2010) has given strong observational support to our theoretical work. GRB 090510 has been analyzed in light of the recent progress achieved in the fireshell theory and the resulting new classification of GRBs. We show that GRB 090510 is an S-GRB, originating in a binary NS merger (see Figure 3). Such systems, by the absence of the associated SN events, are by far the simplest GRBs to be analyzed. Our analysis indicates the presence of three distinct episodes in S-GRBs: the P-GRB, the prompt emission, and the GeV emission. By following the precise identification of successive events predicted by the fireshell theory, we show evidence for the first indication of a Kerr BH or, possibly, a Kerr–Newman BH formation:

1. The P-GRB spectrum of GRB 090510, in the time interval from $T_0 + 0.528$ to $T_0 + 0.644$ s, is best fitted by a Comptonized component (see Figures 7 and 8 and Table 1), which is interpreted as a convolution of thermal spectra originating in a dyadotorus (see Cherubini et al. 2009; Ruffini 2009; see also Figure 1 and Section 2).
2. The prompt emission follows at the end of the P-GRB (see Figure 4). The analysis of the prompt emission within the fireshell model allows us to determine the inhomogeneities in the CBM giving rise to the spiky structure of the prompt emission and to estimate as well an averaged CBM density of $\langle n_{\rm CBM}\rangle = 8.7 \times 10^{-6}$ cm^{-3} obtained from a few CBM clouds of mass $\sim 10^{22}$ g and typical dimensions of $\sim 10^{16}$ cm (see Figure 9). Such a density is typical of galactic halos where binary NSs are expected to migrate due to large natal kicks.
3. The late X-ray emission of GRB 090510 does not follow the characteristic patterns expected in BdHN events (see Figure 5 and Pisani et al. 2013).
4. The GeV emission occurs at the end of the P-GRB emission and is initially concurrent with the prompt emission. This sequence occurs in both S-GRBs (Ruffini et al. 2015b) and BdHNe (Ruffini et al. 2015c). This delayed long-lasting ($\approx$200 s) GeV emission in GRB 090510 is one of the most intense ever observed in any GRB (see Figure 10; see also Ackermann et al. 2013; Ruffini et al. 2016).
5. We then consider accretion on co-rotating and counter-rotating orbits (see Ruffini & Wheeler 1969, in problem 2 of Section 104 in Landau & Lifshitz 2003) around an extreme Kerr BH. Assuming the accretion of the crustal mass $2M_c = 8.60 \times 10^{-5}\ M_\odot$ from a $1.6 + 1.6\ M_\odot$ NS–NS binary, fulfilling global charge neutrality (see Figure 2), geometrical beaming angles of $\theta \gtrsim 0\overset{\circ}{.}81$, for the co-rotating case, and $\theta \gtrsim 2\overset{\circ}{.}70$, for the counter-rotating case, are inferred. In order to fulfill the transparency condition, the initial Lorentz factor of the jetted material has to be $\gamma \gtrsim 550$ (see Section 6.6).
6. While there is evidence that the GeV emission must be jetted, no beaming appears to be present in the P-GRB and in the prompt emission, with important consequences for the estimate of the rate of such events (Ruffini et al. 2016).

7. The energetic and the possible beaming of the GeV emission requires the presence of a Kerr BH, or a Kerr–Newman BH dominated by its angular momentum and with electromagnetic fields not influencing the geometry (see also Section 6.5).
8. The self-consistency of the entire procedure has been verified by estimating, on the ground of the fireshell theory, the cosmological redshift of the source. The theoretical redshift is $z = 0.75 \pm 0.17$ (see Section 6.4), close to and consistent with the spectroscopically measured value $z = 0.903 \pm 0.003$ (Rau et al. 2009).
9. The values of $E_{\rm peak}$ and $E_{\rm iso}$ of GRB 090510 fulfill with excellent agreement the MuRuWaZha relation (see Section 5.2 and Figure 6; see also Ruffini et al. 2015a).

The main result of this article is that the dyadotorus manifests itself by the P-GRB emission and clearly preceeds the prompt emission phase, as well as the GeV emission originating from the newly formed BH. This contrasts with the usual assumption made in almost the totality of works relating BHs and GRBs in which the BH preceeds the GRB emission. In conclusion, in this article, we take GRB 090510 as the prototype of S-GRBs and perform a new time-resoved spectral analysis, in excellent agreement with that performed by the *AGILE* and the *Fermi* teams. Now this analysis, guided by a theoretical approach successfully tested in this new family of S-GRBs, is directed to identify a precise sequence of different events made possible by the exceptional quality of the data of GRB 090510. This includes a new structure in the thermal emission of the P-GRB emission, followed by the onset of the GeV emission linked to the BH formation, allowing us, as well, to derive the strucutre of the CBM from the spiky structure of the prompt emission. This sequence, for the first time, illustrates the formation process of a BH.

It is expected that this very unique condition of generating a jetted GeV emission in such a well-defined scenario of a newly born BH will possibly lead to a deeper understanding of the equally jetted GeV emission observed, but not yet explained, in a variety of systems harboring a Kerr BH. Among these systems we recall binary X-ray sources (see, e.g., Giacconi & Ruffini 1978, and references therein), microquasars (see, e.g., Chaty et al. 2015, and references therein), and, at larger scale, active galactic nuclei (see, e.g., Arsioli et al. 2015, and references therein).

We thank the editor and the referee for their comments, which helped to improve the presentation and the contextualization of our results. We are indebted to Marco Tavani for very interesting comments, as well as for giving us observational supporting evidence. This work made use of data supplied by the UK *Swift* Data Center at the University of Leicester. M.E., M.K., and Y.A. are supported by the Erasmus Mundus Joint Doctorate Program by Grant Numbers 2012-1710, 2013-1471, and 2014-0707, respectively, from the EACEA of the European Commission. C.C. acknowledges INdAM-GNFM for support. M.M. acknowledges the partial support of the project N 3101/GF4 IPC-11 and the target program F.0679 of the Ministry of Education and Science of the Republic of Kazakhstan.

REFERENCES

Ackermann, M., Ajello, M., Asano, K., et al. 2013, ApJS, 209, 11
Ackermann, M., Asano, K., Atwood, W. B., et al. 2010, ApJ, 716, 1178
Aksenov, A. G., Ruffini, R., & Vereshchagin, G. V. 2007, PhRvL, 99, 125003
Aksenov, A. G., Ruffini, R., & Vereshchagin, G. V. 2009, PhRvD, 79, 043008
Amati, L., & Della Valle, M. 2013, IJMPD, 22, 30028
Amati, L., Frontera, F., in't Zand, J. J. M., et al. 2004, A&A, 426, 415
Amati, L., Frontera, F., Tavani, M., et al. 2002, A&A, 390, 81
Antoniadis, J. 2015, ASSP, 40, 1
Arsioli, B., Fraga, B., Giommi, P., Padovani, P., & Marrese, P. M. 2015, A&A, 579, A34
Becerra, L., Bianco, C. L., Fryer, C. L., Rueda, J. A., & Ruffini, R. 2016, arXiv:1606.02523
Becerra, L., Cipolletta, F., Fryer, C. L., Rueda, J. A., & Ruffini, R. 2015, ApJ, 812, 100
Belvedere, R., Pugliese, D., Rueda, J. A., Ruffini, R., & Xue, S.-S. 2012, NuPhA, 883, 1
Belvedere, R., Rueda, J. A., & Ruffini, R. 2014, JKPS, 65, 897
Belvedere, R., Rueda, J. A., & Ruffini, R. 2015, ApJ, 799, 23
Berger, E. 2011, NewAR, 55, 1
Berger, E. 2014, ARA&A, 52, 43
Bianco, C. L., & Ruffini, R. 2005a, ApJL, 620, L23
Bianco, C. L., & Ruffini, R. 2005b, ApJL, 633, L13
Bloom, J. S., Kulkarni, S. R., & Djorgovski, S. G. 2002, AJ, 123, 1111
Bloom, J. S., Prochaska, J. X., Pooley, D., et al. 2006, ApJ, 638, 354
Bucciantini, N., Metzger, B. D., Thompson, T. A., & Quataert, E. 2012, MNRAS, 419, 1537
Calderone, G., Ghirlanda, G., Ghisellini, G., et al. 2015, MNRAS, 448, 403
Cavallo, G., & Rees, M. J. 1978, MNRAS, 183, 359
Cherubini, C., Geralico, A. J. A., Rueda, H., & Ruffini, R 2009, PhRvD, 79, 124002
Cipolletta, F., Cherubini, C., Filippi, S., Rueda, J. A., & Ruffini, R. 2015, PhRvD, 92, 023007
Curran, P. A., Starling, R. L. C., O'Brien, P. T., et al. 2008, A&A, 487, 533
Dai, Z. G., Wang, X. Y., Wu, X. F., & Zhang, B. 2006, Sci, 311, 1127
Damour, T., & Ruffini, R. 1975, PhRvL, 35, 463
Della Valle, M. 2011, IJMPD, 20, 1745
De Pasquale, M., Schady, P., Kuin, N. P. M., et al. 2010, ApJL, 709, L146
Dezalay, J.-P., Barat, C., Talon, R., et al. 1992, in Gamma-ray bursts, Proc. of the Workshop, AIP Conf. Ser. 265, ed. W. S. Paciesas & G. J. Fishman (Melville, NY: AIP), 304
Eichler, D., Livio, M., Piran, T., & Schramm, D. N. 1989, Natur, 340, 126
Enderli, M., Bianco, C. L., Izzo, L., et al. 2014, in Proceedings of Swift: 10 Years of Discovery (SWIFT 10) (Trieste: SISSA) (pos.sissa.it/archive/conferences/233/073/SWIFT%2010_073.pdf)
Endrizzi, A., Ciolfi, R., Giacomazzo, B., Kastaun, W., & Kawamura, T. 2016, arXiv:1604.03445
Fong, W., Berger, E., & Fox, D. B. 2010, ApJ, 708, 9
Fruchter, A. S., Levan, A. J., Strolger, L., et al. 2006, Natur, 441, 463
Fryer, C. L., Rueda, J. A., & Ruffini, R. 2014, ApJL, 793, L36
Gehrels, N., Ramirez-Ruiz, E., & Fox, D. B. 2009, ARA&A, 47, 567
Giacconi, R., & Ruffini, R. (ed.) 1978, Physics and Astrophysics of Neutron Stars and Black Holes (Amsterdam: North Holland Publishing Company), 907
Giuliani, A., Fuschino, F., Vianello, G., et al. 2010, ApJL, 708, L84
Golenetskii, S., Aptekar, R., Mazets, E., et al. 2009, GCN, 9344, 1
Goodman, J. 1986, ApJL, 308, L47
Guiriec, S., Connaughton, V., & Briggs, M. 2009, GCN, 9336, 1
Hansen, B. M. S., & Lyutikov, M. 2001, MNRAS, 322, 695
Heise, J. 2003, in AIP Conf. Ser. 662, Gamma-Ray Burst and Afterglow Astronomy 2001: A Workshop Celebrating the First Year of the HETE Mission, ed. G. R. Ricker & R. K. Vanderspek (Melville, NY: AIP), 229
Hoversten, E. A., Barthelmy, S. D., Burrows, D. N., et al. 2009, GCN, 9331, 1
Izzo, L., Ruffini, R., Penacchioni, A. V., et al. 2012, A&A, 543, A10
Klebesadel, R. W. 1992, in Gamma-Ray Bursts—Observations, Analyses and Theories, ed. C. Ho, R. I. Epstein, & E. E. Fenimore (Cambridge: Cambridge Univ. Press)
Kobayashi, S., Piran, T., & Sari, R. 1997, ApJ, 490, 92
Kopač, D., D'Avanzo, P., Melandri, A., et al. 2012, MNRAS, 424, 2392
Kouveliotou, C., Meegan, C. A., Fishman, G. J., et al. 1993, ApJL, 413, L101
Kumar, P., & Zhang, B. 2015, PhR, 561, 1
Landau, L. D., & Lifshitz, E. M. 2003, The Classical Theory of Fields (Oxford: Butterworth-Heinemann) IV rev. Engl. ed.
Lazzati, D. 2005, MNRAS, 357, 722
Lee, W. H., Ramirez-Ruiz, E., & Page, D. 2004, ApJL, 608, L5
Lithwick, Y., & Sari, R. 2001, ApJ, 555, 540
Longo, F., Moretti, E., Barbiellini, G., et al. 2009, GCN, 9343, 1
Lü, H.-J., & Zhang, B. 2014, ApJ, 785, 74
Mazets, E. P., Golenetskii, S. V., Ilinskii, V. N., et al. 1981, Ap&SS, 80, 3

Meegan, C., Lichti, G., Bhat, P. N., et al. 2009, ApJ, 702, 791
Meszaros, P., & Rees, M. J. 1997, ApJL, 482, L29
Metzger, B. D., Giannios, D., Thompson, T. A., Bucciantini, N., & Quataert, E. 2011, MNRAS, 413, 2031
Mirabel, I. F., Chaty, S., Rodríguez, L. F., & Sauvage, M, M. 2015, in IAU Symp. 313, Extragalactic Jets from Every Angle (Paris: IAU), 370
Muccino, M., Ruffini, R., Bianco, C. L., Izzo, L., & Penacchioni, A. V. 2013a, ApJ, 763, 125
Muccino, M., Ruffini, R., Bianco, C. L., et al. 2013b, ApJ, 772, 62
Nakar, E. 2007, PhR, 442, 166
Narayan, R., Paczynski, B., & Piran, T. 1992, ApJL, 395, L83
Narayan, R., Piran, T., & Shemi, A. 1991, ApJL, 379, L17
Nava, L., Vianello, G., Omodei, N., et al. 2014, MNRAS, 443, 3578
Ohmori, N., Noda, K., Sonoda, E., et al. 2009, GCN, 9355, 1
Ohno, M., & Pelassa, V. 2009, GCN, 9334, 1
Oliveira, F. G., Rueda, J. A., & Ruffini, R. 2014, ApJ, 787, 150
Olofsson, G., Ergon, M., Malesani, D., et al. 2009, GCN, 9338, 1
Omodei, N., Granot, J., Meszaros, P., et al. 2009, GCN, 9350, 1
Paczynski, B. 1986, ApJL, 308, L43
Patricelli, B., Bernardini, M. G., Bianco, C. L., et al. 2012, ApJ, 756, 16
Penacchioni, A. V., Ruffini, R., Izzo, L., et al. 2012, A&A, 538, A58
Perley, D. A., Cenko, S. B., Corsi, A., et al. 2014, ApJ, 781, 37
Piran, T. 2005, RvMP, 76, 1143
Pisani, G. B., Izzo, L., Ruffini, R., et al. 2013, A&A, 552, L5
Popham, R., Woosley, S. E., & Fryer, C. 1999, ApJ, 518, 356
Rau, A., McBreen, S., & Kruehler, T. 2009, GCN, 9353, 1
Rees, M. J., & Meszaros, P. 1992, MNRAS, 258, 41
Rhoades, C. E., & Ruffini, R. 1974, PhRvL, 32, 324
Rosswog, S., Ramirez-Ruiz, E., & Davies, M. B. 2003, MNRAS, 345, 1077
Rotondo, M., Rueda, J. A., Ruffini, R., & Xue, S.-S. 2011a, PhLB, 701, 667
Rotondo, M., Rueda, J. A., Ruffini, R., & Xue, S.-S. 2011b, PhRvC, 83, 045805
Rueda, J. A., & Ruffini, R. 2012, ApJ, 758, L7
Rueda, J. A., & Ruffini, R. 2013, IJMPD, 22, 1360007
Rueda, J. A., Ruffini, R., Wu, Y.-B., & Xue, S.-S. 2014, PhRvC, 89, 035804
Rueda, J. A., Ruffini, R., & Xue, S.-S. 2011, NuPhA, 872, 286
Ruffini, R. 2009, in The Ergosphere and Dyadosphere of Black Holes, ed. D. L. Wiltshire, M. Visser, & S. Scott (Cambridge: Cambridge Univ. Press), 161
Ruffini, R. 2015, in Thirteenth Marcel Grossmann Meeting: On Recent Developments in Theoretical and Experimental General Relativity, Astrophysics and Relativistic Field Theories, Proc. of the MG13 Meeting on General Relativity, ed. K. Rosquist (Singapore: World Scientific Publishing), 242
Ruffini, R., Bernardini, M. G., Bianco, C. L., et al. 2007, in The Obscured Universe, Proc. of the VI INTEGRAL Workshop, ESA SP-622, ed. S. Grebenev, R. Sunyaev, & C. Winkler (Noordwijk: ESA Publication Division), 561
Ruffini, R., Bianco, C. L., Enderli, M., et al. 2015a, GCN, 18296, 1
Ruffini, R., Bianco, C. L., Fraschetti, F., Xue, S.-S., & Chardonnet, P. 2001a, ApJL, 555, L107
Ruffini, R., Bianco, C. L., Fraschetti, F., Xue, S.-S., & Chardonnet, P. 2001b, ApJL, 555, L113
Ruffini, R., Bianco, C. L., Fraschetti, F., Xue, S.-S., & Chardonnet, P. 2001c, ApJL, 555, L117
Ruffini, R., Muccino, M., Bianco, C. L., et al. 2014, A&A, 565, L10
Ruffini, R., Muccino, M., Kovacevic, M., et al. 2015b, ApJ, 808, 190
Ruffini, R., Rueda, J. A., Muccino, M., et al. 2016, arXiv:1602.02732
Ruffini, R., Salmonson, J. D., Wilson, J. R., & Xue, S. 2000, A&A, 359, 855
Ruffini, R., Salmonson, J. D., Wilson, J. R., & Xue, S.-S. 1999, A&A, 350, 334
Ruffini, R., Wang, Y., Enderli, M., et al. 2015c, ApJ, 798, 10
Ruffini, R., & Wilson, J. 1973, PhRvL, 31, 1362
Ruffini, R., & Wilson, J. R. 1975, PhRvD, 12, 2959
Ruffini, R., & Wheeler, J. A. 1969, in Significance of Space Research for Fundamental Physics, Proc. of the ESRO Collaboration, ed. A. F. Moore & V. Hardy (Paris: European Space Research Organization), 45
Ruiz, M., Lang, R. N., Paschalidis, V., & Shapiro, S. L. 2016, ApJL, 824, L6
Sahu, K. C., Livio, M., Petro, L., et al. 1997, Natur, 387, 476
Salmonson, J. D., & Wilson, J. R. 2002, ApJ, 578, 310
Smith, N. 2014, ARA&A, 52, 487
Smith, N., Li, W., Filippenko, A. V., & Chornock, R. 2011, MNRAS, 412, 1522
Soderberg, A. M., Berger, E., Kasliwal, M., et al. 2006a, ApJ, 650, 261
Soderberg, A. M., Kulkarni, S. R., Nakar, E., et al. 2006b, Natur, 442, 1014
Strong, I. B., Klebesadel, R. W., & Evans, W. D. 1975, in Annals of the New York Academy of Sciences 262, Seventh Texas Symp. on Relativistic Astrophysics, ed. P. G. Bergman, E. J. Fenyves, & L. Motz (New York: New York Academy of Sciences), 145
Svensson, K. M., Levan, A. J., Tanvir, N. R., Fruchter, A. S., & Strolger, L.-G. 2010, MNRAS, 405, 57
Tavani, M. 1998, ApJL, 497, L21
Troja, E., King, A. R., O'Brien, P. T., Lyons, N., & Cusumano, G. 2008, MNRAS, 385, L10
Tsang, D., Read, J. S., Hinderer, T., Piro, A. L., & Bondarescu, R. 2012, PhRvL, 108, 011102
van Paradijs, J., Groot, P. J., Galama, T., et al. 1997, Natur, 386, 686
Woosley, S. E. 1993, ApJ, 405, 273
Woosley, S. E., & Bloom, J. S. 2006, ARA&A, 44, 507
Zalamea, I., & Beloborodov, A. M. 2011, MNRAS, 410, 2302
Zel'dovich, Y. B., Ivanova, L. N., & Nadezhin, D. K. 1972, SvA, 16, 209
Zhang, B., & Mészáros, P. 2001, ApJL, 552, L35
Zhang, C. M., Wang, J., Zhao, Y. H., et al. 2011, A&A, 527, A83
Zhang, F.-W., Shao, L., Yan, J.-Z., & Wei, D.-M. 2012, ApJ, 750, 88
Zou, Y.-C., Fan, Y.-Z., & Piran, T. 2011, ApJL, 726, L2

The Astrophysical Journal, 832:136 (24pp), 2016 December 1 doi:10.3847/0004-637X/832/2/136

ON THE CLASSIFICATION OF GRBs AND THEIR OCCURRENCE RATES

R. Ruffini[1,2,3,4], J. A. Rueda[1,2,4], M. Muccino[1,2], Y. Aimuratov[1,2], L. M. Becerra[1,2], C. L. Bianco[1,2], M. Kovacevic[1,2,3], R. Moradi[1,2], F. G. Oliveira[1,2,3], G. B. Pisani[1,2], and Y. Wang[1,2]
[1] Dipartimento di Fisica and ICRA, Sapienza Università di Roma, Piazzale Aldo Moro 5, I-00185 Rome, Italy
[2] ICRANet, Piazza della Repubblica 10, I-65122 Pescara, Italy
[3] Université de Nice Sophia Antipolis, CEDEX 2, Grand Château Parc Valrose, Nice, France
[4] ICRANet-Rio, Centro Brasileiro de Pesquisas Físicas, Rua Dr. Xavier Sigaud 150, 22290-180 Rio de Janeiro, Brazil
Received 2015 December 21; revised 2016 September 6; accepted 2016 September 7; published 2016 November 23

ABSTRACT

There is mounting evidence for the binary nature of the progenitors of gamma-ray bursts (GRBs). For a long GRB, the induced gravitational collapse paradigm proposes as progenitor, or "in-state," a tight binary system composed of a carbon–oxygen core (CO_{core}) undergoing a supernova explosion that triggers hypercritical accretion onto a neutron star (NS) companion. For a short GRB (S-GRB), an NS–NS merger is traditionally adopted as the progenitor. We divide long and S-GRBs into two subclasses, depending on whether or not a black hole (BH) is formed in the merger or in the hypercritical accretion process exceeding the NS critical mass. For long bursts, when no BH is formed, we have the subclass of X-ray flashes (XRFs), with isotropic energy $E_{\rm iso} \lesssim 10^{52}$ erg and rest-frame spectral peak energy $E_{p,i} \lesssim 200$ keV. When a BH is formed, we have the subclass of binary-driven hypernovae (BdHNe), with $E_{\rm iso} \gtrsim 10^{52}$ erg and $E_{p,i} \gtrsim 200$ keV. In analogy, short bursts are similarly divided into two subclasses. When no BH is formed, short gamma-ray flashes (S-GRFs) occur, with $E_{\rm iso} \lesssim 10^{52}$ erg and $E_{p,i} \lesssim 2$ MeV. When a BH is formed, the authentic S-GRBs occur, with $E_{\rm iso} \gtrsim 10^{52}$ erg and $E_{p,i} \gtrsim 2$ MeV. We give examples and observational signatures of these four subclasses and their rate of occurrence. From their respective rates it is possible that "in-states" of S-GRFs and S-GRBs originate from the "out-states" of XRFs. We indicate two additional progenitor systems: white dwarf–NS and BH–NS. These systems have hybrid features between long and short bursts. In the case of S-GRBs and BdHNe evidence is given of the coincidence of the onset of the high-energy GeV emission with the birth of a Kerr BH.

Key words: binaries: general – black hole physics – gamma-ray burst: general – stars: neutron – supernovae: general – white dwarfs

1. INTRODUCTION

On 1974 February, at the same AAAS meeting in San Francisco where the discovery of gamma-ray bursts (GRBs) by the Vela satellites was publicly announced (Strong et al. 1975), the possible relation of GRBs to the "moment of gravitational collapse" leading to a black hole (BH) formation was advanced (see Gursky & Ruffini 1975). Damour & Ruffini (1975) considered, for definiteness, the vacuum polarization process occurring in an overcritical Kerr–Newman BH (KNBH). Evidence was given for (a) the formation of a vast amount of e^+e^--baryon plasma; (b) the energetics of GRBs of the order of $E_{\rm max} \approx 10^{54} M_{\rm BH}/M_\odot$ erg, where $M_{\rm BH}$ is the BH mass, implying their cosmological origin; and (c) ultra-high-energy cosmic rays with energy up to $\sim 10^{20}$ eV originating from such an extreme electrodynamical process. Soon after, the role of an e^+e^- plasma for the origin of GRBs was also considered by Cavallo & Rees (1978). It took almost 30 yr to clarify some of the analogies and differences between these two processes of e^+e^--pair creation leading, respectively, to the alternative concepts of "fireball" and "fireshell" (Aksenov et al. 2007, 2009).

Already in 1989, well before the establishment of the GRB cosmological nature and energetics, Eichler et al. (1989) gave support to the cosmological interpretation of GRBs and indicated in merging neutron star (NS) binaries their possible origin. They also pointed out the relevance of such NS–NS mergers for the occurrence of *r*-process, as well as for the emission of gravitational radiation, indicating the uncertainty in the determination of their rate of occurrence.

Following the launch of the *Compton Gamma Ray Observatory* and the observations by the BATSE detector (Meegan et al. 1992), a phenomenological classification based on the prompt T_{90} duration was advanced: GRBs were classified into long GRBs (L-GRBs) for $T_{90} > 2$ s and short GRBs (S-GRBs) for $T_{90} < 2$ s (Dezalay et al. 1992; Klebesadel 1992, pp. 161–68; Kouveliotou et al. 1993; Tavani 1998).

Shortly after, Narayan et al. (1992) indicated the possible cosmological origin of S-GRBs originating in binary NS mergers. They also introduced the clear indication of the role of $\nu\bar{\nu}$ annihilation leading to the formation of an e^+e^- plasma. This paper was followed by a large number of theoretical works including the gravitational wave emission in Newtonian, post-Newtonian, and general relativistic treatments (see, e.g., Rasio & Shapiro 1999), as well as the $\nu\bar{\nu}$ annihilation leading to an e^+e^- plasma (see, e.g., Salmonson & Wilson 2002 and Rosswog et al. 2003 and references therein).

Soon after the paper by Narayan et al. (1992), Woosley (1993) also supported the cosmological origin of GRBs and introduced the concept of BH accretion disks, produced by the collapse of a very massive star. Such a system was indicated by its author as a *collapsar* and was assumed to be the origin of ultrarelativistic jets expected to occur by the same author in L-GRBs. For a recent review see MacFadyen & Woosley (1999), MacFadyen et al. (2001), and Woosley & Bloom (2006).

After the determination of the cosmological nature of GRBs (Costa et al. 1997; Metzger et al. 1997; van Paradijs et al. 1997) and the confirmation of their outstanding energy ($\approx 10^{54}$ erg), we returned to our GRB scenario (Damour & Ruffini 1975). In

a period of 4 yr, from 1997 to 2001, we developed a fully relativistic GRB theoretical model examining, as well, the dynamics of the e^+e^- plasma originating the GRB emission (the fireshell model; see, e.g., Preparata et al. 1998; Ruffini et al. 1999, 2000, 2001a, 2001b, 2001c; see also Section 2). The fireshell model applies to both S-GRBs and L-GRBs.

The origin of S-GRBs from NS–NS (or NS–BH) binaries as "in-states" has been confirmed by strong observational and theoretical evidence (see, e.g., Goodman 1986; Paczynski 1986; Eichler et al. 1989; Narayan et al. 1991, 1992; Meszaros & Rees 1997; Rosswog et al. 2003; Lee et al. 2004; Berger 2014). In this article we address specifically some of the latest results within the fireshell model (Muccino et al. 2013; Ruffini et al. 2015b) on the possible presence or absence of a BH formation in NS–NS mergers; the consequent classification of short bursts into short gamma-ray flashes (S-GRFs), when no BH is formed (see Section 6), and S-GRBs, when a BH is formed (see Section 7); and the computation of their occurrence rate (see Section 10).

The application of the fireshell model to the case of L-GRBs followed a longer path for reaching a proper understanding of the overall phenomenon. The first application of our model to an L-GRB was implemented on GRB 991216 (Ruffini et al. 2001a, 2001b, 2001c, 2002, 2004, 2006a). In these papers a clear difference between the thermal component observed at the transparency of the e^+e^- plasma, the proper GRB (P-GRB) emission (Ruffini et al. 1999, 2000), and the nonthermal remaining part, later called prompt emission (Ruffini et al. 2001b), was evidenced. This fully relativistic approach was not readily accepted by the GRB community, also in view of its objective technical complexity and novelties in the theoretical physics scenario. Some authors attempted to describe the GRB phenomenon by simplified Newtonian approaches, e.g., those based on the concept of *magnetars* (Usov 1992; Dai & Lu 1998a, 1998b; Kluźniak & Ruderman 1998; Zhang & Mészáros 2001). As detailed observations of the X-ray afterglow by *Swift*-XRT (Evans et al. 2007) were obtained, as well as high-energy emission by *Fermi*-LAT (Atwood et al. 2009), our model has correspondingly evolved, pointing out the precise common power-law behavior of the rest-frame 0.3–10 keV X-ray luminosity light curves (Pisani et al. 2013), as well as the nesting properties (Ruffini et al. 2014b). As pointed out in the present article, the concept of L-GRBs has evolved into X-ray flashes (XRFs) and binary-driven hypernovae (BdHNe), depending on the possible presence or absence of a BH in their formation process (see also Ruffini et al. 2015c).

It is appropriate to recall that the quest for having progenitors for the collapsar hypothesized by Woosley (1993) led to an interesting direction of research dealing with a binary system composed of two very massive stars of $\approx 50\ M_\odot$ each. The large masses involved in these systems were introduced in order to form a BH at the end of their evolution. Similarly, the large amount of angular momentum of the system would guarantee the formation of an accretion disk needed in the collapsar model (Fryer et al. 1999). Up to six different scenarios were there envisaged leading to a *collapsar*, as well as a few leading, alternatively, to a variety of binary compact systems. The need for choosing low-metallicity massive stars followed from the expectation of the formation of large BHs in their evolution (Fryer et al. 1999). The elimination of H from metal-rich massive stars would follow naturally, but the formation of a BH was not expected in their final stage of evolution (Woosley 1993).

The spatial and temporal coincidence of an L-GRB explosion with an optical supernova (SN), first observed in the association between GRB 980425 and SN 1998bw, created a profound conceptual turmoil in the GRB community. Woosley and collaborators postulated the birth of an SN out of a collapsar (see, e.g., Woosley & Bloom 2006, and references therein).

In our approach, GRBs were supposed to originate from the BH formation, while SNe were expected to lead only to NSs (see, e.g., Ruffini 2015, and references therein). We consequently introduced a new paradigm to explain the coincidence of these two qualitative and quantitative different astrophysical events in space and time: the birth of an SN and the occurrence of a GRB. The induced gravitational collapse (IGC) paradigm was then introduced (see, e.g., Ruffini et al. 2001c, 2006b, 2007, 2008; Izzo et al. 2012b; Rueda & Ruffini 2012; Fryer et al. 2014). This approach differs from alternative descriptions of the GRB-SN coincidences occurring, e.g., in the *magnetars* and the *collapsar* models, where the two events are coming from a single progenitor star, and takes full advantage of the recent observations of SNe Ibc in interacting binary systems (Smartt 2009).

In a first formulation we considered a finely tuned process: the GRB triggering the explosion of a binary companion star very close to the onset of the SN (Ruffini et al. 2001c). This scenario soon led to the alternative IGC paradigm in which a CO_{core} undergoes an SN explosion in the presence of an NS companion in a tight binary system. This is also by itself an unlikely event that, in order to occur, needs a fine-tuning of the initial conditions of the binary system. This scenario was shown to be consistent with population synthesis analysis (Fryer et al. 1999, 2015). The SN explosion induces a hypercritical accretion of its ejecta onto the companion NS, leading to the formation of a more massive NS (MNS), when the NS critical mass M_{crit} is not reached, or to the formation of a BH with the associated GRB emission in the opposite case (see, e.g., Rueda & Ruffini 2012; Fryer et al. 2014). The IGC scenario was first tested and verified in GRB 090618 (Izzo et al. 2012b, 2012c). It soon became clear that the occurrence of a GRB is far from being a single event, but it is part of an authentic laboratory composed of a variety of astrophysical relativistic phenomena preceeding and following the prompt GRB emission.

We adopted as progenitor of our CO_{core}–NS binary system the massive binaries independently considered in Fryer et al. (1999) and Nomoto et al. (1994, 1995). In our case, the late evolution of such massive binary systems does not lead to a collapsar, nor to a hypernova, but to a much richer and vast number of possibilities, made possible by our IGC paradigm. Consistently with the considerations by Sakamoto et al. (2005), indicating that XRFs, X-ray-rich bursts, and all L-GRBs are part of the same population, which we show to originate in the hypercritical accretion process of the SN ejecta onto a binary companion NS.

In agreement with the considerations by Soderberg et al. (2006), Guetta & Della Valle (2007), and Liang et al. (2007) for a subclassification of long bursts into low-luminosity and high-luminosity GRBs, we have divided the long bursts into two different scenarios depending on the distance between the CO_{core} and the NS binary companion (Becerra et al. 2015).

Correspondingly, two different subclasses of long bursts, both originating in the hypercritical accretion process of the IGC scenario, have been shown to exist (Becerra et al. 2015; Ruffini et al. 2015c): the XRFs, which clearly include low-luminosity GRBs, such as GRB 060218 (Campana et al. 2006), when no BH is formed (see Section 4), and the BdHNe, such as GRB 130427A (Ruffini et al. 2015c), when a BH is formed (see Section 5). Their occurrence rates have been computed (see Section 10). Instead of proposing just a new classification, we also give the description of its underlying physical origin: the hypercritical accretion process of the SN ejecta onto a binary companion NS, with the full associated theoretical treatments at the basis of the IGC paradigm.

To the above four subclasses of long and short bursts, we have recently added a new hybrid subclass of ultrashort GRBs (U-GRBs), which, as recently pointed out in Fryer et al. (2015), can originate during the further evolution of the BdHNe out-states. Indeed, nearly 100% of the NS–BH binaries that are the outcome of BdHNe remain bound. Their orbital velocities are high, and even large kicks are unlikely to unbind these systems. They represent a new family of NS–BH binaries unaccounted for in current standard population synthesis analyses (see, e.g., Fryer et al. 2015 and Section 8).

The above considerations based on the IGC paradigm and the NS–NS paradigm as progenitors encompass and classify into subclasses most of the known astrophysical systems related to GRBs. We finally recall the existence of a class of L-GRBs occurring in a low-density circumburst medium (CBM) with density $\sim 10^{-3}\,\mathrm{cm}^{-3}$, with hybrid short/long burst properties in their γ-ray light curves: (1) an initial spike-like harder emission and (2) a prolonged softer emission observed for up to 100 s. These bursts do not have an associated SN, even though in the case of a low value of the cosmological redshift its detection would not be precluded. The prototype of such systems is GRB 060614 (Della Valle et al. 2006). The progenitor for this class of long bursts has been identified in a binary system composed of an NS and a white dwarf (WD) (Caito et al. 2009). Their merger leads to an MNS with additional orbiting material, but not to an authentic GRB. We refer to these systems, historically addressed as disguised S-GRBs, as gamma-ray flashes (GRFs; see, e.g., GRB 060614, Caito et al. 2009; and GRB 071227, Caito et al. 2010).

In the following we adopt the term *burst* only for those systems leading to BH formation, namely, S-GRBs, U-GRBs, and BdHNe. We refer to the term *flash*, instead, only for those systems not leading to BH formation, namely, S-GRFs, GRFs, and XRFs.

The main topic addressed in the present article is to estimate the rates of occurrence of the XRFs, BdHNe, S-GRFs, S-GRBs, U-GRBs, and GRFs and to give a general description of these GRB subclasses. In Section 2 we present a short summary on the fireshell model. In Section 3 we discuss the 10^{52} erg lower limit in binary systems leading to BH formation. After describing the observational properties of the above subclasses, their interpretation within the IGC paradigm, the NS–NS merger scenario, and the fireshell scenario, we present some prototypes (see Sections 4, 5, 6, 7, 8, and 9, respectively). We then proceed in Section 10 to estimate their observed occurrence rates and to compare and contrast our results with those outlined in the literature (see, e.g., Soderberg et al. 2006; Guetta & Della Valle 2007; Liang et al. 2007; Virgili et al. 2009, 2011; Rangel Lemos et al. 2010; Wanderman & Piran 2010, 2015; Kovacevic et al. 2014; Sun et al. 2015). We then draw some general conclusions in Section 11.

A standard flat ΛCDM cosmological model with $\Omega_M = 0.27$, $\Omega_\Lambda = 0.73$, and $H_0 = 71\,\mathrm{km\,s^{-1}\,Mpc^{-1}}$ is adopted throughout the paper. A summary of acronyms used throughout the paper is shown in Table 1.

Table 1
Alphabetic Ordered List of the Acronyms Used in This Work

Extended wording	Acronym
Binary-driven hypernova	BdHN
black hole	BH
Carbon–oxygen core	$\mathrm{CO_{core}}$
Circumburst medium	CBM
Equitemporal surfaces	EQTS
Gamma-ray burst	GRB
Gamma-ray flash	GRF
Induced gravitational collapse	IGC
Kerr–Newman black hole	KNBH
Massive neutron star	MNS
Neutron star	NS
New neutron star	νNS
Proper gamma-ray burst	P-GRB
Short gamma-ray burst	S-GRB
Short gamma-ray flash	S-GRF
Supernova	SN
Ultrashort gamma-ray burst	U-GRB
White dwarf	WD
X-ray flash	XRF

2. SUMMARY OF THE FIRESHELL MODEL

The fireshell model for GRBs (see, e.g., Ruffini et al. 2001a, 2001b, 2001c) has been introduced to explain the GRB phenomenon as originating in the gravitational collapse leading to the formation of a BH (Damour & Ruffini 1975). The GRB emission results by taking into proper account relativistic magnetohydrodynamical effects, quantum electrodynamical processes, and relativistic spacetime transformations.

The role of the relativistic magnetohydrodynamical effects arising in the gravitational collapse of a globally neutral magnetized plasma has been first considered in Ruffini & Wilson (1975), where the occurrence of a local charge separation, during a globally neutral accretion process, led to the development of overcritical electric fields at the onset of a KNBH formation.[5] These overcritical fields and, consequently, the vacuum polarization process leading to the creation of an e^+e^- plasma have been considered in Damour & Ruffini (1975), for the sake of definiteness in a KNBH, as the energy source of GRBs:[6] the pair creation process is fully reversible, and as a result, a highly efficient energy extraction mechanism occurs, which may deliver as much as $E_{\mathrm{max}} \approx 10^{54}\, M_{\mathrm{BH}}/M_\odot$ erg.

Later on, the concept of *dyadotorus* for a KNBH (Cherubini et al. 2009; Ruffini 2009) was introduced to describe the region where pair creation occurs, leading to the formation of a BH. The dynamics of an optically thick *fireshell* of e^+e^- plasma of

[5] Overcritical electric fields are defined as larger than the critical value $E_c = m_e^2 c^3/(\hbar e)$, where m_e is the electron mass, c the speed of light in the vacuum, $\hbar$ the reduced Planck constant, and e the electron charge.

[6] The role of an e^+e^- plasma for the origin of GRBs was also considered independently by Cavallo & Rees (1978).

total energy $E^{\rm tot}_{e^+e^-}$, i.e., its expansion and self-acceleration due to its own internal pressure, has been described in Ruffini et al. (1999). The effect of baryonic contamination, i.e., the remnant of the collapsed object, on the dynamics of the fireshell was then considered in Ruffini et al. (2000), where it was shown that even after the engulfment of a baryonic mass M_B, quantified by the baryon load $B = M_B c^2/E^{\rm tot}_{e^+e^-}$, the fireshell remains still optically thick and continues its self-acceleration up to ultrarelativistic velocities (Aksenov et al. 2007, 2009). When the fireshell reaches the transparency condition, a flash of thermal radiation termed P-GRB is emitted (Ruffini et al. 1999, 2000). The dynamics of the fireshell up to the transparency condition is fully described by $E^{\rm tot}_{e^+e^-}$ and B: solutions with $B \leqslant 10^{-2}$ are characterized by regular relativistic expansion; for $B > 10^{-2}$ turbulence and instabilities occur (Ruffini et al. 2000).

The P-GRB emission is followed by the prompt emission (Ruffini et al. 2001b). The prompt emission originates in the collisions of the accelerated baryons left over after transparency, moving at Lorentz factor $\Gamma \approx 100$–1000, with interstellar clouds of the CBM (Ruffini et al. 2002, 2004, 2005). These interactions give rise to a modified blackbody spectrum in the comoving frame (Patricelli et al. 2012). The resulting observed spectral shape, once the constant arrival time effect is taken into account in the equitemporal surfaces (EQTSs; see Bianco & Ruffini 2005a, 2005b), is in general nonthermal, as a result of the convolution of a large number of modified thermal spectra with different Lorentz factors and temperatures. To reproduce the prompt emission light curve and spectra, three additional parameters, all related to the properties of the CBM, are required: the CBM density profile $n_{\rm CBM}$, the filling factor $\mathcal{R}$ that accounts for the size of the effective emitting area, and a low-energy power-law index α of the modified blackbody spectrum (Patricelli et al. 2012). These parameters are obtained by running a trial-and-error simulation of the observed prompt emission light curves and spectra.

To describe the dynamics of such an e^+e^--baryon plasma from the vicinity of a BH all the way up to ultrarelativistic velocities at infinity, both in the P-GRB and in the prompt emission, the appropriate relative spacetime transformation paradigm was discussed in Ruffini et al. (2001a). It relates the observed GRB signal to its past light cone, defining the events on the worldline of the source that is essential for the interpretation of the data. Particular attention has been there given to the explicit equations relating the comoving time, the laboratory time, the arrival time, and the arrival time at the detector corrected by the cosmological effects, consistently with the equation of motion of the system (see also Bianco & Ruffini 2004, 2005a, 2005b, 2006), compared and contrasted with the corresponding treatments in the literature (see, e.g., Sari 1997, 1998; Waxman 1997; Panaitescu & Meszaros 1998; Rees & Meszaros 1998; Chiang & Dermer 1999; Granot et al. 1999; Panaitescu & Mészáros 1999).

As recalled above, the evolution of a baryon-loaded pair plasma is generally described in terms of $E^{\rm tot}_{e^+e^-}$ and B, and it is independent of the way the pair plasma is created. Given this generality, in addition to the specific case of the dyadotorus mentioned above, these concepts can be applied as well in the case of a pair plasma created via the $\nu\bar{\nu} \leftrightarrow e^+e^-$ mechanism in an NS merger as described in Narayan et al. (1992), Salmonson & Wilson (2002), and Rosswog et al. (2003), or in the hyperaccretion disks around BHs as described in Woosley (1993) and Zalamea & Beloborodov (2011), assuming that the created pair plasma is optically thick. The relative role of neutrino and weak interactions versus the electromagnetic interactions in building the dyadotorus is currently the topic of intense research.

In conclusion, the deeper understanding of the GRB phenomenon, occurring under very different initial conditions, has highlighted the possibility of using the general description of the dyadosphere (dyadotorus) for any source of an optically thick baryon-loaded e^+e^- plasma and, consequently, of applying the above fireshell treatment in total generality.

The generality of the fireshell approach clearly differs from alternative treatments purporting late activity from a central engine (see, e.g., the *collapsar* model in Woosley 1993; Popham et al. 1999; Woosley & Bloom 2006 and references therein; and the Newtonian *magnetar* model in Zhang & Mészáros 2001; Dai et al. 2006; Metzger et al. 2011; Bucciantini et al. 2012; Giacomazzo & Perna 2013; Lü & Zhang 2014, and references therein) and proposes a different explanation for the afterglow observations in L-GRBs (see Pisani et al. 2013; Y. Aimuratov et al. 2016, in preparation).

3. ON THE 10^{52} ERG LOWER LIMIT IN BINARY SYSTEMS LEADING TO BH FORMATION

During the hypercritical accretion process onto the NS, the total energy available to be released, e.g., in the form of neutrinos and photons, is given by the gain of gravitational potential energy of the matter being accreted by the NS (Zel'dovich et al. 1972; Ruffini & Wilson 1973; Rueda & Ruffini 2012; Fryer et al. 2014). The total energy released in the star in a time interval dt during the accretion of an amount of mass dM_b with angular momentum $l\dot{M}_b$ is given by (see, e.g., Sibgatullin & Sunyaev 2000; Becerra et al. 2015)

$$L_{\rm acc} = (\dot{M}_b - \dot{M}_{\rm NS})c^2 = \dot{M}_b c^2 \left[1 - \left(\frac{\partial M_{\rm NS}}{\partial J_{\rm NS}}\right)_{M_b} \times l - \left(\frac{\partial M_{\rm NS}}{\partial M_b}\right)_{J_{\rm NS}}\right], \quad (1)$$

where J is the NS angular momentum. The last two terms of the above equation take into due account the change of binding energy of the NS while accreting both matter and angular momentum. We assume, as a norm, a typical NS mass of $\approx 1.4\ M_\odot$, a value observed in galactic NS binaries (Zhang et al. 2011; Antoniadis 2015) and characteristic of the XRFs (Becerra et al. 2016). We also assume an NS critical mass $M_{\rm crit}$ in the range from 2.2 up to 3.4 $M_\odot$ depending on the equations of state and angular momentum (see Cipolletta et al. 2015; Becerra et al. 2016, 2015, for details). $L_{\rm acc}$ is clearly a function of both the NS mass and $M_{\rm crit}$.

Since $L_{\rm acc} \propto \dot{M}_b$, it evolves with time similarly to $\dot{M}_B$. We have shown that the accretion luminosity can be as high as $L_{\rm acc} \sim 0.1\, \dot{M}_b c^2 \sim 10^{47}$–$10^{51}$ erg s^{-1} for accretion rates $\dot{M}_b \sim 10^{-6}$–$10^{-2}\ M_\odot$ s^{-1} (see Becerra et al. 2015, 2016, for details). The duration of the accretion process is given approximately by the flow time of the slowest layers of the SN ejecta to the NS companion. If the velocity of these layers is $v_{\rm inner}$, then $\Delta t_{\rm acc} \sim a/v_{\rm inner}$, where a is the binary separation. For $a \sim 10^{11}$ cm and $v_{\rm inner} \sim 10^8$ cm s^{-1} we obtain $\Delta t_{\rm acc} \sim 10^3$ s, while for shorter binary separation,

Table 2
List of the XRFs Considered in This Work up to the End of 2014

GRB	z	$E_{\rm iso}/(10^{50}$ erg)	GRB	z	$E_{\rm iso}/(10^{50}$ erg)
970508	0.835	65 ± 13	081007	0.5295	17 ± 2
980425	0.0085	0.0064 ± 0.0016	100316D	0.059	0.59 ± 0.05
980613	1.096	50 ± 10	100816A	0.8049	71 ± 9
990712	0.434	69 ± 13	101219B	0.55	63 ± 6
020819B	0.41	69 ± 18	110106B	0.618	$73 \pm$
020903	0.251	0.24 ± 0.06	120121B	0.017	0.0139 ± 0.0002
031203	0.105	0.99 ± 0.10	120422A	0.283	2.4 ± 0.8
050416A	0.6528	11 ± 2	120714B	0.3984	8.0 ± 2.0
060218	0.033	0.54 ± 0.05	130702A	0.145	6.5 ± 1.0
070419	0.97	24 ± 10	130831A	0.4791	46 ± 2

Note. For each source (first and fourth columns) the values of z and $E_{\rm iso} \lesssim 10^{52}$ erg (second, third, fifth, and sixth columns) are listed.

e.g., $a \sim 10^{10}$ cm ($P \sim 5$ minutes), $\Delta t_{\rm acc} \sim 10^2$ s. These estimates are validated by our numerical simulations (see, e.g., Becerra et al. 2015, 2016; Fryer et al. 2015, 2014). From the above results we obtain that for systems with the above short orbital periods the NS collapses to a BH, namely, BdHNe (Becerra et al. 2016), and a total energy larger than the separatrix energy of $\approx 10^{52}$ erg is released during the hypercritical accretion process. For systems with larger separations, in which the hypercritical accretion is not sufficient to induce the collapse of the NS into a BH, namely, the XRFs (Becerra et al. 2016), the value of $\approx 10^{52}$ erg represents a theoretical estimate of the upper limit to the energy emitted by norm in the hypercritical accretion process. These considerations are derived from theoretical expectations based on the above-mentioned masses for the accreting NSs and $M_{\rm crit}$. Indeed, they are in satisfactory agreement with the observations of 20 XRFs and 233 BdHNe (considered up to the end of 2014), which we have used in our sample (see Tables 2 and 3, respectively). The upper limit for the XRFs is $(7.3 \pm 0.7) \times 10^{51}$ erg (see Section 4.1), while the lower limit for the BdHNe is $(9.2 \pm 1.3) \times 10^{51}$ erg (see Section 5.1).

The same arguments apply to the fusion process of two NSs in a binary NS merger (Ruffini et al. 2015b). Therefore, from these general arguments, we can conclude that the energy emitted during the merger process leading to the formation of a BH should be larger than $\approx 10^{52}$ erg. Indeed, we find an upper limit for the S-GRFs of $(7.8 \pm 1.0) \times 10^{51}$ erg (see Section 6.1) and a lower limit for the S-GRBs of $(2.44 \pm 0.22) \times 10^{52}$ erg (see Section 7.1).

Such a separatrix energy is clearly a function of the initial NS mass undergoing accretion, by norm assumed to be $\approx 1.4\ M_\odot$. It is also a function of the yet unknown precise value of $M_{\rm crit}$, for which only an absolute upper limit of $3.2\ M_\odot$ has been established for the nonrotating case (Rhoades & Ruffini 1974). As already pointed out in Ruffini et al. (2015b) for the case of binary NS mergers, the direct observation of the separatrix energy between S-GRFs and S-GRBs, and also (in this case) between BdHNe and XRFs, gives fundamental information for the determination of the actual value of $M_{\rm crit}$, for the minimum mass of the newly formed BH, and for the mass of the accreting NS. It is appropriate to notice that a value of the mass of the accreting NS binary larger than $\approx 1.4\ M_\odot$ is a priori possible and would give interesting observational properties: an exceptional accreting NS with mass close to $M_{\rm crit}$ would lead to a BdHN with a value of the energy lower than the theoretical separatrix of $\approx 10^{52}$ erg. Conversely, the accretion on an NS with mass smaller than $\approx 1.4\ M_\odot$ should lead to an XRF with energy larger than $\approx 10^{52}$ erg. These rare possibilities will be precious in further probing the implications of the IGC paradigm, in estimating the NS masses, and in deriving more stringent limits on $M_{\rm crit}$ directly from observations.

Our theory of the hypercritical accretion, applied in the GRB analysis through the IGC paradigm in binary systems, introduces substantial differences with respect to the traditional ones. To appreciate these differences and gain familiarity in this novel approach, we recommend the reading of all the references quoted in this section.

4. THE X-RAY FLASHES

4.1. General Properties

The observational features of long bursts with energy below $\approx 10^{52}$ erg are listed below and summarized in Figure 2. These bursts are interpreted within the theoretical framework of the IGC as a new class that we indicate as XRFs.

The upper limit on the energetics of the XRFs is $(7.3 \pm 0.7) \times 10^{51}$ erg, as measured in GRB 110106B.

The isotropic energies are in the range $(6.4 \pm 1.6) \times 10^{47}$ erg $\lesssim E_{\rm iso} \lesssim (7.3 \pm 0.7) \times 10^{51}$ erg (see Figure 1 and Amati & Della Valle 2013; Ruffini et al. 2015c).

The spectral peak energies are in the range $4 \lesssim E_{\rm p,i} \lesssim 200$ keV (see Figure 1 and Amati & Della Valle 2013; Ruffini et al. 2015c) and increase monotonically with $E_{\rm iso}$.

The cosmological redshifts are in the range $0.0085 \leqslant z \leqslant 1.096$, with an average value of ≈ 0.43 (see Table 2).

The prompt emission phase has a duration ranging between $\sim 10^2$ and 10^4 s (see Figure 2(a)) with a spectrum generally characterized by a thermal component and power-law component. The radii of the thermal emitter are in the range of 10^{10}–10^{12} cm, and the temperatures vary in the range of 0.1–2 keV (see, e.g., Campana et al. 2006, and Figure 2(c)), depending on the values of the binary period and separation of the progenitor systems.

The long-lasting X-ray afterglow does not exhibit any specific common late power-law behavior (see Figure 2(a)).

For all XRFs at $z \lesssim 1$, an optical SN with a luminosity similar to the one of SN 2010bh (Bufano et al. 2012) occurs after 10–15 days in the cosmological rest frame.

No high-energy emission has ever been observed.

Table 3
List of the BdHNe Considered in This Work up to the End of 2014

GRB	z	$E_{\rm iso}/(10^{52}$ erg)	GRB	z	$E_{\rm iso}/(10^{52}$ erg)
970228	0.695	1.65 ± 0.16	081008	1.969	10.0 ± 1.0
970828	0.958	30.4 ± 3.6	081028	3.038	18.3 ± 1.8
971214	3.42	22.1 ± 2.7	081029	3.8479	12.1 ± 1.4
980329	3.5	267 ± 53	081109	0.9787	1.81 ± 0.12
980703	0.966	7.42 ± 0.74	081118	2.58	12.2 ± 1.2
990123	1.6	241 ± 39	081121	2.512	32.4 ± 3.7
990506	1.3	98.1 ± 9.9	081203A	2.05	32 ± 12
990510	1.619	18.1 ± 2.7	081221	2.26	31.9 ± 3.2
990705	0.842	18.7 ± 2.7	081222	2.77	27.4 ± 2.7
991208	0.706	23.0 ± 2.3	090102	1.547	22.6 ± 2.7
991216	1.02	69.8 ± 7.2	090205	4.6497	1.12 ± 0.16
000131	4.5	184 ± 32	090313	3.375	4.42 ± 0.79
000210	0.846	15.4 ± 1.7	090323	3.57	438 ± 53
000418	1.12	9.5 ± 1.8	090328	0.736	14.2 ± 1.4
000911	1.06	70 ± 14	090418A	1.608	17.2 ± 2.7
000926	2.07	28.6 ± 6.2	090423	8.1	8.8 ± 2.1
010222	1.48	84.9 ± 9.0	090424	0.544	4.07 ± 0.41
010921	0.45	0.97 ± 0.10	090429B	9.3	6.7 ± 1.3
011121	0.36	8.0 ± 2.2	090516	4.109	72 ± 14
011211	2.14	5.74 ± 0.64	090519	3.85	24.7 ± 2.8
020124	3.2	28.5 ± 2.8	090529	2.625	2.56 ± 0.30
020127	1.9	3.73 ± 0.37	090530	1.266	1.73 ± 0.19
020405	0.69	10.6 ± 1.1	090618	0.54	28.6 ± 2.9
020813	1.25	68 ± 17	090715B	3.0	23.8 ± 3.7
021004	2.3	3.47 ± 0.46	090809	2.737	1.88 ± 0.26
021211	1.01	1.16 ± 0.13	090812	2.452	47.5 ± 8.2
030226	1.98	12.7 ± 1.4	090902B	1.822	292 ± 29.2
030323	3.37	2.94 ± 0.92	090926	2.106	228 ± 23
030328	1.52	38.9 ± 3.9	090926B	1.24	4.14 ± 0.45
030329	0.169	1.62 ± 0.16	091003	0.897	10.7 ± 1.8
030429	2.65	2.29 ± 0.27	091020	1.71	8.4 ± 1.1
030528	0.78	2.22 ± 0.27	091024	1.092	18.4 ± 2.0
040912	1.563	1.36 ± 0.36	091029	2.752	7.97 ± 0.82
040924	0.859	0.98 ± 0.10	091109A	3.076	10.6 ± 1.4
041006	0.716	3.11 ± 0.89	091127	0.49	1.64 ± 0.18
050126	1.29	2.47 ± 0.25	091208B	1.063	2.06 ± 0.21
050315	1.95	6.15 ± 0.30	100219A	4.6667	3.93 ± 0.61
050318	1.444	2.30 ± 0.23	100302A	4.813	1.33 ± 0.17
050319	3.243	4.63 ± .0.56	100414A	1.368	55.0 ± 5.5
050401	2.898	37.6 ± 7.3	100513A	4.8	6.75 ± 0.53
050502B	5.2	2.66 ± 0.22	100621A	0.542	2.82 ± 0.35
050505	4.27	16.0 ± 1.1	100728A	1.567	86.8 ± 8.7
050525A	0.606	2.30 ± 0.49	100728B	2.106	3.55 ± 0.36
050603	2.821	64.1 ± 6.4	100814A	1.44	15.3 ± 1.8
050730	3.969	11.8 ± 0.8	100901A	1.408	4.22 ± 0.50
050802	1.71	5.66 ± 0.47	100906A	1.727	29.9 ± 2.9
050814	5.3	9.9 ± 1.1	101213A	0.414	2.72 ± 0.53
050820	2.615	103 ± 10	110128A	2.339	1.58 ± 0.21
050904	6.295	133 ± 14	110205A	2.22	48.3 ± 6.4
050908	3.347	1.54 ± 0.16	110213A	1.46	5.78 ± 0.81
0509220	2.199	5.6 ± 1.8	110213B	1.083	8.3 ± 1.3
051022	0.8	56.0 ± 5.6	110422A	1.77	79.8 ± 8.2
051109A	2.346	6.85 ± 0.73	110503A	1.613	20.8 ± 2.1
051111	1.55	15.4 ± 1.9	110715A	0.82	4.36 ± 0.45
060115	3.533	5.9 ± 3.8	110731A	2.83	49.5 ± 4.9
060124	2.296	43.8 ± 6.4	110801A	1.858	10.9 ± 2.7
060202	0.785	1.20 ± 0.09	110818A	3.36	26.6 ± 2.8
060206	4.056	4.1 ± 1.9	111008A	4.9898	24.7 ± 1.2
060210	3.91	32.2 ± 3.2	111107A	2.893	3.76 ± 0.55
060306	3.5	7.6 ± 1.0	111209A	0.677	5.14 ± 0.62
060418	1.489	13.5 ± 2.7	111228A	0.716	2.75 ± 0.28
060510B	4.9	19.1 ± 0.8	120119A	1.728	27.2 ± 3.6
060522	5.11	6.47 ± 0.63	120326A	1.798	3.27 ± 0.33
060526	3.22	2.75 ± 0.37	120327A	2.813	14.42 ± 0.46

Table 3
(Continued)

GRB	z	$E_{iso}/(10^{52}$ erg)	GRB	z	$E_{iso}/(10^{52}$ erg)
060605	3.773	4.23 ± 0.61	120404A	2.876	4.18 ± 0.34
060607A	3.075	11.9 ± 2.8	120624B	2.197	319 ± 32
060707	3.424	4.3 ± 1.1	120711A	1.405	180 ± 18
060708	1.92	1.06 ± 0.08	120712A	4.175	21.2 ± 2.1
060714	2.7108	7.67 ± 0.44	120716A	2.486	30.2 ± 3.0
060814	1.923	56.7 ± 5.7	120802A	3.796	12.9 ± 2.8
060906	3.6856	7.81 ± 0.51	120811C	2.671	6.41 ± 0.64
060908	1.884	7.2 ± 1.9	120815A	2.358	1.65 ± 0.27
060926	3.2086	2.29 ± 0.37	120909A	3.93	87 ± 10
060927	5.46	12.0 ± 2.8	121024A	2.298	4.61 ± 0.55
061007	1.262	90.0 ± 9.0	121027A	1.773	3.29 ± 0.17
061110B	3.4344	17.9 ± 1.6	121128A	2.2	8.66 ± 0.87
061121	1.314	23.5 ± 2.7	121201A	3.385	2.52 ± 0.34
061126	1.1588	31.4 ± 3.6	121229A	2.707	3.7 ± 1.1
061222A	2.088	30.0 ± 6.4	130408A	3.758	35.0 ± 6.4
070110	2.3521	4.98 ± 0.30	130418A	1.218	9.9 ± 1.6
070125	1.547	84.1 ± 8.4	130420A	1.297	7.74 ± 0.77
070306	1.4959	8.26 ± 0.41	130427A	0.334	92 ± 13
070318	0.84	3.64 ± 0.17	130427B	2.78	5.04 ± 0.48
070411	2.954	8.31 ± 0.45	130505A	2.27	347 ± 35
070508	0.82	7.74 ± 0.29	130514A	3.6	52.4 ± 9.2
070521	1.35	10.8 ± 1.8	130518A	2.488	193 ± 19
070529	2.4996	12.8 ± 1.1	130606A	5.91	28.3 ± 5.1
070611	2.0394	0.92 ± 0.13	130610A	2.092	6.99 ± 0.46
070721B	3.6298	24.2 ± 1.4	130701A	1.155	2.60 ± 0.09
071003	1.604	38.3 ± 4.5	130907A	1.238	304 ± 19
071010B	0.947	2.32 ± 0.40	130925A	0.347	18.41 ± 0.37
071020	2.145	10.0 ± 4.6	131105A	1.686	34.7 ± 1.2
071031	2.6918	4.99 ± 0.97	131117A	4.042	1.02 ± 0.16
071117	1.331	5.86 ± 2.7	140206A	2.74	35.93 ± 0.73
080207	2.0858	16.4 ± 1.8	140213A	1.2076	9.93 ± 0.15
080210	2.6419	4.77 ± 0.29	140226A	1.98	5.8 ± 1.1
080310	2.4274	8.58 ± 0.90	140304A	5.283	13.7 ± 1.1
080319B	0.937	118 ± 12	140311A	4.954	11.6 ± 1.5
080319C	1.95	14.9 ± 3.0	140419A	3.956	186 ± 77
080325	1.78	9.55 ± 0.84	140423A	3.26	65.3 ± 3.3
080411	1.03	16.2 ± 1.6	140428A	4.7	1.88 ± 0.31
080413A	2.433	8.6 ± 2.1	140430A	1.6	1.54 ± 0.23
080413B	1.1	1.61 ± 0.27	140506A	0.889	1.12 ± 0.06
080514B	1.8	18.1 ± 3.6	140508A	1.027	23.24 ± 0.26
080603B	2.69	6.0 ± 3.1	140509A	2.4	3.77 ± 0.44
080604	1.4171	1.05 ± 0.12	140512A	0.725	7.76 ± 0.18
080605	1.64	28 ± 14	140515A	6.32	5.41 ± 0.55
080607	3.036	200 ± 20	140518A	4.707	5.89 ± 0.59
080710	0.8454	1.68 ± 0.22	140614A	4.233	7.3 ± 2.1
080721	2.591	134 ± 23	140629A	2.275	6.15 ± 0.90
080804	2.205	12.0 ± 1.2	140703A	3.14	1.72 ± 0.09
080805	1.5042	5.05 ± 0.22	140801A	1.32	5.69 ± 0.05
080810	3.35	47.8 ± 5.5	140808A	3.29	11.93 ± 0.75
080905B	2.3739	4.55 ± 0.37	140907A	1.21	2.29 ± 0.08
080913	6.695	9.2 ± 2.7	141026A	3.35	7.17 ± 0.90
080916A	0.689	0.98 ± 0.10			
080916C	4.35	407 ± 86			
080928	1.692	3.99 ± 0.91			

Note. For each source (first and fourth columns) the values of z and E_{iso} (second, third, fifth, and sixth columns) are listed.

In view of the observed values of $E_{p,i}$ that occur in the X-ray domain and also because of the low values of their $E_{iso} < 10^{52}$ erg, we adopted the name XRFs for these soft and less energetic long bursts, a terminology already used in the literature on purely morphological grounds (see, e.g., Heise 2003; Amati et al. 2004; Soderberg et al. 2006).

4.2. Theoretical Interpretation of XRFs within the IGC Paradigm

In the IGC paradigm an XRF occurs when the CO_{core}–NS binary separation a is so large (typically $a > 10^{11}$ cm; see, e.g., Becerra et al. 2015) that the accretion of the SN ejecta onto the NS is not sufficient for the NS to reach M_{crit}. Correspondingly,

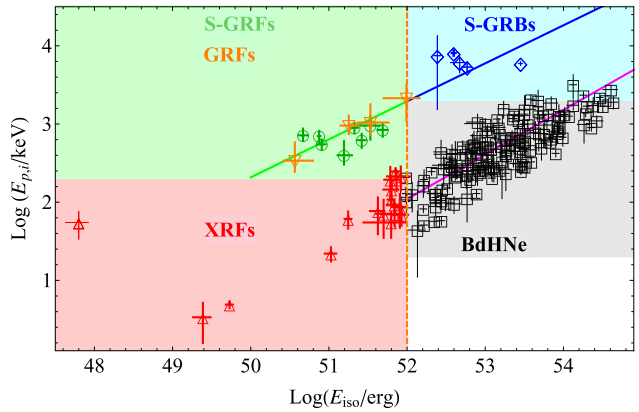

Figure 1. $E_{p,i}$–E_{iso} plane for XRFs, BdHNe, S-GRBs, S-GRFs, and the initial spike-like emission of the GRFs. The XRFs (red triangles) cluster in the red shaded region ($E_{p,i} \lesssim 200$ keV and $E_{iso} \lesssim 10^{52}$ erg), while the BdHNe (black squares) cluster in the gray shaded one ($E_{p,i} \gtrsim 200$ keV and $E_{iso} \gtrsim 10^{52}$ erg); the Amati relation (Amati & Della Valle 2013) fulfilled by the BdHNe is plotted with a magenta solid line. The S-GRFs (green circles) and the initial spike-like emission of the GRFs (orange downward-pointing triangles) cluster in the green shaded region ($E_{p,i} \lesssim 2$ MeV and $E_{iso} \lesssim 10^{52}$ erg), while the S-GRBs (blue diamonds) cluster in the blue shaded one ($E_{p,i} \gtrsim 2$ MeV and $E_{iso} \gtrsim 10^{52}$ erg); the relation for short bursts (Zhang et al. 2012; Calderone et al. 2015; Ruffini et al. 2015b) is plotted with a green solid line for the S-GRFs and the GRFs, and in blue for the S-GRBs.

there is a critical or maximum value of the orbital period P_{max} (e.g., $P_{max} \approx 28$ minutes for an NS with initial mass of 1.4 $M_\odot$) for which the NS collapses to a BH, namely, for $P > P_{max}$ the accretion rate is not sufficient to induce the gravitational collapse of the companion NS into a BH (see Figures 2(d)).

The hypercritical accretion of the SN ejecta onto the NS binary companion occurs at rates $<10^{-2}\,M_\odot$ s^{-1} and can last from several hundreds of seconds all the way up to $\sim 10^4$ s, until the whole SN ejecta flies beyond the NS binary orbit (see Figure 2(a)). The photons are trapped in the accreting material, and the accretion energy is lost through a large associated neutrino emission (see, e.g., Zel'dovich et al. 1972; Ruffini & Wilson 1973; Rueda & Ruffini 2012; Fryer et al. 2014, and references therein). The upper limit of 10^{52} erg for these sources is explainable by estimating the gravitational energy of the matter accreted onto the NS reaching a mass below M_{crit} at the end of the accretion process (see Section 3).

The resulting emission, dubbed Episode 1, exhibits a spectrum composed of a thermal component, possibly originating from the outflow within the NS atmosphere driven out by Rayleigh–Taylor convection instabilities, and a power-law component. The shorter the binary period, the larger the accretion rate (see Figure 2(f)) and the values of E_{iso} and $E_{p,i}$, and correspondingly the shorter the prompt emission duration (see Figure 2(a)). The excess of angular momentum of the system necessarily leads to a jetted emission, manifested in the power-law spectral component (Becerra et al. 2015). Indeed, in the IGC simulations the typical radii inferred from the evolving thermal component coincide with the observed ones of 10^{10}–10^{12} cm.

In the IGC paradigm the in-state is represented by an exploding CO_{core} and a companion NS. The out-state is a multiple system composed of an MNS, resulting from the accretion of part of the SN ejecta onto the binary companion NS, a νNS, originating from the SN event, and the remaining part of the SN ejecta shocked by the hypercritical accretion emission of the XRF. This energy injection into the SN ejecta leads to the occurrence of a broad-lined SN Ic (*hypernova*; see, e.g., Maeda & Nomoto 2003) with a kinetic energy larger than that of the traditional SNe Ic. The presence of ^{56}Ni in the SN ejecta leads to the observed SN emission after $\approx$10–15 days in the cosmological rest frame, which is observable for sources at $z \lesssim 1$.

Clearly the absence of hard γ-ray and GeV emissions is implicit in the nature of the hypercritical accretion process not leading to a BH and the corresponding rate of neutrino emission (see also the Appendix).

4.3. Prototypes

In Figure 2(a) we reproduce the rest-frame 0.3–10 keV luminosity light curves of four selected XRFs: GRB 980425 (Pian et al. 2000; Kouveliotou et al. 2004; Pian et al. 2004), associated with SN 1998bw (Galama et al. 1998), GRB 060218 associated with SN 2006aj (Campana et al. 2006; Soderberg et al. 2006), GRB 070419A (Evans et al. 2007, 2009) with an optical SN bump (Hill et al. 2007), and GRB 101219B (Evans et al. 2007, 2009) associated with SN 2010ma (Sparre et al. 2011). Their prompt emissions are represented by the above-mentioned Episode 1. In Figure 2(c) we plot the evolution of both temperature and radius inferred from the thermal component observed in the Episode 1 emission of GRB 060218. The increasing radius and almost constant temperature are obtained from the thermal component observed in GRB 060218 (Campana et al. 2006). Details will appear in forthcoming publications (Pisani et al. 2016; Becerra et al. 2016). A complete list of XRFs is shown in Table 2.

5. THE BINARY-DRIVEN HYPERNOVAE

5.1. General Properties

The observational features of long bursts with energy above $\approx 10^{52}$ erg are listed below and summarized in Figure 3. These bursts are interpreted within the theoretical framework of the IGC as a new class that we indicate as BdHNe.

The lower limit on the energetics of the BdHNe is $(9.2 \pm 1.3) \times 10^{51}$ erg as measured in GRB 070611.

The observed isotropic energies are in the range $(9.2 \pm 1.3) \times 10^{51}$ erg $\lesssim E_{iso} \lesssim (4.07 \pm 0.86) \times 10^{54}$ erg (see Figure 1 and Amati & Della Valle 2013; Ruffini et al. 2015c) and are in principle dependent on the NS mass, which we have assumed, as an example, to be $\approx 1.4\ M_\odot$ (see Section 3).

The spectral peak energies are in the range $0.2 \lesssim E_{p,i} \lesssim 2$ MeV (see Figure 1 and Amati & Della Valle 2013; Ruffini et al. 2015c) and increase monotonically with E_{iso}.

The cosmological redshifts are in the range $0.169 \leqslant z \leqslant 9.3$, with an average value of ≈ 2.42 (see Table 3).

The prompt emission phase of BdHNe exhibits a more complex structure than that of XRFs. Indeed, three different regimes are found:

(a) A thermal emission with a decreasing temperature following a broken power-law behavior and an additional nonthermal spectral component (a power law) dominate the early emission in selected BdHNe (see, e.g., Izzo et al. 2012c, and Figure 3(a)). The existence of this

thermal component was first identified in the GRB BATSE data by Ryde (2004, 2005). It was then shown to occur in the case of BdHNe as GRB 090618 (Izzo et al. 2012c, and Figure 3(a)), GRB 101023 (Penacchioni et al. 2012), GRB 110709B (Penacchioni et al. 2013), and GRB 970828 (Ruffini et al. 2015a). The characteristic radii inferred from the cooling thermal component are of the order of 10^9–10^{10} cm, and the average expansion speed is $\sim 10^8$–10^9 cm s^{-1} (Izzo et al. 2012c; Penacchioni et al. 2012, 2013; Ruffini et al. 2015a).

(b) This early emission is followed by the characteristic GRB emission (see Figure 3(d)), encompassing a thermal precursor, the P-GRB (Ruffini et al. 1999, 2000), followed by the prompt emission (Ruffini et al. 2002, 2004, 2005).

(c) The prompt emission is followed by a steep decay, then by a plateau and a late power-law decay. These features have been first reported in Nousek et al. (2006) and Zhang et al. (2006).

The late decay has typical slopes of $-1.7 \lesssim \alpha_X \lesssim -1.3$ (Pisani et al. 2013) and shows a characteristic power-law behavior both in the optical and in X-rays. When computed in the source cosmological rest frame, the late power-law decay in X-rays exhibits new features: overlapping and nesting (see Figure 3(c)). Overlapping has been proven in a sample of six BdHNe: GRBs 060729, 061007, 080319B, 090618, 091127, and 111228 (Izzo et al. 2012a; Pisani et al. 2013). The nested property of the BdHNe has been discussed in Ruffini et al. (2014b), where it has been shown that the duration (the luminosity) of the plateau phase is inversely (directly) proportional to the energy of the GRB emission: the more energetic the source, the smaller (higher) the duration (the luminosity) of the plateau.

For all BdHNe at $z \lesssim 1$, an optical SN with a luminosity similar to the one of SN 1998bw (Galama et al. 1998) occurs after 10–15 days in the cosmological rest frame.

A distinctive high-energy emission observed up to 100 GeV shows a luminosity light curve following a precise power-law behavior with index ≈ -1.2 (Figure 3(d) and Nava et al. 2014). The turn-on of this GeV emission occurs after the P-GRB emission and during the prompt emission phase.

5.2. Theoretical Interpretation of BdHNe within the IGC Paradigm

In the IGC paradigm a BdHN occurs when the CO_{core}–NS binary is more tightly bound ($a \lesssim 10^{11}$ cm; see, e.g., Becerra et al. 2015). The larger accretion rate of the SN ejecta, e.g., $\gtrsim 10^{-2}$–$10^{-1}\, M_\odot\, s^{-1}$, leads the companion NS to easily reach its critical mass M_{crit} (Rueda & Ruffini 2012; Fryer et al. 2014; Becerra et al. 2015), leading to the formation of a BH. The electrodynamical conditions encountered in the final accretion phase explain the existence of a vacuum polarization process leading to the creation of an e^+e^- plasma and to the formation of a KNBH with a large variety of new astrophysical phenomena. For the sake of clarity and independence on the physical regime encountered, in the IGC paradigm we have divided the activities of the BdHNe in a numbered set of distinct episodes.

Episode 1 of BdHNe originates in the same hypercritical accretion process as the corresponding one of XRFs. The corresponding spectrum again exhibits an expanding thermal component and a power-law function (Izzo et al. 2012c; Ruffini et al. 2015a). The typical radii inferred from the thermal component are of the order of 10^9–10^{10} cm, and the average expansion speed is $\sim 10^8$–10^9 cm s^{-1} (see Figure 3(a) and Izzo et al. 2012c; Ruffini et al. 2015a).

Episode 2 corresponds to the authentic L-GRB emission (see Figure 3(b)), stemming from the collapse of the companion NS to a BH. For its theoretical description we adopt the traditional fireshell model (see Ruffini et al. 2001a, 2001b, 2001c, and Section 2). The GRB emission occurs at a Lorentz factor at the transparency of $\Gamma = 10^2$–10^3 (Izzo et al. 2012c; Ruffini et al. 2015a), and the spatial extension of the interaction of the fireshell with the CBM goes all the way up to $\sim 10^{16}$–10^{17} cm, reached at the end of Episode 2 (Izzo et al. 2012c). The BdHNe have $E_{iso} \gtrsim 10^{52}$ erg, and their $E_{p,i} \gtrsim 200$ keV is in the hard γ-ray domain.

Episode 3 in BdHNe originates from the SN ejecta (Ruffini et al. 2015c). In this case an extra energy injection is delivered by the interaction of the GRB outflow with the SN ejecta, resulting in an isotropic energy emission of 10^{51}–10^{52} erg. This interaction produces a flare at the beginning of Episode 3 (typically at a rest-frame time of $\sim 10^2$ s) with the typical signature of an expanding thermal component in its spectrum. The radii inferred from this thermal component are $\sim 10^{12}$–10^{13} cm, and their evolution reveals a mildly relativistic expansion at $\Gamma \approx 2$ (Ruffini et al. 2014b, 2015c). The rest-frame 0.3–10 keV luminosity light is then followed by a plateau phase and a late power-law decay. The late decay has been shown to exhibit a common power-law behavior and a nested structure (see, e.g., Pisani et al. 2013; Ruffini et al. 2014b, and Figure 3(c)). The possibility of using the late X-ray emission as a distance indicator has been explored by inferring the redshifts of GRBs 101023 and 110709B (Penacchioni et al. 2012, 2013) and has been applied to predict the occurrence of the SN associated with GRB 130427A after $\sim$10–15 days in the cosmological rest frame before its discovery (Ruffini et al. 2013), later confirmed by the observations (de Ugarte Postigo et al. 2013; Levan et al. 2013; Watson et al. 2013; Xu et al. 2013).

Episode 4, as predicted in the IGC paradigm and in analogy to XRFs, corresponds to the optical SN emission observable in all BdHNe at $z \lesssim 1$ after $\approx$10–15 days in the cosmological rest frame. It is remarkable that these SNe have a standard luminosity, like the one of SN 1998bw (see, e.g., Melandri et al. 2014).

A new Episode 5, here introduced, is identified with the long-lived GeV emission. This emission is conceptually distinct in its underlying physical process from that of Episode 3. When LAT data are available, the majority of BdHNe observed by the *Fermi* satellite (Atwood et al. 2009) exhibit such an emission, similar to the one observed in S-GRBs (see Section 6). In Ruffini et al. (2015c) the further accretion of matter onto the newly formed BH has been indicated as the origin of this GeV emission. An outstanding exception is GRB 151027A (M. Kovacevic et al. 2016, in preparation).

Also for BdHNe the in-state is composed of an exploding CO_{core} and a companion NS. The out-state is again a multiple system. First, there is a GRB composed of the P-GRB and its prompt emission. Then there is a newly formed BH, produced by the hypercritical accretion of part of the SN ejecta onto the binary companion NS reaching M_{crit}. Again, there is a νNS originating from the SN explosion. Finally, there is the

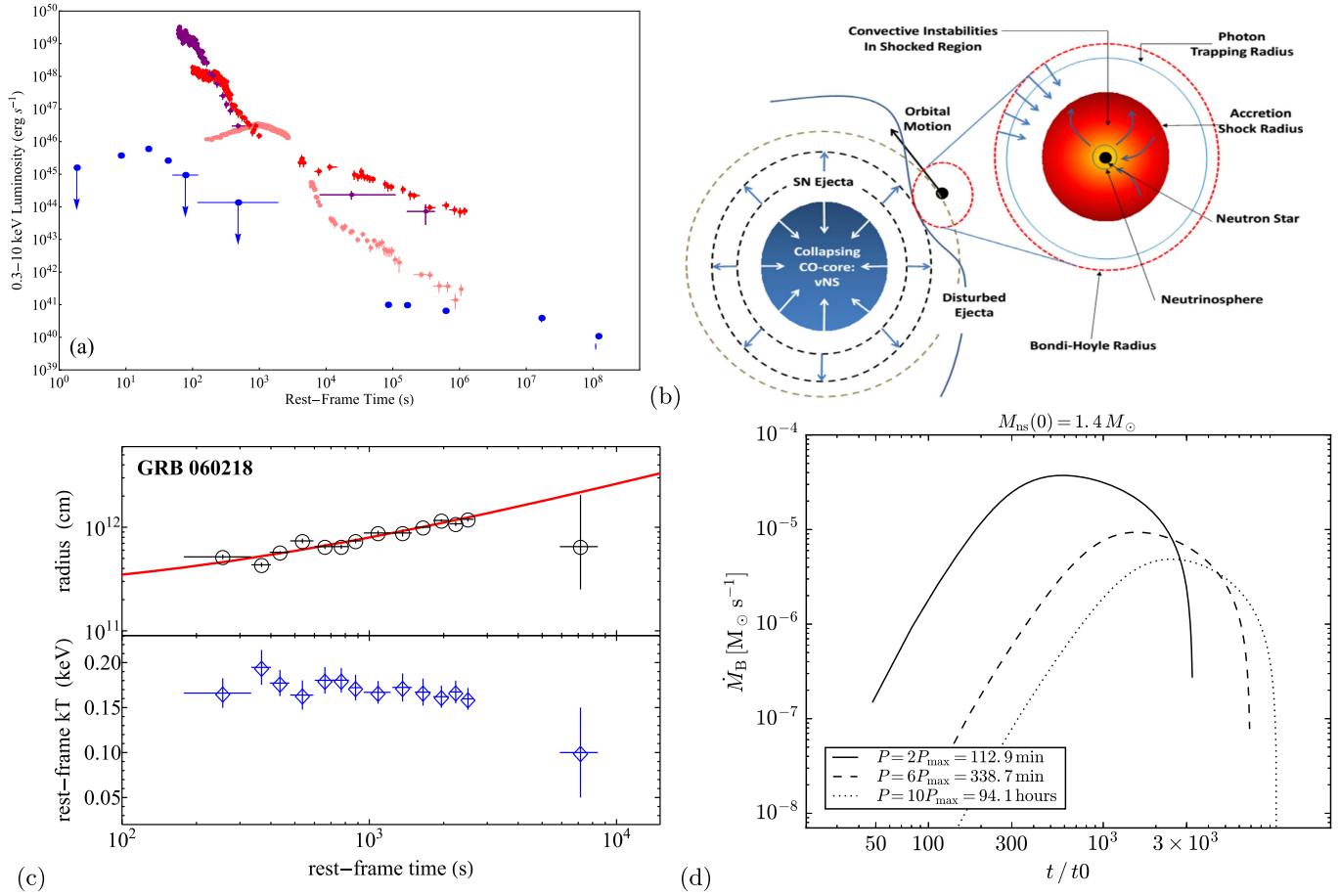

Figure 2. (a) Rest-frame 0.3–10 keV luminosity light curves of four selected XRFs: GRB 980425 (blue), GRB 060218 (pink), GRB 070419A (purple), and GRB 101219B (red). (b) Sketch of the CO_{core}–NS binary progenitor and the hypercritical accretion process in the IGC scenario (reproduced from Fryer et al. 2014). (c) Upper panel: evolution of the radius of the thermal component detected in GRB 060218 (black circles) and its linear fit (solid red curve). Lower panel: decay of the corresponding rest-frame temperature (blue diamonds). Reproduced from Campana et al. (2006). (d) Mass accretion rate $\dot{M}_B$ of the SN ejecta onto an NS companion of initial mass 1.4 $M_\odot$, as a function of time. Three cases are plotted for various selected orbital periods $P > P_{max}$ (see legend).

remaining part of the SN ejecta shocked by the GRB emission. The energy injection into the SN ejecta from both the hypercritical accretion phase and the GRB emission leads also in this case to the occurrence of a broad-lined SN Ic (*hypernova*; see, e.g., Maeda & Nomoto 2003) with a kinetic energy larger than that of the traditional SNe Ic.

5.3. Prototypes

In the following selected prototypes of BdHNe are given and illustrated in Figure 3.

The first systematic time-resolved spectral analysis of an Episode 1 of a BdHN has been performed for GRB 090618 (Izzo et al. 2012c). In this source the typical radii inferred from the cooling thermal component are of the order of 10^9–10^{10} cm and the average expansion speed is $\sim 10^8$–10^9 cm s^{-1} (see Figure 3(a)). Similar results have been obtained for GRB 101023 (Penacchioni et al. 2012), GRB 110907B (Penacchioni et al. 2013), and GRB 980828 (Ruffini et al. 2015a).

The selected prototypes of Episode 2 emission have isotropic energies ranging from $E_{iso} = 1.60 \times 10^{53}$ erg in GRB 970828 (Ruffini et al. 2015a) to $E_{iso} = 1.32 \times 10^{54}$ erg in GRB 080319B (Patricelli et al. 2012). The amount of baryonic matter loaded before the P-GRB emission, the baryon load $B \equiv M_B c^2/E^{tot}_{e^+e^-}$, where $E^{tot}_{e^+e^-}$ is the pair plasma energy and M_B the engulfed baryon mass, is in the range from $B = 1.98 \times 10^{-3}$ for GRB 090618 (Izzo et al. 2012c) to $B = 7.0 \times 10^{-3}$ for GRB 970828 (Ruffini et al. 2015a). Correspondingly, their transparency emission occurs at Lorentz factors at the transparency ranging from $\Gamma = 143$ in GRB 970828 (Ruffini et al. 2015a) to $\Gamma = 490$ in GRB 090618 (Izzo et al. 2012c). The average density of the CBM in these prototypes, inferred from description of the interaction with the fireshell after its transparency (Ruffini et al. 2002, 2004, 2005), varies from 0.6 cm^{-3} in GRB 090618 (Izzo et al. 2012c) to $\approx 10^3$ cm^{-3} in GRB 970828 (Ruffini et al. 2015a). The size of the corresponding emitting region, $\sim 10^{16}$–10^{17} cm, is clearly incompatible with the radii inferred from Episodes 1 and 3. This points to the different origins in the emission mechanisms of the above three episodes.

The radii inferred from the expanding thermal components observed in the spectra of the flares at the beginning of Episode 3 are typically $\sim 10^{12}$–10^{13} cm. This has been found in the cases of GRB 090618 (see, e.g., Starling et al. 2010; Ruffini et al. 2014b) and GRB 130427A (Ruffini et al. 2015c). In both these sources, the expansion of the thermal emitter of Episode 3 proceeds at $\Gamma \approx 2$ (Ruffini et al. 2014b, 2015c). After the initial emission in the spike of Episode 3, the rest-frame

0.3–10 keV luminosity light curve is then followed by a plateau phase and a late power-law decay. The overlapping of the late power-law decay and the nested structure is reproduced in Figure 3(c) for selected sources: GRB 060729, GRB 061007, GRB 080319B, GRB 090618, GRB 091127B, and GRB 111228A (considered in Pisani et al. 2013), GRB 061121 and GRB 130427A (considered in Ruffini et al. 2014b, 2015c), GRB 090423 (Ruffini et al. 2014a), and GRB 140512A (introduced here).

Episode 4 has been spectroscopically identified for the two closest BdHNe, e.g., GRB 091127–SN 2009 nz (Cobb et al. 2010) and GRB 130427A–SN 2013cq (Xu et al. 2013). In the cases of GRB 060729 (Cano et al. 2011), GRB 080319B (Kann et al. 2008), GRB 090618 (Cano et al. 2011), and GRB 111228A (D'Avanzo et al. 2012), at $z \lesssim 1$, the identification was possible through the detection of bumps in their Episode 3 optical light curves.

Turning now to Episode 5 of BdHNe, the GeV emission has been studied in detail in the case of GRB 130427A (Ruffini et al. 2015c), as well as in other selected BdHNe (see Figure 3(d) and Ackermann et al. 2013). The turn-on has been identified as the onset of the emission from the newly formed BH (Ruffini et al. 2015c).

A complete list of BdHNe is shown in Table 3.

The ultralong GRBs (Levan et al. 2014; Boër et al. 2015) are certainly BdHNe on the ground of their late X-ray rest-frame luminosity (Pisani et al., 2016).

6. THE SHORT GAMMA-RAY FLASHES

6.1. General Properties

The observational features of short bursts with energy below $\approx 10^{52}$ erg are listed below and summarized in Figure 4. These bursts are interpreted within the theoretical framework of the NS–NS merger paradigm in the fireshell model as a new class that we indicate as S-GRFs.

The upper limit on the energetics of the S-GRFs is $(7.8 \pm 1.0) \times 10^{51}$ erg, as measured in GRB 100117A.

The isotropic energies are in the range $(8.5 \pm 2.2) \times 10^{48}$ erg $\lesssim E_{\rm iso} \lesssim (7.8 \pm 1.0) \times 10^{51}$ erg (see Figure 1 and Zhang et al. 2012; Calderone et al. 2015; Ruffini et al. 2015b).

The spectral peak energies are in the range $0.2 \lesssim E_{\rm p,i} \lesssim 2$ MeV (see Figure 1 and Zhang et al. 2012; Calderone et al. 2015; Ruffini et al. 2015b) and increase monotonically with $E_{\rm iso}$.

The cosmological redshifts are in the range $0.111 \leqslant z \leqslant 2.609$, with an average value of ≈ 0.71 (see Table 4).

The prompt emission phase has a duration of a few seconds and is expected to crucially be a function of the masses of the binary NSs.

The long-lasting X-ray afterglow does not exhibit any specific common late power-law behavior (see Figure 4(a)).

For all S-GRFs no SN association is expected, nor observed.

No high-energy GeV emission is expected or observed in absence of BH formation.

6.2. Theoretical Interpretation of S-GRFs within the NS–NS Merger Paradigm in the Fireshell Model

As noted in the Introduction, current paradigms indicate mergers of NS–NS or NS–BH binaries as progenitors.

The extension of the IGC paradigm considerations to NS–NS mergers has led to a new classification of short bursts into two subclasses depending on the mass of the merged core, namely, whether or not a BH is formed out of the merger (see Figure 4(d) and Ruffini et al. 2015b). This, in turn, depends on the NS equation of state and on the adoption of a global neutrality model, as opposed to the case of absence of electromagnetic structures when local charge neutrality is imposed (see, e.g., Belvedere et al. 2012, and references therein; see also Figure 4(c)). Also relevant is the very different density distribution in the crust and in the core between these two treatments, which could play an important role in the NS–NS mergers (see Figure 4(d) and Oliveira et al. 2014).

S-GRFs originate from NS–NS mergers with initial total mass $m_1 + m_2$ leading to a merged core with mass smaller than $M_{\rm crit}$; therefore, their outcomes are an MNS with additional orbiting material, or even a binary NS or WD companion (see, e.g., Bildsten & Cutler 1992, and references therein), due to the energy and momentum conservation laws (Ruffini et al. 2015b). As discussed in Section 2, even though a BH is not formed out of the merger, also for these systems the general description of the fireshell model can be applied. A viable mechanism for S-GRFs can be the creation of a pair plasma via $\nu\bar{\nu} \leftarrow e^+e^-$ in an NS–NS merger (see, e.g., Narayan et al. 1992; Salmonson & Wilson 2002; Rosswog et al. 2003), where the maximum energy attainable in the process is $\approx 10^{52}$ erg, which represents indeed the upper limit to the energetics of these systems. Their energies are very similar to those emitted in XRFs. However, S-GRFs have $E_{p,i}$ as high as $\sim$2 MeV (see, e.g., Zhang et al. 2012; Calderone et al. 2015; Ruffini et al. 2015b); therefore, in view of the hardness of their spectra, we adopted the name of S-GRFs to distinguish them from the corresponding XRFs.

S-GRFs coincide with the majority of the systems extensively discussed in Berger (2014). All S-GRFs have an extended X-ray afterglow (Berger 2014; Ruffini et al. 2015b). Similarly to XRFs, the rest-frame 0.3–10 keV luminosity light curve does not exhibit either a late common power-law behavior or the nesting discovered in the BdHNe (see Figure 4(a)). At the moment, there are still a large number of possible candidates for the description of the origin of the late X-ray afterglow emission: (a) the interaction of the MNS with orbiting material or with a less massive binary NS or WD companion, (b) the accelerated baryons interacting with the CBM after the P-GRB emission, or (c) the possible radioactive decay of heavy elements synthesized in the ejecta of a compact binary merger (Li & Paczyński 1998). In this light we recall the possibility of a *macronova* emission, a near-infrared/optical transient (a bump) in the late afterglow (see the case of GRB 130603B in Berger et al. 2013; Tanvir et al. 2013).

As a general conclusion, in Ruffini et al. (2015b) the necessary absence of an SN was indicated. It has been predicted there that, since no BH is produced in the merger, S-GRFs should never exhibit high-energy GeV emission, which is expected to originate in the newly born BH (Ruffini et al. 2015b). No counterexample has been found as of today. In Ruffini et al. (2016) it has been shown that the absence of detection of GeV emission, necessary within the fireshell model, is indeed supported by the observations. The entire Section 6.5 of that paper is dedicated to the GeV emission of S-GRFs and S-GRBs. As evidenced there, it is concluded that S-GRFs, due to the upper limits of the LAT observations, have,

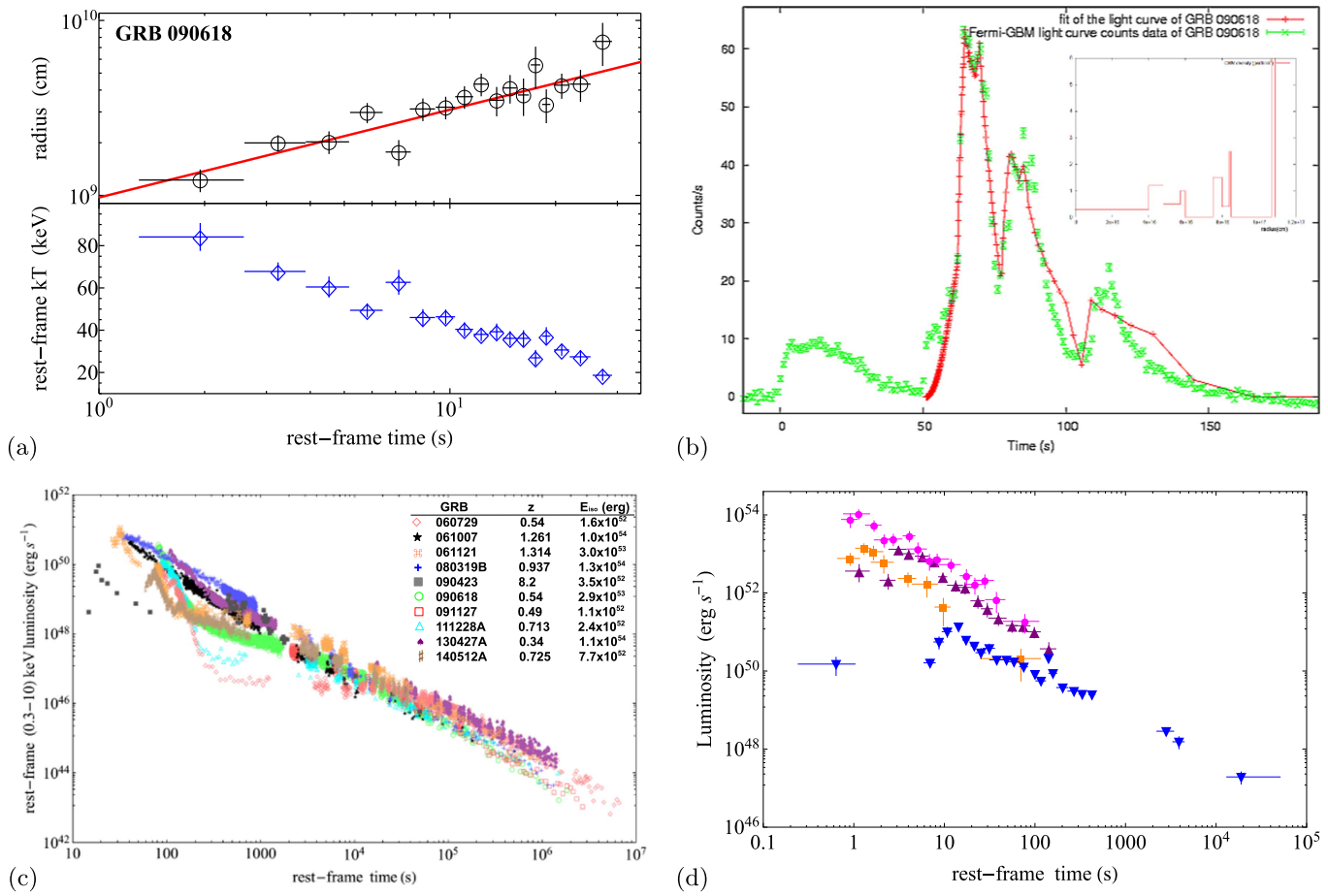

Figure 3. (a) Upper panel: evolution of the radius of the thermal component detected in Episode 1 of GRB 090618 (black circles) and its linear fit (solid red curve). Lower panel: decay of the corresponding rest-frame temperature (blue diamonds). Reproduced from Izzo et al. (2012c). (b) Fireshell simulation (red line) of the light curve of Episode 2 of the prototype GRB 090618 (green data). The small inset reproduces the CBM profile required for the simulation. Reproduced from Izzo et al. (2012c). (c) Rest-frame 0.3–10 keV luminosity light curves of selected BdHNe. All these sources exhibit the overlapping of the late power-law decay, outlined in Pisani et al. (2013), and a nested structure, as outlined in Ruffini et al. (2014b). (d) Rest-frame 0.1–100 GeV luminosity light curves of selected BdHNe (reproduced from Ackermann et al. 2013): GRB 080916C (magenta circles), GRB 090902B (purple triangles), GRB 110731A (orange squares), GRB 130427A (blue downward-pointing triangles).

if any, GeV fluxes necessarily 10^5–10^6 times weaker than those of S-GRBs, although their $E_{\rm iso}$ is only a factor of 10^2 smaller (see also the Appendix).

6.3. Prototypes

In Table 4 we indicate the selected prototypes of S-GRFs. For each of them, we list the values of $E_{\rm iso}$ and z used in order to evaluate their rate.

7. THE SHORT GRBs

7.1. General Properties

The observational features of short bursts with energy above $\approx 10^{52}$ erg are listed below and summarized in Figure 5. These bursts are interpreted within the theoretical framework of the NS–NS merger paradigm in the fireshell model as a new class that we indicate as S-GRBs.

The lower limit on the energetics of the S-GRBs is $(2.44 \pm 0.22) \times 10^{52}$ erg as measured in GRB 081024B.

The isotropic energies are in the range $(2.44 \pm 0.22) \times 10^{52} \lesssim E_{\rm iso} \lesssim (2.83 \pm 0.15) \times 10^{53}$ erg (see Figure 1 and Zhang et al. 2012; Muccino et al. 2013; Calderone et al. 2015; Ruffini et al. 2015b).

The spectral peak energies are in the range $2 \lesssim E_{\rm p,i} \lesssim 8$ MeV (see Figure 1 and Zhang et al. 2012; Muccino et al. 2013; Calderone et al. 2015; Ruffini et al. 2015b) and increase monotonically with $E_{\rm iso}$.

The cosmological redshifts are in the range $0.903 \leqslant z \leqslant 5.52$, with an average value of $\approx$2.48 (see Table 5).

The P-GRB and the prompt emission components have a total duration of a few seconds, which is expected to crucially be a function of the masses of the binary NSs (see Figures 5(a) and (b)).

Only in the case of GRB 090510 has an X-ray afterglow been observed not conforming to any known afterglow (see Figure 5(c)).

For all S-GRBs no SN association is expected or observed.

In all S-GRBs an extremely high energy GeV emission has been observed (see Figure 5(d)). It is interesting that even in one case, which was outside the nominal *Fermi*-LAT field of view, evidence for high-energy emission has been found (Ackermann et al. 2013; R. Ruffini & Y. Wang 2016, in preparation).

Table 4
List of the S-GRFs Considered in This Work up to the End of 2014

GRB	z	$E_{\rm iso}/(10^{50}$ erg)	GRB	z	$E_{\rm iso}/(10^{50}$ erg)
050509B	0.225	0.085 ± 0.022	090927	1.37	27.6 ± 3.5
050709	0.161	0.80 ± 0.08	100117A	0.915	78 ± 10
051221A	0.546	26.3 ± 3.3	100206A	0.408	4.67 ± 0.61
060502B	0.287	4.33 ± 0.53	100625A	0.453	7.50 ± 0.30
061201	0.111	1.51 ± 0.73	100724A	1.288	16.4 ± 2.4
061217	0.827	42.3 ± 7.2	101219A	0.718	48.8 ± 6.8
070429B	0.902	4.75 ± 0.71	111117A	1.3	34 ± 13
070724A	0.457	0.60 ± 0.14	120804A	1.3	70 ± 15
070729	0.8	11.3 ± 4.4	130603B	0.356	21.2 ± 2.3
070809	0.473	2.76 ± 0.37	131004A	0.717	12.7 ± 0.9
080123	0.495	11.7 ± 3.9	140622A	0.959	0.70 ± 0.13
080905A	0.122	6.58 ± 0.96	140903A	0.351	1.41 ± 0.11
090426	2.609	44.5 ± 6.6	141004A	0.573	21.0 ± 1.9
090515	0.403	0.094 ± 0.014			

Note. For each source (first and fourth columns) the values of z and $E_{\rm iso}$ (second, third, fifth, and sixth columns) are listed.

7.2. Theoretical Interpretation of S-GRBs within the NS–NS Merger Paradigm in the Fireshell Model

S-GRBs originate from NS–NS mergers with initial total mass $m_1 + m_2$ leading to a merged core with mass larger than $M_{\rm crit}$ so that a BH is formed (Ruffini et al. 2015b). In order to conserve energy and momentum, the outcome of such S-GRBs is a KNBH with additional orbiting material, or a binary companion (Bildsten & Cutler 1992; Ruffini et al. 2015b). If we compare and contrast the different episodes encountered in the description of the BdHNe (see Section 5) with those of S-GRBs, we find some remarkable analogies but also some differences in view of the simplicity of the underlying physical system of S-GRBs, which, unlike the BdHNe, do not exhibit any of the extremely complex activities related to the SN (see Section 5).

Episode 1 corresponds here to the activity of the NS–NS merger before the gravitational collapse into a BH. Because of the compactness of the systems, this process at times is not observable, or it possibly corresponds to faint precursors observed in some short bursts (see, e.g., Troja et al. 2010 and Ruffini et al. 2016).

Episode 2 corresponds to the GRB emission stemming from the NS–NS merger. It is described within the fireshell model as composed of two components (see Section 2): the P-GRB emission, with a mainly thermal spectrum (see Figure 5(a)), and the prompt emission, with a characteristic nonthermal spectrum (see Figure 5(b)). Typically in all S-GRBs so far analyzed (see, e.g., GRB 090227B, Muccino et al. 2013; GRB 140619B, Ruffini et al. 2015b) the baryon load is standard, e.g., $B \approx 10^{-5}$, and is consistent with the crustal masses of NS–NS mergers (Belvedere et al. 2014; Ruffini et al. 2015b). The average densities of the CBM where S-GRBs occur are $\langle n_{\rm CBM}\rangle \approx 10^{-5}\,{\rm cm}^{-3}$, typical of the halos of GRB host galaxies (see, e.g., Muccino et al. 2013; Ruffini et al. 2015b). Most remarkable is that this model gives the theoretical explanation for the fulfillment of the $E_{\rm p,i}$–$E_{\rm iso}$ relation for the short bursts (see Figure 1 and Zhang et al. 2012; Calderone et al. 2015; Ruffini et al. 2015b).

Episode 3, which corresponds to the traditional X-ray afterglow, is missing here in view of the absence of the SN and of all the characteristic processes originating from the interaction between the GRB and the SN ejecta, as in the case of BdHNe (see Section 5). At times S-GRBs have nonprominent X-ray or optical emissions (see Figure 5(c)).

Episode 4, identified with the optical emission of an SN, is here missing.

Episode 5 coincides with the long-lived GeV emission. All S-GRBs consistently exhibit this emission, which appears to be strictly correlated to the one observed in the BdHNe. By analogy with BdHNe, we assume that the GeV emission originates from the activity of the newly born KNBH produced in the merger (Ruffini et al. 2015b). Indeed, the presence of a BH is the only commonality between BdHNe and S-GRBs. By comparing and contrasting Figures 3(d) and 5(d), we see that the turn-on of the GeV emission in S-GRBs occurs earlier and is energetically more prominent than the corresponding one of the BdHNe. To emphasize this point in Figure 5(d) we have represented by a dashed line the minimal turn-on time of the GeV emission of BdHNe (see Ruffini et al. 2016; R. Ruffini et al. 2016, in preparation). The very high angular momentum, expected to occur in NS–NS mergers, and the very high luminosities of the S-GRBs, originating in the corresponding BH formation, offer a great opportunity to analyze some of the features expected in a KNBH.

7.3. Prototypes

In Table 5 we list all the S-GRBs identified so far.

The first identified S-GRB, GRB 090227B, has been analyzed by Muccino et al. (2013). The analysis of its P-GRB emission has found a baryon load $B = 4.13 \times 10^{-5}$ and a Lorentz factor at the transparency condition $\Gamma = 1.44 \times 10^4$. The fit of the light curve of the prompt emission allowed the determination of the average number density of the CBM, i.e., $\langle n_{\rm CBM}\rangle = 1.9 \times 10^{-5}\,{\rm cm}^{-3}$, which is typical of galactic halos where NS–NS mergers migrate, owing to natal kicks imparted to the binaries at birth (see, e.g., Berger 2014). These values are strikingly similar to those inferred for other S-GRBs: GRB 081024B ($B = 4.80 \times 10^{-5}$, $\Gamma = 1.07 \times 10^4$, and $\langle n_{\rm CBM}\rangle = 5.0 \times 10^{-6}\,{\rm cm}^{-3}$; Y. Aimuratov et al. 2016, in preparation), GRB 090510 ($B = 5.54 \times 10^{-5}$, $\Gamma = 1.04 \times 10^4$, and $\langle n_{\rm CBM}\rangle = 8.7 \times 10^{-6}\,{\rm cm}^{-3}$; Ruffini et al. 2016), and GRB 140619B ($B = 5.52 \times 10^{-5}$, $\Gamma = 1.08 \times 10^4$, and $\langle n_{\rm CBM}\rangle = 4.7 \times 10^{-5}\,{\rm cm}^{-3}$; Ruffini et al. 2015b).

With the exception of GRB 090227B, which was outside the nominal *Fermi*-LAT field of view (Ackermann et al. 2013), the GeV luminosity light curves of the above four S-GRBs and that of the additional example recently identified, GRB 140402A (R. Ruffini et al. 2016, in preparation), follow a common behavior when computed in the source rest frame (see Figure 5(d)).

8. ULTRASHORT GRBs

As pointed out in the Introduction, U-GRBs originate from the NS–BH binaries produced in the BdHNe, and nearly 100% of these binaries remain bound (Fryer et al. 2015). The lack of any observed source to date is mainly due to the extremely short duration of these systems (Fryer et al. 2015).

Interesting considerations, which may be of relevance for describing the U-GRB subclass, can be found in Popham et al. (1999).

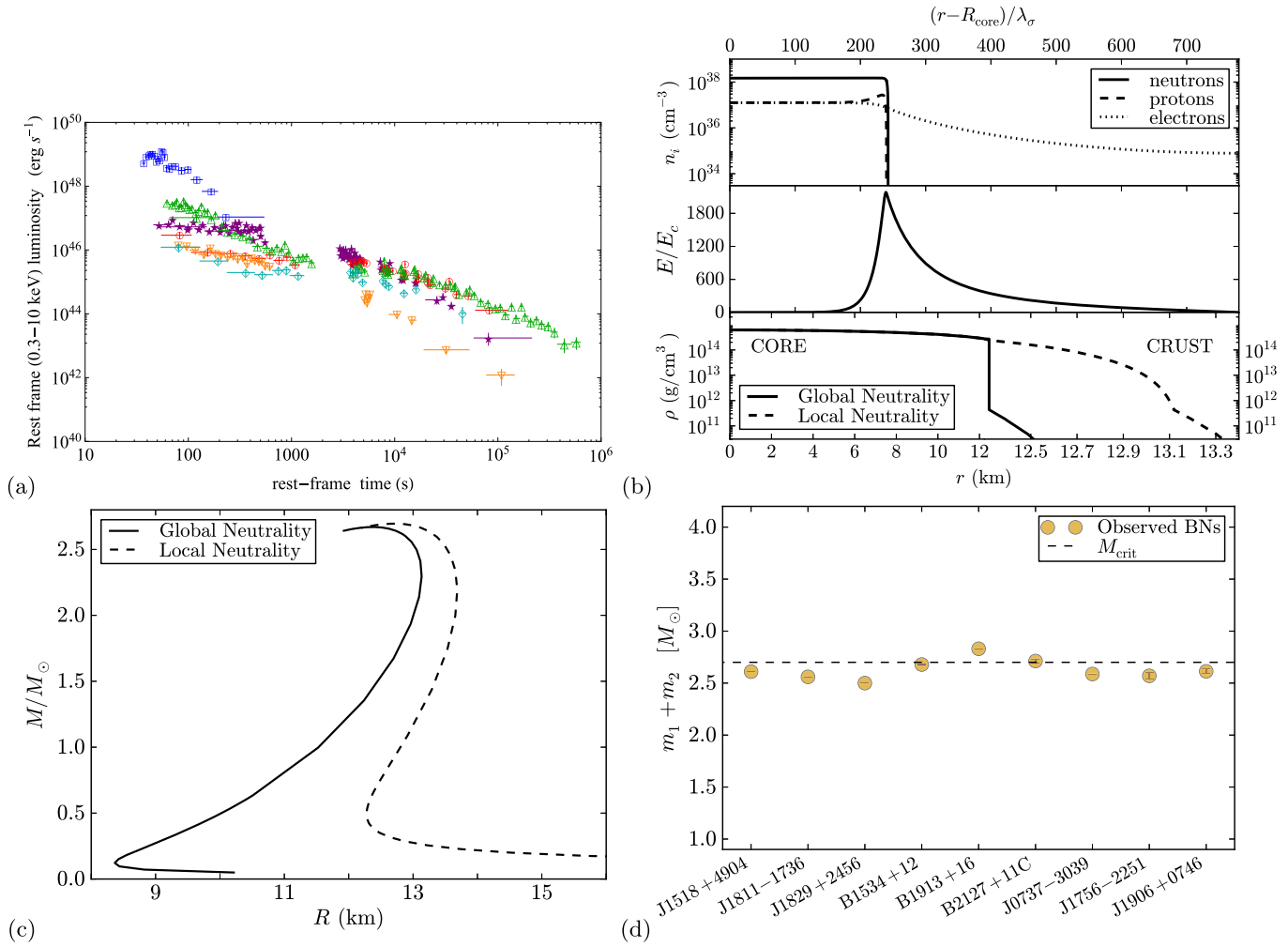

Figure 4. (a) Rest-frame 0.3–10 keV luminosity light curves of some selected S-GRFs: GRB 051210 (blue squares), GRB 051221 (green triangles), GRB 061201 (orange downward-pointing triangles), GRB 070809 (light-blue diamonds), GRB 130603B (purple stars), and GRB 140903A (red circles). See Table 4 for details on the sources. (b) Upper panel: particle density profiles in the NS core–crust boundary interface. Middle panel: electric field in the core–crust transition layer in units of E_c. Lower panel: density profile inside an NS with central density $\rho \sim 5\rho_{\rm nuc}$, where $\rho_{\rm nuc}$ is the nuclear density, from the solution of the Tolman–Oppenheimer–Volkoff (TOV) equations (locally neutral case) and the globally neutral solution presented in Belvedere et al. (2012). Here the density at the edge of the crust is the neutron drip density $\rho_{\rm drip} = 4.3 \times 10^{11}$ g cm^{-3}, and $\lambda_\sigma = \hbar/(m_\sigma c) \sim 0.4$ fm denotes the σ-meson Compton wavelength. Reproduced from Oliveira et al. (2014) with their kind permission. (c) Mass–radius relation obtained with the local and the new global neutrality equilibrium configurations, by applying the NL3 nuclear model, with a critical mass of 2.67 $M_\odot$ for nonrotating NSs (Belvedere et al. 2012). Figure reproduced from Belvedere et al. (2012). (d) Plot of the galactic binary NSs with known total masses ($m_1 + m_2$, in solar masses). The horizontal dashed line marks the NS critical mass: systems beyond this value lead to BH formation. Reproduced from Ruffini et al. (2015b).

Table 5
List of the S-GRBs Considered in This Work up to the End of 2014

GRB	z	$E_{\rm iso}/(10^{52}$ erg)	GRB	z	$E_{\rm iso}/(10^{52}$ erg)
060801	1.13	3.27 ± 0.49	090510	0.903	3.95 ± 0.21
081024B	3.05	2.44 ± 0.22	140402A	5.52	4.7 ± 1.1
090227B	1.61	28.3 ± 1.5	140619B	2.67	6.03 ± 0.79

Note. For each source (first and fourth columns) the values of z and $E_{\rm iso}$ (second, third, fifth, and sixth columns) are listed.

9. THE GAMMA-RAY FLASHES

9.1. General Properties

The observational features of short bursts followed by an extended emission with energy below $\approx 10^{52}$ erg are listed below and summarized in Figure 6. These bursts are interpreted within the theoretical framework of a binary merger of an NS and a massive WD (della Valle et al. 1992, 1994) in the fireshell model as a new class that we indicate as GRFs.

The upper limit on the energetics of the GRFs is $(9.8 \pm 2.4) \times 10^{51}$ erg, as measured in GRB 070714B.

The isotropic energies are in the range $(8.9 \pm 1.6) \times 10^{49} \lesssim E_{\rm iso}$ erg $\lesssim (9.8 \pm 2.4) \times 10^{51}$ erg.

The spectral peak energies are in the range $0.2 \lesssim E_{\rm p,i} \lesssim 2$ MeV.

The cosmological redshifts are in the range $0.089 \leqslant z \leqslant 2.31$, with an average value of ≈ 0.54 (see Table 6).

The γ-ray emission is composed of (1) an initial spike-like harder emission and (2) a prolonged softer emission observed for up to 100 s (see Figure 6(a)).

The long-lasting X-ray afterglow does not exhibit any specific common late power-law behavior (see Figure 6(b)).

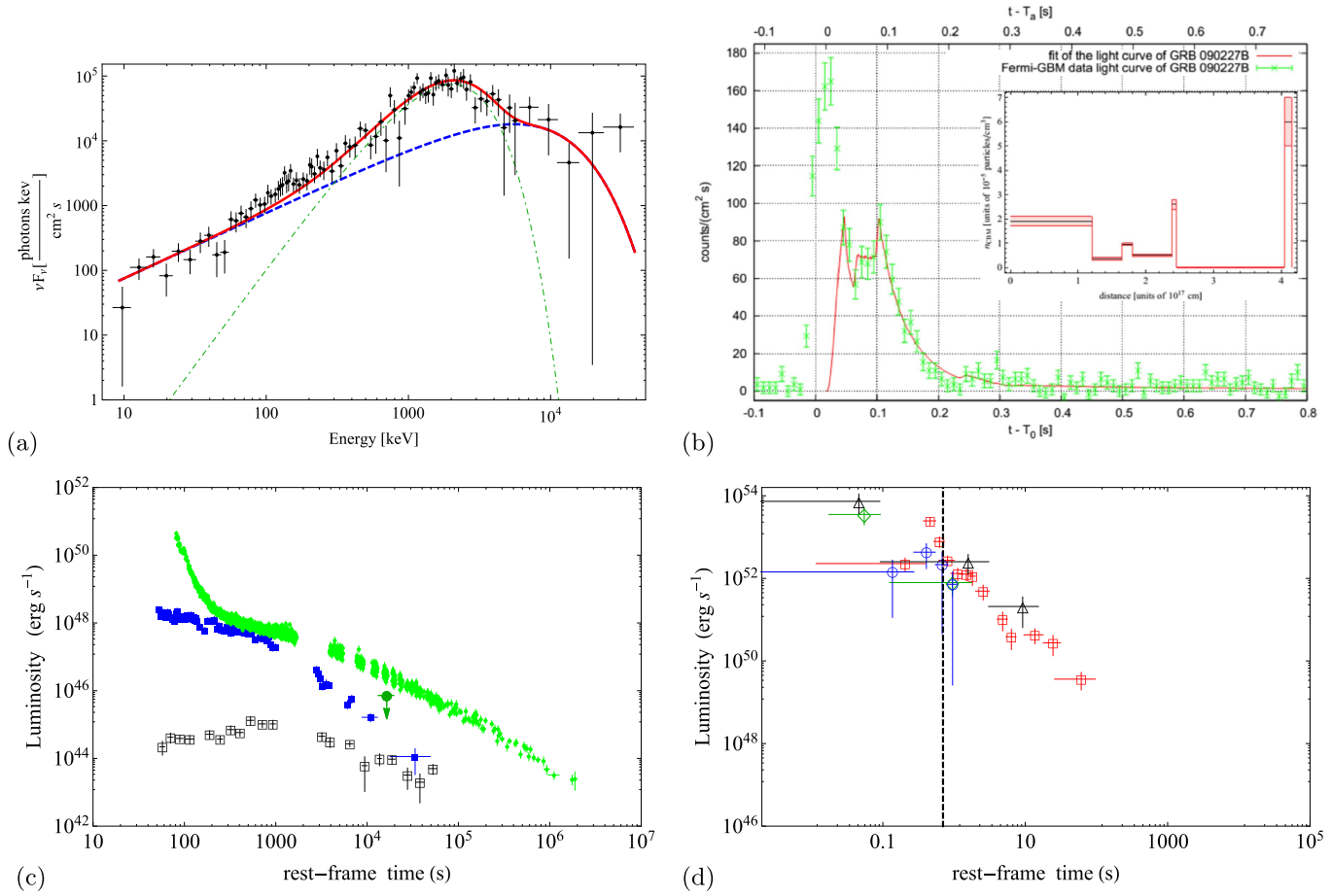

Figure 5. (a) Simulation of the observed P-GRB spectrum of the prototypical S-GRB 090227B: the dot-dashed green line represents the BB emission, and the dashed blue line corresponds to the early onset of the prompt emission within the P-GRB computed from the fireshell simulation in the energy band 8–40,000 keV; the sum of the two components is shown as a solid red line. Reproduced from Muccino et al. (2013). (b) NaI-n2 light curve of the prompt emission of the S-GRB 090227B (green data) and the simulation within the fireshell model (red curve). The inset reproduces the CBM profile required for the simulation. Reproduced from Muccino et al. (2013). (c) Available X-ray and optical luminosities of S-GRBs: the X-ray rest-frame 0.3–10 keV (blue filled squares) and the optical rest-frame 2–7 eV (black open squares, taken from De Pasquale et al. 2010) luminosity light curves of GRB 090510, and the X-ray rest-frame 0.3–10 keV upper limit of GRB 140619B (green filled circle; see, e.g., Ruffini et al. 2015b). For comparison the rest-frame 0.3–10 keV luminosity light curve of one of the prototypes of BdHNe, GRB 090618 (green circles), is shown. (d) Rest-frame 0.1–100 GeV luminosity light curves of the S-GRBs 081024B (green diamonds), 090510 (red squares), 140402A (black triangles), and 140619B (blue circles). The dashed vertical line marks the minimal turn-on time of the GeV emission of BdHNe. It is clear that in the case of S-GRBs the GeV emission turns on at shorter timescales and exhibits larger luminosities.

No SN association is expected or observed also in the case of nearby sources (Della Valle et al. 2006).

No high-energy GeV emission is expected or observed in the absence of BH formation.

9.2. Theoretical Interpretation of GRFs within the NS–WD Merger Paradigm in the Fireshell Model

As we mentioned, the mergers of NS–WD binaries, notoriously very common astrophysical systems (Cadelano et al. 2015), can be the progenitors of another GRB subclass: the GRFs. Possible evolutionary scenarios leading to NS–WD mergers have been envisaged, e.g., in Lazarus et al. (2014) and Tauris et al. (2000). Another less likely but possible scenario is the merger of an NS–WD binary produced, as recalled in Section 6.2, from an S-GRF, namely, the merger of a mass-asymmetric NS–NS binary with total mass $m_1 + m_2$ smaller than $M_{\rm crit}$, which produces an MNS with a low-mass WD companion (see, e.g., Bildsten & Cutler 1992, and references therein), due to the energy and momentum conservation laws (Ruffini et al. 2015b).

With the term GRFs we dubbed a class of L-GRBs occurring in a CBM environment with low density, e.g., $\sim 10^{-3}$ cm^{-3}, with a light curve in γ-rays composed of an initial spike-like hard emission, identified with the P-GRB, and prolonged softer emission, explained as the prompt emission (see Figure 6(a) and Caito et al. 2009, 2010). No associated SN has ever been observed, although in the case of the low value of the cosmological redshift its detection would not have been precluded (Della Valle 2006). The prototype of such systems is GRB 060614 (Caito et al. 2009).

Apart from the absence of any SN associated with a GRF, the identification of NS–WD binaries as progenitor systems of the GRFs comes from the following observational and theoretical evidence: (a) the initial spike-like emission fulfills the $E_{\rm p,i}$–$E_{\rm iso}$ relation for S-GRFs and S-GRBs (Zhang et al. 2012; Calderone et al. 2015; Ruffini et al. 2015b), both originating in NS–NS mergers (Ruffini et al. 2015b); (b) the value of the baryon load, $B \approx 10^{-3}$ (Caito et al. 2009, 2010) points to a system more baryon contaminated than the simpler and more compact NS–NS merger ($B \approx 10^{-5}$, see, e.g., Ruffini

Table 6
List of the GRFs Considered in This Work up to the End of 2014

GRB	z	$E_{\rm iso}/(10^{50}$ erg)	GRB	z	$E_{\rm iso}/(10^{50}$ erg)
050724	0.257	6.19 ± 0.74	061021	0.3462	50 ± 11
050911	0.165	0.89 ± 0.16	061210	0.409	0.24 ± 0.06
060505	0.089	2.35 ± 0.42	070506	2.31	51.3 ± 5.4
060614	0.125	21.7 ± 8.7	070714B	0.923	98 ± 24
061006	0.438	17.9 ± 5.6	071227	0.381	8.0 ± 1.0

Note. For each source (first and fourth columns) the values of z and $E_{\rm iso}$ (second, third, fifth, and sixth columns) are listed.

et al. 2015b); (c) the fit of the prompt emission within the fireshell model provides the CBM with low density, e.g., $\sim 10^{-3}$ cm^{-3}, typical of the halos of the GRB host galaxies (Caito et al. 2009, 2010); (d) the presence of a macronova emission in the optical afterglow of the prototype GRF 060614 (Jin et al. 2015).

In summary, we list below the different episodes observed (or not) in GRFs.

Episode 1 does not exist due to the compactness of the NS–WD merger.

Episode 2 corresponds to the γ-ray emission stemming from the NS–WD merger. The fireshell theory still applies to these systems in view of the considerations presented in Section 2. Also in this case a viable mechanism consists in the pair creation via $\nu\bar{\nu} \leftarrow e^+e^-$ during an NS–WD merger (see, e.g., Paschalidis et al. 2011). This is in line with an upper limit to the energetics of these systems in γ-rays of $E_{\rm iso} \approx 10^{52}$ erg.

Episode 3 in GRFs, like in the cases of XRFs and S-GRFs, does not exhibit either a late common power-law behavior or the nesting discovered in the rest-frame 0.3–10 keV luminosity light curves of BdHNe (see Figure 6(b)). Also for GRFs, possible candidates for the explanation of the late X-ray afterglow emission are (a) the accelerated baryons interacting with the CBM after the P-GRB emission or (b) the possible radioactive decay of heavy elements synthesized in the ejecta of a compact binary merger (Li & Paczyński 1998).

Episode 4 is missing in view of the absence of the SN.

Episode 5, namely, the GeV emission, does not occur for NS–WD mergers. This fact, together with the energetics of these systems, $E_{\rm iso} < 10^{52}$ erg, implies that both of these necessary and sufficient conditions for the BH formation are not fullfilled. Therefore, in an NS–WD merger, in view of the limited mass of the WD component, the NS critical mass is never reached in the accretion process during the merger.

9.3. Prototypes

In Table 6 we list all the GRFs identified so far.

The prototype of GRFs is GRB 060614 and has been analyzed by Caito et al. (2009). From the analysis of its P-GRB emission a baryon load $B = 2.8 \times 10^{-3}$ and a Lorentz factor at the transparency condition $\Gamma = 346$ have been found. From the fit of the light curve of the prompt emission it has been inferred that this burst occurred in a CBM with density $n_{\rm CBM} = 2.3 \times 10^{-5}$–$4.8 \times 10^{-3}$ cm^{-3}, which is typical of galactic halos where NS–NS and NS–WD mergers occur (see, e.g., Berger 2014). Analogous results were obtained for the GRF 071227: $B = 2.0 \times 10^{-4}$ and $n_{\rm CBM} = 1.0 \times 10^{-4}$–$1.0 \times 10^{-2}$ cm^{-3} (Caito et al. 2010).

Further analyses on other GRF examples will be presented elsewhere.

10. THE OBSERVED RATES OF SHORT AND LONG BURSTS

The observed GRB occurrence rate is defined by the convolution of both (likely redshift-dependent) luminosity function, which describes the fraction of bursts with isotropic equivalent luminosities in the interval $\log L$ and $\log L + d\log L$, and cosmic GRB occurrence rate, which gives the number of sources at different redshifts. The definition of both of these functions is still an open issue and depends on a priori assumptions, and some investigations have been carried out in the literature (see, e.g., Soderberg et al. 2006; Guetta & Della Valle 2007; Liang et al. 2007; Virgili et al. 2009; Rangel Lemos et al. 2010; Wanderman & Piran 2010; Guetta et al. 2011; Kovacevic et al. 2014, for long bursts; Virgili et al. 2011; Wanderman & Piran 2015, for short bursts; and Sun et al. 2015, for both long and short bursts). To complicate the matter, also the instrumental sensitivity threshold, the field of view Ω_i, and the operational time T_i of the various detectors i observing GRBs introduce additional uncertainties to the problem.

In the following we ignore the possible redshift evolution of the luminosity function. Thus, if ΔN_i events are detected by various detectors in a finite logarithmic luminosity bin from $\log L$ to $\log L + \Delta \log L$, the total local event rate density of bursts between observed minimum and maximum luminosities, $L_{\rm min}$ and $L_{\rm max}$, respectively, is defined as (see Sun et al. 2015)

$$\rho_0 \simeq \sum_i \sum_{\log L_{\rm min}}^{\log L_{\rm max}} \frac{4\pi}{\Omega_i T_i} \frac{1}{\ln 10} \frac{1}{g(L)} \frac{\Delta N_i}{\Delta \log L} \frac{\Delta L}{L}, \tag{2}$$

where

$$g(L) = \int_0^{z_{\rm max}(L)} \frac{f(z)}{1+z} \frac{dV(z)}{dz} dz, \tag{3}$$

and the comoving volume is given by

$$\frac{dV(z)}{dz} = \frac{c}{H_0} \frac{4\pi d_L^2}{(1+z)^2 [\Omega_M (1+z)^3 + \Omega_\Lambda]^{1/2}}, \tag{4}$$

where d_L is the luminosity distance. The dimensionless function $f(z)$ describes the GRB cosmic redshift-dependent event rate density. In the following we assume no redshift dependency; therefore, we set $f(z) = 1$. The maximum redshift $z_{\rm max}(L)$ in Equation (3) defines the maximum volume inside which an event with luminosity L can be detected. This redshift can be computed from the 1 s bolometric peak luminosity L, k-corrected from the observed detector energy band into the burst cosmological rest-frame energy band 1–10^4 keV (Schaefer 2007), and the corresponding 1 s threshold peak flux $f_{\rm th}$, which is the limiting peak flux to allow the burst detection (see Band 2003, for details). Therefore, $z_{\rm max}$ can be defined via (see, e.g., Zhang et al. 2009; Ruffini et al. 2014a)

$$f_{\rm th} = \frac{L}{4\pi d_L^2(z_{\rm max}) k}, \tag{5}$$

where we duly account for the k-correction.

Within the assumptions that the GRB luminosity function does not evolve with redshift and that $f(z) = 1$, we investigate the evolution with the redshift of the GRB rates by separating the bursts into several redshift bins. As suggested in Sun et al. (2015), this can be done in each redshift interval $z_j \leqslant z \leqslant z_{j+1}$ by changing the integration limits of Equation (3) into z_j and min $[z_{j+1}, z_{\max,j}(L)]$, where $z_{\max,j}(L)$ is the maximum redshift for the jth redshift bin. Finally, from Equation (2) we derive an event rate ρ_0^z in each redshift bin around z.

In the following we adopt the following fields of view and operational times for various detectors: *BeppoSAX*, $\Omega_{\rm BS} = 0.25$ sr, $T_{\rm BS} = 7$ yr; BATSE, $\Omega_{\rm B} = \pi$ sr, $T_{\rm B} = 10$ yr, *HETE*-2, $\Omega_{\rm H} = 0.8$ sr, $T_{\rm H} = 7$ yr; *Swift*-BAT, $\Omega_{\rm S} = 1.33$ sr, $T_{\rm S} = 10$ yr; *Fermi*-GBM, $\Omega_{\rm F} = 9.6$ sr, $T_{\rm F} = 7$ yr. We assume no beaming correction in computing the rates of the GRB subclasses.

10.1. Rate of S-GRFs

The local rate of S-GRFs, obtained from the sample of sources listed in Table 4, is $\rho_0 = 3.6^{+1.4}_{-1.0}\,{\rm Gpc}^{-3}\,{\rm yr}^{-1}$, and it is in agreement with the estimates obtained from the whole short-burst population detected by the *Swift*-BAT detector (and, therefore, including also S-GRBs and GRFs) and reported in the literature (1–10 $\rm Gpc^{-3}\,yr^{-1}$; see, e.g., Clark et al. 2015, and references therein). In particular, our local rates with $f(z) = 1$ agree with recent more precise estimates: (a) $4.1^{+2.3}_{-1.9}\,{\rm Gpc}^{-3}\,{\rm yr}^{-1}$ for $L_{\rm min} = 5 \times 10^{49}\,{\rm erg\,s}^{-1}$ and for $f(z)$ described by a power-law merger delay model (Wanderman & Piran 2015); (b) $4.2^{+1.3}_{-1.0}$, $3.9^{+1.2}_{-0.9}$, and $7.1^{+2.2}_{-1.7}\,{\rm Gpc}^{-3}\,{\rm yr}^{-1}$ for $L_{\rm min} = 7 \times 10^{49}\,{\rm erg\,s}^{-1}$ and $f(z)$ described as Gaussian, lognormal, and power-law merger delay models, respectively (Sun et al. 2015).

The evolution of the S-GRF rate in various redshift bins is shown in Figure 7(c). This rate decreases as a power law from the local value in the interval $0.1 \leqslant z \leqslant 0.4$ to a value of $0.042^{+0.046}_{-0.025}\,{\rm Gpc}^{-3}\,{\rm yr}^{-1}$ in the interval $1.0 \leqslant z \leqslant 2.7$. Also in the case of S-GRFs the increasing sampled comoving universe volume and the threshold of the detectors play a fundamental role in the observed decrease of their rate at larger distances.

10.2. Rate of S-GRBs

Previously we have identified and described four S-GRBs in Ruffini et al. (2015b): GRB 081024B, GRB 090227B, GRB 090510, and GRB 140619B. Here we present two additional new members of this class: GRB 060801 (at $z \approx 1.13$ and with $z_{\max} \approx 2.04$, in this work) and GRB 140402A (at $z \approx 5.52$ and with $z_{\max} \approx 7.16$; R. Ruffini et al. 2016, in preparation). From these six S-GRBs detected by the *Fermi* and *Swift* satellites, we obtain via Equations (2)–(3) a local rate $\rho_0 = (1.9^{+1.8}_{-1.1}) \times 10^{-3}\,{\rm Gpc}^{-3}\,{\rm yr}^{-1}$.

With only six sources, we could not build the evolution with the redshift of such systems.

10.3. Rate of XRFs

In Kovacevic et al. (2014), we have estimated an updated observed rate for the XRFs at $z < 0.1$ based on the method outlined in Soderberg et al. (2006) and Guetta & Della Valle (2007). In this work, we consider the complete list of XRFs shown in Table 2 and the method outlined in Sun et al. (2015). From Equations (2)–(3) the local rate of XRFs is $\rho_0 = 100^{+45}_{-34}$ $\rm Gpc^{-3}\,yr^{-1}$, where the attached errors are determined from the 95% confidence level of the Poisson statistic (Gehrels 1986). Within the extent of our different classification criteria and different choices for $f(z)$, our estimate is in agreement with those reported for low-luminosity L-GRBs in Liang et al. (2007) and Virgili et al. (2009), and in particular with the value of 164^{+98}_{-65} $\rm Gpc^{-3}\,yr^{-1}$, obtained by Sun et al. (2015) with the same method.

In the IGC scenario the XRF out-states are NS–NS binary systems. For a reasonable set of binary initial conditions, population synthesis simulations performed by Fryer et al. (1999) provide an NS–NS formation rate of 0.2–1600 $\rm Gpc^{-3}\,yr^{-1}$. The NS–NS formation rate accounts for other possible channels in the population synthesis models, in addition to the one we considered from the XRFs. It is interesting, nevertheless, that our predicted rate is consistent with that obtained by Fryer et al. (1999).

For the same reason, our rate of XFRs can also be compared with the NS–NS merger rate proposed by Eichler et al. (1989). In this historical paper, the NS–NS merger rate is derived from the strong assumption that each merger ejects always the same amount of material r-process classified and the heavy r-process material. Eichler et al. (1989) obtain a rough estimate of 140–14,000 $\rm Gpc^{-3}\,yr^{-1}$, which is marginally consistent with the upper value of the local XRF rate.

The evolution of the XRF rate in various redshift bins is shown in Figure 7(a). It decreases from a value of 95^{+123}_{-63} $\rm Gpc^{-3}\,yr^{-1}$ in the interval $0 \leqslant z \leqslant 0.1$ to a value of $0.8^{+1.1}_{-0.5}$ $\rm Gpc^{-3}\,yr^{-1}$ in the interval $0.7 \leqslant z \leqslant 1.1$. This effect is mainly due to the intrinsic low luminosities of the bulk of the XRF population (10^{46}–10^{48} $\rm erg\,s^{-1}$; see, e.g., Bromberg et al. 2011) and to the threshold of the detectors: at increasing sampled universe comoving volumes, these low-luminosity XRFs become undetectable; therefore, at higher redshifts the total XRF rate decreases.

10.4. Rate of BdHNe

We proceed now in estimating the rate of BdHNe from the total sample of 233 sources (see Table 3). From Equations (2)–(3) the local rate of BdHNe is $\rho_0 = 0.77^{+0.09}_{-0.08}\,{\rm Gpc}^{-3}\,{\rm yr}^{-1}$. Our estimate is in agreement with two recent estimates obtained from long bursts with $L \geqslant 10^{50}\,{\rm erg\,s}^{-1}$ and by assuming $f(z) \neq 1$: (a) the value of $1.3^{+0.6}_{-0.7}\,{\rm Gpc}^{-3}\,{\rm yr}^{-1}$ obtained by Wanderman & Piran (2010), even though limited to the *Swift* long bursts and including some long bursts with $E_{\rm iso} < 10^{52}$ erg, obtained from a GRB-inferred cosmic rate independent of the star formation rate; (b) the value of $0.8^{+0.1}_{-0.1}\,{\rm Gpc}^{-3}\,{\rm yr}^{-1}$ obtained by Sun et al. (2015) with the same method and including the star formation rate dependence.

In the IGC scenario the BdHNe out-states are NS–BH binary systems. Following again the work by Fryer et al. (1999), population synthesis simulations (which also accounts for alternative scenarios to that of the IGC model) provide an NS–BH formation rate of 0.02–1000 $\rm Gpc^{-3}\,yr^{-1}$. Also in this case, even though a straightforward comparison is not possible, the BdHN rate is consistent with the NS–BH formation rate obtained by Fryer et al. (1999).

The evolution of the BdHN rate in various redshift bins is shown in Figure 7(b). It slightly decreases from the local value in the interval $0.1 \leqslant z \leqslant 0.4$ to a value of $0.17^{+0.05}_{-0.04}\,{\rm Gpc}^{-3}\,{\rm yr}^{-1}$ in the interval $3.6 \leqslant z \leqslant 9.3$. As stated for the case of XRFs, this effect occurs because for increasing sampled universe comoving volumes, only the most luminous BdHNe are

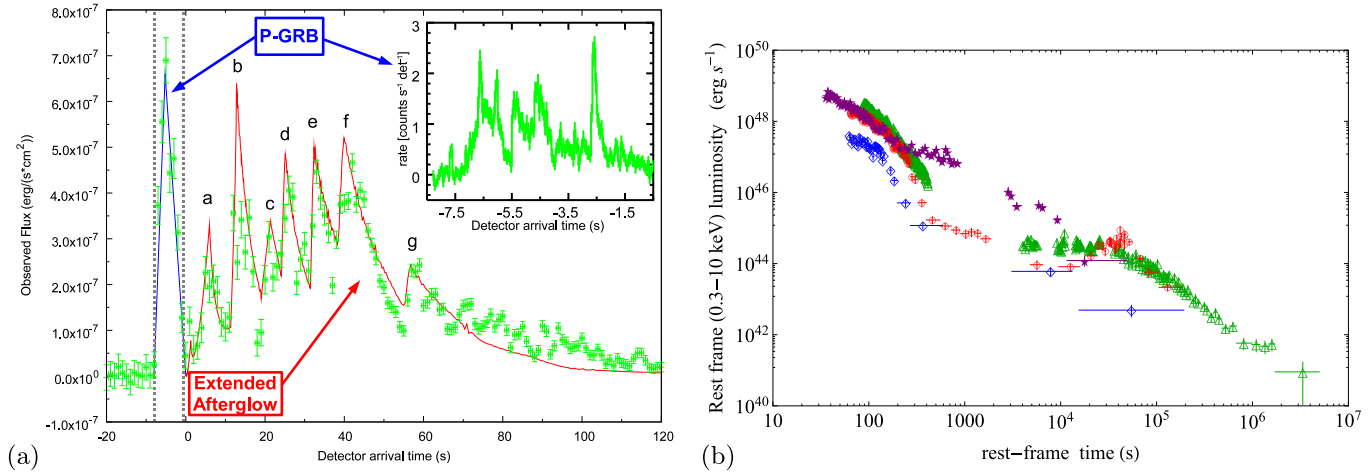

Figure 6. (a) Fireshell simulation of the *Swift*-BAT prompt emission of GRB 060614 (taken from Caito et al. 2009). (b) Rest-frame 0.3–10 keV luminosity light curves of selected GRFs: GRB 050724 (red circles), GRB 060614 (green triangles), GRB 070714B (purple stars), and GRB 071227 (blue diamonds).

detectable, even though in a less marked way than the case of the XRFs.

10.5. Rate of U-GRBs

As pointed out in Section 8, nearly 100% of the BdHNe lead to bound NS–BH binaries, which are the progenitor systems of U-GRBs (Fryer et al. 2015). If we include the possibility of other channels of formation for these NS–BH binaries, we can safely assume the BdHN local rate as a lower limit for these U-GRBs, e.g., $\rho_0 = 0.77^{+0.09}_{-0.08}\ \mathrm{Gpc}^{-3}\ \mathrm{yr}^{-1}$. From this consideration, it appears that the U-GRBs have the second higher rate among the short bursts after the S-GRFs.

10.6. Rate of GRFs

We proceed now in estimating the rate of GRFs from the total sample of 10 sources (see Table 6). From Equations (2)–(3) we obtain a local rate $\rho_0 = 1.02^{+0.71}_{-0.46}\ \mathrm{Gpc}^{-3}\ \mathrm{yr}^{-1}$ and represent the first estimate for these kinds of bursts originating from NS–WD mergers.

Due to the limited number of sources in our sample, we limited the study of the GRF rate evolution to two redshift bins, as shown in Figure 7(d). The rate ranges from a value consistent with the above local rate, in the redshift interval $0 \leqslant z \leqslant 0.35$, to a value of $0.080^{+0.088}_{-0.048}\ \mathrm{Gpc}^{-3}\ \mathrm{yr}^{-1}$, in the interval $0.35 \leqslant z \leqslant 2.31$. Also for GRFs, the cutoff in the rate at higher redshift occurs because for increasing sampled universe comoving volumes only the most luminous sources are detectable. However, this effect, as in the case of S-GRFs, is more pronounced due to their intrinsically weaker luminosities, when compared to those of S-GRBs.

11. CONCLUSIONS

The remarkable progress reached in understanding the GRB phenomenon has been made possible by the outstanding spectral and temporal information acquired from X-rays, γ-rays, and high-energy observatories, as well as from optical and radio data obtained by telescopes all over the planet. At the same time, this result has been fostered by a novel deeper theoretical understanding in the physics and astrophysics of WDs (see, e.g., Boshkayev et al. 2013), NSs (see, e.g., Belvedere et al. 2014; Cipolletta et al. 2015), and BHs (see, e.g., Ruffini et al. 2010). Consequently, the understanding of the GRB phenomenon has evolved from an elementary paradigm based on a single jetted emission process as postulated in the fireball model (see, e.g., Sari et al. 1998; Piran 2005; Meszaros 2006; Gehrels et al. 2009, and references therein) to an authentic astrophysical laboratory involving many-body interactions between different astrophysical systems encountering previously unexplored regimes and observational evidence.

In the Introduction we reviewed the increasing number of GRB observations that have likewise led to the theoretical progress in the understanding of the GRB phenomena. While the role of NS–NS (or NS–BH) binaries as "in-states" of S-GRBs has been widely accepted and confirmed by strong observational and theoretical evidence (see, e.g., Goodman 1986; Paczynski 1986; Eichler et al. 1989; Narayan et al. 1991, 1992; Meszaros & Rees 1997; Rosswog et al. 2003; Lee et al. 2004; Berger 2014; Ruffini et al. 2015b, and figure 8), the identification of the progenitor systems for L-GRBs followed a more difficult path. Initially, theoretical models based on a single progenitor were proposed: a *collapsar* (Woosley 1993) or a *magnetar* (see, e.g., Zhang & Mészáros 2001). Then, the role of binary progenitor systems composed of two very massive stars for L-GRBs was recognized by Fryer et al. (1999), where several different scenarios were there envisaged leading to a *collapsar* (Woosley 1993), as well as a few leading, alternatively, to a variety of binary compact systems. These considerations were addressed by our group in a set of papers assuming that the birth of an SN and the occurrence of a GRB were qualitatively and quantitatively different astrophysical events in space and time. This led to the necessity of introducing the IGC paradigm (see, e.g., Ruffini et al. 2001c, 2006b, 2007, 2008, 2015c; Izzo et al. 2012b; Rueda & Ruffini 2012; Fryer et al. 2014). In the IGC paradigm the L-GRB–SN coincidence originates from $\mathrm{CO}_{\mathrm{core}}$–NS binary progenitor systems (see Figure 8). This approach differs from alternative descriptions, e.g., the *magnetar* and the *collapsar* models, where the two events are coming from a single progenitor star.

In Section 2 we reviewed the fireshell model for GRBs (see, e.g., Ruffini et al. 2001a, 2001b, 2001c) and its general description, which can be applied to any source of an optically

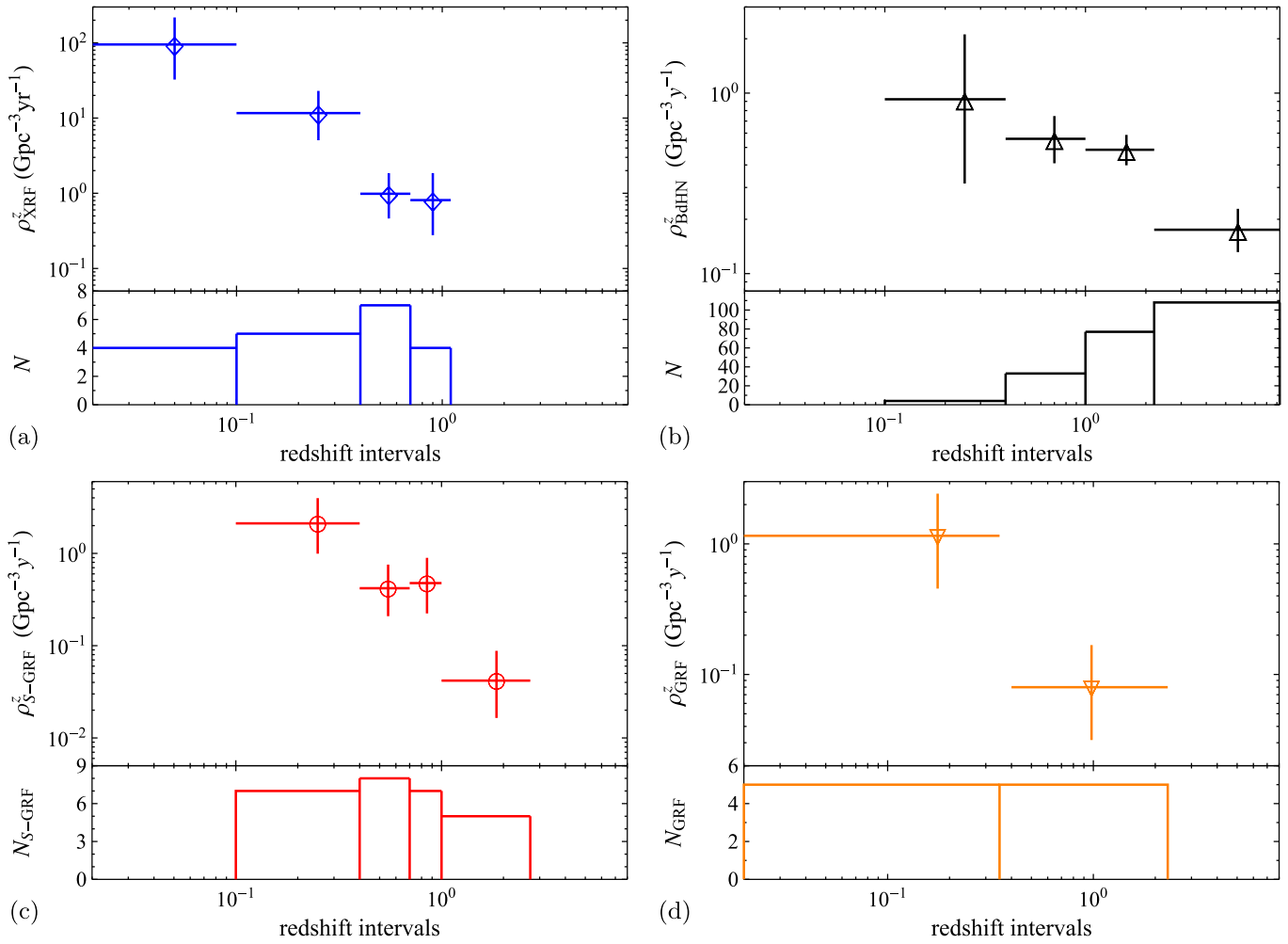

Figure 7. Evolution of the rate with redshift for the considered GRB subclasses: (a) the XRFs, (b) the BdHNe, (c) the S-GRFs, and (d) the GRFs. In each plot the upper panel shows the evolution rate with redshift, while the lower panel displays the number of observed sources in each redshift bin. Because of the limited amount of sources, for S-GRBs no redshift bin evolution is shown. In the case of U-GRBs, there are no current detections.

thick baryon-loaded e^+e^- plasma, i.e., in the quantum electrodynamical process expected in the formation of a BH (see, e.g., Preparata et al. 1998; Ruffini et al. 2000, 1999 Cherubini et al. 2009; Ruffini 2009), as well as in the case of a pair plasma created via $\nu\bar{\nu} \leftrightarrow e^+e^-$ mechanism in an NS–NS merger (Narayan et al. 1992; Salmonson & Wilson 2002; Rosswog et al. 2003), or in the hyperaccretion disks around BHs (Woosley 1993; Zalamea & Beloborodov 2011).

In Section 3 we discussed the role of the 10^{52} erg energy critical value introduced to discriminate between binary systems leading to the formation of an MNS (XRFs, S-GRFs, and GRFs), with energy lower than the above critical value, and those leading to the formation of a BH (BdHNe, S-GRBs, and U-GRBs), with energy larger than the above critical value. The value of 10^{52} erg is derived by considering the hypercritical accretion process onto an NS leading to an energy release in the form of neutrinos and photons, given by the gain of gravitational potential energy of the matter accreted in the NS. This includes the change of binding energy of the NS while accreting both matter and angular momentum (Becerra et al. 2016). A typical NS mass of $\approx$1.4 $M_\odot$ has been assumed, as observed in galactic NS binaries (Zhang et al. 2011; Antoniadis 2015). An NS critical mass in the range from 2.2 up to 3.4 $M_\odot$, depending on the equations of state and angular momentum (see Cipolletta et al. 2015; Becerra et al. 2016, 2015, for details), has been assumed.

In Section 4 we described the properties of XRFs (see Figure 1). In these systems the distance between the CO_{core} and the NS companion is $a > 10^{11}$ cm. The hypercritical accretion process is not sufficient to push the NS beyond its M_{crit}, and an MNS is formed (see, e.g., Becerra et al. 2015, 2016). In Table 2 we list the XRFs considered in this work, as well as the spectral, temporal, and luminosity analysis of a selected prototype, e.g., GRB 060218. The complete theoretical simulation of this prototype is presented in Becerra et al. (2016).

In Section 5 we considered the BdHNe, for which the binary separation between the CO_{core} and the NS binary companion is $a < 10^{11}$ cm and the hypercritical accretion process triggers the gravitational collapse of the NS into a BH (see, e.g., Becerra et al. 2015, 2016). We show here an updated list of BdHNe (see Table 3), as well as a diagram summarizing some of the key properties and prototypes (see Figure 1), analyzed within the IGC paradigm and the fireshell model (see, e.g., GRB 090618 and GRB 130427A).

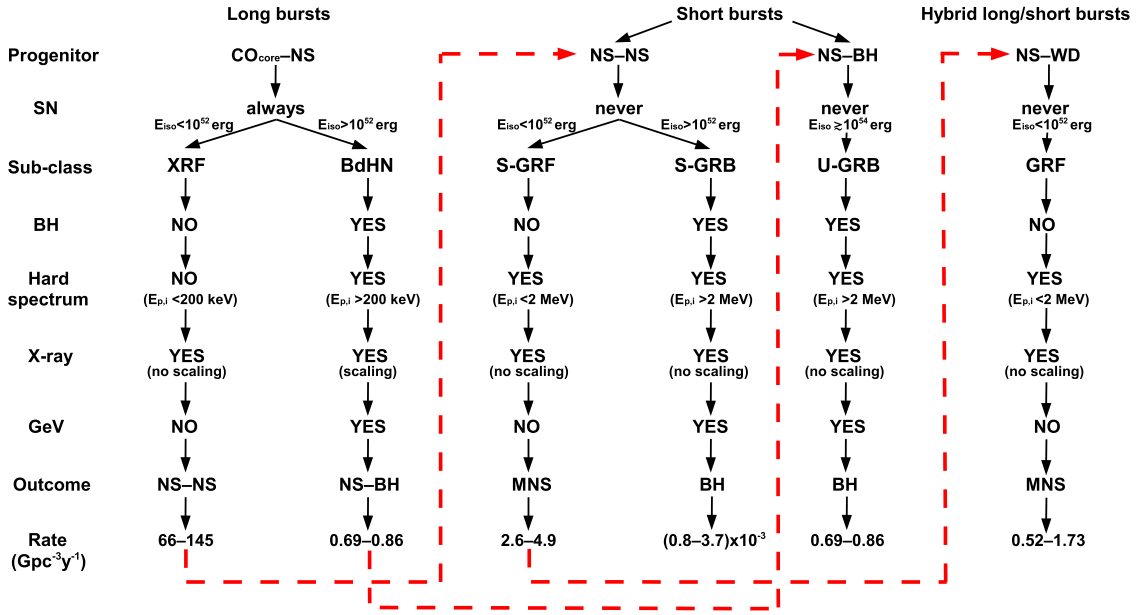

Figure 8. Summary of the properties of long, short, and hybrid long/short burst subclasses discussed in the Introduction. The red dashed lines indicate the evolutionary tracks linking the out-states and the in-states of some of the subclasses considered in this work.

In Section 6 we outlined the properties of S-GRFs listed in Table 4 and shown in Figure 1. These systems coincide with the short bursts considered in Berger (2014). They originate in NS–NS mergers leading to the formation of an MNS and possibly a binary companion, in order to fulfill the conservation of energy and momentum (Ruffini et al. 2015b).

In Section 7 we presented S-GRBs originating in NS–NS mergers leading to the formation of a BH (see Figure 1). We give, in Table 5, their updated list. We then described their prototypes, analyzed within the fireshell model (see, e.g., GRB 090227B and GRB 140619B), and outlined the key role of the P-GRB identification for their description, as well as the analysis of the GeV emission.

In Section 8, motivated by the results obtained by Fryer et al. (2015), where it was shown that nearly 100% of the NS–BH binaries, namely, the out-states of the BdHNe, remain bound, we added the description of this not yet observed but theoretically predicted subclass of U-GRBs, unaccounted for in current standard population synthesis analyses.

In Section 9 we reviewed the properties of the GRFs listed in Table 6 and shown in Figure 1. We recall and describe the results obtained from the sources analyzed within the fireshell model (see, e.g., GRB 060614, Caito et al. 2009; GRB 071227, Caito et al. 2010).

The most important result of the present article is the estimate of the rates of occurrence of the XRFs, BdHNe, S-GRFs, S-GRBs, U-GRBs, and GRFs. In Section 10 we introduced the procedure outlined in Sun et al. (2015) for estimating the local rates and their evolution with the redshift of the above subclasses of long and short bursts, assuming no beaming (note: the recent observation of the absence of GeV emission associated with a BdHN may limit this assumption). By ignoring possible redshift evolution of the GRB subclasses' luminosity functions and assuming that the GRB cosmic event rate density is redshift independent (e.g., $f(z) = 1$), the above method duly takes into account observational constraints, i.e., the detector solid angle coverage of the sky Ω and sensitivities, which in turn define a maximum volume of observation depending on the intrinsic luminosity of the sources (see Section 10 and Soderberg et al. 2006; Guetta & Della Valle 2007; Liang et al. 2007; Virgili et al. 2009, 2011; Rangel Lemos et al. 2010; Wanderman & Piran 2010, 2015; Kovacevic et al. 2014; Sun et al. 2015, for details). We obtain

- an S-GRF local rate of $\rho_0 = 3.6^{+1.4}_{-1.0}\,\mathrm{Gpc}^{-3}\,\mathrm{yr}^{-1}$ (see Section 10.1);
- an S-GRB local rate of $\rho_0 = (1.9^{+1.8}_{-1.1}) \times 10^{-3}\,\mathrm{Gpc}^{-3}\,\mathrm{yr}^{-1}$ (see Section 10.2);
- an XRF local rate of $\rho_0 = 100^{+45}_{-34}\ \mathrm{Gpc}^{-3}\ \mathrm{yr}^{-1}$ (see Section 10.3);
- a BdHN local rate of $\rho_0 = 0.77^{+0.09}_{-0.08}\,\mathrm{Gpc}^{-3}\,\mathrm{yr}^{-1}$ (see Section 10.4; for the above reason this rate coincides with that of the U-GRBs; see Section 10.5);
- a GRF local rate of $\rho_0 = 1.02^{+0.71}_{-0.46}\,\mathrm{Gpc}^{-3}\,\mathrm{yr}^{-1}$ (see Section 10.6).

The local rates of S-GRFs, XRFs, and BdHNe are in agreement, within the extent of the different classification criteria, with those reported in the literature. The local rates of S-GRBs and GRFs are, instead, new ones following from the classification proposed in this work. The evolution with redshift of the rates of XRFs, BdHNe, S-GRFs, and GRFs is shown in Figure 7. It is certainly of interest to compare and contrast these results obtained from the direct observations of the sources in our new classification with the results computed from population synthesis models. Any possible disagreement will give the opportunity to identify possible missing links in the evolutionary phases within population synthesis analysis.

We are now in a position to apply the above rates of S-GRFs, S-GRBs, and U-GRBs to assess the detectability and the expected number of gravitational wave detections by LIGO from NS–NS and NS–BH binaries (Ruffini et al. 2016). We are also ready to apply the above BdHN rate to give an estimate of the contribution of GRBs to cosmic rays (R. Ruffini et al. 2016, in preparation).

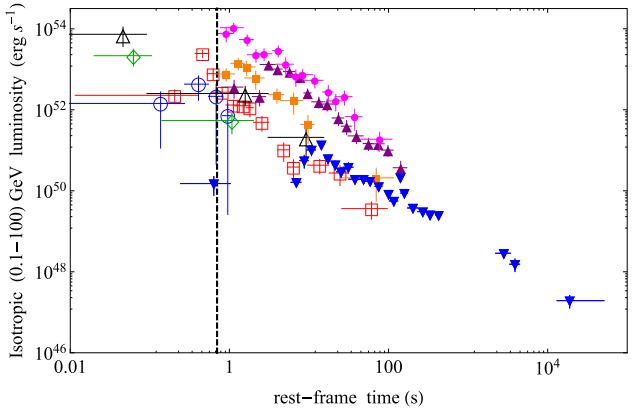

Figure 9. Rest-frame 0.1–100 GeV isotropic luminosity light curves of selected BdHNe (filled symbols) and all S-GRBs with available LAT data (open symbols). BdHNe: GRB 080916C (magenta circles), GRB 090902B (purple triangles), GRB 110731A (orange squares), GRB 130427A (blue downward-pointing triangles). S-GRBs: GRB 081024B (green diamonds), GRB 090510 (red squares), GRB 140402A (black triangles), GRB 140619B (blue circles). Also in this case the dashed vertical line marks the minimal turn-on time of the GeV emission of BdHNe.

Table 7
List of the Prompt and GeV Emission Properties of Selected BdHNe and S-GRBs

Source	z	$E_{p,i}$ (MeV)	$E_{\rm iso}$ (10^{52} erg)	$E_{\rm LAT}$ (10^{52} erg)
		S-GRBs		
081024B	2.6 ± 1.6	8.7 ± 4.9	2.44 ± 0.22	2.70 ± 0.93
090510	0.903	7.89 ± 0.76	3.95 ± 0.21	5.78 ± 0.60
140402A	5.52 ± 0.93	6.1 ± 1.6	4.7 ± 1.1	16.6 ± 5.3
140619B	2.67 ± 0.37	5.34 ± 0.79	6.03 ± 0.79	2.34 ± 0.91
		BdHNe		
080916C	4.35	2.76 ± 0.37	407 ± 86	440 ± 47
090902B	1.822	2.19 ± 0.22	292 ± 29	110 ± 5
110731A	2.83	1.16 ± 0.12	49.5 ± 4.9	42.5 ± 7.4
130427A	0.3399	1.25 ± 0.15	92 ± 13	19.9 ± 2.9

Note. We listed z, $E_{\rm p,i}$, $E_{\rm iso}$ (in the rest-frame energy band 1–10,000 keV), and $E_{\rm LAT}$ (in the rest-frame energy band 0.1–100 GeV).

Before concluding, in support of the classification proposed in this article, we recall that the luminosity light curves of the GeV emission are uniquely observed in both BdHNe and S-GRBs. In both cases it follows a precise power-law behavior with time $\propto t^{-1.2}$ (see Nava et al. 2014; Ruffini et al. 2016; see also Figure 9). An outstanding conclusion of this paper is that in both BdHNe and S-GRBs, where the presence of the BH is predicted, the turn-on of this GeV emission occurs after the P-GRB emission and at the beginning of the prompt emission phase (see Figures 3(d) and 5(d)). This commonality, in such different systems, and their energy requirements (see Table 7 and Figure 9) are naturally explained if we assume, as indicated in Ruffini et al. (2015c, 2015b), that this GeV emission originates by accretion processes in the newly born BH. We have pointed out in Ruffini et al. (2016) how the total energy of the GeV emission can be expressed in terms of the gravitational binding energy of matter accretion into Kerr BHs (see Ruffini & Wheeler 1969, in problem 2 of Section 104 in Landau & Lifshitz 2003). This energetics requirement could not be fulfilled in the case of accretion onto an NS, in view of the much smaller value of the gravitational binding energy when compared to the case of a rotating BH (see, e.g., Sibgatullin & Sunyaev 2000). On the general issue of the origin of the jetted GeV emission, and not just of its energetics, we refer to the last paragraph of the conclusions of Ruffini et al. (2016).

We have added a Table 7 with the values of the GeV emission for the case of both S-GRBs and BdHNe. These energy releases up to $\approx 10^{54}$ erg can be explained by the occurrence of accretion onto a rotating BH with mass in the range of 3–10 $M_\odot$. It is also clear from Figure 9 that S-GRBs and BdHNe have GeV emission sharing a common luminosity pattern and originating, in both cases, from a newly born Kerr BH (Ruffini et al. 2015c, 2015b). This picture includes also the first scenario of an IGC considered in Ruffini et al. (2001c) where an exploding $CO_{\rm core}$ is in a close binary system with an already formed BH companion. In view of the hypercritical accretion process of the SN ejecta onto an already formed BH, these systems have $E_{\rm iso} \gtrsim 10^{54}$ erg and $E_{\rm p,i} \gtrsim 2$ MeV. Their "out-states" are a binary composed of a more massive BH and a νNS. Such systems, which we refer to as BH-SNe, are expected to be the late evolutionary stages of X-ray binaries such as Cyg X-1 or Cyg X-3 (see, e.g., Giacconi & Ruffini 1978).

In conclusion, we have computed the occurence rate of short and long bursts following a new classification and obtaining figures in good agreement with the ones derived from population synthesis models. Essential to the classification have been the following new considerations:

(1) the binary nature of the progenitors and their separation;
(2) the essential role of the hypercritical accretion process onto an NS member of a close binary system, and the possible reaching of $M_{\rm crit}$ by the accretion process and the formation of a BH;
(3) the activity of the newly born BHs originating the energetic prominent GeV emission, which can be explained in terms of the gravitational energy release by accreting matter onto a Kerr BH.

This classification is now open to a verification by the addition of new GRB sources and offers new possibilities of theoretical and observational activities, including:

(1) the reaching of new observational constraints on the value of the NS critical mass $M_{\rm crit}$ and the minimum mass of a BH, which play a fundamental role in defining the separatrix among the different classes of our classification.
(2) having elucidated the role of the activities of the newly born BH in explaining the energetics of the GeV emission, in order to identify its microphysical process, the study of fundamental issues of general relativistic quantum electrodynamical processes appears to be open to further lines of inquiry (see, e.g., Ruffini et al. 2010, and references therein);
(3) it is conceivable that the sizable enlargement of the database of GRBs and of their spectral and luminosity time varability may open the possibilty of further enlarging the above classification.

We thank the editor and the referee for their comments, which helped to improve the presentation and the

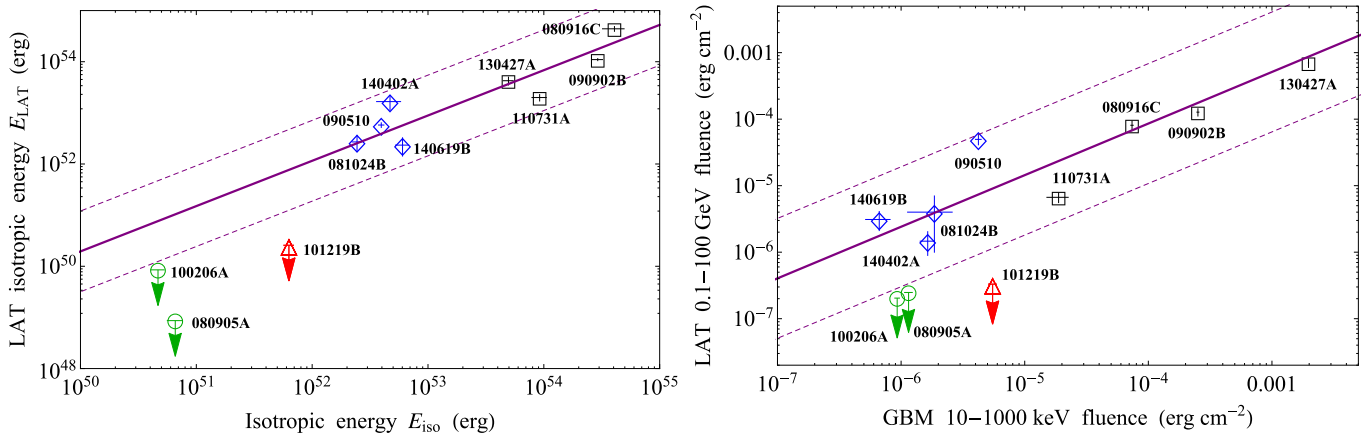

Figure 10. For the sources in Table 7 (BdHNe as black squares and S-GRBs as blue diamonds), as well as for two S-GRFs (green circles) and one XRF (red triangle) that did not exhibit GeV emission although they were in the optimal position (<65° from the LAT boresight) for its detection, we plot (left) the relation between E_{iso} of the prompt emission observed by the *Fermi*-GBM instrument and the total isotropic energy in the 0.1–100 GeV energy band observed by the *Fermi*-LAT instrument (or the corresponding upper limit if not detected) and (right) the relation between the 10–1000 keV fluence observed by the *Fermi*-GBM instrument and the total 0.1–100 GeV fluence observed by the *Fermi*-LAT instrument (or the corresponding upper limit if not detected). The purple solid line is the relation between the plotted quantities of BdHNe and S-GRBs, and the dashed lines are the corresponding dispersion.

contextualization of our results. This work made use of data supplied by the UK Swift Science Data Center at the University of Leicester. J.A.R. acknowledges the support by the International Cooperation Program CAPES-ICRANet financed by the CAPES-Brazilian Federal Agency for Support and Evaluation of Graduate Education within the Ministry of Education of Brazil. M.K. and Y.A. are supported by the Erasmus Mundus Joint Doctorate Program Grant N. 2013–1471 and 2014-0707, respectively, from EACEA of the European Commission. M. M. acknowledges the partial support of the project N 3101/GF4 IPC-11 and the target program F.0679 of the Ministry of Education and Science of the Republic of Kazakhstan.

APPENDIX
ON THE NONOBSERVED GEV EMISSION IN S-GRFs AND XRFs

In Figure 10 we compare and contrast the sources in Table 7, all exhibiting a GeV emission, with two S-GRFs and one XRF that, as theoretically expected within the fireshell model, do not exhibit any GeV emission. All these sources were in the optimal position (<65° from the LAT boresight) for the detection of the GeV emission.

In the left panel we plot the values of E_{iso} and of the isotropic energy in the *Fermi*-LAT energy band, or the corresponding upper limits if not observed. These upper limits were obtained by using the unbinned likelihood analysis that was performed assuming an integration time of 100 s after the flash trigger, a radius of the source region of 10°, and a zenith angle cut of 100°. This plot observationally supports the theoretical expectation, made in Ruffini et al. (2016) and quoted in Section 6.2 above, that S-GRFs have, if any, GeV fluxes necessarily 10^5–10^6 times weaker than those of S-GRBs, although their E_{iso} is only a factor of 10^2 smaller.

Motivated by a request of the referee, we also plotted, in the right panel, the values of the fluence observed by *Fermi*-GBM and by *Fermi*-LAT, or the corresponding upper limits if not observed (computed as above).

From both plots it is clear that the upper limits to the GeV emission of S-GRFs and XRFs are much lower than what one may expect from the extrapolation to lower energies of the one observed in BdHNe and S-GRBs. This is a further clear observational support to the absence, theoretically implied by the fireshell model, of any GeV emission associated with S-GRFs and XRFs (see Sections 4.2 and 6.2).

REFERENCES

Ackermann, M., Ajello, M., Asano, K., et al. 2013, ApJS, 209, 11
Aksenov, A. G., Ruffini, R., & Vereshchagin, G. V. 2007, PhRvL, 99, 125003
Aksenov, A. G., Ruffini, R., & Vereshchagin, G. V. 2009, PhRvD, 79, 043008
Amati, L., & Della Valle, M. 2013, IJMPD, 22, 30028
Amati, L., Frontera, F., in't Zand, J. J. M., et al. 2004, A&A, 426, 415
Antoniadis, J. 2015, ASSP, 40, 1
Atwood, W. B., Abdo, A. A., Ackermann, M., et al. 2009, ApJ, 697, 1071
Band, D. L. 2003, ApJ, 588, 945
Becerra, L., Bianco, C. L., Fryer, C. L., Rueda, J. A., & Ruffini, R. 2016, arXiv:1606.02523
Becerra, L., Cipolletta, F., Fryer, C. L., Rueda, J. A., & Ruffini, R. 2015, ApJ, 812, 100
Belvedere, R., Boshkayev, K., Rueda, J. A., & Ruffini, R. 2014, NuPhA, 921, 33
Belvedere, R., Pugliese, D., Rueda, J. A., Ruffini, R., & Xue, S.-S. 2012, NuPhA, 883, 1
Berger, E. 2014, ARA&A, 52, 43
Berger, E., Fong, W., & Chornock, R. 2013, ApJL, 774, L23
Bianco, C. L., & Ruffini, R. 2004, ApJL, 605, L1
Bianco, C. L., & Ruffini, R. 2005a, ApJL, 620, L23
Bianco, C. L., & Ruffini, R. 2005b, ApJL, 633, L13
Bianco, C. L., & Ruffini, R. 2006, ApJL, 644, L105
Bildsten, L., & Cutler, C. 1992, ApJ, 400, 175
Boër, M., Gendre, B., & Stratta, G. 2015, ApJ, 800, 16
Boshkayev, K., Rueda, J. A., Ruffini, R., & Siutsou, I. 2013, ApJ, 762, 117
Bromberg, O., Nakar, E., & Piran, T. 2011, ApJL, 739, L55
Bucciantini, N., Metzger, B. D., Thompson, T. A., & Quataert, E. 2012, MNRAS, 419, 1537
Bufano, F., Pian, E., Sollerman, J., et al. 2012, ApJ, 753, 67
Cadelano, M., Pallanca, C., Ferraro, F. R., et al. 2015, ApJ, 812, 63
Caito, L., Amati, L., Bernardini, M. G., et al. 2010, A&A, 521, A80
Caito, L., Bernardini, M. G., Bianco, C. L., et al. 2009, A&A, 498, 501
Calderone, G., Ghirlanda, G., Ghisellini, G., et al. 2015, MNRAS, 448, 403
Campana, S., Mangano, V., Blustin, A. J., et al. 2006, Natur, 442, 1008
Cano, Z., Bersier, D., Guidorzi, C., et al. 2011, MNRAS, 413, 669
Cavallo, G., & Rees, M. J. 1978, MNRAS, 183, 359
Cherubini, C., Geralico, A., Rueda, J. A., & Ruffini, R, H. 2009, PhRvD, 79, 124002
Chiang, J., & Dermer, C. D. 1999, ApJ, 512, 699
Cipolletta, F., Cherubini, C., Filippi, S., Rueda, J. A., & Ruffini, R. 2015, PhRvD, 92, 023007

Clark, J., Evans, H., Fairhurst, S., et al. 2015, ApJ, 809, 53
Cobb, B. E., Bloom, J. S., Perley, D. A., et al. 2010, ApJL, 718, L150
Costa, E., Frontera, F., Heise, J., et al. 1997, Natur, 387, 783
Dai, Z. G., & Lu, T. 1998a, A&A, 333, L87
Dai, Z. G., & Lu, T. 1998b, PhRvL, 81, 4301
Dai, Z. G., Wang, X. Y., Wu, X. F., & Zhang, B. 2006, Sci, 311, 1127
Damour, T., & Ruffini, R. 1975, PhRvL, 35, 463
D'Avanzo, P., Melandri, A., Palazzi, E., et al. 2012, GCN, 13069, 1
Della Valle, M. 2006, in AIP Conf. Ser. 836, Gamma-Ray Bursts in the Swift Era, ed. S. S. Holt, N. Gehrels, & J. A. Nousek (Melville, NY: AIP), 367
della Valle, M., Bianchini, A., Livio, M., & Orio, M. 1992, A&A, 266, 232
Della Valle, M., Chincarini, G., Panagia, N., et al. 2006, Natur, 444, 1050
della Valle, M., Rosino, L., Bianchini, A., & Livio, M. 1994, A&A, 287, 403
De Pasquale, M., Schady, P., Kuin, N. P. M., et al. 2010, ApJL, 709, L146
de Ugarte Postigo, A., Xu, D., Leloudas, G., et al. 2013, GCN, 14646, 1
Dezalay, J.-P., Barat, C., Talon, R., et al. 1992, in AIP Conf. Ser. 265, Gamma-ray Bursts, Proc. of the Workshop, ed. W. S. Paciesas & G. J. Fishman (Huntsville: Univ. Alabama), 304
Eichler, D., Livio, M., Piran, T., & Schramm, D. N. 1989, Natur, 340, 126
Evans, P. A., Beardmore, A. P., Page, K. L., et al. 2007, A&A, 469, 379
Evans, P. A., Beardmore, A. P., Page, K. L., et al. 2009, MNRAS, 397, 1177
Fryer, C. L., Oliveira, F. G., Rueda, J. A., & Ruffini, R. 2015, PhRvL, 115, 231102
Fryer, C. L., Rueda, J. A., & Ruffini, R. 2014, ApJL, 793, L36
Fryer, C. L., Woosley, S. E., & Hartmann, D. H. 1999, ApJ, 526, 152
Galama, T. J., Vreeswijk, P. M., van Paradijs, J., et al. 1998, Natur, 395, 670
Gehrels, N. 1986, ApJ, 303, 336
Gehrels, N., Ramirez-Ruiz, E., & Fox, D. B. 2009, ARA&A, 47, 567
Giacomazzo, B., & Perna, R. 2013, ApJL, 771, L26
Giacconi, R., & Ruffini, R. 1978, Physics and Astrophysics of Neutron Stars and Black Holes (Amsterdam: North Holland)
Goodman, J. 1986, ApJL, 308, L47
Granot, J., Piran, T., & Sari, R. 1999, ApJ, 513, 679
Guetta, D., & Della Valle, M. 2007, ApJL, 657, L73
Guetta, D., Pian, E., & Waxman, E. 2011, A&A, 525, A53
Gursky, H., & Ruffini, R. (ed.) 1975, in Proc. Annual Meeting, Astrophysics and Space Science Library, Vol. 48, Neutron Stars, Black Holes and Binary X-ray Sources (Dordrecht: Reidel)
Heise, J. 2003, in AIP Conf. Ser. 662, Gamma-Ray Burst and Afterglow Astronomy 2001: A Workshop Celebrating the First Year of the HETE Mission, ed. G. R. Ricker & R. K. Vanderspek (Melville, NY: AIP), 229
Hill, J., Garnavich, P., Kuhn, O., et al. 2007, GCN, 6486, 1
Izzo, L., Pisani, G. B., Muccino, M., et al. 2012a, arXiv:1210.8034
Izzo, L., Rueda, J. A., & Ruffini, R. 2012b, A&A, 548, L5
Izzo, L., Ruffini, R., Penacchioni, A. V., et al. 2012c, A&A, 543, A10
Jin, Z.-P., Li, X., Cano, Z., et al. 2015, ApJL, 811, L22
Kann, D. A., Schulze, S., & Updike, A. C. 2008, GCN, 7627, 1
Klebesadel, R. W. 1992, in Gamma-Ray Bursts—Observations, Analyses and Theories, ed. C. Theories, R. I. Ho, & E. E. Epstein (Cambridge: Cambridge Univ. Press)
Kluźniak, W., & Ruderman, M. 1998, ApJL, 505, L113
Kouveliotou, C., Meegan, C. A., Fishman, G. J., et al. 1993, ApJL, 413, L101
Kouveliotou, C., Woosley, S. E., Patel, S. K., et al. 2004, ApJ, 608, 872
Kovacevic, M., Izzo, L., Wang, Y., et al. 2014, A&A, 569, A108
Landau, L. D., & Lifshitz, E. M. 2003, The Classical Theory of Fields (4th Engl. ed.; Oxford: Butterworth-Heinemann)
Lazarus, P., Tauris, T. M., Knispel, B., et al. 2014, MNRAS, 437, 1485
Lee, W. H., Ramirez-Ruiz, E., & Page, D. 2004, ApJL, 608, L5
Levan, A. J., Fruchter, A. S., Graham, J., et al. 2013, GCN, 14686, 1
Levan, A. J., Tanvir, N. R., Starling, R. L. C., et al. 2014, ApJ, 781, 13
Li, L.-X., & Paczyński, B. 1998, ApJL, 507, L59
Liang, E., Zhang, B., Virgili, F., & Dai, Z. G. 2007, ApJ, 662, 1111
Lü, H.-J., & Zhang, B. 2014, ApJ, 785, 74
MacFadyen, A. I., & Woosley, S. E. 1999, ApJ, 524, 262
MacFadyen, A. I., Woosley, S. E., & Heger, A. 2001, ApJ, 550, 410
Maeda, K., & Nomoto, K. 2003, ApJ, 598, 1163
Meegan, C. A., Fishman, G. J., Wilson, R. B., et al. 1992, Natur, 355, 143
Melandri, A., Pian, E., D'Elia, V., et al. 2014, A&A, 567, A29
Meszaros, P. 2006, RPPh, 69, 2259
Meszaros, P., & Rees, M. J. 1997, ApJL, 482, L29
Metzger, B. D., Giannios, D., Thompson, T. A., Bucciantini, N., & Quataert, E. 2011, MNRAS, 413, 2031
Metzger, M. R., Djorgovski, S. G., Kulkarni, S. R., et al. 1997, Natur, 387, 878
Muccino, M., Ruffini, R., Bianco, C. L., Izzo, L., & Penacchioni, A. V. 2013, ApJ, 763, 125
Narayan, R., Paczynski, B., & Piran, T. 1992, ApJL, 395, L83
Narayan, R., Piran, T., & Shemi, A. 1991, ApJL, 379, L17
Nava, L., Vianello, G., Omodei, N., et al. 2014, arXiv:1406.6693
Nomoto, K., Yamaoka, H., Pols, O. R., et al. 1994, Natur, 371, 227
Nomoto, K. I., Iwamoto, K., & Suzuki, T. 1995, PhR, 256, 173
Nousek, J. A., Kouveliotou, C., Grupe, D., et al. 2006, ApJ, 642, 389
Oliveira, F. G., Rueda, J. A., & Ruffini, R. 2014, ApJ, 787, 150
Paczynski, B. 1986, ApJL, 308, L43
Panaitescu, A., & Meszaros, P. 1998, ApJL, 493, L31
Panaitescu, A., & Mészáros, P. 1999, ApJ, 526, 707
Paschalidis, V., Liu, Y. T., Etienne, Z., & Shapiro, S. L. 2011, PhRvD, 84, 104032
Patricelli, B., Bernardini, M. G., Bianco, C. L., et al. 2012, ApJ, 756, 16
Penacchioni, A. V., Ruffini, R., Bianco, C. L., et al. 2013, A&A, 551, A133
Penacchioni, A. V., Ruffini, R., Izzo, L., et al. 2012, A&A, 538, A58
Pian, E., Amati, L., Antonelli, L. A., et al. 2000, ApJ, 536, 778
Pian, E., Giommi, P., Amati, L., et al. 2004, AdSpR, 34, 2711
Piran, T. 2005, RvMP, 76, 1143
Pisani, G. B., Izzo, L., Ruffini, R., et al. 2013, A&A, 552, L5
Pisani, G. B., Ruffini, R., Aimuratov, Y., et al. 2016, arXiv:1610.05619
Popham, R., Woosley, S. E., & Fryer, C. 1999, ApJ, 518, 356
Preparata, G., Ruffini, R., & Xue, S. 1998, A&A, 338, L87
Rangel Lemos, L. J., Bianco, C. L., Mosquera Cuesta, H. J., Rueda, J. A., & Ruffini, R. 2010, in XXV Texas Symp. Relativistic Astrophysics, ed. F. M. Rieger, C. van Eldik, & W. Hofmann, 204
Rasio, F. A., & Shapiro, S. L. 1999, CQGra, 16, R1
Rees, M. J., & Meszaros, P. 1998, ApJL, 496, L1
Rhoades, C. E., & Ruffini, R. 1974, PhRvL, 32, 324
Rosswog, S., Ramirez-Ruiz, E., & Davies, M. B. 2003, MNRAS, 345, 1077
Rueda, J. A., & Ruffini, R. 2012, ApJL, 758, L7
Ruffini, R. 2009, in The Ergosphere and Dyadosphere of Black Holes, ed. D. L. Wiltshire, M. Visser, & S. Scott. (Cambridge: Cambridge Univ. Press), 161
Ruffini, R. 2015, ARep, 59, 591
Ruffini, R., Bernardini, M. G., Bianco, C. L., et al. 2005, in AIP Conf. Ser. 782, XIth Brazilian School of Cosmology and Gravitation, ed. M. Novello & S. E. Perez Bergliaffa (Melville, NY: AIP), 42
Ruffini, R., Bernardini, M. G., Bianco, C. L., et al. 2006a, AdSpR, 38, 1291
Ruffini, R., Bernardini, M. G., Bianco, C. L., et al. 2006b, in The Tenth Marcel Grossmann Meeting, ed. M. Novello, S. Perez Bergliaffa, & R. Ruffini (Singapore: World Scientific), 369
Ruffini, R., Bernardini, M. G., Bianco, C. L., et al. 2007, in Proc. VI INTEGRAL Workshop, ESA SP-622, The Obscured Universe, ed. S. Grebenev, R. Sunyaev, & C. Winkler (Noordwijk: ESA), 561
Ruffini, R., Bernardini, M. G., Bianco, C. L., et al. 2008, in Proc. MG11 Meeting on General Relativity, The Eleventh Marcel Grossmann Meeting, ed. H. Kleinert, R. T. Jantzen, & R. Ruffini (Singapore: World Scientific), 368
Ruffini, R., Bianco, C. L., Chardonnet, P., Fraschetti, F., & Xue, S. 2002, ApJL, 581, L19
Ruffini, R., Bianco, C. L., Enderli, M., et al. 2013, GCN, 14526, 1
Ruffini, R., Bianco, C. L., Fraschetti, F., Xue, S.-S., & Chardonnet, P. 2001a, ApJL, 555, L107
Ruffini, R., Bianco, C. L., Fraschetti, F., Xue, S.-S., & Chardonnet, P. 2001b, ApJL, 555, L113
Ruffini, R., Bianco, C. L., Fraschetti, F., Xue, S.-S., & Chardonnet, P. 2001c, ApJL, 555, L117
Ruffini, R., Bianco, C. L., Xue, S.-S., et al. 2004, IJMPD, 13, 843
Ruffini, R., Izzo, L., Bianco, C. L., et al. 2015a, ARep, 59, 626
Ruffini, R., Izzo, L., Muccino, M., et al. 2014a, A&A, 569, A39
Ruffini, R., Muccino, M., Aimuratov, Y., et al. 2016, ApJ, in press (arXiv:1607.02400v2)
Ruffini, R., Muccino, M., Bianco, C. L., et al. 2014b, A&A, 565, L10
Ruffini, R., Muccino, M., Kovacevic, M., et al. 2015b, ApJ, 808, 190
Ruffini, R., Rodriguez, J., Muccino, M., et al. 2016, ApJ, arXiv:1602.03545
Ruffini, R., Salmonson, J. D., Wilson, J. R., & Xue, S. 2000, A&A, 359, 855
Ruffini, R., Salmonson, J. D., Wilson, J. R., & Xue, S.-S. 1999, A&A, 350, 334
Ruffini, R., Vereshchagin, G., & Xue, S. 2010, PhR, 487, 1
Ruffini, R., Wang, Y., Enderli, M., et al. 2015c, ApJ, 798, 10
Ruffini, R., & Wheeler, J. A. 1969, in Significance of Space Research for Fundamental Physics, Proc. of the ESRO Collaboration, ed. A. F. Moore & V. Hardy, 52, 45
Ruffini, R., & Wilson, J. 1973, PhRvL, 31, 1362
Ruffini, R., & Wilson, J. R. 1975, PhRvD, 12, 2959
Ryde, F. 2004, ApJ, 614, 827
Ryde, F. 2005, ApJL, 625, L95

Sakamoto, T., Lamb, D. Q., Kawai, N., et al. 2005, ApJ, 629, 311
Salmonson, J. D., & Wilson, J. R. 2002, ApJ, 578, 310
Sari, R. 1997, ApJL, 489, L37
Sari, R. 1998, ApJL, 494, L49
Sari, R., Piran, T., & Narayan, R. 1998, ApJL, 497, L17
Schaefer, B. E. 2007, ApJ, 660, 16
Sibgatullin, N. R., & Sunyaev, R. A. 2000, AstL, 26, 772
Smartt, S. J. 2009, ARA&A, 47, 63
Soderberg, A. M., Kulkarni, S. R., Nakar, E., et al. 2006, Natur, 442, 1014
Sparre, M., Sollerman, J., Fynbo, J. P. U., et al. 2011, ApJL, 735, L24
Starling, R. L. C., Wiersema, K., Levan, A. J., et al. 2010, arXiv:1004.2919
Strong, I. B., Klebesadel, R. W., & Evans, W. D. 1975, in Seventh Texas Symp. Relativistic Astrophysics 262, Annals of the New York Academy of Sciences 262, ed. P. G. Bergman, E. J. Fenyves, & L. Motz 145
Sun, H., Zhang, B., & Li, Z. 2015, ApJ, 812, 33
Tanvir, N. R., Levan, A. J., Fruchter, A. S., et al. 2013, Natur, 500, 547
Tauris, T. M., van den Heuvel, E. P. J., & Savonije, G. J. 2000, ApJL, 530, L93
Tavani, M. 1998, ApJL, 497, L21
Troja, E., Rosswog, S., & Gehrels, N. 2010, ApJ, 723, 1711
Usov, V. V. 1992, Natur, 357, 472
van Paradijs, J., Groot, P. J., Galama, T., et al. 1997, Natur, 386, 686
Virgili, F. J., Liang, E.-W., & Zhang, B. 2009, MNRAS, 392, 91
Virgili, F. J., Zhang, B., O'Brien, P., & Troja, E. 2011, ApJ, 727, 109
Wanderman, D., & Piran, T. 2010, MNRAS, 406, 1944
Wanderman, D., & Piran, T. 2015, MNRAS, 448, 3026
Watson, A. M., Butler, N., Kutyrev, A., et al. 2013, GCN, 14666, 1
Waxman, E. 1997, ApJL, 491, L19
Woosley, S. E. 1993, ApJ, 405, 273
Woosley, S. E., & Bloom, J. S. 2006, ARA&A, 44, 507
Xu, D., de Ugarte Postigo, A., Kruehler, T., et al. 2013, GCN, 14597, 1
Zalamea, I., & Beloborodov, A. M. 2011, MNRAS, 410, 2302
Zel'dovich, Y. B., Ivanova, L. N., & Nadezhin, D. K. 1972, SvA, 16, 209
Zhang, B., Fan, Y. Z., Dyks, J., et al. 2006, ApJ, 642, 354
Zhang, B., & Mészáros, P. 2001, ApJL, 552, L35
Zhang, B., Zhang, B., Virgili, F. J., et al. 2009, ApJ, 703, 1696
Zhang, C. M., Wang, J., Zhao, Y. H., et al. 2011, A&A, 527, A83
Zhang, F.-W., Shao, L., Yan, J.-Z., & Wei, D.-M. 2012, ApJ, 750, 88

The Astrophysical Journal, 833:107 (21pp), 2016 December 10 doi:10.3847/1538-4357/833/1/107

ON THE INDUCED GRAVITATIONAL COLLAPSE SCENARIO OF GAMMA-RAY BURSTS ASSOCIATED WITH SUPERNOVAE

L. Becerra[1,2], C. L. Bianco[1,2], C. L. Fryer[3], J. A. Rueda[1,2,4], and R. Ruffini[1,2,4]
[1] Dipartimento di Fisica and ICRA, Sapienza Università di Roma, Piazzale Aldo Moro 5, I-00185 Rome, Italy
[2] ICRANet, Piazza della Repubblica 10, I-65122 Pescara, Italy
[3] CCS-2, Los Alamos National Laboratory, Los Alamos, NM 87545, USA
[4] ICRANet-Rio, Centro Brasileiro de Pesquisas Físicas, Rua Dr. Xavier Sigaud 150, 22290-180 Rio de Janeiro, Brazil
Received 2016 June 8; revised 2016 October 5; accepted 2016 October 15; published 2016 December 12

ABSTRACT

Following the induced gravitational collapse (IGC) paradigm of gamma-ray bursts (GRBs) associated with type Ib/c supernovae, we present numerical simulations of the explosion of a carbon–oxygen (CO) core in a binary system with a neutron-star (NS) companion. The supernova ejecta trigger a *hypercritical* accretion process onto the NS thanks to a copious neutrino emission and the trapping of photons within the accretion flow. We show that temperatures of 1–10 MeV develop near the NS surface, hence electron–positron annihilation into neutrinos becomes the main cooling channel leading to accretion rates of 10^{-9}–$10^{-1}\,M_{\odot}\ \mathrm{s}^{-1}$ and neutrino luminosities of 10^{43}–$10^{52}\ \mathrm{erg\ s}^{-1}$ (the shorter the orbital period the higher the accretion rate). We estimate the maximum orbital period, P_{max}, as a function of the NS initial mass, up to which the NS companion can reach by hypercritical accretion the critical mass for gravitational collapse leading to black hole formation. We then estimate the effects of the accreting and orbiting NS companion onto a novel geometry of the supernova ejecta density profile. We present the results of a 1.4×10^{7} particle simulation which show that the NS induces accentuated asymmetries in the ejecta density around the orbital plane. We elaborate on the observables associated with the above features of the IGC process. We apply this framework to specific GRBs: we find that X-ray flashes (XRFs) and binary-driven hypernovae are produced in binaries with $P > P_{\mathrm{max}}$ and $P < P_{\mathrm{max}}$, respectively. We analyze in detail the case of XRF 060218.

Key words: accretion, accretion disks – stars: black holes – gamma-ray burst: general – stars: neutron – supernovae: general

1. INTRODUCTION

Recently, Ruffini et al. (2016) proposed a binary nature for the progenitors of both long and short gamma-ray bursts (GRBs). In this work we focus on long GRBs associated with supernovae. For such systems the *induced gravitational collapse* (IGC) paradigm (see, e.g., Ruffini et al. 2006, 2008; Izzo et al. 2012a; Rueda & Ruffini 2012; Fryer et al. 2014) indicates as the progenitor a binary system composed of a CO core and a neutron-star (NS) in a tight orbit. Such a binary system emerged first as a necessity for the explanation of a set of observational features of long GRBs associated with SNe Ic (Rueda & Ruffini 2012). It also appears in the final stages of a well defined evolutionary path which includes the presence of interacting binaries responsible for the formation of stripped-envelope stars, such as CO cores leading to SNe Ic (Rueda & Ruffini 2012; Becerra et al. 2015; Fryer et al. 2015).

The core-collapse of the CO star produces a supernova explosion ejecting material that triggers an accretion process onto the binary NS companion; hereafter indicated as NS. Ruffini et al. (2016) suggested the existence of two classes of long GRBs depending on whether or not a black hole (BH) is formed in the hypercritical accretion process onto the NS:

1. First, there is the subclass of binary-driven hypernovae (BdHNe), long GRBs with isotropic energy $E_{\mathrm{iso}} \gtrsim 10^{52}$ erg and rest-frame spectral peak energy $0.2 \lesssim E_{p,i} \lesssim 2$ MeV. Their prompt emission lasts up to ∼100 s and is at times preceded by an X-ray emission in the 0.3–10 keV band lasting up to 50 s and characterized by a thermal and a power-law component (i.e., Episode 1 in GRB 090618 in Izzo et al. 2012a). They have a long lasting X-ray afterglow generally composed by a spike, a plateau, followed by a common late power-law behavior when measured in the common source rest-frame (Pisani et al. 2013). For all BdHNe at $z \lesssim 1$, an optical supernova with luminosity similar to the one of supernova 1998bw (Galama et al. 1998) has been observed after 10–15 days in the cosmological rest-frame (see, e.g., Melandri et al. 2014). It has been proposed that this class of GRBs occurs when the NS reaches its critical mass through the above accretion process and forms a BH (see Figure 1). Under these conditions, the GeV emission becomes observable and it has been proposed to originate from the newly formed BH (Ruffini et al. 2016). This GRB subclass occurs in compact binaries with orbital periods as short as $P \sim 5$ minutes or binary separations $a \lesssim 10^{11}$ cm (Fryer et al. 2014).
2. Second, there is the subclass of X-ray flashes (XRFs), long GRBs with isotropic energies in the range $E_{\mathrm{iso}} \approx 10^{47}$–$10^{52}$ erg; spectral peak energies $E_{p,i} \approx 4$–200 keV (Amati & Della Valle 2013; Ruffini et al. 2015, 2016). Their prompt emission phase lasts $\sim 10^{2}$–10^{4} s and is generally characterized by a spectrum composed by a thermal component (with radii 10^{10}–10^{12} cm and temperatures 0.1–2 keV, Campana et al. 2006) and power-law component. They have long lasting X-ray afterglows without the characteristic common late power-law behavior encountered in the BdHNe (Pisani et al. 2013), nor the characteristic X-ray spike. For all XRFs at $z \lesssim 1$, an optical supernova with luminosity

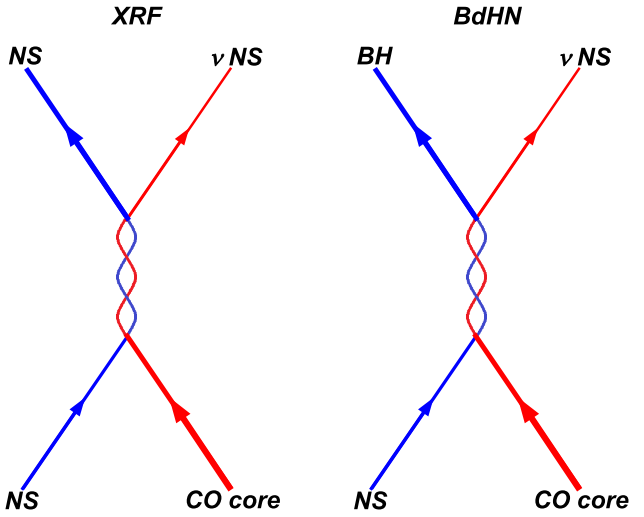

Figure 1. Cosmic-matrix of XRFs and BdHNe as introduced in Ruffini (2015a, pp. 242–314, 2015b), Ruffini et al. (2015). See text for details.

similar to the one of supernova 2010bh (Bufano et al. 2012) has been observed after 10–15 days in the cosmological rest-frame. These sources have been associated within the IGC paradigm to binaries of a CO core and an NS in which there is no BH formation (see Figure 1): when the accretion is not sufficient to bring the NS to reach the critical mass. This occurs in binaries with orbital periods longer than $P \sim 5$ minutes or binary separations $a \gtrsim 10^{11}$ cm (Ruffini et al. 2016; Becerra et al. 2015).

The complexity of the above processes leading to two possible outcomes can be summarized schematically within the concept of a *Cosmic-Matrix (C-matrix)* as first introduced in Ruffini (2015a, pp. 242–314, 2015b), Ruffini et al. (2015). The C-matrix describes these systems as a four-body problem in analogy to the case of particle physics (see Figure 1). The *in-state* is represented by the CO core and the NS companion. The interaction between these two objects given by the hypercritical accretion process triggered by the supernova explosion onto the NS companion, and which is examined in this work, leads to two possible *out-states*: in the case of a BdHN it is formed by the νNS, i.e., the neutron star left by the supernova explosion of the CO core, and a BH formed from the gravitational collapse of the NS companion of the CO core in the in-state. As we have mentioned, in XRFs the accretion is not enough to lead to the gravitational collapse of the NS. Thus, in this case the out-state is νNS and another NS (of course more massive than the initial one present in the in-state).

It is clear that the observational properties of the IGC binaries are sensitive to the binary parameters which can change the fate of the system. The first estimates of the accretion rate and the possible fate of the accreting NS in an IGC binary were presented in Rueda & Ruffini (2012). To obtain an analytic expression of the accretion rate, such a first simple model assumed:

1. a pre-supernova homogeneous density profile;
2. an homologous expansion of the density;
3. constant mass of the NS ($\approx$1.4 $M_\odot$) and the supernova ejecta ($\approx$4–8 $M_\odot$). The first application of this model was presented in Izzo et al. (2012a) for the explanation of the Episode 1 of GRB 090618.

Fryer et al. (2014) presented 1D numerical simulations which improved the above model. Specific density and ejection velocity profiles were adopted from numerical simulations of CO core-collapses producing SNe Ic. The hydrodynamic evolution of the material entering the NS accretion region was computed on the basis of models of hypercritical accretion in supernova fallback. The integration was followed up to the point where it is finally accreted by the NS on its surface.

In Fryer et al. (2015) the evolution of the gravitational binding energy of the BdHNe was analyzed and it was shown that most of these systems would remain bound after the occurrence of the supernova explosion. This conclusion is in contradiction with the traditional assumption of instantaneous mass ejection which leads to the well-known limit that the system becomes unbound when the binary loses more than half of the total mass. This novel result was obtained by the accurate consideration of two ingredients: the accretion process which changes the mass and the momentum of the binary, and the orbital period which can be as short as the explosion timescale.

Becerra et al. (2015) estimated the amount of angular momentum transported by the ejecta entering the Bondi–Hoyle region, and how much of it can be transferred to the NS when it is finally accreted. The ejecta density profile was adopted as a power-law in radius and its evolution with time homologous. It is important to recall some of the conclusions obtained in that work:

1. The angular momentum of the ejecta inside the accretion region is such that it circularizes around the NS forming a disk-like structure;
2. The timescale of the disk angular momentum loss is shorter than the timescale at which matter is being captured, so the accretion timescale dominates the evolution;
3. For binary periods shorter than some critical value, i.e., $P \lesssim P_{\rm max}$, the NS can reach either the mass-shedding or secular axisymmetric instability (critical mass point) which induces its gravitational collapse to a BH. In systems with $P > P_{\rm max}$ the NS gains both mass and angular momentum but not enough to trigger its collapse to a BH. The value of the critical mass was calculated including the effects of rotation (Cipolletta et al. 2015).

The value of $P_{\rm max}$ was computed as a function of the initial NS mass, but only for masses larger than $\approx$1.67 $M_\odot$, and it was assumed that half of the angular momentum of the disk at the inner disk radius is transferred to the NS.

Although all the above works have already shown that indeed the supernova can induce, by accretion, the gravitational collapse of the NS to a BH, there is still the need to explore systematically the entire, physically plausible, space of parameters of these systems, as well as to characterize them observationally. The main aims of this work are:

1. To improve the estimate of the accretion rate with respect to the one in Becerra et al. (2015) by including effects of the finite size/thickness of the density profile and, for different CO core progenitors leading to different ejected masses.
2. To extend the analysis performed in Becerra et al. (2015) and identify the separatrix of systems in which a BH is

formed and the ones where there is no BH formation. This is equivalent to improving the determination of $P_{\rm max}$. We extend here the possible range of the initial NS mass and allow for different values of the angular momentum transfer efficiency.
3. To compute the expected luminosity emitted during the hypercritical accretion process onto the NS for a wide range of binary periods shorter (BdHNe) and longer (XRFs) than $P_{\rm max}$. With this we can establish the energetic budget that characterizes both XRFs and BdHNe.

In parallel,

a. We apply the above considerations to specific GRBs by analyzing in detail the specific case of XRF 060218.
b. We estimate in that specific case the asymmetries created by the orbiting and accreting NS on the ejected matter density profile and the structure of the prompt radiation.
c. We explore the influence of the prompt X-ray radiation in the late X and optical emission of the supernova and the afterglow.

The article is organized as follows. In Section 2 we summarize the framework of the hypercritical accretion of the supernova ejecta onto the NS. Section 3 gives details on the computation of the time evolution of both the (gravitational and baryonic) mass and angular momentum of the accreting NS. In Section 4 we compute the maximum orbital period, $P_{\rm max}$, up to which the IGC of the NS to a BH by accretion can occur. We show in Section 5 the asymmetries that the accreting NS produces on the supernova ejecta. In Section 6 we summarize the hydrodynamics inside the accretion region, including convective instabilities, and the properties of the neutrino emission. We present in Section 7 estimates of the expected luminosities during the hypercritical accretion process. Section 8 shows how the radiation from the accretion process as well as the asymmetries in the ejecta influence the supernova emission both in X-rays and in the optical. Finally in Section 9 we summarize the results of this work. Additional technical details are presented in a series of appendices.

2. HYPERCRITICAL ACCRETION INDUCED BY THE SUPERNOVA

In order to model the hypercritical accretion process onto the NS, we use the formalism introduced in Becerra et al. (2015). The accretion rate of the ejected material onto the NS is given by (Hoyle & Lyttleton 1939; Bondi & Hoyle 1944; Bondi 1952):

$$\dot{M}_B = \pi \rho_{\rm ej} R_{\rm cap}^2 \sqrt{v_{\rm rel}^2 + c_{\rm s,ej}^2}, \tag{1}$$

where $R_{\rm cap}$ is the NS gravitational capture radius

$$R_{\rm cap} = \frac{2GM_{\rm NS}}{v_{\rm rel}^2 + c_{\rm s,ej}^2}. \tag{2}$$

Here $\rho_{\rm ej}$ and $c_{\rm s,ej}$ are the density and sound velocity of the ejecta, $M_{\rm NS}$ the NS mass and $\boldsymbol{v}_{\rm rel} = \boldsymbol{v}_{\rm ej} - \boldsymbol{v}_{\rm orb}$, the velocity of the ejecta as seen from an observer at the NS, and G is the gravitational constant. The orbital velocity is $v_{\rm orb} = \sqrt{GM/a}$, where $M = M_{\rm NS} + M_{\rm CO}$ is the total binary mass, $M_{\rm CO} = M_{\rm env} + M_{\rm Fe}$ the total mass of the CO core which is given by the envelope mass $M_{\rm env}$ and the central iron core mass $M_{\rm Fe} = 1.5\,M_\odot$. The latter is the mass of the new NS formed in the core-collapse supernova process, hereafter indicated as νNS and its mass $M_{\nu\rm NS}$, i.e., we adopt $M_{\nu\rm NS} = M_{\rm Fe} = 1.5\,M_\odot$ in agreement with the range of masses predicted under the convective supernova paradigm (Fryer et al. 2012). For the ejecta velocities, we adopt a homologous explosion model for the supernova expansion, i.e., a velocity proportional to the radius:

$$v_{\rm ej} = n\frac{r}{t}, \tag{3}$$

where n is the so-called *expansion parameter*. Within this approximation, the density profile evolves as (see, e.g., Cox 1968):

$$\rho_{\rm ej}(x,\,t) = \rho_{\rm ej}^0(x)\left(\frac{R_{\rm star}^0}{R_{\rm star}(t)}\right)^3 \frac{M_{\rm env}(t)}{M_{\rm env}^0}, \tag{4}$$

where $x \equiv r/R_{\rm star}(t)$, $M_{\rm env}$ is the mass ejected (i.e., the mass available to be accreted by the NS), $\rho_{\rm ej}^0$ is the pre-supernova density profile and $R_{\rm star}$ is the outermost layer of the supernova ejecta. From the velocity profile law we have that $R_{\rm star}$ evolves as:

$$R_{\rm star}(t) = R_{\rm star}^0\left(\frac{t}{t_0}\right)^n, \tag{5}$$

where $t_0 = nR_{\rm star}^0/v_{\rm star,0}$, $v_{\rm star,0}$ being the velocity of the outermost layer $R_{\rm star}^0$.

The pre-supernova density profile of the CO envelope can be well approximated by a power-law profile, i.e.,

$$\rho_{\rm ej}^0 = \rho_{\rm core}\left(\frac{R_{\rm core}}{r}\right)^m, \qquad R_{\rm core} < r < R_{\rm star}^0. \tag{6}$$

We show in Table 1 the properties of the pre-supernova CO cores produced by low-metallicity progenitors with initial zero-age main sequence (ZAMS) masses $M_{\rm ZAMS} = 15$, 20, and $30\,M_\odot$ obtained with the *Kepler* stellar evolution code (Woosley et al. 2002).

We now improve the treatment in Becerra et al. (2015) taking into account the finite size of the envelope. We thus modify the above density profile by introducing boundaries to the supernova ejecta through density cut-offs at the outermost and innermost layers of the ejecta, namely:

$$\rho_{\rm ej}^0 = \hat{\rho}_{\rm core}\ln\left(\frac{r}{\hat{R}_{\rm core}}\right)\left(\frac{R_{\rm star}}{r} - 1\right)^m, \tag{7}$$

Table 1
Properties of the Pre-supernova CO Cores

Progenitor $M_{\rm ZAMS}$ ($M_\odot$)	$\rho_{\rm core}$ (10^8 g cm^{-3})	$R_{\rm core}$ (10^7 cm)	$M_{\rm env}$ ($M_\odot$)	$R_{\rm star}^0$ (10^9 cm)	m
15	3.31	5.01	2.079	4.49	2.771
20	3.02	7.59	3.89	4.86	2.946
30	3.08	8.32	7.94	7.65	2.801

Note. CO cores obtained for the low-metallicity ZAMS progenitors with $M_{\rm ZAMS} = 15$, 20, and $30\,M_\odot$ in Woosley et al. (2002). The central iron core is assumed to have a mass $M_{\rm Fe} = 1.5\,M_\odot$, which will be the mass of the νNS, denoted here as $M_{\nu\rm NS}$, formed out of the supernova process.

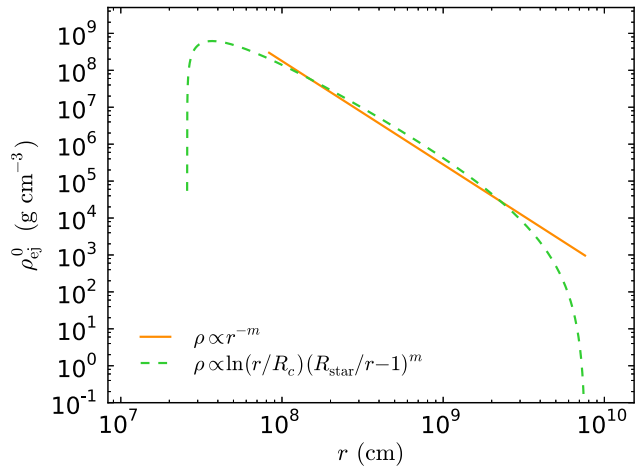

Figure 2. Pre-supernova density profile produced by the $M_{\rm ZAMS} = 30\,M_\odot$ progenitor of Table 1. We compare and contrast the power-law density profile (solid curve) with a modified profile (dashed curve) with density cut-offs at the outermost and innermost ejecta layers following Equations (6) and (7). The two profiles have the same envelope mass.

where $\hat{R}_{\rm core} < r < R_{\rm star}$. The condition that the modified profile has the same ejecta mass with respect to the unmodified power-law profile implies $\hat{R}_{\rm core} < R_{\rm core}$.

Figure 2 shows the pre-supernova density profile described by Equations (6) and (7) for the $M_{\rm ZAMS} = 30\,M_\odot$. For these parameters we have $\hat{R}_{\rm core} = 0.31\,R_{\rm core}$ and $\hat{\rho}_{\rm core} = 567.67$ g cm^{-3}.

Introducing the homologous expansion for the description of the evolution of the supernova ejecta, Equation (1) becomes:

$$\frac{\dot{\mu}_{\rm B}(\tau)}{(1-\chi\mu_{\rm B}(\tau))M_{\rm NS}^2} = \frac{\tau^{(m-3)n}}{\hat{r}^m}\ln\left(\frac{\hat{r}}{\hat{r}_c\tau^n}\right)\frac{(\hat{r}_s-\hat{r}\tau^{-n})^m}{[1+\eta\hat{r}/\tau^{\,2}]^{3/2}}, \tag{8}$$

where

$$\tau \equiv \frac{t}{t_0}, \quad \mu_{\rm B}(\tau) \equiv \frac{M_{\rm B}(\tau)}{\Sigma_{\rm B}}, \quad \hat{r} \equiv 1 - \frac{R_{\rm cap}}{a}, \tag{9}$$

and the parameters χ, Σ_B and η depend on the properties of the binary system before the supernova explosion:

$$\Sigma_{\rm B} = \frac{4\pi\hat{\rho}_c G^2 M_\odot^2 t_0}{v_{\rm orb}^3}, \quad \chi = \frac{\Sigma_{\rm B}}{M^0_{\rm env}}, \quad \eta = \left(\frac{n\,a}{t_0 v_{\rm orb}}\right)^2, \tag{10}$$

where $M^0_{\rm env} \equiv M_{\rm env}(t=t_0) = M_{\rm env}(\tau=1)$.

Figure 3 shows the time evolution of the mass accretion rate onto the NS of initial 1.4 $M_\odot$ and selected orbital periods. The other binary parameters are: expansion parameter $n = 1$, ejecta outermost layer velocity $v_{\rm star,0} = 2\times10^9$ cm s^{-1}, and the supernova ejecta profile is the one obtained for the CO core of the $M_{\rm ZAMS} = 20\,M_\odot$ progenitor of Table 1.

We can see from Figure 3 that the shorter(smaller) the orbital period(separation) the higher the accretion rate and the shorter the time it peaks. In Appendix A we derive, following simple arguments, analytic formulas for the peak accretion rate and time which can be useful to get straightforward estimates of these systems.

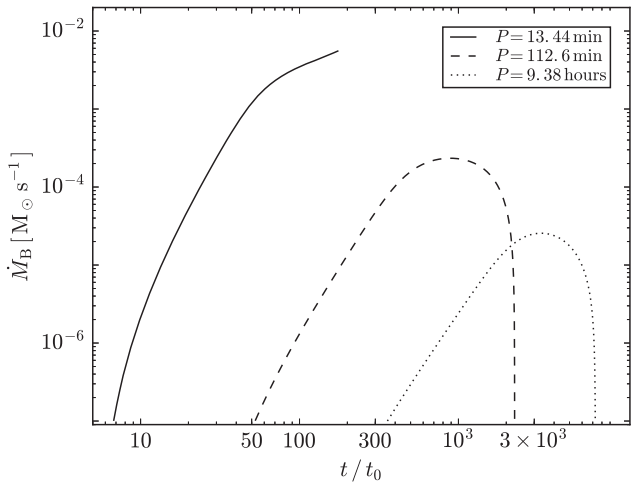

Figure 3. Time evolution of the accretion rate onto a NS of initial mass 1.4 $M_\odot$ for the following binary parameters: expansion parameter $n = 1$, an ejecta outermost layer velocity $v_{\rm star,0} = 2\times10^9$ cm s^{-1} and the supernova ejecta profile is the one obtained for the CO core of the $M_{\rm ZAMS} = 20\,M_\odot$ progenitor of Table 1. For the above progenitor and velocity $t_0 = 2.4$ s. Three selected orbital periods are shown: $P = 13.44$ minutes, 112.6 minutes and 9.38 hr which correspond to binary separation distances $a = 2.46\times10^{10}$ cm, 1.01×10^{11} cm, and 2.96×10^{11} cm, respectively. The solid line corresponds to a case in which the NS reaches the critical mass and collapses to a BH (end point of the curve). In the two other cases, owing to the longer orbital period, there is no induced gravitational collapse of the NS to a BH (see Figure 5 in Section 4 for further details).

3. TIME EVOLUTION OF THE ACCRETING NS

Becerra et al. (2015) showed that the supernova ejecta has enough angular momentum to circularize around the NS in a sort of disk-like structure. Thus, the accreted material will transfer both baryonic mass and angular momentum to the NS.

The equilibrium NS configurations form a two-parameter family given by the mass (baryonic or gravitational) and angular momentum (or angular velocity). Namely, the NS gravitational mass, $M_{\rm NS}$, is in general a function of the NS baryonic mass, $M_{\rm b}$, and angular momentum, $J_{\rm NS}$. In a similar way the angular momentum contributes to the mass of a BH (Christodoulou & Ruffini 1971). It is then clear that the evolution of the NS gravitational mass is given by:

$$\dot{M}_{\rm NS}(t) = \left(\frac{\partial M_{\rm NS}}{\partial M_{\rm b}}\right)_J \dot{M}_{\rm b} + \left(\frac{\partial M_{\rm NS}}{\partial J_{\rm NS}}\right)_{M_{\rm b}} \dot{J}_{\rm NS}. \tag{11}$$

We assume that all the (baryonic) mass entering the NS capture region will be accreted by the NS, i.e.,

$$M_{\rm b}(t) = M_{\rm b}(t_0) + M_{\rm B}(t), \tag{12}$$

then $\dot{M}_{\rm b} \equiv \dot{M}_{\rm B}$.

For the relation between the NS gravitational mass, the baryonic mass, and the angular momentum for the NS equilibrium configurations, namely the NS gravitational binding energy formula, we use the recent result obtained in Cipolletta et al. (2015):

$$\frac{M_{\rm b}}{M_\odot} = \frac{M_{\rm NS}}{M_\odot} + \frac{13}{200}\left(\frac{M_{\rm NS}}{M_\odot}\right)^2\left(1+\frac{1}{137}j_{\rm NS}^{1.7}\right), \tag{13}$$

where $j_{\rm NS} \equiv cJ_{\rm NS}/(GM_\odot^2)$, and which is independent on the nuclear equation of state (EOS).

The torque on the NS by the accreted matter is given by

$$\dot{J}_{\rm NS} = \xi l(R_{\rm in})\dot{M}_{\rm B}, \tag{14}$$

where $R_{\rm in}$ is the disk inner boundary radius, $l(R_{\rm in})$ is the angular momentum per unit mass of the material located at $r = R_{\rm in}$, and $\xi \leqslant 1$ is a parameter that accounts for the efficiency of the angular momentum transfer. The precise value of ξ depends mainly: (1) on possible angular momentum losses (e.g., by jetted emission during accretion) and (2) on the deceleration of the matter in the disk inner radius zone.

The inner disk radius is given by the maximum between the radius of the last stable circular orbit, $r_{\rm lso}$, and the NS radius, $R_{\rm NS}$. Namely, $R_{\rm in} = \max(r_{\rm lso}, R_{\rm NS})$. When the disk extends up to the NS surface, $l(R_{\rm in})$ is given by the Keplerian orbit with radius equal to the NS equatorial radius. On the other hand, if $R_{\rm NS} < r_{\rm lso}$, $l(R_{\rm in})$ is given by the last stable circular orbit. Summarizing:

$$l(R_{\rm in}) = \begin{cases} l_{\rm K}(R_{\rm NS}), & \text{for } R_{\rm NS} > r_{\rm lso} \Rightarrow R_{\rm in} = R_{\rm NS}, \\ l_{\rm lso}, & \text{for } R_{\rm NS} \leqslant r_{\rm lso} \Rightarrow R_{\rm in} = r_{\rm lso}. \end{cases} \tag{15}$$

We show hereafter the results for three selected NS nuclear EOSs: NL3, TM1 and GM1 (Cipolletta et al. 2015). For these EOSs and assuming that the NS is initially non-rotating, we have that $r_{\rm lso} = 6GM_{\rm NS}/c^2 > R_{\rm NS}$ for $M_{\rm NS} \gtrsim [1.78, 1.71, 1.67]\, M_\odot$, for the NL3, TM1 and GM1 EOSs, respectively.

For the axially symmetric exterior spacetime around a rotating NS, $l_{\rm lso}$ is well approximated by (Becerra et al. 2015):

$$l_{\rm lso} \approx 2\sqrt{3}\frac{GM_{\rm NS}}{c}\left[1 - \frac{1}{10}\left(\frac{j_{\rm NS}}{M_{\rm NS}/M_\odot}\right)^{0.85}\right], \tag{16}$$

for co-rotating particles.

On the contrary, for $M_{\rm NS} \lesssim 1.7\, M_\odot$ we have $r_{\rm lso} < R_{\rm NS}$ and thus $R_{\rm in} = R_{\rm NS}$. We shall adopt for this case Hartle's slow-rotation approximation. The angular momentum per unit mass of a Keplerian orbit with a radius equal to the NS radius is, within this approximation, given by (Boshkayev et al. 2016)

$$l_{\rm K}(u) = \frac{GM_{\rm NS}}{c\sqrt{u(1-3u)}}\left[1 - j_{\rm NS}\frac{3\,u^{3/2}(1-2u)}{1-3u} + j_{\rm NS}^2\frac{u^4(3-4u)}{(1-2u)^2(1-3u)}\right], \tag{17}$$

where $u \equiv GM_{\rm NS}/(c^2 R_{\rm NS})$. This formula can be also obtained by taking the second order slow rotation limit of the angular momentum of the last stable circular orbit around a Kerr BH (Rees et al. 1974; Boshkayev et al. 2012, 2016).

Therefore, by solving (numerically) simultaneously Equations (8) and (14), with the aid of Equations (11)–(17), it is possible to follow the evolution of the NS mass and angular momentum during the accretion process.

4. IGC OF THE NS

We proceed now to calculate the binary parameters which discriminate systems in which the NS can reach by accretion its critical mass ($M_{\rm crit}$) and consequently collapse to a BH, from the systems in which the accretion is not sufficient to induce such a collapse.

Table 2
Critical Mass (and Corresponding Radius) for Selected Parameterizations of Nuclear EOS Obtained in Cipolletta et al. (2015)

EOS	$M_{\rm crit}^{J=0}$ ($M_\odot$)	$R_{\rm crit}^{J=0}$ (km)	$M_{\rm max}^{J\neq0}$ ($M_\odot$)	$R_{\rm max}^{J\neq0}$ (km)	p	k	f_K (kHz)
NL3	2.81	13.49	3.38	17.35	1.68	0.006	1.34
GM1	2.39	12.56	2.84	16.12	1.69	0.011	1.49
TM1	2.20	12.07	2.62	15.98	1.61	0.017	1.40

Note. In the last column we have also reported the rotation frequency of the critical mass configuration in the rotating case. This value corresponds to the frequency of the last configuration along the secular axisymmetric instability line, i.e., the configuration that intersects the Keplerian mass-shedding sequence.

The stability of the accreting NS is limited by two main instability conditions: the mass-shedding or Keplerian limit, and the secular axisymmetric instability. Mass-shedding occurs when the centrifugal force balances the gravitational one. Thus, for a given gravitational mass (or central density), it is given by the rotating configuration with angular velocity equal to the the Keplerian velocity of test-particles orbiting at the star's equator. In this limit the matter at the surface is marginally bound to the star and small perturbations will cause mass loss to make the star stable again, or otherwise to bring it to a point of dynamical instability (Stergioulas 2003).

At the secular axisymmetric instability point the star is unstable against axisymmetric perturbations. It is expected to evolve, first quasi-stationarily, and then to find a dynamical instability point where gravitational collapse takes place (Stergioulas 2003). Using the turning-point method (Friedman et al. 1988), Cipolletta et al. (2015) computed the critical mass due to this instability point for the NL3, GM1 and TM1 EOSs. They showed that the numerical results of the critical NS mass are well fitted, with a maximum error of 0.45%, by the formula

$$M_{\rm NS}^{\rm crit} = M_{\rm crit}^{J=0}(1 + kj_{\rm NS}^p), \tag{18}$$

where the parameters k and p depend on the nuclear EOS and $M_{\rm crit}^{J=0}$ is the critical mass in the non-rotating case (see Table 2). It can be checked that the latter is, as expected, below the $3.2\, M_\odot$ critical mass upper bound by (Rhoades & Ruffini 1974).

Thus, a NS with initial mass $M_{\rm NS}(t_0)$ can reach $M_{\rm crit}$ if it accretes an amount of mass $\Delta M_{\rm acc} = M_{\rm crit} - M_{\rm NS}(t_0)$ from the supernova ejecta. Given the initial NS mass, the CO core mass, and the supernova ejecta profile and its velocity, the accretion rate increases for shorter binary separation, namely for shorter orbital periods (Fryer et al. 2014; Becerra et al. 2015). Therefore, there exists a maximum orbital period, denoted here as $P_{\rm max}$, up to which, given $M_{\rm NS}(t_0)$ (and all the other binary parameters), the NS can accrete this precise amount of mass, $\Delta M_{\rm acc}$.

For example, for a NS with an initial gravitational mass $M_{\rm NS}(t_0) = 2\ M_\odot$ accreting the ejected material from the supernova explosion of the $30\, M_\odot$ ZAMS progenitor (see Table 1), $v_{\rm star,0} = 2 \times 10^9\,{\rm cm\,s^{-1}}$, expansion parameter $n = 1$ and angular momentum transfer efficiency $\xi = 0.5$, we find $P_{\rm max} \approx 26$ minutes. Figure 4 shows the evolution of such a NS for two different binary periods, $P = 5$ minutes $< P_{\rm max}$ and $P = 50$ minutes $> P_{\rm max}$. We can see that only for the system

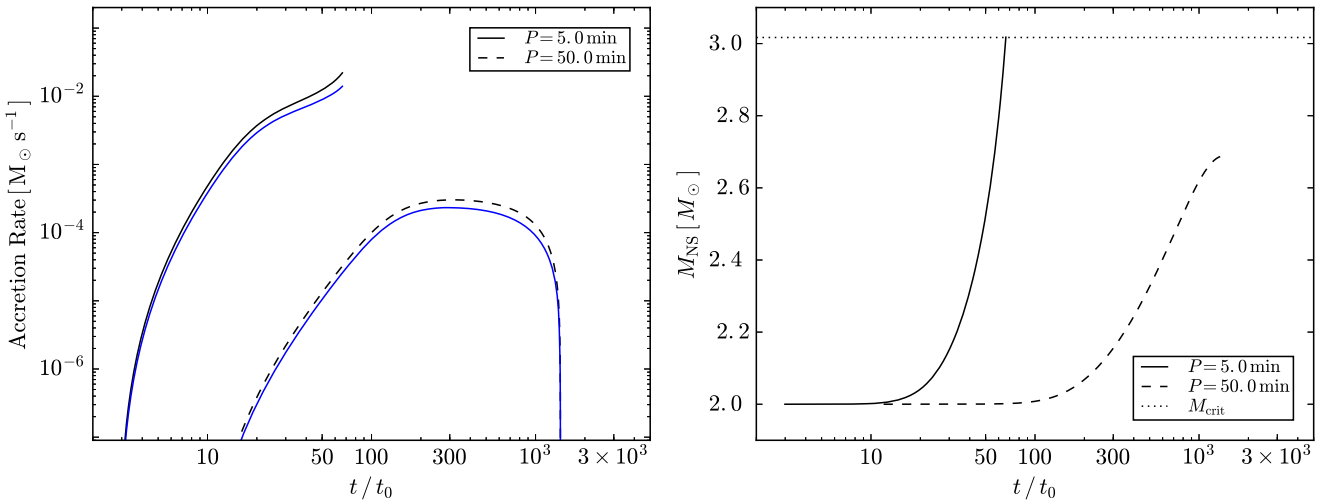

Figure 4. Left panel: time evolution of the baryonic mass accretion rate (black curve) obtained from Equation (8) and rate of increase of the NS gravitational mass obtained from Equation (11). Right panel: evolution of the NS gravitational mass. We use here the ejecta from the explosion of a CO core by the 30 $M_\odot$ ZAMS progenitor, $v_{\rm star,0} = 2 \times 10^9$ cm s^{-1}, expansion parameter $n = 1$ and angular momentum transfer efficiency $\xi = 0.5$. Two binary periods are used here: $P = 5$ minutes $< P_{\rm max}$ (solid curves) and $P = 50$ minutes $> P_{\rm max}$ (dashed curves). For these binary parameters, $P_{\rm max} \approx 26$ minutes. It can be seen that only the NS in the system with $P < P_{\rm max}$ accretes enough matter to reach the critical mass (dotted line) for gravitational collapse.

with $P < P_{\rm max}$ the NS accretes enough matter to reach the critical mass for gravitational collapse, given by Equation (18).

Figure 5 shows $P_{\rm max}$, obtained from our numerical simulations, for different values of the NS initial gravitational mass, keeping all the other binary parameters fixed. In this figure we show the results for pre-supernova properties listed in Table 1 for the CO progenitors with $M_{\rm ZAMS} = 20\,M_\odot$ (left panel) and $30\,M_\odot$ (right panel), a free expansion for the supernova explosion ($n = 1$), and a velocity of the outermost supernova ejecta layer, $v_{\rm star,0} = 2 \times 10^9$ cm s^{-1}.

A few comments on Figure 5 are in order:

1. The increase of $P_{\rm max}$ with the initial NS mass value $M_{\rm NS}(0)$ can be easily understood from the fact that the larger $M_{\rm NS}(0)$, the lower the amount of mass needed to reach the critical NS mass.
2. There is a transition in the behavior at $M_{\rm NS}(0) \approx 1.7\ M_\odot$. This occurs because configurations with $M_{\rm NS}(0) \lesssim 1.7\ M_\odot$ have the disk extending up to the NS surface, correspondingly we used the angular momentum per unit mass given by Equation (17). For larger initial masses, accretion occurs from the last stable orbit and we used Equation (16). Thus, the difference around this transition point is attributable to the use of the slow rotation approximation for masses $M_{\rm NS}(0) < 1.7\ M_\odot$. We recall that Becerra et al. (2015) considered only initial NS masses $M_{\rm NS}(0) \gtrsim 1.7\ M_\odot$ so this transition is not observed there.
3. In Becerra et al. (2015) an angular momentum transfer efficiency parameter $\xi = 0.5$ was adopted. In order to see the effect of such a parameter we adopted here in the simulations the maximum possible value $\xi = 1$. Values of ξ lower than unity account for possible angular momentum losses between the inner disk radius and the NS surface. This implies that the values of $P_{\rm max}$ in Figure 5 are upper limits to the maximum orbital period for BH formation. Namely, a value $\xi < 1$ leads to lower values of $P_{\rm max}$. For instance, in the right panel of Figure 5 we see that for $M_{\rm NS}(0) = 1.8\,M_\odot$ and the NL3 EOS, $P_{\rm max} \approx 70$ minutes. We checked that, for $\xi = 0.5$, the same initial mass and EOS would instead lead to $P_{\rm max} \approx 20$ minutes.
4. Because of the highly efficient angular momentum transfer ($\xi = 1$), the NS in the systems of Figure 5 ends at the mass-shedding limit. In the case of lower values of ξ, the NS might end directly at the secular axisymmetric instability with lower values of the critical mass with respect to the maximum mass along the Keplerian mass-shedding sequence. We have checked, for instance in the case of $\xi = 0.5$ (the one adopted in Becerra et al. 2015) and the NL3 EOS, that this occurs when the initial NS mass is close to the non-rotating critical mass value, e.g., for $M_{\rm NS}(0) \gtrsim 2.2\ M_\odot$.
5. We recall that in Becerra et al. (2015) only the case of the $M_{\rm ZAMS} = 30\,M_\odot$ progenitor was analyzed. Here, we studied different progenitors. At first sight, it might appear contradictory that the left panel of Figure 5, which is for a less massive CO core with respect to the one the right panel, shows longer values of the maximum orbital period for BH formation. The reason for this is as follows. First, the binary separation satisfies $a \propto (M_{\rm t} P^2)^{1/3}$ where $M_{\rm t}$ is the total binary mass. Thus, for a given NS mass and binary period, a less massive CO core implies a less massive binary and a smaller orbit by a factor $a_1/a_2 = (M_{\rm t1}/M_{\rm t2})^{1/3}$. A tighter orbit implies a supernova ejecta density at the NS position that is higher by a factor $\rho_{\rm ej,1}/\rho_{\rm ej,2} = (a_2/a_1)^3 = M_{\rm t2}/M_{\rm t1}$, hence the accretion rate which is proportional to the density (see Equation (1)).

Thus we have shown that in systems with $P \leqslant P_{\rm max}$ the IGC of the accreting NS to a BH occurs. These systems explain the BdHNe (Fryer et al. 2014, 2015; Becerra et al. 2015). We do not simulate in this work the complex process of gravitational collapse; rather we assume BH formation at the moment when the NS reaches the critical mass value. We also adopt the mass of the newly formed BH as given by the critical NS mass value.

In systems with $P > P_{\rm max}$, the NS does not accrete enough matter from the supernova ejecta and the collapse to a BH does

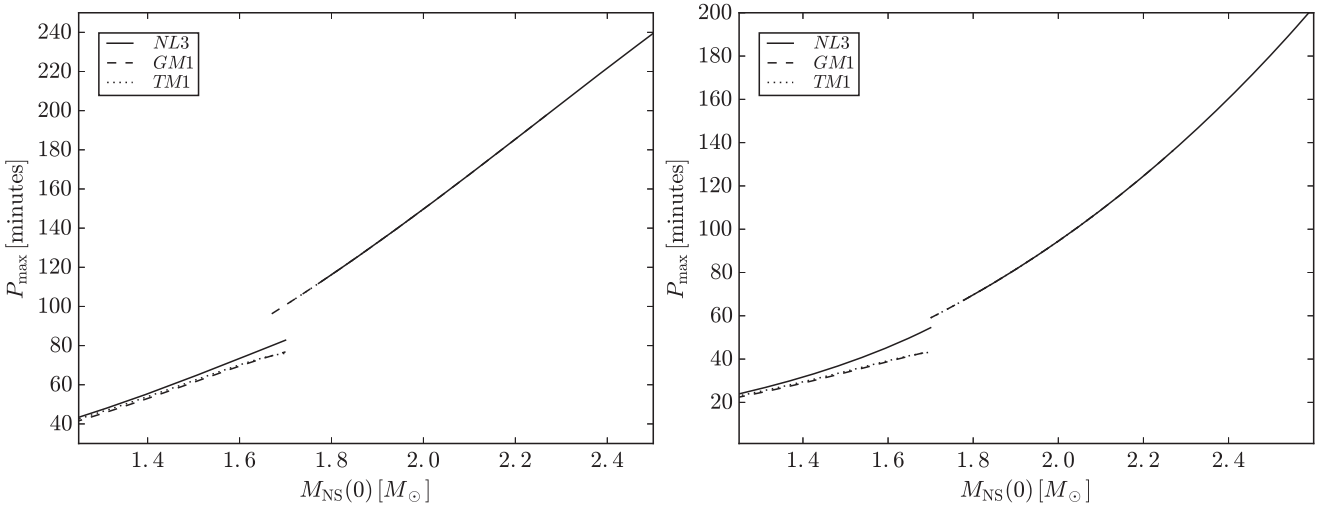

Figure 5. Maximum orbital period for which the NS with initial mass $M_{\rm NS}(0)$ collapses to a BH by accretion of supernova ejecta material. We have adopted a free expansion for the supernova ejecta ($n = 1$), an outermost supernova layer velocity $v_{\rm star,0} = 2 \times 10^9$ cm s^{-1}. The left and right panels show the results for CO cores left by $M_{\rm ZAMS} = 20\,M_\odot$ and $30\,M_\odot$ progenitors, respectively (see Table 1). The apparent transition at $M_{\rm NS}(0) \approx 1.7\ M_\odot$ is explained as follows: configurations with $M_{\rm NS}(0) \lesssim 1.7\ M_\odot$ have the disk extending up to the NS surface, correspondingly we used the angular momentum per unit mass given by Equation (17). In contrast, for larger initial masses the accretion occurs from the last stable orbit, and we used Equation (16). Thus, the difference around this transition point is attributable to the use of the slow rotation approximation for masses $M_{\rm NS}(0) < 1.7\ M_\odot$. See the text for more details.

not occur. As we show below, these systems explain XRFs (see also Ruffini et al. 2016, in preparation, for more details).

5. SUPERNOVA EJECTA ASYMMETRIES INDUCED BY THE NS

For isolated supernova explosions, or for very wide binaries with negligible accretion rates, the density of the supernova ejecta would approximately follow the homologous evolution given by Equation (4) with constant ejecta mass, i.e., $M_{\rm env}(t) = M^0_{\rm env}$, i.e., the density will decrease with time following a simple power-law $\rho_{\rm ej}(t) \propto t^{-3n}$, with n the expansion parameter, keeping its spherical symmetry about the explosion site (see, e.g., Figure 6). However, for explosions occurring in close binaries with compact companions such as NSs or BHs, the supernova ejecta is subjected to a strong gravitational field which produces at least two non-negligible effects: (1) an accretion process on the NS that subtracts part of the ejecta mass, and (2) a deformation of the supernova fronts closer to the accreting NS companion. As we show below, the conjunction of these effects can generate large changes in the density profile of the ejecta in a region around the orbital plane.

In order to visualize the above effects we have simulated the evolution of the supernova layers in the presence of the NS during the accretion process (see Figures 6 and 7). Thus, we followed the three-dimensional motion of N particles in the gravitational field of the orbiting NS. Following Becerra et al. (2015), we consider the gravitational field of the NS on the supernova ejecta including the effects of the orbital motion as well as the changes in the NS gravitational mass as described above in Section 2 via the Bondi formalism. The supernova matter is described as being formed by point-like particles whose trajectory was computed by solving the Newtonian equation of motion. We plan to do an SPH simulation of this process and expect to present the results in a forthcoming publication.

The initial conditions of the supernova ejecta are computed assuming the supernova layers move via a homologous velocity distribution in free expansion (i.e., evolving with $n = 1$). The initial power-law density profile of the CO envelope is simulated by populating the inner layers with more particles, as follows. The total number of particles is $N = N_r \times N_\theta \times N_\phi$ and for symmetry reasons we simulate only the north hemisphere of the supernova; thus the polar and azimuthal angles are divided as $\Delta\theta = (\pi/2)/N_\theta$ and $\Delta\phi = 2\pi/N_\phi$, respectively. For the radial coordinate we first introduce the logarithmic coordinate $x = \log(r)$ and $\Delta x = (x_s - x_c)/N_r$, where $x_s = \log(R_{\rm star})$ and $x_c = \log(R_{\rm core})$. Thus, the thickness of each layer is $\Delta r = r_i(10^{\Delta x} - 1)$, where r_i is the location of the layer. The mass of each particle of the i-layer is: $m_i = 4\pi r_i^3 \ln(10)\Delta x \rho(r_i)/(2N_\theta N_\phi)$.

Let us assume, for the sake of example, the $M_{\rm ZAMS} = 30\,M_\odot$ progenitor of Table 1 which gives a CO core with envelope profile $\rho^0_{\rm ej} \approx 3.1 \times 10^8 (8.3 \times 10^7/r)^{2.8}$ g cm^{-3} and $R^0_{\rm star} = 7.65 \times 10^9$ cm. This implies that, for a total number of $N = 10^6$ particles in the simulation, the particles of the innermost radius $r_i = R_{\rm core} = 8.3 \times 10^7$ cm with density $\rho^0_{\rm ej}(r_i) = 3.1 \times 10^8$ g cm^{-3} have mass $m_i \approx 2 \times 10^{-5}\,M_\odot$, while the particles of the outermost radius, $r_i = R^0_{\rm star}$, would have $m_i \approx 6 \times 10^{-6}\,M_\odot$. In addition, we assume that particles crossing the Bondi–Hoyle radius are captured and accreted by the NS so we removed them from the system as they reach that region. We removed these particles according to the results obtained from the numerical integration of Equation (8).

Figure 6 shows in detail the orbital plane of an IGC binary at selected times of its evolution. The NS has an initial mass of $2.0\,M_\odot$; the CO core is the one obtained by the $M_{\rm ZAMS} = 30\,M_\odot$ progenitor (see Table 1), which leads to a total ejecta with mass $7.94\,M_\odot$ and an iron core that left a νNS of $1.5\,M_\odot$. The orbital period of the binary is $P \approx 5$ minutes, i.e., a binary separation $a \approx 1.5 \times 10^{10}$ cm, and we have adopted an angular momentum transfer efficiency parameter $\xi = 0.5$. The evolution of the accretion rate and the gravitational mass of the NS in this system are the ones shown in

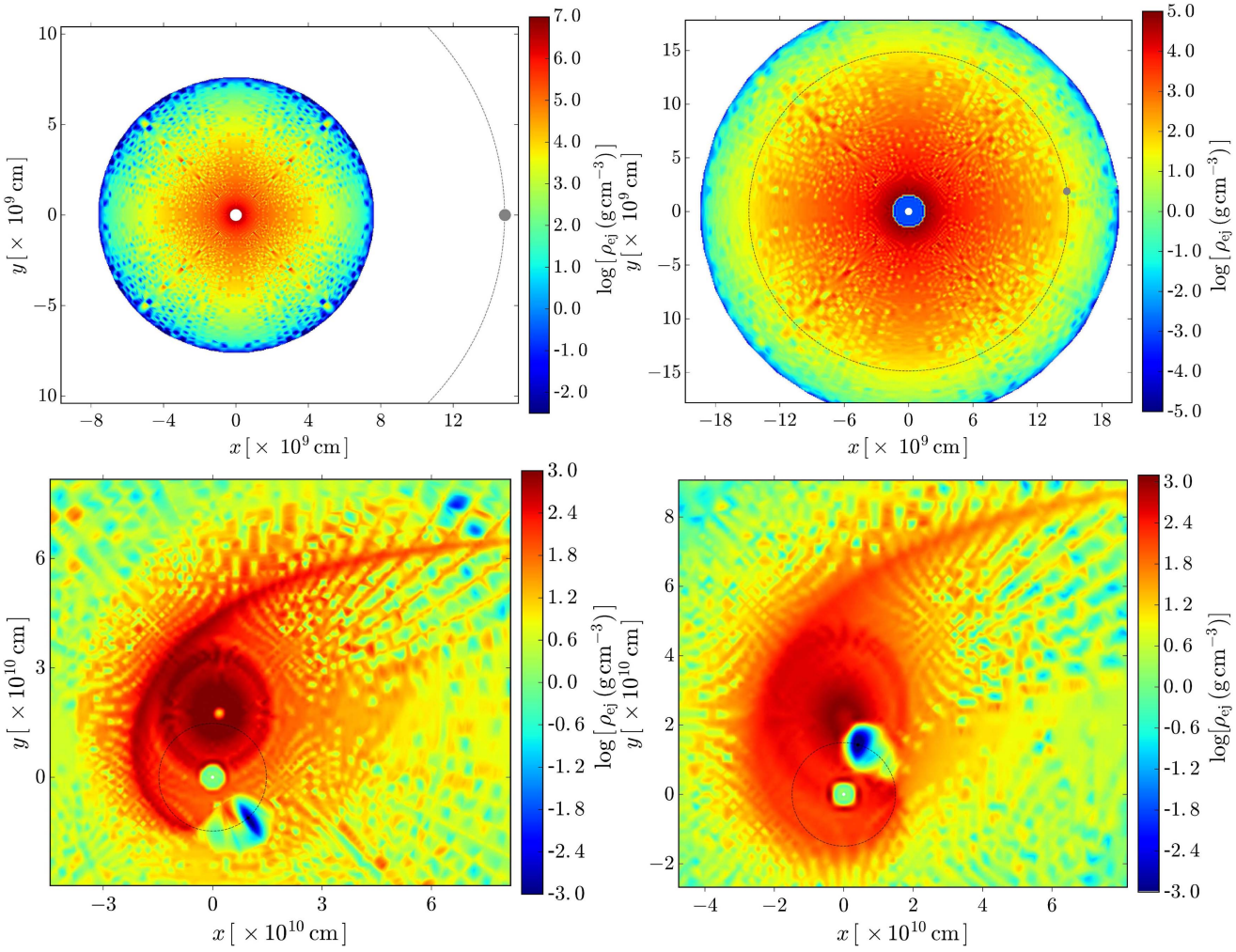

Figure 6. Snapshots of the IGC binary system and the supernova ejecta density at selected times of the evolution. In this example we have adopted the $M_{\rm ZAMS} = 30\,M_\odot$ progenitor with an ejecta mass of 7.94 $M_\odot$ and a core that left a νNS of 1.5 $M_\odot$. We assume homologous evolution of the supernova ejecta with expansion parameter $n = 1$ and ejecta outermost layer velocity $v_{0,\rm star} = 2 \times 10^9$ cm s^{-1}. For the NS we adopt an initial mass 2.0 $M_\odot$. The binary has an orbital period $P \approx 5$ minutes, i.e., a binary separation distance $a \approx 1.5 \times 10^{10}$ cm. The evolution of the accretion rate and the gravitational mass of the NS are shown in Figure 4. The coordinate system is centered on the νNS born in the supernova: it is here represented with a white-filled circle located at (0, 0). The NS, represented by the gray-filled circle, is orbiting counterclockwise in this time-evolution and we have indicated its trajectory with a thin-dashed circle. The color bar indicates values of ejecta density. We have chosen a thickness Δz around the orbital plane to estimate the ejecta density: $\Delta z \approx 0.05a \approx 7.1 \times 10^8$ cm for all these figures. We note that, in order to better show the features of the system at different times, we have chosen for each plot different ranges of the x–y scales and of the color bar. Left upper panel: initial time of the process, $t = t_0 = R^0_{\rm star}/v_{\rm star,0} = 3.82$ s. The supernova ejecta starts to expand radially outward and the NS (black filled circle) is located at the position (a, 0). Right upper panel: beginning of the accretion process, i.e., passage of the first supernova ejecta layers through the NS gravitational capture region. Thus, this time is $t = t_{\rm acc,0} \approx a/v_{0,\rm star} = 7.7$ s. Left lower panel: instant when the NS reaches, by accretion, the critical mass and collapses to a BH. This occurs at $t = t_{\rm coll} \approx 254$ s $\approx 0.85P$. The BH, here represented by the black-filled circle, has a mass set by the critical NS mass, i.e., $M_{\rm BH} = M_{\rm crit} \approx 3\,M_\odot$ (see Figure 4). The asymmetry of the induced supernova ejecta density that has been generated by the nearby presence of the NS, and the accretion process onto it, can be seen here. We can also see at this stage a stream of matter (of negligible mass) being expelled (i.e., reaching escape velocity) from the system. Right lower panel: system 100 s after the BH formation, namely $t = t_{\rm coll} + 100$ s $= 354$ s $\approx 1.2P$. This figure shows the new binary system composed by the νNS (white-filled circle at the (0, 0) position) out of the supernova, and a BH [black-filled circle at the (0.5, 1.7) position] out of the gravitational collapse of the NS due to the hypercritical accretion process. The asymmetry of the supernova ejecta is now even larger than the one showed by the left lower panel figure. The asymmetry of the supernova ejecta is such that its "center" has been displaced from the explosion site originally at the position (0, 0) to the approximate position (0, 2), due to the action of the orbiting NS.

Figure 4. As it can be seen, for the above parameters the NS reaches the critical mass and collapses to form a BH (see also Figure 5 and conclusion 3 in Section 6).

In the simulation shown in Figure 6 we adopted two millions of particles per solar mass of ejecta, so in this simulation we have followed the three-dimensional motion of $N = 2 \times 10^6 (M^0_{\rm env}/M_\odot) \approx 1.6 \times 10^7$ particles in the gravitational field of the orbiting NS. To estimate the ejecta density we have chosen a thickness Δz around the orbital plane. For the plots in Figure 6 we have adopted $\Delta z \approx 0.05a \approx 7.1 \times 10^8$ cm.

The left upper panel shows the binary at the initial time of the process, i.e., $t = t_0 = R^0_{\rm star}/v_{\rm star,0} = 3.82$ s, the first instant of the ejecta radial expansion.

The right upper panel shows the instant at which the accretion process begins, namely at $t = t_{\rm acc,0} \approx a/v_{0,\rm star} = 7.7$ s. Owing to their fast velocity, the accretion rate of the first layers is low and they escape almost undisturbed, so the supernova ejecta at these times keeps its original spherical symmetry.

The left lower panel shows the binary at the instant in which the accreting NS reaches the critical mass, hence the instant of

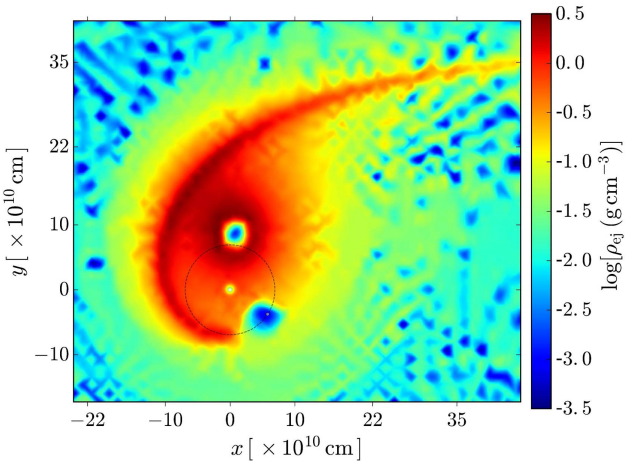

Figure 7. Snapshot of an IGC binary system analogous to the one of Figure 6 but with an orbital period of $P \approx 50$ minutes (i.e., binary separation $a \approx 7 \times 10^{10}$ cm). In this case the accreting NS (gray-filled circle), which is orbiting counterclockwise (thin-dashed circle), does not collapse to a BH. The νNS left by the supernova is represented by the white filled circle at the position (0, 0). The asymmetry of the supernova ejecta is clear from this figure: indeed the supernova "center" has been displaced from the explosion site originally at the position (0, 0) to the approximate position (0, 9), due to the action of the orbiting NS. The snapshot corresponds to a time $t = 2667$ s ≈ 44 minutes, which corresponds to roughly 1/4 the total accretion process. To estimate the ejecta density we have adopted $\Delta z = 0.08a \approx 5.3 \times 10^9$ cm.

formation of the BH, at $t = t_{\rm coll} = 254$ s $\approx 0.85P$. The BH mass is thus set by the critical NS mass, i.e., $M_{\rm BH} = M_{\rm crit} \approx 3\,M_\odot$ (see Figure 4). This figure also evidences the asymmetry on the supernova density as being induced by the presence of the companion and its increasing gravitational field due to the ongoing accretion process onto it. Indeed, one can see how the supernova "center" has been shifted from the explosion site originally at the (0, 0) position (see left upper panel) to the approximate position (0, 2). Thus, the layers of the ejecta are displaced as a result of the gravitational attraction of the orbiting NS. This can be understood as follows. When the NS passes over the northern hemisphere, it attracts the northern region of the ejecta toward it. Consequently, that part of the ejecta gains velocity in the northern direction. The same effect occurs in the other regions of the orbit, however the effect is asymmetric because, by the time the NS passes, say over the southern hemisphere, it attracts layers moving at slower velocity with respect to the ones it had attracted in the northern hemisphere before. The reason for this is that the southern fastest layers have moved further already while the NS was passing the northern side. This effect is indeed incorporated in our simulation which follows the trajectory of each of the 14 million particles.

One can also see in this figure a stream of matter (one-armed flow) of negligible mass with respect to the total mass escaping from the system. As we have mentioned above, the NS attracts some layers, increasing their velocity. As a result some material can reach escape velocity to leave the binary system forming this unbound debris. The appearance of a one-armed flow (instead of two-armed flows) is because the center-of-mass is located roughly at the CO core position, thus the NS is, in practice, orbiting the CO core. If the two masses were of comparable mass, (e.g., as in the case of binary NS mergers), they would move around a common center-of-mass lying in-between them. In such systems the momentum transfer is more symmetric leading to a symmetric two-armed flow structure. The one-armed flow in our system is, in this sense, more similar to the one that appears in the tidal disruption of a small body by a supermassive BH.

The right lower panel shows the system 100 s after the BH formation, namely at $t = t_{\rm coll} + 100$ s $= 354$ s $\approx 1.2P$. Thus, this figure shows the new binary system formed by the νNS, out of the supernova, and the BH from the gravitational collapse of the NS. The νNS is at the (0, 0) position and it is represented by the white filled circle. The BH is in this instant of time located at the (0.5, 1.7) position and it is represented by the black filled circle. One can see the increasing asymmetry of the supernova ejecta around the orbital plane. We note the presence of ejecta in the vicinity of the newly formed BH, the latter sited at the approximate position (0.5, 1.5). It is interesting that part of these ejecta can indeed cause a subsequent accretion process onto the newly formed BH. The possible outcomes of this process deserve further attention which will be analyzed elsewhere.

We have shown above the evolution of an IGC binary with a very short orbital period of $P \approx 5$ minutes, for which the gravitational collapse of the NS of the CO core occurs. Besides the formation of a BH, we have evidenced the asymmetry caused by the presence and accretion onto the NS on the supernova ejecta density. It is natural to ask if these asymmetries also appear for less compact binaries. For comparison, we show in Figure 7 the results of a numerical simulation for a binary with orbital period $P \approx 50$ minutes, in which the NS does not reach the critical mass during the entire accretion process (see Section 6). The evolution of the accretion rate and the gravitational mass of the NS in this system are shown in Figure 4.

In these kinds of systems, all the ejecta layers pass the NS position. Thus, the total duration of the accretion process, denoted here $t_{\rm acc}$, is approximately given by the time it takes the innermost layer of the ejecta to overcome the NS position, i.e., $t_{\rm acc} \approx a/v_{\rm inner}$, where $v_{\rm inner} = (\hat{R}_{\rm core}/R^0_{\rm star})v_{\rm star,0}$ using the homologous expansion assumption. The snapshot corresponds to a time $t = 2667$ s ≈ 44 minutes $\approx t_{\rm acc}/4$. To estimate the ejecta density we have chosen in this example $\Delta z = 0.08a \approx 5.3 \times 10^9$ cm. It is interesting that although the NS is in this case further away from the CO core, it still induces a high asymmetry on the supernova ejecta. We shall investigate elsewhere if this mechanism could explain the asymmetries observed in some type Ibc supernovae (see, e.g., Tanaka et al. 2009; Taubenberger et al. 2009). We here constrain ourselves in Section 8, instead, to the consequences that the ejecta asymmetries have on the supernova emission (both in X-rays and in the optical).

6. HYDRODYNAMICS INSIDE THE ACCRETION REGION

We turn now to analyze in detail the properties of the system inside the Bondi–Hoyle accretion region. Figure 3 shows the mass accretion rate onto the NS of initial mass $1.4\,M_\odot$. We can see that the accretion rate can be as high as $\sim 10^{-1}\,M_\odot$ s^{-1}. For these high accretion rates we can draw some general properties:

1. We can neglect the effect of the NS magnetic field since for $\dot{M}_{\rm B} > 2.6 \times 10^{-8}\,M_\odot$ s^{-1} the magnetic pressure remains much smaller than the random pressure of the

infalling material (Fryer et al. 1996; Rueda & Ruffini 2012).

2. The photons are trapped in the accretion flow. The trapping radius, defined as the point at which the photons emitted diffuse outward at a slower velocity than the one of the infalling material, is (Chevalier 1989):

$$r_{\rm trapping} = \min\{\dot{M}_{\rm B}\kappa/(4\pi c), R_{\rm cap}\}, \quad (19)$$

where κ is the opacity. For the CO core, Fryer et al. (2014) estimated a Rosseland mean opacity roughly 5×10^3 cm^2 g^{-1}. For the range of accretion rates, we obtain $\dot{M}_{\rm B}\kappa/(4\pi c) \sim 10^{13}$–$10^{19}$ cm, a radius much bigger than the NS capture radius which is in our simulations at most $1/3$ of the binary separation. Thus, in our systems the trapping radius extends all the way to the Bondi–Hoyle region, hence the Eddington limit does not apply and hypercritical accretion onto the NS occurs. See Figures 15 and 16 in Appendix B.3 for details.

3. Under these conditions of photons being trapped within the accretion flow, the gain of gravitational energy of the accreted material is mainly radiated via neutrino emission (Zel'dovich et al. 1972; Ruffini & Wilson 1973; Fryer et al. 1996; Rueda & Ruffini 2012; Fryer et al. 2014). See Figures 15 and 16 in Appendix B.3 for details.

4. Figure 3 shows that the evolution of the accretion rate has a shape composed of a rising part, followed by an almost flat maximum and finally it decreases with time. The rising part corresponds to the passage and accretion of the first layers of the ejecta. The sharpness of the density cut-off of the outermost ejecta layer defines the sharpness of this rising accretion rate. The maximum rate is given by the accretion of the ejecta layers with velocities of the same order as the orbital velocity of the NS. These layers are located very close to the innermost part of the supernova ejecta. Then, the rate starts to decrease with the accretion of the innermost layers whose density cut-off determines the sharpness of this decreasing part of the mass accretion rate. See also Appendix A for further details.

5. The longer the orbital period/larger binary separation, the lower the accretion rate (see Figure 11 in Appendix A for details.); hence the lower the accretion luminosity and the longer the time at which peak luminosity occurs. These features confirm what was advanced in Ruffini et al. (2015, 2016), Becerra et al. (2015), namely that less energetic long GRBs correspond to the binaries with wider orbits. Specifically, XRFs correspond to the binaries in which the NS does not reach the point of gravitational collapse to a BH (see below). Since there is a limiting orbital period, $P_{\rm max}$, up to which the NS can reach the critical mass and collapse to a BH (these systems are the BdHNe Fryer et al. 2015, 2014), the XRFs are the binaries with $P > P_{\rm max}$ (see Section 5 for details).

6.1. Convective Instabilities

As the material piles onto the NS and the atmosphere radius, the accretion shock moves outward. The post-shock entropy is a decreasing function of the shock radius position which creates an atmosphere unstable to Rayleigh–Taylor convection during the initial phase of the accretion process (see Appendix B for additional details). These instabilities can accelerate above the escape velocity driving outflows from the accreting NS with final velocities approaching the speed of light (Fryer et al. 2006; Fryer 2009). Assuming that radiation dominates, the entropy of the material at the base of the atmosphere is (Fryer et al. 1996):

$$S_{\rm bubble} \approx 16\left(\frac{M_{\rm NS}}{1.4\,M_\odot}\right)^{7/8}\left(\frac{\dot{M}_{\rm B}}{M_\odot\ {\rm s}^{-1}}\right)^{-1/4}\left(\frac{r}{10^6\ {\rm cm}}\right)^{-3/8}, \quad (20)$$

in units of $k_{\rm B}$ per nucleon.

This material will rise and expand, cooling adiabatically, i.e., $T^3/\rho =$ constant, for radiation dominated gas. If we assume a spherically symmetric expansion, then $\rho \propto 1/r^3$ and we obtain

$$k_{\rm B}T_{\rm bubble} = 195\ S_{\rm bubble}^{-1}\left(\frac{r}{10^6\ {\rm cm}}\right)^{-1}\ {\rm MeV}. \quad (21)$$

However, it is more likely that the bubbles expand in the lateral but not in the radial direction (Fryer 2009), thus we have $\rho \propto 1/r^2$, i.e.,

$$T_{\rm bubble} = T_0(S_{\rm bubble})\left(\frac{r_0}{r}\right)^{2/3}, \quad (22)$$

where $T_0(S_{\rm bubble})$ is given by Equation (21) evaluated at $r = r_0 \approx R_{\rm NS}$.

This temperature implies a bolometric blackbody flux at the source from the bubbles

$$F_{\rm bubble} = \sigma T_{\rm bubble}^4 \approx 2 \times 10^{40}\left(\frac{M_{\rm NS}}{1.4\,M_\odot}\right)^{-7/2}\left(\frac{\dot{M}_{\rm B}}{M_\odot\ {\rm s}^{-1}}\right) \times \left(\frac{R_{\rm NS}}{10^6\ {\rm cm}}\right)^{3/2}\left(\frac{r_0}{r}\right)^{8/3}\ {\rm erg\ s^{-1}\ cm^{-2}}, \quad (23)$$

where σ is the Stefan–Boltzmann constant.

In Fryer et al. (2014) it was shown that the above thermal emission from the rising bubbles produced during the hypercritical accretion process can explain the early ($t \lesssim 50$ s) thermal X-ray emission observed in GRB 090618 (Izzo et al. 2012a, 2012b). In that case $T_{\rm bubble}$ drops from 50 keV to 15 keV expanding from $r \approx 10^9$ cm to 6×10^9 cm, for an accretion rate $10^{-2}\,M_\odot$ s^{-1}.

From the above formulas we can explain the blackbody emission observed in XRF 060218 (Campana et al. 2006). The observed temperature ($k_{\rm B}T \approx 0.2$ keV) and radius of the emitter (a few 10^{11} cm) are consistent with the temperature and surface radius of the above bubbles formed in a system with a NS of initial mass $1.4\,M_\odot$, supernova-progenitor of $20\,M_{\rm ZAMS}$, and orbital period 2.5 hr: it can be easily checked via Equation (22) that for $r \sim 10^{11}$ cm and an accretion rate of the order of $10^{-6}\,M_\odot$ s^{-1}, the bubbles would have a temperature consistent with the one observed in XRF 060218. Further details on this specific case and additional examples will be presented elsewhere.

It is worth mentioning the possibility that, as discussed in Fryer et al. (2006), r-process nucleosynthesis occurs in these outflows. This implies that long GRBs can be also r-process sites with specific signatures from the decay of the produced heavy elements, possibly similar to the case of the *kilonova* emission in short GRBs (see, e.g., Tanvir et al. 2013, and references therein). The signatures of this phenomenon in

XRFs and BdHNe, and its comparison with kilonovae, deserve to be explored. However, this is out of the scope of the present work and it will be presented elsewhere.

6.2. Neutrino Emission During Hypercritical Accretion

Most of the energy from the accretion is lost through neutrino emission and the neutrino luminosities are proportional to the accretion rate (see Appendix B.2 for details). For the accretion rate conditions characteristic of our models $\sim 10^{-4}$–$10^{-2}\,M_\odot\ \mathrm{s}^{-1}$ (see Section 2 and Appendix A), pair annihilation dominates the neutrino emission and electron neutrinos remove the bulk of the energy (see Fryer 2009, and Figures 15 and 16 in Appendix B.3 for details). The temperature of these neutrinos can be roughly approximated by assuming that the inflowing material generally flows near to the NS surface before shocking and emitting neutrinos (see Appendices B.1 and B.2). The pressure from this shock is given by (Fryer et al. 2006):

$$P_{\rm shock} = \frac{1}{2}(\gamma + 1)\rho_{\rm acc} v_{\rm acc}^2 \tag{24}$$

where, if we assume the accretion occurs nearly at free-fall,

$$v_{\rm acc} = \left(\frac{2GM_{\rm NS}}{R_{\rm NS}}\right)^{1/2} \tag{25}$$

and

$$\rho_{\rm acc} = \frac{\dot{M}_{\rm acc}}{4\pi R_{\rm NS}^2 v_{\rm acc}} \tag{26}$$

where $\dot{M}_{\rm acc} = \dot{M}_{\rm B}$ is the accretion rate onto the NS. The EOS $\gamma = 4/3$ for the radiation-dominated conditions in this material, leads to the temperature of this material:

$$T_{\rm acc} = \left(\frac{3P_{\rm shock}}{4\sigma/c}\right)^{1/4} = \left(\frac{7}{8}\frac{\dot{M}_{\rm acc} v_{\rm acc} c}{4\pi R_{\rm NS}^2 \sigma}\right)^{1/4}. \tag{27}$$

The electron–positron pairs producing the neutrinos are thermalized at this temperature and the resulting neutrino temperature can be estimated by this formula. For accretion rates lying between $\sim 10^{-4}$–$10^{-2}\,M_\odot\ \mathrm{s}^{-1}$, we estimate neutrino temperatures lying between 1.7–5.2 MeV (i.e., neutrino energies $E_\nu \approx 3k_BT \approx$ 5–15 MeV; see Appendix B.2), predicting energies only slightly below those produced by detailed calculations (Fryer 2009). A detailed study of the neutrino emission will be presented elsewhere (see also Appendices B.1 and B.2).

As we show in Appendix B.2, for the developed temperatures (say $k_BT \sim$ 1–10 MeV) near the NS surface (see Figures 13 and 14), the dominant neutrino emission process is the electron–positron annihilation leading to neutrino–antineutrino. This process produces a neutrino emissivity proportional to the ninth power of the temperature (see Equation (54)). The accretion atmosphere near the NS surface is characterized by a temperature gradient (see Figure 13 in Appendix B.1) with a typical scale height $\Delta r_{\rm ER} \approx 0.7\,R_{\rm NS}$, obtained from Equation (53). Owing to the aforementioned strong dependence of the neutrino emission on temperature, most of the neutrino emission occurs in the region $\Delta r_{\rm ER}$ above the NS surface.

These conditions lead to the neutrinos being efficient in balancing the gravitational potential energy gain, as indicated in Equation (52), allowing the hypercritical accretion rates. We show in Appendix B.3 (see Figures 15 and 16) that when photons are trapped within the flow the Eddington limit does not apply in this system. As discussed in Fryer et al. (1996), the neutrinos can efficiently balance the gravitational energy gain. The effective accretion onto the NS can be estimated as:

$$\dot{M}_{\rm eff} \approx \Delta M_{\rm ER}\frac{L_{\rm ER}}{E_{\rm er}}, \tag{28}$$

where $\Delta M_{\rm ER}$, $L_{\rm ER}$ are the mass and neutrino luminosity in the emission region (i.e., $\Delta r_{\rm ER}$), and $E_{\rm ER}$ is half the gravitational potential energy gained by the material falling from infinity to the $R_{\rm NS} + \Delta r_{\rm ER}$. Since $L_{\rm ER} \approx 2\pi R_{\rm NS}\Delta r_{\rm ER}\,\epsilon_{e^-e^+}$ with $\epsilon_{e^-e^+}$ the electron–positron pair annihilation process emissivity given by Equation (54), and $E_{\rm ER} = (1/2)GM_{\rm NS}\Delta M_{\rm ER}/(R_{\rm NS} + \Delta r_{\rm ER})$, it can be checked that for $M_{\rm NS} = 1.4\,M_\odot$ this accretion rate leads to values $\dot{M}_{\rm eff} \approx 10^{-9}$–$10^{-1}\,M_\odot\ \mathrm{s}^{-1}$ for temperatures $k_BT =$ 1–10 MeV.

The neutrino signal from this accretion can be similar to the one from accretion in supernovae with fallback. Fallback begins immediately after the launch of the supernova explosion and, after peaking, decays with time ($t^{-5/3}$: Chevalier 1989). Depending upon the total fallback mass, the fallback accretion rate can remain above $10^{-4}\,M_\odot\ \mathrm{s}^{-1}$ for 10^3–10^4 s (Wong et al. 2014).

7. ACCRETION LUMINOSITY

In order to make a comparison with observed light-curves we need to estimate the luminosity produced during the accretion process. The gain of gravitational potential energy in the accretion process is the total one available to be released e.g., by neutrinos and photons. The total energy released in the star in a time-interval dt during the accretion of an amount of mass $dM_{\rm b}$ with angular momentum $l\dot{M}_{\rm b}$, is given by (see, e.g., Sibgatullin & Sunyaev 2000; Becerra et al. 2015):

$$\begin{aligned} L_{\rm acc} &= (\dot{M}_{\rm b} - \dot{M}_{\rm NS})c^2 \\ &= \dot{M}_{\rm b}c^2\left[1 - \left(\frac{\partial M_{\rm NS}}{\partial J_{\rm NS}}\right)_{M_{\rm b}} l - \left(\frac{\partial M_{\rm NS}}{\partial M_{\rm b}}\right)_{J_{\rm NS}}\right], \end{aligned} \tag{29}$$

where we have used Equation (11). This upper limit to the energy released is just the amount of gravitational energy gained by the accreted matter by falling to the NS surface and which is not spent in changing the gravitational binding energy of the NS. The total energy releasable during the accretion process, $\Delta E_{\rm acc} \equiv \int L_{\rm acc}\,dt$, is thus given by the difference in binding energies of the initial and final NS configurations. The typical luminosity will be $L_{\rm acc} \approx \Delta E_{\rm acc}/\Delta t_{\rm acc}$ where $\Delta t_{\rm acc}$ is the duration of the accretion process.

The duration of the accretion process is given approximately by the flow time of the slowest layers of the supernova ejecta to the NS. If the velocity of these layers is $v_{\rm inner}$, then $\Delta t_{\rm acc} \sim a/v_{\rm inner}$, where a is the binary separation. For $a \sim 10^{11}$ cm and $v_{\rm inner} \sim 10^8\,\mathrm{cm\,s}^{-1}$ we obtain $\Delta t_{\rm acc} \sim 10^3$ s, while for shorter binary separation, e.g., $a \sim 10^{10}$ cm ($P \sim 5$ minutes), $\Delta t_{\rm acc} \sim 10^2$ s, as validated by the results of our numerical integrations shown e.g., in Figures 3 and 4. See also Appendix A.

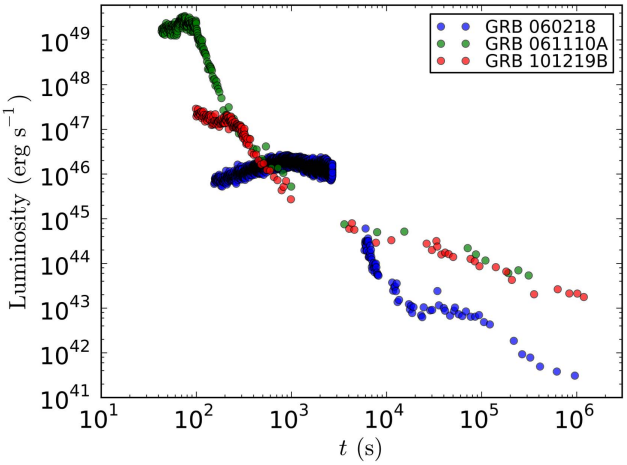

Figure 8. Observed 0.3–10 keV XRT light curves of some XRFs.

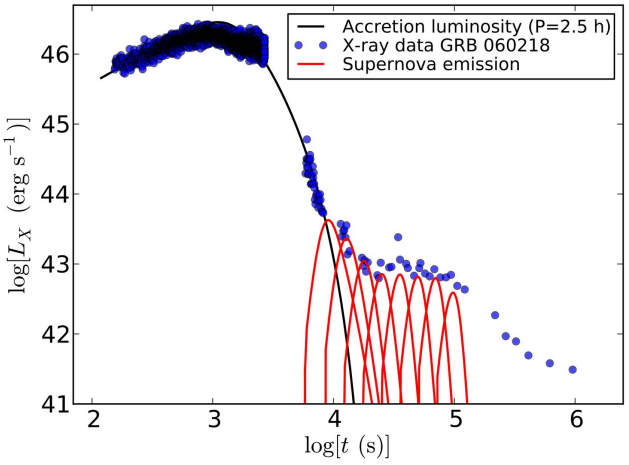

Figure 9. Comparison of the accretion luminosity given by Equation (29) and the supernova luminosity with the observed X-ray luminosity of XRF 060218. The binary system has the following parameters: supernova velocity $v_{\rm star,0} = 2 \times 10^9$ cm s^{-1}, a pre-supernova core obtained from the $M_{\rm ZAMS} = 20\,M_\odot$ evolution (see Table 1), initial NS mass $M_{\rm NS}(t_0) = 1.4\ M_\odot$, and orbital period of 2.5 hr. In this example the initial explosion energy is 2×10^{51} erg, ranging the spherical equivalent-mass from 0.05–4 $M_\odot$. It can be seen that at early times $t \lesssim 10^4$ s the luminosity is dominated by the accretion process. The supernova X-ray light curves rise quickly at $t \approx 10^4$ s for the lowest mass, to $t \sim 10^5$ s for the 4 $M_\odot$ explosion, which corresponds to total ejecta mass from our supernova.

We have shown in Figure 4 the evolution of both the baryonic mass $\dot{M}_{\rm b}$ and the gravitational mass $\dot{M}_{\rm NS}$ for a specific example. We have seen that these two quantities show a similar behavior, therefore we should expect that the difference between them, which gives the available energy to be released (29), evolves with time analogously. In addition, we can see that the NS in the system with $P = 5$ minutes accretes $\approx$1 $M_\odot$ in $\Delta t_{\rm acc} \approx 100$ s. With the aid of Equation (13) we can estimate the difference in binding energies between a 2 $M_\odot$ and a 3 $M_\odot$ NS, i.e., $\Delta E_{\rm acc} \approx 13/200(3^2\text{–}2^2)\ M_\odot c^2 \approx 0.32\ M_\odot c^2$ leading to a maximum luminosity $L_{\rm acc} \approx 3 \times 10^{-3}\, M_\odot c^2 \approx 0.1 \dot{M}_{\rm b} c^2$.

Such an accretion power could lead to signatures observable in long GRBs (see, e.g., Izzo et al. 2012a; Fryer et al. 2014) since it could be as high as $L_{\rm acc} \sim 0.1 \dot{M}_{\rm b} c^2 \sim 10^{47}$–$10^{51}$ erg s^{-1} for accretion rates in the range $\dot{M}_{\rm b} \sim 10^{-6}$–$10^{-2}\, M_\odot$ s^{-1}. Figure 8 shows a few examples of light curves of XRFs. It can be shown that the accretion luminosity can explain the observed early emission ($t \lesssim 10^3$ s) in these examples (see Section 8).

8. INFLUENCE OF THE HYPERCRITICAL ACCRETION ON THE SUPERNOVA EMISSION

The duration of the accretion is shorter than that of the long-lasting X-ray emission (at times $t \sim 10^3$–10^6 s). We shall show below (see Section 8) such a long-lasting emission can be explained from the supernova powered by the prompt radiation, i.e., the X-ray radiation occurring during the accretion process onto the NS. In the case of the tightest binaries leading to BdHNe, the supernova is in addition powered by the prompt radiation following the BH formation.

We now analyze the emission of the supernova at early stages. Traditionally, the supernova shock breaks out of the star producing a burst of X-ray emission which, in a spherically symmetric model, behaves as a sharp rise and equally fast decay as the forward shock cools. However, in our models, the supernova shock has distinct asymmetries caused by the accretion onto the NS (see Figures 6–7 in Section 5). In addition, the X-rays emitted from this hypercritical accretion add energy to the explosion. To calculate the shock breakout luminosity, we use the simplified light-curve code described in Bayless et al. (2015) and De La Rosa (2016). This code assumes homologous outflow for the ejecta velocities, modeling the radiative transport using a single group diffusion scheme with prescriptions for recombination opacities and energies. Energy released in the accretion onto the neutron star is injected as an energy source at the base of the explosion. Because these calculations are one-dimensional, we mimic the asymmetry in the explosion by modeling a series of spherical explosions with different densities. Each of these densities produces a different light curve with the more massive models producing later shock breakout times.

In Figure 9 we compare and contrast the luminosity expected from the accretion process given by Equation (29) and from the accretion-powered supernova, with the observed X-ray luminosity of XRF 060218. The parameters characterizing the binary are: orbital period of 2.5 hr, supernova velocity $v_{\rm star,0} = 2 \times 10^9$ cm s^{-1}, a pre-supernova core obtained from the $M_{\rm ZAMS} = 20\,M_\odot$ evolution which leads to a CO core envelope mass $\sim$4 $M_\odot$ (see Table 1), and initial NS mass $M_{\rm NS}(t_0) = 1.4\ M_\odot$. For these binary parameters, the NS does not collapse to a BH, in agreement with the fact that XRFs, such as XRF 060218, should be explained by these kinds of binaries.

For this burst, our model assumes an initial explosion energy of 2×10^{51} erg, ranging the spherical equivalent-mass from 0.05–4 $M_\odot$. Figure 9 shows light curves rising quickly at $t \lesssim 10^4$ s for the lowest mass to $\sim 10^5$ s for the 4 $M_\odot$ explosion. This maximum mass corresponds to the ejecta mass from our supernova. The corresponding CO core mass of our progenitor is this ejecta mass plus the mass of the νNS, roughly 5.4 $M_\odot$. It is possible that the mass is slightly larger for our progenitors, and the emission from the breakout could be longer, but peak X-ray emission from shock breakout beyond a few times 10^5 s will be difficult to achieve. The observed emission would come from the sum of this full range of explosions. The close match of our models (fitted to our expected progenitor mass) to this X-ray plateau demonstrates that this sequence of shock

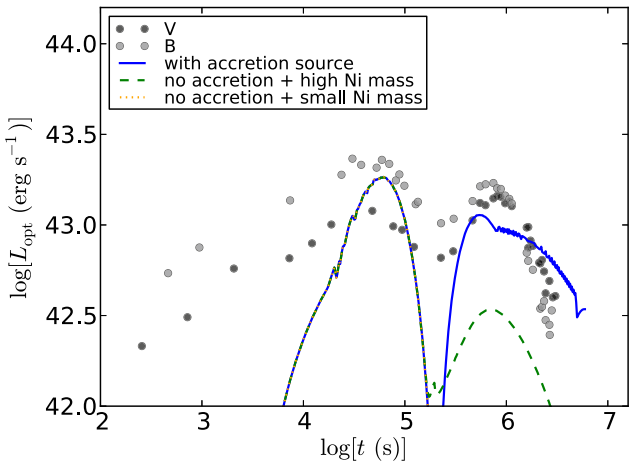

Figure 10. Optical and UV luminosity of XRF 060218 (Pian et al. 2006). The light curve shows a double-peaked structure. The red dotted curve shows the supernova optical emission without either ^{56}Ni decay or accretion energy; it can be seen that it explains only the first peak. The blue solid curve includes the energy deposition from the accretion onto the NS (which is a power source of 4×10^{46} erg s^{-1} over a 2500 s duration). This simulation reproduces both the first peak at ~50,000 s as well as the second peak at ~500,000 s. The dashed green curve shows that a second peak can also be produced without accretion power by increasing the total ^{56}Ni yield. However, even if we assume half of the total ejecta is ^{56}Ni, the produced second peak cannot explain the observational data.

breakouts is certainly a viable and natural explanation for this emission (see Figure 9).

We have shown that the X-ray plateau in the afterglow is powered almost entirely by a sequence of shock breakouts and the expanding photosphere. We turn now to the the optical emission which is more complex. The optical emission can be powered by the expanding photosphere, ^{56}Ni decay and the energy deposited by the accreting NS. For XRF 060218, the light curve in the optical and UV exhibits a double-peaked structure suggestive of multiple power sources and, using our light-curve code, we can test out different scenarios. Just like the X-ray, geometry effects will modify the optical light-curve. Here we merely probe the different emission mechanisms to determine the viability of each to explain the XRF 060218 optical light-curve.

Figure 10 shows the V and B band light curves for XRF 060218 (Pian et al. 2006). The light curve in both bands peaks first near 50,000 s and then again at 500,000 s. Using our 1 $M_{\odot}$ 1D model from our X-ray emission, we simulate the V and B band light curves. Without either ^{56}Ni decay or accretion energy, the supernova explosion only explains the first peak. However, if we include the energy deposition from the accretion onto the NS (for our energy deposition, we use 4×10^{46} erg s^{-1} over a 2500 s duration), our simulations produce a second peak at roughly 500,000 s. A second peak can also be produced by increasing the total ^{56}Ni yield. However, even if we assume half of the total ejecta is ^{56}Ni, the second peak remains too dim to explain the observations.

The accretion energy in our model provides a natural explanation for the double-peaked features observed in the optical emission of XRF 060218. However, our simple model makes a series of approximations: e.g., we use gray transport, estimating the V and B emission assuming a blackbody, we assume the opacities are dominated by electron scattering, etc. Our simplified picture cannot accurately reproduce the first slowly rising part of the optical data which could be due to a combination of (1) the low-energy tail of the X-ray bubbles and (2) the geometry asymmetries which, just like for the X-rays, cause 1D effective mass ejecta to be lower along some lines of sight, leading to some optical emission. The simulation of these details are out of the scope of the present article and will be the subject of future simulations. We have shown that, although approximate, the accretion mechanism can power the observed XRF 060218 light curve.

9. CONCLUSIONS

We have analyzed in detail the IGC paradigm of GRBs associated with supernovae. The progenitor is a binary system composed of a CO core and a NS in which the explosion of the CO core as a supernova triggers a hypercritical accretion process onto the NS. For the given supernova parameters (total CO core mass, density profile, ejecta mass and velocity) and an initial mass of the NS, the fate of the NS depends only on the binary separation/orbital period. The picture that arises from the simulation of the accretion process as a function of the orbital period is as follows.

1. Since the accretion rate decreases for increasing values of the orbital period, there exists a specific value over which BH formation is not possible because the NS does not accrete sufficient matter to reach the critical mass. We denoted this maximum period for gravitational collapse as $P_{\rm max}$ and computed it as a function of the initial NS mass for selected pre-supernova CO cores (see Figure 5). Therefore, in systems with $P \leqslant P_{\rm max}$ BH formation occurs and these systems, within the IGC paradigm, can explain BdHNe (Fryer et al. 2014, 2015; Becerra et al. 2015). In systems with $P > P_{\rm max}$, the NS does not accrete enough matter from the supernova ejecta and the collapse to a BH does not occur: these systems, within the IGC paradigm, are used to explain the nature of XRFs.
2. We have shown that the early emission ($t \lesssim 10^3$ s) of an IGC binary is powered by the accretion luminosity. This luminosity explains the prompt emission of XRFs as presented here in the case of XRF 060218 (see Figure 9). We are planning to extend this conclusion to additional XRFs.
3. We have shown that convection instabilities arising from the NS accretion atmosphere can drive hot outflows emitting X-rays observable in the early emission of GRBs. It has been shown in Fryer et al. (2014) that the emission from such outflows is consistent with the early ($t \lesssim 50$ s) thermal X-ray emission observed in the BdHN GRB 090618 (Izzo et al. 2012a, 2012b). We have shown consistency with the thermal emission of XRF 060218. The observational verification in the case of additional XRFs will be presented elsewhere. Details of the structure of the accretion region are presented in Appendix B.
4. Neutrino emission is the main energy sink of the system, allowing the hypercritical accretion to occur. We have given estimates of the neutrino flux and energy. Typical neutrino energies are in the range 1–15 MeV. A detailed study of the neutrino emission will be presented elsewhere. Details are also presented in Appendix B.2.
5. We have shown that the presence of the NS in very compact orbit produces large asymmetries in the supernova ejecta around the orbital plane (see Figures 6 and 7). These asymmetries are the combined effect of the

accretion and of the action of the gravitational field of the NS on the supernova layers.

6. The above supernova asymmetries lead to observable effects in the supernova emission. The shocked material becomes transparent at different times with different luminosities along different directions owing to the asymmetry created in the supernova ejecta by the orbiting and accreting NS (see Figures 6 and 7). The sequence of shock breakout luminosities is thus influenced by the asymmetries in the explosion: the light curve produced along the more massive directions produced later shock breakout times. We have shown that the observed long-lasting, $t > t_{\rm acc}$, afterglow X-ray emission observed in XRFs can be powered by this mechanism and presented as an example XRF 060218 (see Figure 9). The specific example is here presented for XRF 060218 and evidence that this mechanism is also observed in additional XRFs will be presented elsewhere.
7. We have exemplified the above mechanism for late X-ray emission observed in XRF 060218. The supernova ejecta asymmetries are even more pronounced in more compact binaries in which the NS, by accretion, reaches the critical mass and collapses to a BH (see Figure 6). This implies that this mechanism is also at work in the X-ray afterglow of BdHNe with specific additional features in the spike, in the plateau and in the late power-law emission.
8. We have shown that not only asymmetries caused by the close accreting NS modify the classic picture of supernova emission. The X-rays emitted from the accretion add energy to the supernova explosion. We have simulated the optical emission of the supernova and compared and contrasted our theoretical expectation with the optical luminosity of XRF 060218 which shows a peculiar double-peaked shape. We have shown that without either ^{56}Ni decay or accretion energy, the supernova explosion can explain only the first peak. We then showed that the inclusion of ^{56}Ni decay produces indeed a double-peaked light curve but with a second peak which is too dim to explain the observed optical emission. This conclusion holds even adopting unphysically high amounts of ^{56}Ni mass of up to half of the ejecta mass. Instead, we demonstrated that the source of energy given by the hypercritical accretion onto the NS provides a double-peaked light curve consistent with the observational data. See Figure 10 for details.
9. We have shown how the radiation during the continuous accretion process affects the supernova emission both in X-rays and in the optical. We have simulated this effect for binaries in which the NS does not collapse to a BH, namely for XRFs (e.g., XRF 060218). For systems with shorter orbital periods in which a BH is formed, namely for BdHNe, besides the initial interaction of the supernova with the radiation from the accretion process, the supernova interacts with the radiation from the prompt radiation following the BH formation. The interaction of the electron–positron pairs (moving with Lorentz factor $\Gamma \sim 10^2$) with the supernova material at a distance of $r \sim 10^{12}$ cm and moving at $\Gamma \sim 1$ can originate the flare observed around $t \sim 100$ s after the GRB trigger time in the X-ray data of BdHNe. The theoretical and observational details of this process will be presented elsewhere.

It is interesting that in parallel to the above conclusions we can also draw some inferences on the astrophysics of NS–NS binaries. Our results suggest that the systems in which the accreting NS does not reach the critical mass (i.e., the XRFs) are natural candidates to produce such binaries (Ruffini et al. 2016). We have shown that this will occur for CO–NS binaries with long orbital periods; thus it is possible that many of these systems become unbound by the supernova explosion produced by the CO core. The XRF to BdHN occurrence rate ratio can shed light on the ratio of bound/unbound IGC binaries Fryer et al. (2015). The short orbital periods $P < P_{\rm max}$ needed for BdHNe obtained from our theoretical model imply that XRF must be much more common than BdHNe, as it is indeed observed (see, e.g., Guetta & Della Valle 2007; Ruffini et al. 2016, and references therein). The few systems which will keep bound become NS–NS binaries where at least one of the components can be massive and with a rotation period in the millisecond region. If the NS accretes from the LSO, then at the end of the process it will have an angular momentum $J_{\rm NS} \sim 2\sqrt{3}\,GM_{\rm acc}M_{\rm NS}/c \approx 4.3 \times 10^{48}\ [M_{\rm acc}/(0.1M_\odot)]\ [M_{\rm NS}/(1.4M_\odot)]\ {\rm g\,cm^2\,s^{-2}}$, where $M_{\rm acc}$ is the total accreted mass. Thus, the NS will have a rotation period $P = 2\pi I_{\rm NS}/J_{\rm NS} \approx 1.6(0.1M_\odot/M_{\rm acc})(R_{\rm NS}/10^6\ {\rm cm})^2$ ms, where $I_{\rm NS} \sim 2/5 M_{\rm NS}R_{\rm NS}^2$ is the NS moment of inertia. That known binary millisecond pulsars could be formed in XRFs is a very exciting result that deserves further scrutiny.

We thank the referee for the comments and suggestions. L.B. acknowledges the support given by the International Relativistic Astrophysics Ph. D Program (IRAP-PhD). J.A.R. acknowledges the support by the International Cooperation Program CAPES-ICRANet financed by CAPES, Brazilian Federal Agency for Support and Evaluation of Graduate Education within the Ministry of Education of Brazil. J.A.R. acknowledges partial support of the project No. 3101/GF4 IPC-11/2015 and the target program of the Ministry of Education and Science of the Republic of Kazakhstan.

APPENDIX A
ANALYTIC APPROXIMATION FOR THE PEAK ACCRETION RATE

We can see from Figure 3 that the shorter(smaller) the orbital period(separation) the higher the peak accretion rate $\dot{M}_{\rm peak}$ and the shorter the peak time, $t_{\rm peak}$. Indeed, we can derive such a feature from simple arguments. The accretion rate (1) increases for higher densities and lower velocities, so we should expect as indeed shown in Figure 3, it increases with time as the inner ejecta layers, which are denser and slower (see Equations (4) and (3)), reach and passed the accretion region. The accretion rate starts to peak at the passage of the innermost densest layer, $r_{\rm inner}$, through the capture region. Such a layer moves with velocity $v_{\rm inner} = (r_{\rm inner}/R^0_{\rm star})v_{\rm star,0}$ as given by the homologous expansion assumption.

Thus, the accretion rate peaks around the peak time:

$$t_{\rm peak} = \frac{a - R_{\rm cap}}{v_{\rm inner}} = \frac{(a - R_{\rm cap})R^0_{\rm star}}{r_{\rm inner}\,v_{\rm star,0}}, \tag{30}$$

namely the time when $r_{\rm inner}$ reaches the capture region which is located at a distance $r = a - R_{\rm cap}$ from the CO core center.

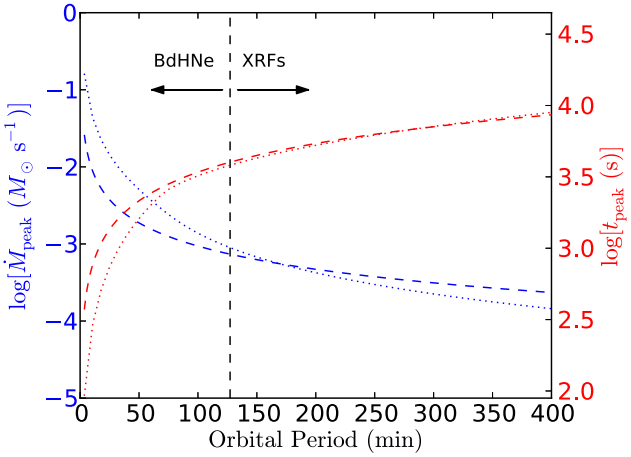

Figure 11. Peak accretion rate ($\dot{M}_{\rm peak}$, blue curves and left y-scale) and peak time ($t_{\rm peak}$, red curves and right y-scale) as a function of the orbital period. The dashed curves give the analytic peak accretion rate and time (34) and (33), respectively, while the dotted curves correspond to the values obtained from the numerical integration of the equations in Section 2. This example corresponds to the following binary parameters: a CO core from the $M_{\rm ZAMS} = 20\,M_\odot$ progenitor of Table 1, an initial NS mass $2.0\,M_\odot$, and a velocity of the outermost ejecta layer $v_{\rm star,0} = 2\times10^9\,{\rm cm\,s^{-1}}$. For these parameters we have $\eta \approx 0.41$ from Equation (32). The black dashed vertical line marks the maximum orbital period (for these system parameters, $P_{\rm max} \approx 127$ minutes) for which the NS reaches, by accretion, the critical mass and collapses to a BH (see Figure 5 in Section 4). We recall that within the IGC interpretation systems with $P < P_{\rm max}$ lead to BdHNe while systems with $P > P_{\rm max}$ lead to XRFs.

The radius $r_{\rm inner}$ is the maximum of the density profile (7), namely the root of the equation:

$$r_{\rm inner} - R^0_{\rm star} + R^0_{\rm star}\, m \ln\left(\frac{r_{\rm inner}}{\hat{R}_{\rm core}}\right) = 0, \tag{31}$$

where we recall $\hat{R}_{\rm core} \approx 0.31 R_{\rm core}$. Since $r_{\rm inner} \approx \hat{R}_{\rm core}$, we can obtain the approximate solution:

$$r_{\rm inner} \approx \eta R_{\rm core}, \qquad \eta \equiv \frac{R^0_{\rm star}}{R_{\rm core}}\frac{1+m}{1+m(R^0_{\rm star}/\hat{R}_{\rm core})}. \tag{32}$$

Since $v_{\rm inner} < v_{\rm orb}$, we can approximate the relative velocity as given only by the orbital one, i.e., $v_{\rm rel} \approx v_{\rm orb}$, and within this approximation, the capture radius reduces to $R_{\rm cap} \approx (2M_{\rm NS}/M)a$. Then, Equation (30) becomes

$$t_{\rm peak} \approx \left(1 - \frac{2M_{\rm NS}}{M}\right)\left(\frac{GM}{4\pi^2}\right)^{1/3}\left(\frac{R^0_{\rm star}}{\eta R_{\rm core}}\right)\frac{P^{2/3}}{v_{\rm star,0}}. \tag{33}$$

We can now evaluate Equation (1) at the above $t = t_{\rm peak}$ and applying the same approximations, we obtain for the peak accretion rate

$$\dot{M}_{\rm peak} \approx 2\pi^2 \frac{(2M_{\rm NS}/M)^{5/2}}{(1-2M_{\rm NS}/M)^3}\eta^{3-m}\frac{\rho_{\rm core}\,R^3_{\rm core}}{P}, \tag{34}$$

where we recall $M = M_{\rm CO} + M_{\rm NS}$ is the total binary mass, being $M_{\rm CO} = M_{\rm env} + M_{\nu{\rm NS}}$ the total mass of the CO core given by the envelope mass and the central iron core mass leading to the formation of the νNS.

Figure 11 shows the behavior of Equations (34) and (33) as a function of the orbital period and compares them with the corresponding values obtained from the numerical integration of the accretion equations presented in Section 2. This example is for the binary parameters: a CO core from the $M_{\rm ZAMS} = 20\,M_\odot$ progenitor of Table 1, an initial NS mass $2.0\,M_\odot$, and a velocity of the outermost ejecta layer $v_{\rm star,0} = 2\times10^9\,{\rm cm\,s^{-1}}$. For these parameters, $\eta \approx 0.41$ from Equation (32). It can be seen that the accuracy of the above simple analytic formulas increases for the systems with $P > P_{\rm max}$. This is expected since, as we have mentioned, only for these systems the innermost ejecta layers passed the NS position. In systems with $P < P_{\rm max}$, the NS collapses to a BH before the passage of the innermost layers. In those cases, the maximum accretion rate is not reached at the passage of $r_{\rm inner}$ but at the passage of a layer located at $r_{\rm max} > r_{\rm inner}$, hence with velocity $v_{\rm max} = v(r = r_{\rm max}) > v_{\rm inner}$, and thus $v_{\rm max} \gtrsim v_{\rm orb}$. In any case, it is clear that the above formulas for $\dot{M}_{\rm peak}$ and $t_{\rm peak}$ remain valid to obtain typical (order-of-magnitude) estimates of the accretion process in these binaries. The consistency of the numerical and analytic results (within their range of validity) shown here also serves as an indicator of the reliability of the numerical results (see also Appendix C).

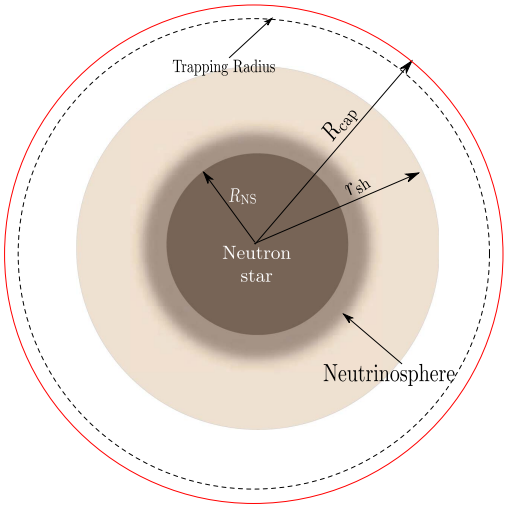

Figure 12. Structure of the NS accretion atmosphere. The ejecta from the supernova enter the NS capture region (red circle) at a distance $r = R_{\rm cap}$ (see Equation (2)) from the NS center and start to fall to the NS surface. The material shocks as it piles on top the NS surface. The shock decelerates the material while it moves toward the NS and near the surface, at the *neutrinosphere*, it loses energy by the emission of neutrinos. The neutrino emission allows the material to reduce its entropy to be finally accreted by the NS.

APPENDIX B
PHYSICS INSIDE THE ACCRETION REGION

In this appendix we analyze the NS accretion zone following the theoretical framework established for supernova fallback accretion (Chevalier 1989; Houck & Chevalier 1991; Fryer et al. 1996). Figure 12 shows schematically the structure of the NS atmosphere: the supernova material entering the NS capture region shocks as it piles up onto the NS surface. As the atmosphere compresses, it becomes sufficiently hot to emit neutrinos allowing the matter to reduce its entropy and be incorporated into the NS.

B.1. Accretion Zone Structure and EOS

In order to model the evolution of the NS accretion zone, we assume that it passes through a sequence of quasi-steady state envelopes, each characterized by the mass accretion rate $\dot{M}$, the NS mass, $M_{\rm NS}$ and its radius $R_{\rm NS}$. The spacetime outside the NS is described by the Schwarzschild metric:

$$ds^2 = -\left(1 - \frac{r_{\rm sch}}{r}\right)dt^2 + \left(1 - \frac{r_{\rm sch}}{r}\right)^{-1}dr^2 + r^2(d\theta^2 + \sin^2\theta d\phi^2), \quad (35)$$

where $r_{\rm sch} = 2GM_{\rm NS}/c^2$ is the Schwarzschild radius. The steady-state relativistic fluid equations for mass, momentum and energy conservation in this geometry are:

$$\frac{1}{r^2}\frac{d}{dr}(r^2\rho u) = 0, \quad (36)$$

$$\frac{1}{2}\frac{d}{dr}\left(\frac{u}{c}\right)^2 + \frac{r_{\rm sch}}{2r} + \frac{1}{w}\frac{dP}{dr}\left[\left(\frac{u}{c}\right)^2 + 1 - \frac{r_{\rm sch}}{r}\right] = 0, \quad (37)$$

$$\frac{d}{dr}(\rho c^2 + U) - \frac{w}{\rho}\frac{d\rho}{dr} + \frac{Q_\nu}{u} = 0, \quad (38)$$

where u is the radial component of the four-velocity, Q_ν is the total energy loss rate per unit volume by neutrino cooling, $w = \rho c^2 + U + P$ is the relativistic enthalpy, ρ is the mass density, P is the pressure and U is the internal energy density.

The boundary conditions are determined by the the conservation of mass, momentum and energy flows through the shock front at $r = R_s$. These are expressed by the Rankine–Hugoniot conditions (Landau & Lifshitz 1959):

$$\rho_p u_p - \rho_{\rm sh} u_{\rm sh} = 0, \quad (39)$$

$$w_p u_p^t u_p - w_{\rm sh} u_{\rm sh}^t u_{\rm sh} = 0, \quad (40)$$

$$w_p u_p^2 + P_p - w_{\rm sh} u_{\rm sh}^2 - P_{\rm sh} = 0, \quad (41)$$

where u^t is the time component of the four-velocity, determined by the condition $g_{\mu\nu}u^\mu u^\nu = -c^2$. The indexes "$p$" and "sh" denote the quantities in the pre-shock and post-shock zone, respectively. Outside the shock front, the material is in approximate free fall, thus:

$$u_p = \sqrt{\frac{2GM_{\rm ns}}{r}}, \qquad \rho_p = \frac{\dot{M}}{4\pi r^2 v_p}, \qquad P_p = \frac{1}{2}\rho_p v_p^2. \quad (42)$$

We consider a gas of electrons, positrons, ions and photons. Then, the total pressure and density energy are:

$$P_{\rm tot}(\rho, T) = P_\gamma + P_{\rm ion} + P_{e^-} + P_{e^+}, \quad (43)$$

$$U_{\rm tot}(\rho, T) = U_\gamma + U_{\rm ion} + U_{e^-} + U_{e^+}. \quad (44)$$

For the pressure and the internal energy of the radiation field, we adopt a blackbody in thermodynamical equilibrium:

$$P_\gamma = \frac{1}{3}aT^4, \qquad U_\gamma = 3P_\gamma, \quad (45)$$

with $a = 4\sigma/c = 7.56 \times 10^{-15}$ erg cm^{-3} K^{-4}, where σ is the Stefan–Boltzmann constant.

For the ion gas, we assume a perfect gas:

$$n_{\rm ion} = \frac{\rho}{Am_u}, \qquad P_{\rm ion} = n_{\rm ion}\kappa_{\rm B}T, \qquad U_{\rm ion} = \frac{3}{2}P_{\rm ion}, \quad (46)$$

where $n_{\rm ion}$ is the ion number density, $m_u = 1.6604 \times 10^{-24}$ g is the atomic mass unit and $\kappa_{\rm B}$ is the Boltzmann constant.

Finally, the electrons and positrons are described by the Fermi–Dirac distributions:

$$n_{e^\pm} = \frac{m_e^3 c^3}{\pi^2\hbar^3}\sqrt{2}\,\beta^{3/2}[\mathcal{F}_{1/2}(\eta_{e^\pm}, \beta) + \beta\mathcal{F}_{3/2}(\eta_{e^\pm}, \beta)], \quad (47)$$

$$P_{e^\pm} = \frac{8\,m_e^4 c^5}{3\sqrt{2}\,\pi^2\hbar^3}\beta^{5/2}\left[\mathcal{F}_{3/2}(\eta_{e^\pm}, \beta) + \frac{1}{2}\beta\mathcal{F}_{5/2}(\eta_{e^\pm}, \beta)\right], \quad (48)$$

$$U_{e^\pm} = \frac{m_e c^2}{\pi^2}\frac{2\sqrt{2}\,m_e^3 c^3}{\hbar^3}\beta^{5/2} \times [\mathcal{F}_{3/2}(\eta_{e^\pm}, \beta) + \beta\mathcal{F}_{5/2}(\eta_{e^\pm}, \beta)], \quad (49)$$

where $\mathcal{F}_k(\eta, \beta) \equiv \int_0^\infty \frac{x^k(1 + 0.5x\beta)^{1/2}dx}{e^{x-\eta} + 1}$ is the relativistic Fermi–Dirac integral, $\beta \equiv \kappa_{\rm B}T/(m_e c^2)$ is the relativity parameter and $\eta \equiv (\mu - m_e c^2)/\kappa_{\rm B}T$ is the degeneracy parameter, with μ the chemical potential. Since the electrons and positrons are in equilibrium with radiation ($e^+ + e^- \rightarrow \gamma + \gamma$), their chemical potential are related by $\mu_{e^-} + \mu_{e^+} = 0$ and then $\eta_{e^+} = -\eta_{e^-} - 2/\beta$. Finally, for each value of density and temperature, η_{e^-} is determined from the charge neutrality condition:

$$n_{e^-} - n_{e^+} = \frac{Z}{A}\frac{\rho}{m_u} = Zn_{\rm ion}. \quad (50)$$

As an example, we show in Figure 13 the entropy, temperature, density and pressure profile from the NS surface (we have assumed a NS of $M_{\rm NS} = 2.0\,M_\odot$ with $R_{\rm NS} = 10^6$ cm) to the shock radius for a specific value of the mass accretion rate $10^{-2}\,M_\odot\,{\rm s}^{-1}$. For the ions we adopt here $Z = 6$ and $A = 12$. It can be seen here that the entropy gradient of the NS atmosphere is negative, and it is thus subjected to convective instabilities (see Section 6.1).

B.2. Neutrino Emission and Shock Position

We turn now to discuss the neutrino emission processes taken into account in our calculations. We follow the results reported in Itoh et al. (1996) for the neutrino energy loss rates computed within the Weinberg–Salam theory (Weinberg 1967; Salam 1968). We use here the formulas which fit the numerical results in the following regime of density and temperature: $10^0\,{\rm g\,cm^{-3}} < \rho < 10^{14}\,{\rm g\,cm^{-3}}$ and $10^7\,{\rm K} < T < 10^{11}\,{\rm K}$ (Itoh et al. 1996).

We consider the following channels of neutrino emission. (i) Pair annihilation: $e^+ + e^- \rightarrow \nu + \bar{\nu}$ (Munakata et al. 1985; Itoh et al. 1989); this neutrino energy loss rate is here denoted by $\epsilon_{e^-e^+}$. (ii) Photo-neutrino process: $\gamma + e^\pm \rightarrow e^\pm + \nu + \bar{\nu}$ (Munakata et al. 1985; Itoh et al. 1989), denoted by ϵ_γ. (iii) Plasmon decay: $\bar{\gamma} \rightarrow \nu + \bar{\nu}$ (Kohyama et al. 1986, 1994), denoted by $\epsilon_{\rm pl}$. (iv) Bremsstrahlung processes (Itoh & Kohyama 1983; Itoh et al. 1984a, 1984b, 1984c), denoted by $\epsilon_{\rm BR}$, which can be due to electron–nucleon interaction $e^\pm + N \rightarrow N + \nu + \bar{\nu}$ or to nucleon–nucleon interaction $N + N \rightarrow N + N + \nu + \bar{\nu}$. It is important to mention that two different expressions for the total Bremsstrahlung emission are shown in Itoh et al. (1996) depending on whether the Coulomb parameter, $\Gamma \equiv (Ze)^2/(r_i k_{\rm B}T)$ where $r_i = [3/(4\pi n_{\rm ion})]^{1/3}$, is higher or lower than the critical value

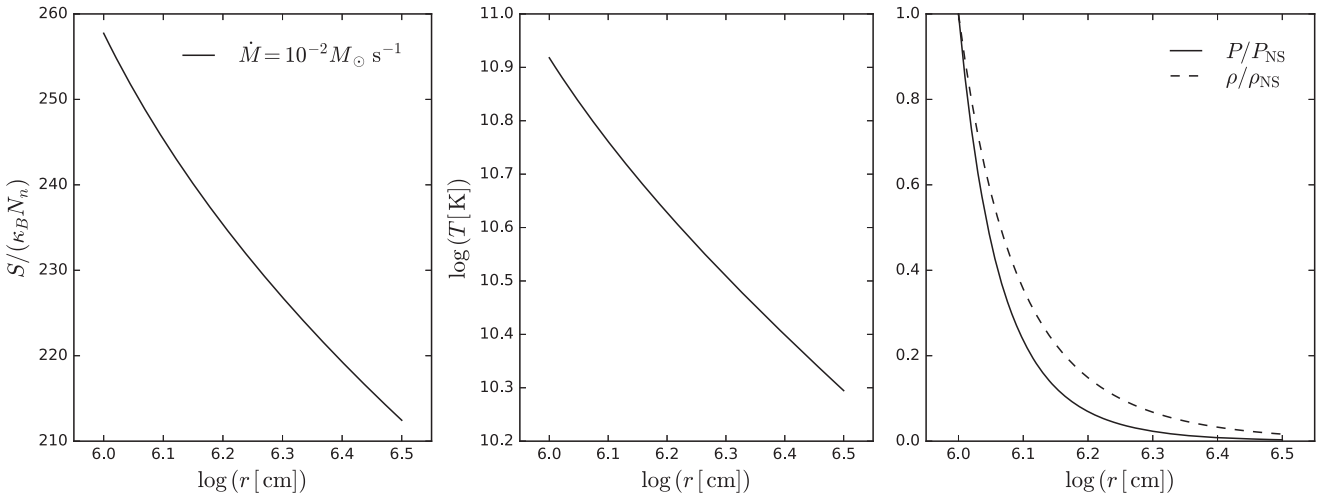

Figure 13. Entropy, temperature, density and pressure profile for a NS accreting atmosphere for $\dot{M} = 10^{-2}\,M_\odot$ s^{-1}. The pressure and density are normalized to $P_{\rm NS} \approx 3.28 \times 10^{29}$ dyn cm^{-2} and $\rho_{\rm NS} \approx 7.5 \times 10^{8}$ g cm^{-3}, respectively.

$\Gamma \approx 180$, over which the system crystallizes. So the total energy loss rate per unit volume due to neutrino emission is $Q_\nu = \epsilon_{e^-e^+} + \epsilon_\gamma + \epsilon_{\rm pl} + \epsilon_{\rm BR}$.

Since the infalling material is strongly decelerated by the accretion shock, the post-shock kinetic energy is much less that the internal and gravitational energy. Then, assuming a polytropic gas [$P = (\gamma - 1)U \propto \rho^\gamma$] and subsonic velocities inside the shock radius, $(v/c)^2 \ll 1$, Equation (38) can be solved for the radial dependence of the fluid variables ρ, P and u as (Houck & Chevalier 1991):

$$\rho = \rho_{\rm sh} f(r)^{\frac{1}{\gamma-1}}, \quad P = P_{\rm sh} f(r)^{\frac{\gamma}{\gamma-1}},$$
$$u = \frac{u_{\rm sh}}{r^2} f(r)^{\frac{1}{1-\gamma}}, \quad f(r) \equiv \frac{\left(1 - \frac{r_{\rm sch}}{r}\right)^{-1/2} - 1}{\left(1 - \frac{r_{\rm sch}}{R_{\rm ns}}\right)^{-1/2} - 1}. \qquad (51)$$

The approximation of a polytropic EOS was validated by numerical simulations in Fryer et al. (1996), who showed the infall NS atmosphere is well approximated by a polytropic gas of index $\gamma = 1.4$.

Since neutrinos are the main energy sink of the system (see below), the position of the shock can be estimated from the balance between the neutrino emission and the release of the potential gravitational energy due to the accretion process, i.e.,

$$\left(\frac{4\pi R_{\rm NS}^2 \Delta r_{\rm ER}}{\sqrt{1 - \frac{2GM_{\rm NS}}{c^2 R_{\rm NS}}}}\right) Q_\nu \approx c^2 \dot{M}\left[\left(1 - \frac{2GM_{\rm NS}}{c^2 R_{\rm NS}}\right)^{-1/2} - 1\right], \qquad (52)$$

where we have assumed the rate at which gravitational energy is released as the kinetic energy gained in the free fall from infinity, and we have considered the proper volume of the cooling region and the proper cooling rate. We have also introduced the thickness of the neutrino emission region at the base of the atmosphere, $\Delta r_{\rm ER}$, which in view of the strong dependence of the neutrino emission processes on the temperature, can be estimated as one temperature scale height, i.e.,

$$\Delta r_{\rm ER} \approx H_T = \frac{T}{|(dT/dr)|},$$
$$\frac{dT}{dr} = \left(\frac{\partial \ln T}{\partial \ln \rho}\right)_P \frac{d \ln \rho}{dr} + \left(\frac{\partial \ln T}{\partial \ln P}\right)_\rho \frac{d \ln P}{dr}. \qquad (53)$$

Figure 14 shows the NS surface temperature and the shock position as a function of the mass accretion rate. The thickness of the neutrino emission region is very poorly dependent on the accretion rate; indeed Equation (53) gives $\Delta r_{\rm ER} \approx 0.76$–$0.77\ R_{\rm NS}$ for $\dot{M} = 10^{-8}$–$10^{-1}\ M_\odot$ s^{-1}.

Under the conditions (non-degenerate, relativistic, hot plasma) of our hypercritically accreting NS, the most efficient neutrino emission is given by the e^+e^- pair annihilation (see Figure 16). In these T–ρ conditions, $\epsilon_{e^-e^+}$ reduces to the simple expression (Yakovlev et al. 2001):

$$\epsilon_{e^-e^+} = 1.39 \times 10^{25} \left(\frac{k_{\rm B} T}{1\ {\rm MeV}}\right)^9 \ {\rm erg\ cm^{-3}\ s^{-1}}. \qquad (54)$$

B.3. Neutrino and Photon Optical Depth

We have assumed that the neutrinos produced at the base of the NS surface are the main sink of the gravitational potential energy gained by the infalling material. We proceed now to assess the validity of this statement through the calculation of the neutrino opacity.

The total neutrino opacity is:

$$\kappa_\nu = \kappa_{\nu,{\rm abs}} + \kappa_{\nu,{\rm scat}}, \qquad (55)$$

where $\kappa_{\nu,{\rm abs}}$ and $\kappa_{\nu,{\rm scat}}$ correspond to the opacity produced by absorption and scattering processes. In general, the opacity can be written as

$$\kappa = \frac{\sigma_i n_i}{\rho}, \qquad (56)$$

where n_i is the particle density and σ_i is the process cross section. We adopt the following scattering and absorption process:

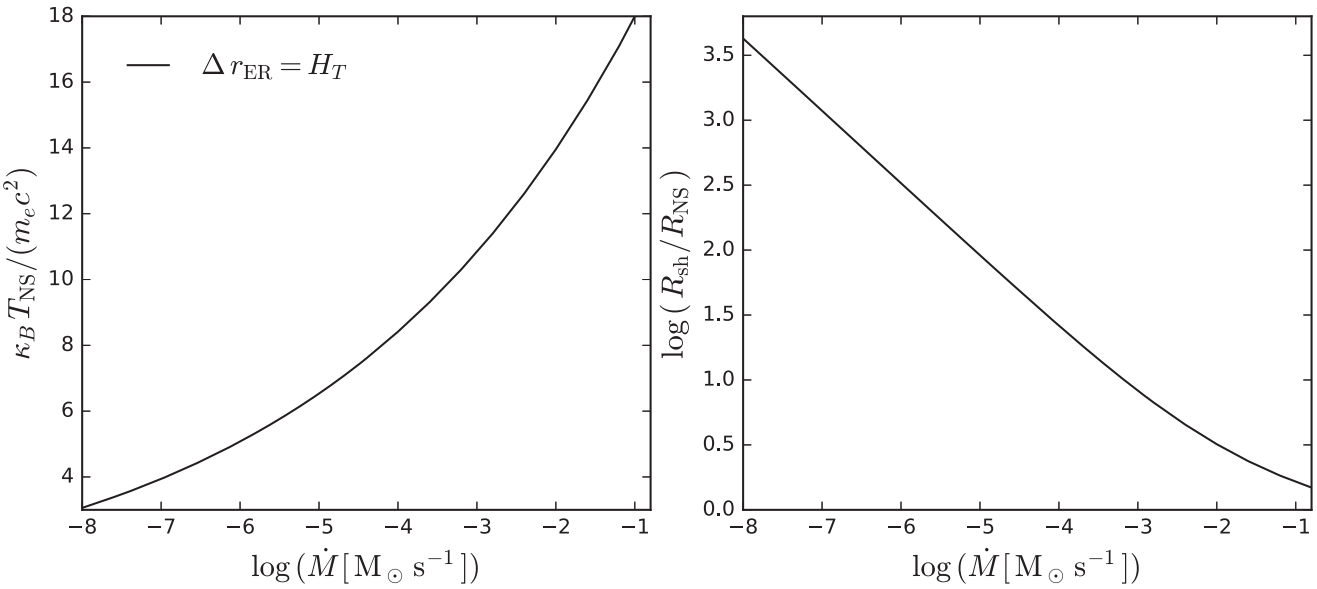

Figure 14. Temperature of the NS surface (left panel) and ratio between the shock radius and the NS radius (right plot) as a function of the mass accretion rate in the range $\dot{M} = 10^{-8}$–$10^{-1}\ M_\odot\ {\rm s}^{-1}$.

Scattering processes: neutrinos transfer momentum to the matter by the scattering off nuclei and electrons and positrons:

1. Coherent neutrino nucleus scattering: $\nu + (A, Z) \rightarrow \nu + (A, Z)$ (Tubbs & Schramm 1975)

$$\sigma_A = \frac{1}{16}\sigma_0\left(\frac{E_\nu}{m_e c^2}\right)^2 A^2\left[1 - \frac{Z}{A} + (4\sin^2\theta_w - 1)\frac{Z}{A}\right]^2$$
$$\text{with}\quad \sigma_0 = \frac{4G_{\rm F}^2\,(m_e c^2)^2}{\pi\,(\hbar c)^4} \approx 1.71 \times 10^{-44}\ {\rm cm}^2 \qquad (57)$$

   where $G_{\rm F}$ is the Fermi weak neutrino coupling constant and $\theta_w =$ is the Weinberg angle, $\sin^2\theta_w = 0.23$. The scattering is coherent in the sense that the nucleus acts as a single particle and the initial and final neutrino energy are nearly equal.
2. Neutrino–electron scattering (Bowers & Wilson 1982; Burrows & Thompson 2002):

$$\sigma_e(E) = \frac{3}{8}\sigma_0\beta\frac{E}{m_e c^2}\left(1 + \frac{\eta_e}{4}\right)\left[(C_v + C_a)^2 + \frac{1}{3}(C_v + Ca)^2\right] \qquad (58)$$

   where $C_v = 1/2 + 2\sin^2\theta_w$ for electron neutrino and antineutrino types, $C_a = 1/2$ for neutrino and $C_a = -1/2$ for antineutrinos.

Absorption processes: Since we have shown that the most efficient neutrino cooling process near the NS surface is electron–positron annihilation, the inverse process, namely the annihilation of neutrinos, $\nu + \bar{\nu} \rightarrow e^- + e^+$, represents the main source of opacity. The total average cross sections are given by (Goodman et al. 1987):

$$\sigma_\nu(E_\nu) = \frac{4}{3}K_{\nu\bar{\nu}}\sigma_0\langle E_\nu\rangle\langle E_{\bar{\nu}}\rangle,$$
$$\sigma_{\bar{\nu}}(E_{\bar{\nu}}) = \frac{4}{3}K_{\nu\bar{\nu}}\sigma_0\langle E_{\bar{\nu}}\rangle\langle E_\nu\rangle, \qquad (59)$$

where $K_{\nu\bar{\nu}} = (1 + 4\sin^2\theta_w + 8\sin^4\theta_w)/12 = 0.195$. The energy of the neutrino and antineutrinos are calculated assuming they are described by the Fermi–Dirac distribution with zero chemical potential:

$$\langle E_\nu\rangle = \langle E_{\bar{\nu}}\rangle = \frac{U_\nu}{n_\nu} = \frac{\mathcal{F}_3(0,0)}{\mathcal{F}_2(0,0)}k_{\rm B}T = 3.15 k_{\rm B}T,$$
$$\langle E_\nu^2\rangle = \frac{\mathcal{F}_4(0,0)}{\mathcal{F}_2(0,0)}(k_{\rm B}T)^2 = 12.93(k_{\rm B}T)^2. \qquad (60)$$

Then, the total neutrino opacity is:

$$\kappa_\nu = \left[\sigma_A\left(\frac{\rho}{A m_u}\right) + \sigma_e(E_\nu)n_{e^-} + \sigma_\nu(E_\nu)n_\nu\right]/\rho, \qquad (61)$$

The neutrino optical depth can then be obtained as:

$$d\,\tau_\nu = \kappa_\nu\,\rho\,dr = \frac{dr}{\lambda_\nu}, \qquad (62)$$

where λ_ν is the neutrino mean free path:

$$\lambda_\nu = \frac{1}{\kappa_\nu\,\rho}. \qquad (63)$$

Thus, the optical depth at the base of the neutrino emission region can be estimated as: $\tau_{\nu,{\rm ER}} \approx \kappa_\nu\,\rho_{\rm NS}\Delta r_{\rm ER} = \Delta r_{\rm ER}/\lambda_{\nu,{\rm ER}}$. Large values for the optical depth ($\tau_\nu \gg 1$) implies that the neutrinos are reabsorbed by the matter and cannot freely escape from the system.

In order to verify that photons are trapped in the infalling material, we evaluate the photon mean free path and photon emissivity:

$$\tau_\gamma = \kappa_R\,\rho\Delta r_{\rm ER}, \qquad \dot{q}_\gamma \approx \frac{1}{\Delta\,r_{\rm ER}}\frac{\sigma T^4}{\tau_\gamma}, \qquad (64)$$

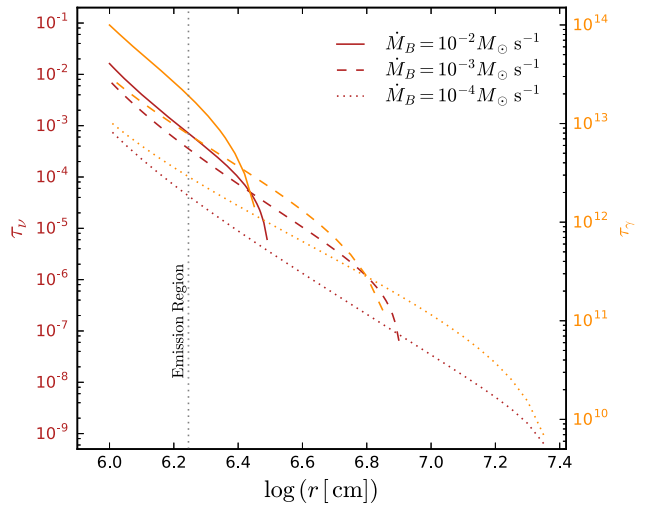

Figure 15. Neutrino (left y-scale, τ_ν) and photon (right y-scale, τ_γ) optical depths in the NS star accretion region (from the shock radius to the NS surface) for selected accretion rates.

where σ is the Stefan–Boltzmann constant, τ_γ is the photon optical depth, and κ_R is the Rosseland mean opacity:

$$\kappa_R = 0.4 + 0.64 \times 10^{23} \left(\frac{\rho}{\mathrm{g\ cm^{-3}}}\right)\left(\frac{T}{K}\right)^{-3} \mathrm{g^{-1}\,cm^2}, \quad (65)$$

being the first term due to the electron scattering and the second one to the free–free absorption.

We show in Figure 15 the neutrino and photon optical depth profile in the NS accretion region for three different values of the mass accretion rate. We can see the photon optical depth is much higher than unity for photons, implying that they are indeed trapped at any radius. On the contrary, the neutrino optical depth is much lower than unity, implying that they efficiently cool the atmosphere which allows the system to continue the accretion at hypercritical rates.

We show in Figure 16 the T–ρ diagram of the NS surface for accretion rates $\dot{M} = 10^{-8}$–$10^{-1}\ M_\odot\ \mathrm{s}^{-1}$ which covers both XRFs and BdHNe (see, e.g., Figure 11). Higher temperatures and densities correspond to higher accretion rates. We show contours indicating where the neutrino emissivities of the different neutrino emission processes are equal. It can be seen from these two figures that: (1) pair annihilation neutrino processes are highly dominant over the other neutrino emission mechanisms; (2) neutrinos can efficiently escape taking away most of the energy (high emissivity); (3) photons are trapped hence they have negligible emissivity; (4) even for the largest accretion rates the neutrino optical depth in the accretion zone is below unity and so the system is not opaque to neutrinos.

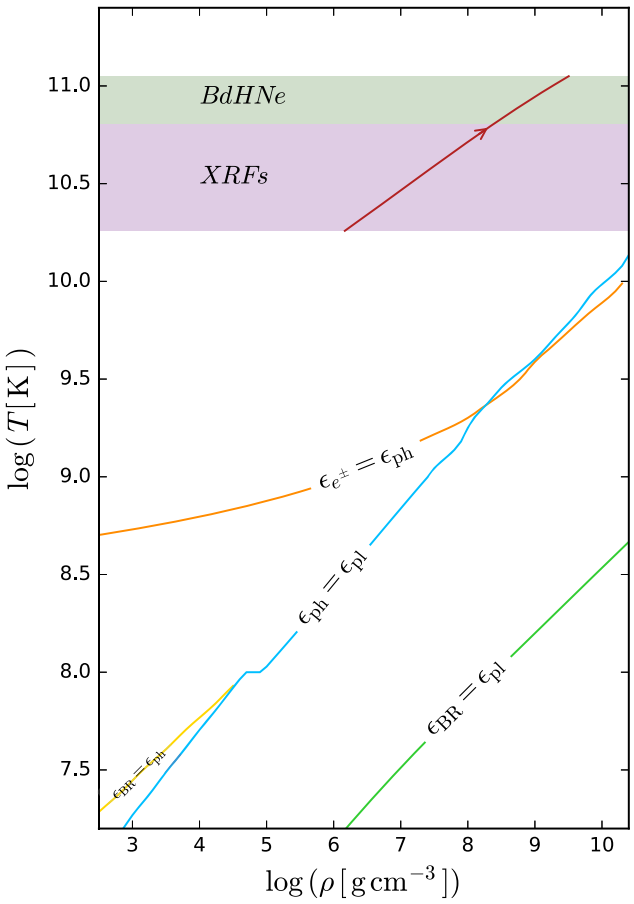

Figure 16. Temperature–density diagram of the accreting atmosphere equation of state. In order to see the dominant neutrino processes, we show contours where the emissivities of the different neutrinos process become equal: $\epsilon_{e^\pm}$ corresponds to the pair annihilation process, ϵ_γ to the photo-neutrino emission, ϵ_{pl} to the plasmon decay, and ϵ_{BR} to the Bremsstralung emission. The solid red curve shows the corresponding T–ρ values of the NS surface in the range of accretion $\dot{M} = 10^{-8}$–$10^{-1}\ M_\odot\ \mathrm{s}^{-1}$ which covers typical rates achieved in XRFs and BdHNe (see Figure 11). The arrow indicates the direction of increasing accretion rate. Thus, while accreting, the NS moves from the left lower part of the red curve to the right upper part of it. It is clear that in this regime of XRFs and BdHNe, the electron–positron pair annihilation dominates the neutrino emission.

APPENDIX C
CONVERGENCE TESTS

We proceed now to perform a convergence test of the results of our numerical integration. We will perform the test for four important quantities, as a function of the dimensionless time $\tau = t/t_0$: the NS accreted mass $M_{\mathrm{acc}}(\tau)$, gravitational mass $M_{\mathrm{NS}}(\tau)$, angular momentum $J_{\mathrm{NS}}(\tau)$ and gravitational capture radius measured from the supernova center normalized to the binary separation, i.e., $\hat{r} = 1 - R_{\mathrm{cap}}(\tau)/a$.

We use for the numerical integration the Adams method implemented in the Python library SciPy version 0.17.1. This requires that the user sets, besides the system of ordinary different equations, a minimum and a maximum integration stepsize. For the integration we set both to the same value, say $\Delta\tau$. To perform this test we select five values of the stepsize: $\Delta\tau_i \equiv \tau_{\mathrm{acc},0}/N_i$ with $N_i = 1, 20, 50, 200, 500$ for $i = 1,\ldots,5$ and $\tau_{\mathrm{acc},0} = t_{\mathrm{acc},0}/t_0$ is the dimensionless time at which the accretion process starts, i.e., the instant at which the first ejecta layer reaches the NS capture radius. We denote as $A_{\Delta\tau_i}$ the numerical value of the quantity A computed with the stepsize $\Delta\tau_i$, and then compute the relative error with respect to the computed value using a reference stepsize, i.e., $\mathrm{Er}(A) \equiv |A_{\Delta\tau_{\mathrm{ref}}} - A_{\Delta\tau_i}|/A_{\Delta\tau_{\mathrm{ref}}}$. Figure 17 shows the convergence test for a binary system with the following parameters: the CO core of the $M_{\mathrm{ZAMS}} = 20\,M_\odot$ progenitor, an initial NS mass of $2\,M_\odot$, and an orbital period $P = 3$ hr. For these parameters we have $\tau_{\mathrm{acc},0} \approx 29$ and so the stepsizes are: $\Delta\tau_i = 0.0581, 0.1453, 0.5812, 9.6874, 29.062,$ respectively

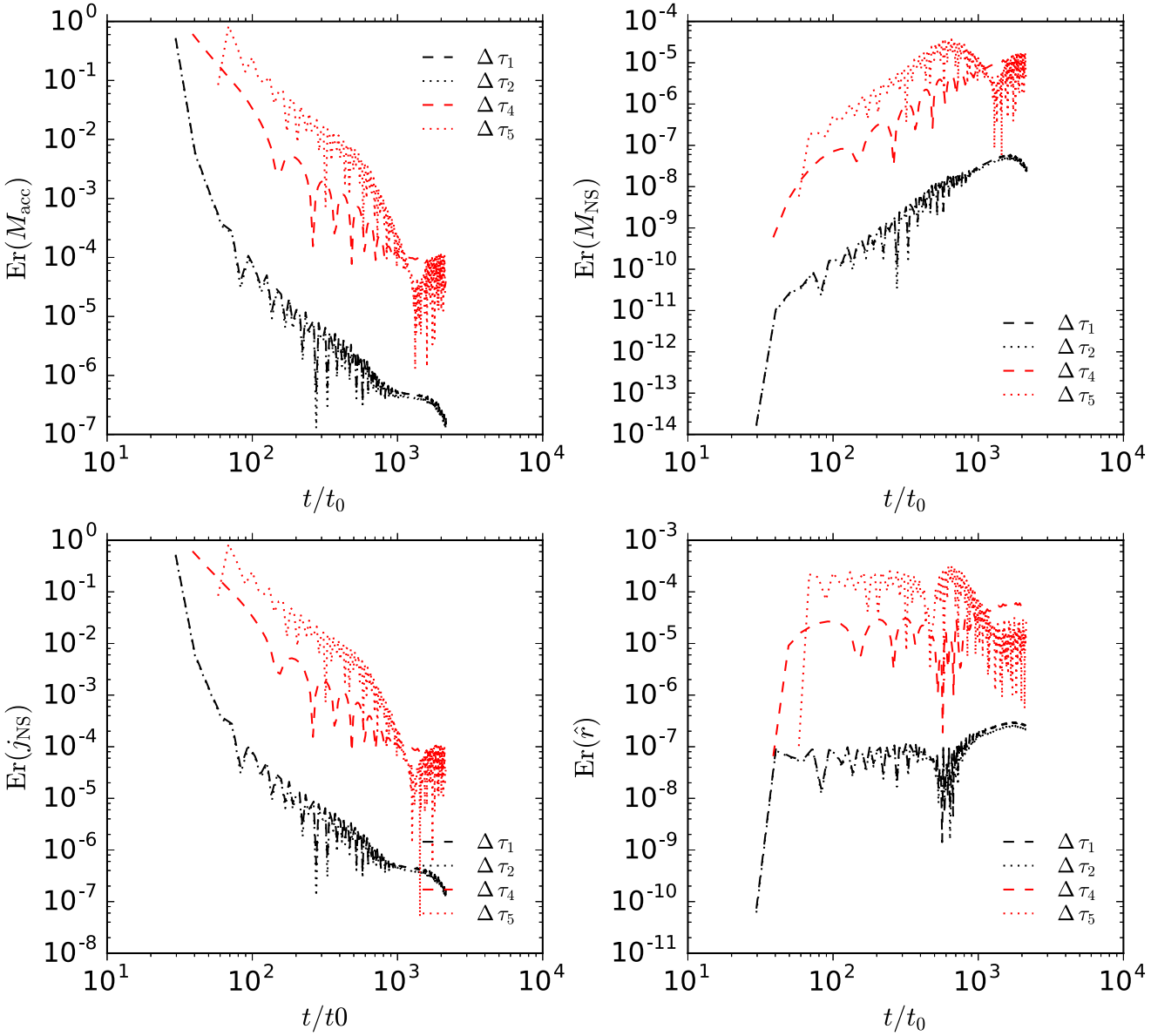

Figure 17. Convergence test for the NS accreted mass $M_{\rm acc}(\tau)$, gravitational mass $M_{\rm NS}(\tau)$, angular momentum $J_{\rm NS}(\tau)$ and the gravitational capture radius measured from the supernova center normalized to the binary separation, i.e., $\hat{r} = 1 - R_{\rm cap}(\tau)/a$. We select here five values of the stepsize: $\Delta\tau_i = 0.0581, 0.1453, 0.5812, 9.6874, 29.062$ for $i = 1,\ldots,5$. The parameters of the binary system in this example are: the CO core of the $M_{\rm ZAMS} = 20\,M_\odot$ progenitor, an initial NS mass of $2\,M_\odot$, and an orbital period $P = 3$ hr. The relative error increases for stepsizes higher than $\Delta\tau_3$ and decreases for stepsizes lower than it, which indicates convergence.

for $i = 1,\ldots,5$. The stepsize of reference in this test is $\Delta\tau_{\rm ref} = \Delta\tau_3 = 0.5812$. We can see that, as expected, the relative error increases for stepsizes higher than $\Delta\tau_3$ and decreases for stepsizes lower than it, indicating convergence. All the results shown in this article are for $\Delta\tau_3$, which corresponds to a different numerical value for different binary systems, since the value of $\tau_{\rm acc,0}$ is specific to each system.

REFERENCES

Amati, L., & Della Valle, M. 2013, IJMPD, 22, 1330028
Bayless, A. J., Even, W., Frey, L. H., et al. 2015, ApJ, 805, 98
Becerra, L., Cipolletta, F., Fryer, C. L., Rueda, J. A., & Ruffini, R. 2015, ApJ, 812, 100
Bondi, H. 1952, MNRAS, 112, 195
Bondi, H., & Hoyle, F. 1944, MNRAS, 104, 273
Boshkayev, K., Quevedo, H., & Ruffini, R. 2012, PhRvD, 86, 064043
Boshkayev, K. A., Quevedo, H., Abutalip, M. S., Kalymova, Z. A., & Suleymanova, S. S. 2016, IJMPA, 31, 1641006
Bowers, R. L., & Wilson, J. R. 1982, ApJS, 50, 115
Bufano, F., Pian, E., Sollerman, J., et al. 2012, ApJ, 753, 67
Burrows, A., & Thompson, T. A. 2002, arXiv:astro-ph/0211404
Campana, S., Mangano, V., Blustin, A. J., et al. 2006, Natur, 442, 1008
Chevalier, R. A. 1989, ApJ, 346, 847
Christodoulou, D., & Ruffini, R. 1971, PhRvD, 4, 3552
Cipolletta, F., Cherubini, C., Filippi, S., Rueda, J. A., & Ruffini, R. 2015, PhRvD, 92, 023007
Cox, J. P. 1968, Principles of Stellar Structure, Vol. 1: Physical Principles, Vol. 2: Applications to Stars (New York: Gordon and Breach)
de la Rosa, J., Roming, P., Pritchard, T., & Fryer, C. 2016, ApJ, 820, 74
Friedman, J. L., Ipser, J. R., & Sorkin, R. D. 1988, ApJ, 325, 722
Fryer, C. L. 2009, ApJ, 699, 409
Fryer, C. L., Belczynski, K., Wiktorowicz, G., et al. 2012, ApJ, 749, 91
Fryer, C. L., Benz, W., & Herant, M. 1996, ApJ, 460, 801

Fryer, C. L., Herwig, F., Hungerford, A., & Timmes, F. X. 2006, ApJL, 646, L131
Fryer, C. L., Oliveira, F. G., Rueda, J. A., & Ruffini, R. 2015, PhRvL, 115, 231102
Fryer, C. L., Rueda, J. A., & Ruffini, R. 2014, ApJL, 793, L36
Galama, T. J., Vreeswijk, P. M., van Paradijs, J., et al. 1998, Natur, 395, 670
Goodman, J., Dar, A., & Nussinov, S. 1987, ApJL, 314, L7
Guetta, D., & Della Valle, M. 2007, ApJL, 657, L73
Houck, J. C., & Chevalier, R. A. 1991, ApJ, 376, 234
Hoyle, F., & Lyttleton, R. A. 1939, PCPS, 35, 405
Itoh, N., Adachi, T., Nakagawa, M., Kohyama, Y., & Munakata, H. 1989, ApJ, 339, 354
Itoh, N., Hayashi, H., Nishikawa, A., & Kohyama, Y. 1996, ApJS, 102, 411
Itoh, N., & Kohyama, Y. 1983, ApJ, 275, 858
Itoh, N., Kohyama, Y., Matsumoto, N., & Seki, M. 1984a, ApJ, 280, 787
Itoh, N., Kohyama, Y., Matsumoto, N., & Seki, M. 1984b, ApJ, 285, 304
Itoh, N., Matsumoto, N., Seki, M., & Kohyama, Y. 1984c, ApJ, 279, 413
Izzo, L., Rueda, J. A., & Ruffini, R. 2012a, A&A, 548, L5
Izzo, L., Ruffini, R., Penacchioni, A. V., et al. 2012b, A&A, 543, A10
Kohyama, Y., Itoh, N., & Munakata, H. 1986, ApJ, 310, 815
Kohyama, Y., Itoh, N., Obama, A., & Hayashi, H. 1994, ApJ, 431, 761
Landau, L. D., & Lifshitz, E. M. 1959, Fluid Mechanics (Oxford: Pergamon)
Melandri, A., Pian, E., D'Elia, V., et al. 2014, A&A, 567, A29
Munakata, H., Kohyama, Y., & Itoh, N. 1985, ApJ, 296, 197
Pian, E., Mazzali, P. A., Masetti, N., et al. 2006, Natur, 442, 1011
Pisani, G. B., Izzo, L., Ruffini, R., et al. 2013, A&A, 552, L5
Rees, M., Ruffini, R., & Wheeler, J. A. 1974, Black Holes, Gravitational Waves and Cosmology (New York: Gordon and Breach)
Rhoades, C. E., & Ruffini, R. 1974, PhRvL, 32, 324
Rueda, J. A., & Ruffini, R. 2012, ApJL, 758, L7
Ruffini, R. 2015a, in 13th Marcel Grossmann Meeting, Recent Developments in Theoretical and Experimental General Relativity, Astrophysics and Relativistic Field Theories, ed. K. Rosquist (Singapore: World Scientific)
Ruffini, R. 2015b, ARep, 59, 591
Ruffini, R., Bernardini, M. G., Bianco, C. L., et al. 2006, in 10th Marcel Grossmann Meeting, ed. M. Novello, S. Perez Bergliaffa, & R. Ruffini (Singapore: World Scientific), 369
Ruffini, R., Bernardini, M. G., Bianco, C. L., et al. 2008, in 11th Marcel Grossmann Meeting, Recent Developments in Theoretical and Experimental General Relativity, Gravitation and Relativistic Field Theories, ed. H. Kleinert, R. T. Jantzen, & R. Ruffini (Singapore: World Scientific), 368
Ruffini, R., Rueda, J. A., Muccino, M., et al. 2016, arXiv:1602.02732
Ruffini, R., Wang, Y., Enderli, M., et al. 2015, ApJ, 798, 10
Ruffini, R., & Wilson, J. 1973, PhRvL, 31, 1362
Salam, A. 1968, Elementary Particle Physics (Stockholm: Almqvist and Wiksells)
Sibgatullin, N. R., & Sunyaev, R. A. 2000, AstL, 26, 772
Stergioulas, N. 2003, LRR, 6, 3
Tanaka, M., Kawabata, K. S., Maeda, K., et al. 2009, ApJ, 699, 1119
Tanvir, N. R., Levan, A. J., Fruchter, A. S., et al. 2013, Natur, 500, 547
Taubenberger, S., Valenti, S., Benetti, S., et al. 2009, MNRAS, 397, 677
Tubbs, D. L., & Schramm, D. N. 1975, ApJ, 201, 467
Weinberg, S. 1967, PhRvL, 19, 1264
Wong, T.-W., Fryer, C. L., Ellinger, C. I., Rockefeller, G., & Kalogera, V. 2014, arXiv:1401.3032
Woosley, S. E., Heger, A., & Weaver, T. A. 2002, RvMP, 74, 1015
Yakovlev, D. G., Kaminker, A. D., Gnedin, O. Y., & Haensel, P. 2001, PhR, 354, 1
Zel'dovich, Y. B., Ivanova, L. N., & Nadezhin, D. K. 1972, SvA, 16, 209

The Astrophysical Journal, 833:159 (12pp), 2016 December 20 doi:10.3847/1538-4357/833/2/159

ON THE UNIVERSAL LATE X-RAY EMISSION OF BINARY-DRIVEN HYPERNOVAE AND ITS POSSIBLE COLLIMATION

G. B. Pisani[1,2], R. Ruffini[1,2,3,4], Y. Aimuratov[1,3], C. L. Bianco[1,2], M. Kovacevic[1,3], R. Moradi[1,2], M. Muccino[1,2], A. V. Penacchioni[5,6], J. A. Rueda[1,2,4], S. Shakeri[2,7], and Y. Wang[1,2]
[1] Dipartimento di Fisica, Sapienza Università di Roma and ICRA, Piazzale Aldo Moro 5, I-00185 Roma, Italy
[2] ICRANet, Piazza della Repubblica 10, I-65122 Pescara, Italy
[3] Université de Nice Sophia-Antipolis, Grand Château Parc Valrose, Nice, CEDEX 2, France
[4] CRANet-Rio, Centro Brasileiro de Pesquisas Fisicas, Rua Dr. Xavier Sigaud 150, Rio de Janeiro, RJ, 22290-180, Brazil
[5] University of Siena, Department of Physical Sciences, Earth and Environment, Via Roma 56, I-53100 Siena, Italy
[6] ASI Science Data Center, via del Politecnico s.n.c., I-00133 Rome, Italy
[7] Department of Physics, Isfahan University of Technology, Isfahan 84156-83111, Iran
Received 2016 August 5; revised 2016 October 4; accepted 2016 October 12; published 2016 December 14

ABSTRACT

It has previously been discovered that there is a universal power-law behavior exhibited by the late X-ray emission (LXRE) of a "golden sample" of six long energetic GRBs, when observed in the rest frame of the source. This remarkable feature, independent of the different isotropic energy ($E_{\rm iso}$) of each GRB, has been used to estimate the cosmological redshift of some long GRBs. This analysis is extended here to a new class of 161 long GRBs, all with $E_{\rm iso} > 10^{52}$ erg. These GRBs are indicated as binary-driven hypernovae (BdHNe) in view of their progenitors: a tight binary system composed of a carbon–oxygen core ($\rm CO_{core}$) and a neutron star undergoing an induced gravitational collapse (IGC) to a black hole triggered by the $\rm CO_{core}$ explosion as a supernova (SN). We confirm the universal behavior of the LXRE for the "enlarged sample" (ES) of 161 BdHNe observed up to the end of 2015, assuming a double-cone emitting region. We obtain a distribution of half-opening angles peaking at $\theta = 17.62°$, with a mean value of 30.05°, and a standard deviation of 19.65°. This, in turn, leads to the possible establishment of a new cosmological candle. Within the IGC model, such universal LXRE behavior is only indirectly related to the GRB and originates from the SN ejecta, of a standard constant mass, being shocked by the GRB emission. The fulfillment of the universal relation in the LXRE and its independence of the prompt emission, further confirmed in this article, establishes a crucial test for any viable GRB model.

Key words: binaries: general – gamma-ray burst: general – stars: neutron – supernovae: general

1. INTRODUCTION

The initial observations by the BATSE instrument on board the Compton γ-ray Observatory satellite have evidenced what has later become known as the prompt radiation of GRBs. On the basis of their hardness as well as their duration, GRBs were initially classified into short and long at a time when their cosmological nature was still being disputed (Dezalay et al. 1992, pp. 161–168; Klebesadel 1992; Kouveliotou et al. 1993; Mazets et al. 1981; Tavani 1998).

The advent of the *BeppoSAX* satellite (Boella et al. 1997) introduced a novel approach to GRBs by introducing joint observations in the X-rays and γ-rays thanks to its instruments: the Gamma-ray Burst Monitor (40–700 keV), the Wide Field Cameras (2–26 keV), and the Narrow Field Instruments (2 −10 keV). The unexpected and welcome discovery of the existence of a well separate component in the GRB soon appeared: the afterglow radiation lasting up to 10^5–10^6 s after the emission of the prompt radiation (see Costa et al. 1997b, 1997a; Frontera et al. 1998, 2000; de Pasquale et al. 2006). Beppo-SAX clearly indicated the existence of a power-law behavior in the late X-ray emission (LXRE; see Figure 1).

The coming of the *Swift* satellite (Gehrels et al. 2004; Evans et al. 2007, 2010), significantly extending the observation in the X-ray band thanks to its X-ray Telescope (XRT band: 0.3–10 keV), has allowed us for the first time to cover the unexplored region between the end of the prompt radiation and the power-law late X-ray behavior discovered by *BeppoSAX*: in some long GRBs a steep decay phase was observed followed by a plateau leading then to a typical LXRE power-law behavior (Evans et al. 2007, 2010).

Already, Pisani et al. (2013) noticed the unexpected result that the LXREs of a "golden sample" (GS) of six long, closeby ($z \lesssim 1$), energetic ($E_{\rm iso} > 10^{52}$ erg) GRBs, when measured in the rest-frame of the sources, were showing a common power-law behavior (see Figure 2), independently from the isotropic energy $E_{\rm iso}$ coming from the prompt radiation (see Figure 3). More surprising was the fact that the plateau phase luminosity and duration before merging in the common LXRE power-law behavior were clearly functions of the $E_{\rm iso}$ (see Figure 3, and Ruffini et al. 2014c), while the late power law remains independent from the energetic of the prompt radiation (see Figures 2–3, and Pisani et al. 2013; Ruffini et al. 2014c). For this reason, this remarkable scaling law has been used as a standard candle to independently estimate the cosmological redshift of some long GRBs by requiring the overlap of their LXRE (see, e.g., Penacchioni et al. 2012, 2013; Ruffini et al. 2013b, 2013c, 2014a), and also to predict, 10 days in advance, the emergence of the typical optical signature of the supernova SN 2013cq, associated with GRB 130427A (de Ugarte Postigo et al. 2013; Levan et al. 2013; Ruffini et al. 2015, 2013a).

The current analysis is based on the paradigms introduced in Ruffini et al. (2001a) for the spacetime parametrization of the GRBs, in Ruffini et al. (2001b) for the interpretation of the structure of the GRB prompt emission, and in Ruffini et al. (2001c) for the induced gravitational collapse (IGC) process, further evolved in Ruffini et al. (2007), Rueda & Ruffini

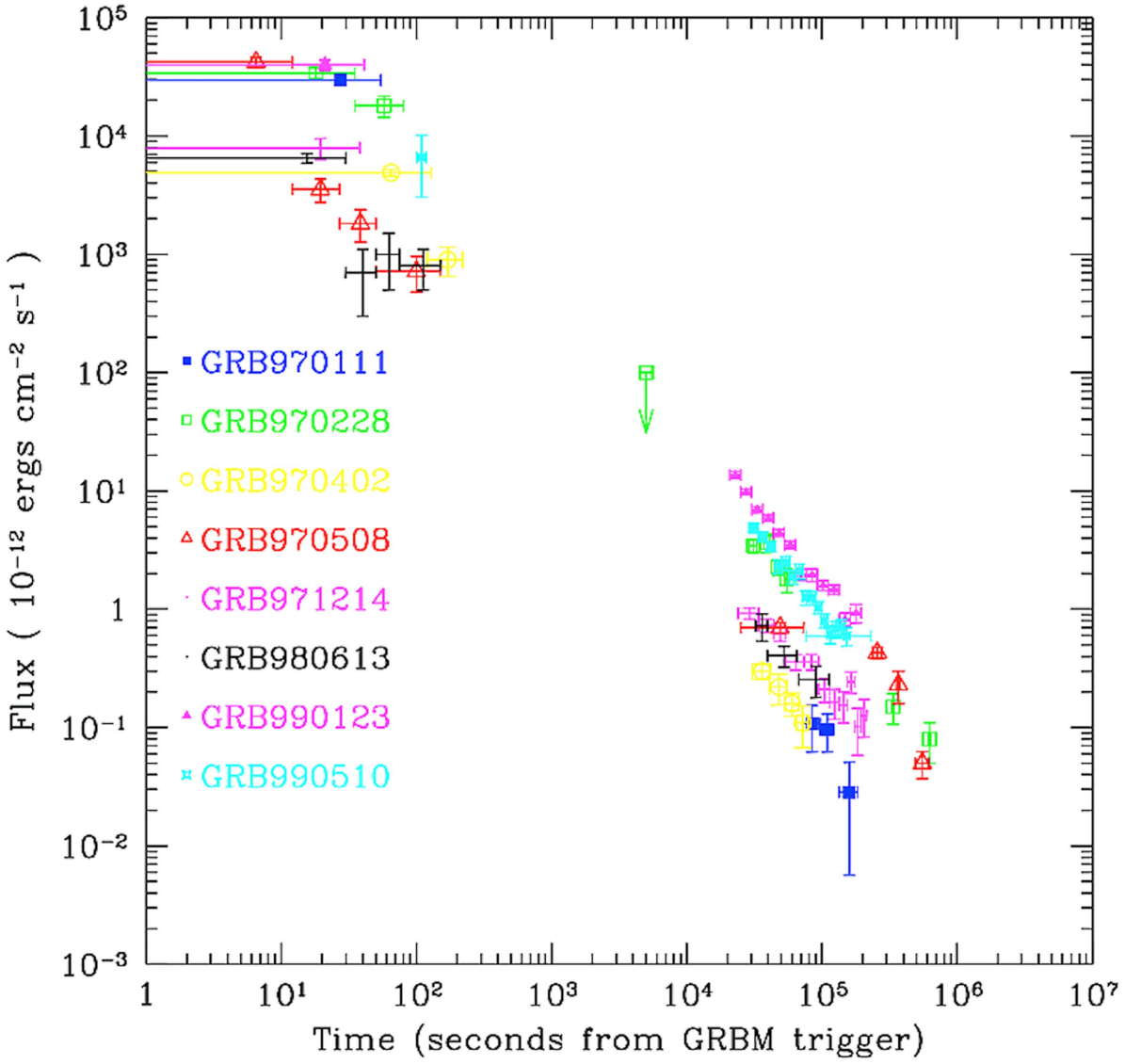

Figure 1. Collection of X-ray afterglow light curves observed by the Italian–Dutch satellite *BeppoSAX*.

(2012), Fryer et al. (2014), and Ruffini et al. (2016). In the present case, the phenomenon points to an IGC occurring when a tight binary system composed of a carbon–oxygen core (CO_{core}) undergoes a supernova (SN) explosion in the presence of a binary NS companion (Ruffini et al. 2001b, 2007; Izzo et al. 2012a; Rueda & Ruffini 2012; Fryer et al. 2014; Ruffini et al. 2015). When the IGC leads the NS to accrete enough matter and therefore to collapse to a black hole (BH), the overall observed phenomenon is called binary-driven hypernova (BdHN; Fryer et al. 2014; Ruffini et al. 2015, 2016).

A crucial further step has been the identification as a BdHN of GRB 090423 (Ruffini et al. 2014b) at the extreme redshift of $z = 8.2$ (Salvaterra et al. 2009; Tanvir et al. 2009). On top of that, the LXRE of GRB 090423 overlaps perfectly with the ones of the GS (see Figure 4), extending such a scaling law up to extreme cosmological distances. This result led to the necessity of checking such an universal behavior of the LXREs in BdHNe at redshifts larger than $z \sim 1$ (see the sample list in Table 2).

It is clear by now that the afterglow analysis is much more articulated than previously expected and contains new specific signatures. When theoretically examined within our framework, these new signatures lead to specific information on the astrophysical nature of the progenitor systems (Ruffini et al. 2016). In the present paper, we start by analyzing the signatures contained in the LXREs at $t_{rf} \gtrsim 10^4$ s, where t_{rf} is the rest-frame time after the initial GRB trigger. In particular, we probe a further improvement for the existence of such an LXRE universal behavior of BdHNe by the introduction of a collimation correction.

In Section 2, we present an "enlarged sample" (ES) of 161 BdHNe observed up to the end of 2015. In particular, we express for each BdHN: (1) redshift; (2) E_{iso}; and (3) the LXRE power-law properties. We probe the universality of the LXRE power-law behavior as well as the absence of correlation with the prompt radiation phase of the GRB. In Section 3, we introduce the collimation correction for the LXRE of BdHNe. This, in turn, will aim to the possible establishment of a new cosmological candle, up to $z \gtrsim 8$. In Section 4, we present the

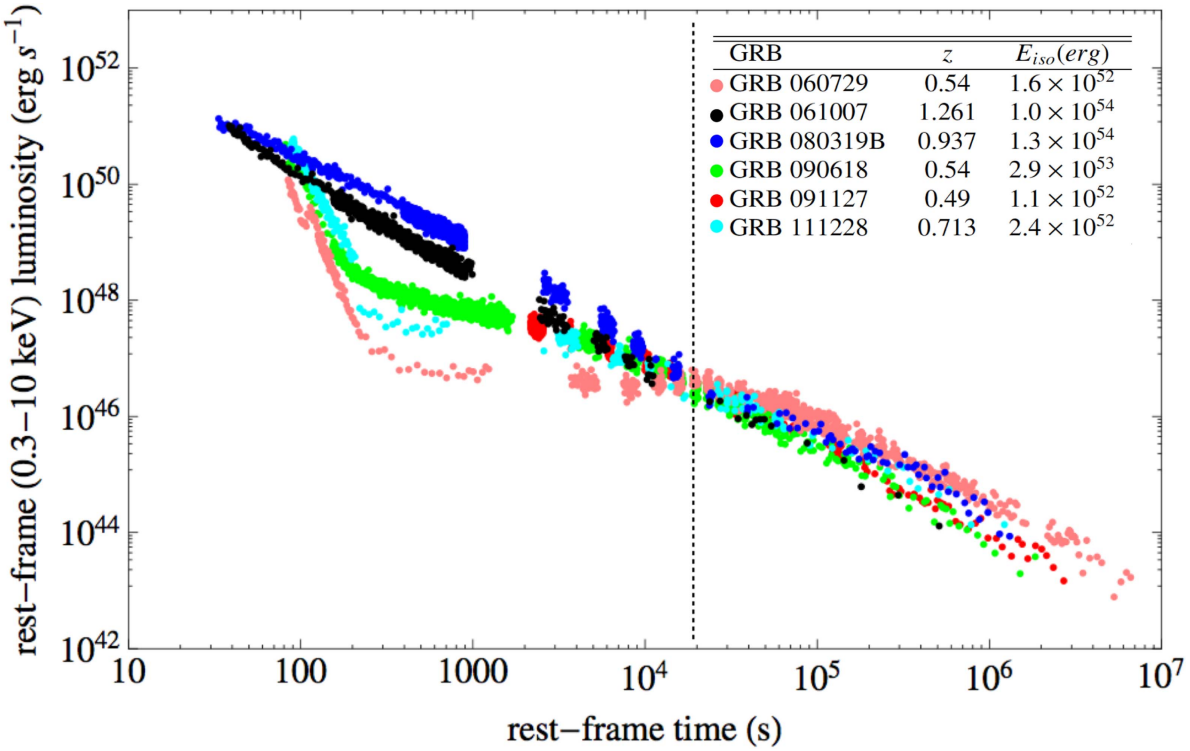

Figure 2. Scaling law found in the isotropic X-ray late times luminosity within the GS by Pisani et al. (2013). Despite the different early behavior, the different light curves join all together the same power law after a rest-frame time of $t_{rf} \sim 2 \times 10^4$ s.

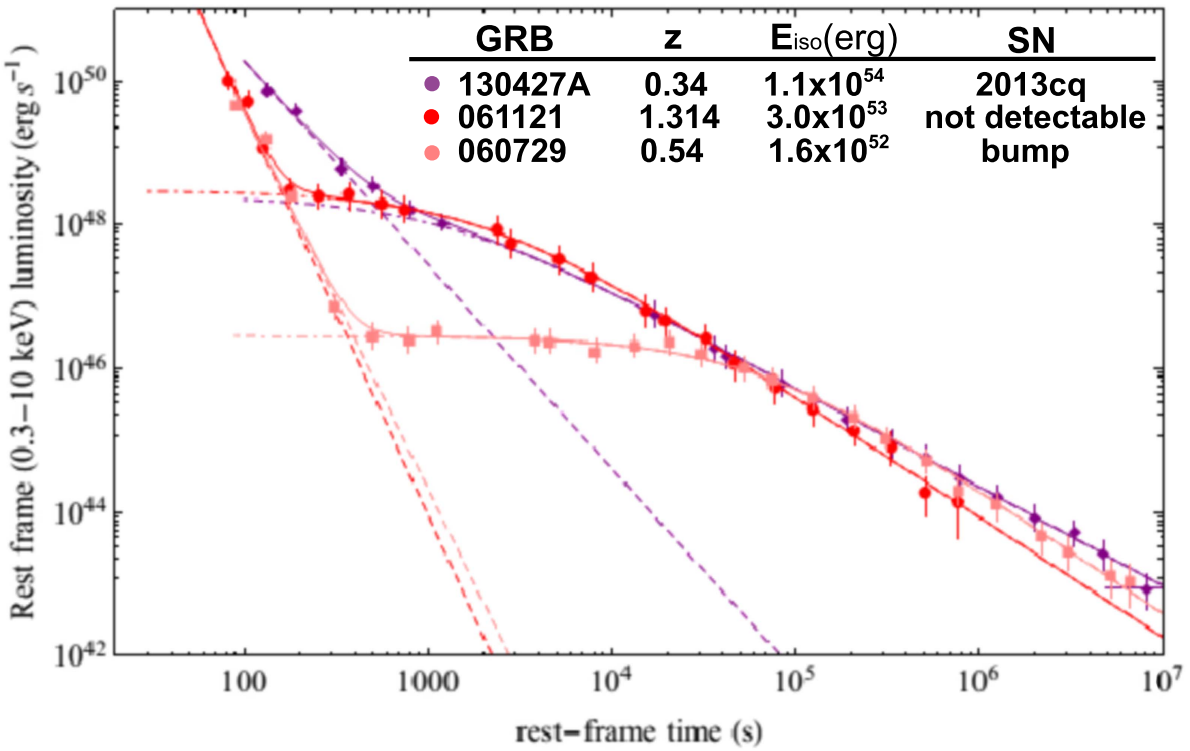

Figure 3. Nested structure of the isotropic X-ray luminosity of the BdHNe. This includes the previously mentioned scaling law of the late power-law and leads to an inverse proportionality between the luminosity of the plateau and the rest-frame time delimiting its end and the beginning of the late power-law decay Ruffini et al. (2014c).

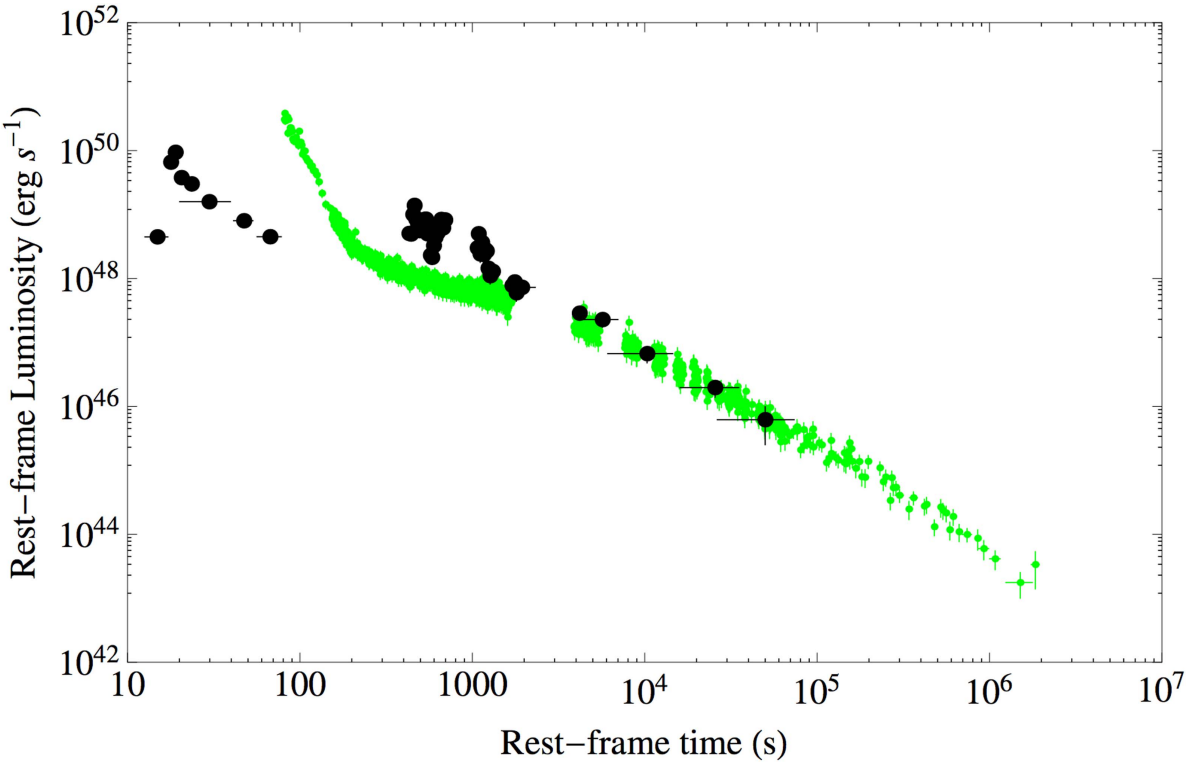

Figure 4. X-ray luminosity of GRB 090423 (black points) compared with the one of GRB 090618 (green points), the prototype BdHN, by Ruffini et al. (2014b).

inferences for the understading of the afterglow structure, and, in Section 5, we draw our conclusions.

2. THE BDHNE ENLARGED SAMPLE

We have built a new sample of BdHNe, which we name "enlarged sample" (ES), under the following selection criteria:

1. measured redshift z;
2. GRB rest-frame duration larger than 2 s;
3. isotropic energy $E_{\rm iso}$ larger than 10^{52} erg; and
4. presence of associated *Swift*/XRT data lasting at least up to $t_{\rm rf} = 10^4$ s.

We collected 161 sources, which satisfy our criteria, covering 11 years of *Swift*/XRT observations, up to the end of 2015, see Table 2. The $E_{\rm iso}$ of each source has been estimated using the measured redshift z together with the best-fit parameters of the γ-ray spectrum published in the GCN circular archive.[8] The majority of the ES sources, 102 out of 161, have γ-ray data provided by *Fermi*/GBM and Konus-WIND, which, with their typical energy bands being 10–1000 keV and 20–2000 keV, respectively, lead to a reliable estimate of the $E_{\rm iso}$, computed in the "bolometric" 1–10^4 keV band (Bloom et al. 2001). The remaining sources of the ES have had their γ-ray emission observed by *Swift*/BAT only, with the sole exception of one source observed by *HETE*. The energy bands of these last two detectors, being 15–150 keV and 8–400 keV, respectively, lead to a standard estimate of $E_{\rm iso}$ by extrapolation in the "bolometric" 1–10^4 keV band (Bloom et al. 2001).

We compare the *Swift*/XRT isotropic luminosity light curve $L_{\rm rf}^{\rm iso}$ for 161 GRBs of the ES in the common rest-frame energy range of 0.3–10 keV. We initially convert the observed *Swift*/XRT flux $f_{\rm obs}$ as if it had been observed in the 0.3–10 keV rest-frame energy range. In the detector frame, the 0.3–10 keV rest-frame energy range becomes $[0.3/(1+z)]$–$[10/(1+z)]$ keV, where z is the redshift of the GRB. We assume a simple power-law function as the best fit for the spectral energy distribution of the *Swift*/XRT data[9]:

$$\frac{dN}{dA\ dt\ dE} \propto E^{-\gamma}. \tag{1}$$

Therefore, we can compute the flux light curve in the 0.3–10 keV rest-frame energy range, $f_{\rm rf}$, multiplying the observed one, $f_{\rm obs}$, by the k-correction factor:

$$f_{\rm rf} = f_{\rm obs} \frac{\int_{\frac{0.3\ {\rm keV}}{1+z}}^{\frac{10\ {\rm keV}}{1+z}} E^{1-\gamma} dE}{\int_{0.3\ {\rm keV}}^{10\ {\rm keV}} E^{1-\gamma} dE} = f_{\rm obs}\,(1+z)^{\gamma-2}. \tag{2}$$

Then, to compute the isotropic X-ray luminosity $L_{\rm iso}$, we have to multiply $f_{\rm rf}$ by the spherical surface having the luminosity distance as radius

$$L_{\rm iso} = 4\,\pi\,d_l^2(z) f_{\rm rf}\,, \tag{3}$$

where we assume a standard cosmological ΛCDM model with $\Omega_m = 0.27$ and $\Omega_\Lambda = 0.73$. Finally, we convert the observed

[8] http://gcn.gsfc.nasa.gov/gcn3_archive.html

[9] http://www.swift.ac.uk/

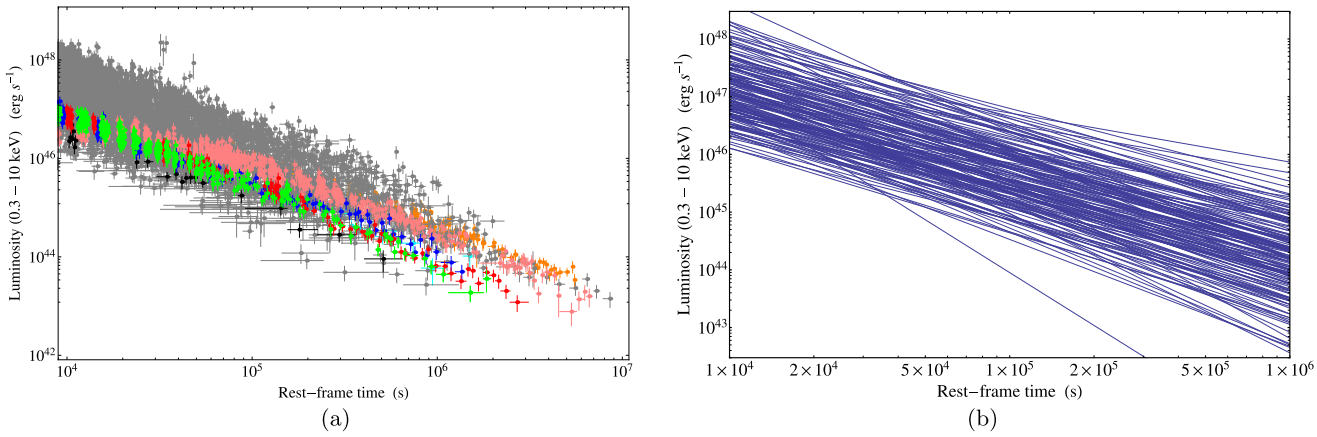

Figure 5. Panel (a): LXRE luminosity light curves of all 161 sources of the ES (gray) compared with the ones of the GS: GRB 060729 (pink), GRB 061007 (black), GRB 080913B (blue), GRB 090618 (green), GRB 091127 (red), and GRB 111228 (cyan), plus GRB 130427A (orange; Pisani et al. 2013; Ruffini et al. 2015). Panel (b): power laws that best fit the luminosity light curves of the X-ray emissions of all 161 sources of the ES.

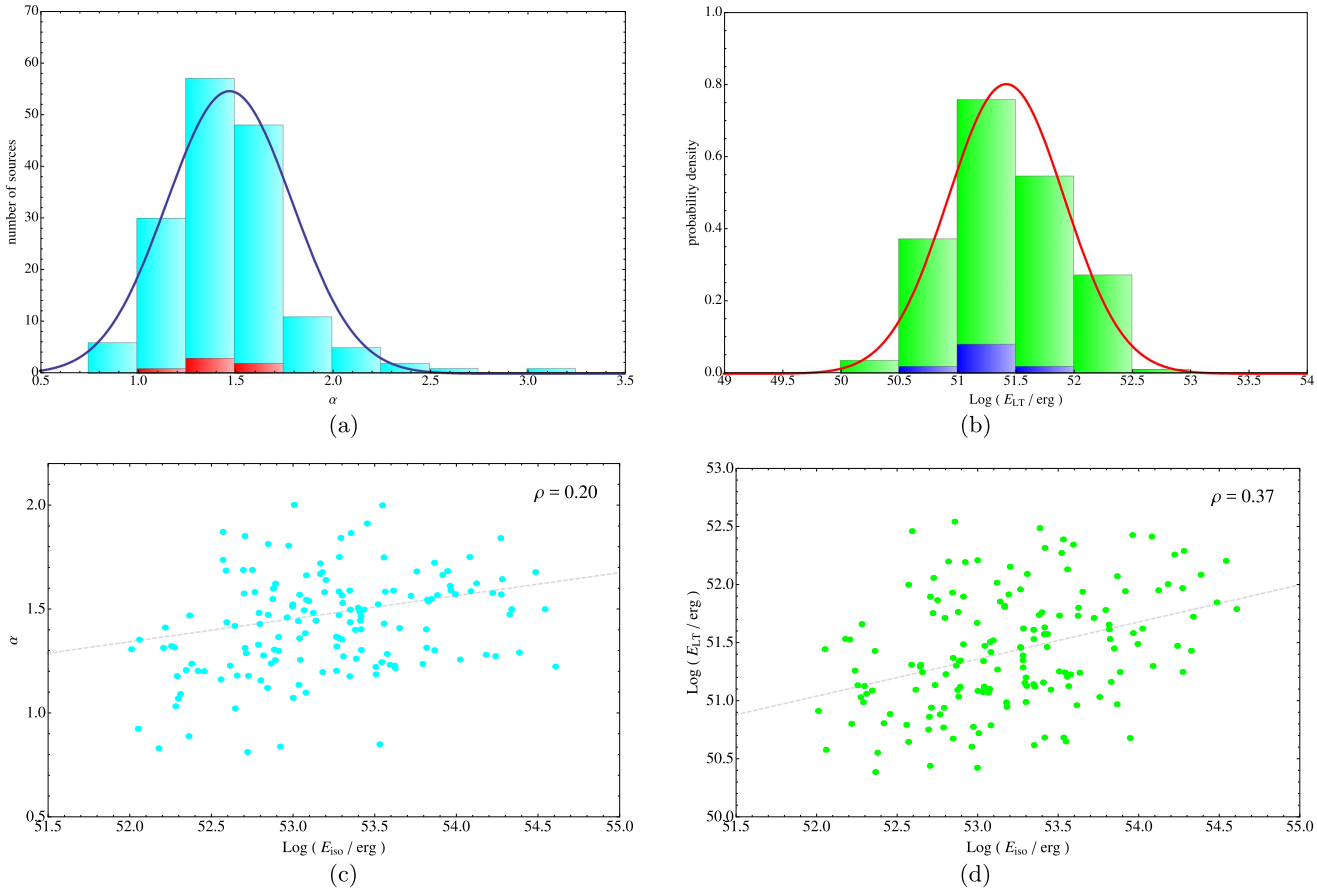

Figure 6. Panel (a): distribution of the LXRE power-law indexes α within the ES (cyan) compared to one of the GS (red). Such a distribution Gaussian behavior (blue line) with a mean value of $\mu_\alpha = 1.48$ and a standard deviation of $\sigma_\alpha = 0.32$ follows. Panel (b): probability distribution of the LXRE integrated energies within the time interval 10^4–10^6 s in the rest-frame after the initial GRB trigger for all the sources of the ES (in green) compared with the GS (in blue). The solid red line represents the Gaussian function, which best fits the ES data in logarithmic scale. Its mean value is $\mu_{\mathrm{Log}_{10}(E_{LT})} = 51.40$, while its standard deviation is $\sigma_{\mathrm{Log}_{10}(E_{LT})} = 0.47$. Panel (c): scatter plot of α vs. E_{iso} (cyan points) in logaritcmic scale. The dashed gray line is the best linear fit on such points. If we look at the correlation coefficient of these data points, $\rho = 0.20$, we conclude that there is no evidence for correlation between the two quantities. Panel (d): scatter plot of E_{LT} vs. E_{iso} (green points) in logaritcmic scale. The dashed gray line is the best linear fit on such points. If we look at the correlation coefficient of these data points, $\rho = 0.37$, we conclude that there is no evidence for correlation between the two quantities.

times into rest-frame times $t_{\rm rf}$:

$$t_{\rm rf} = \frac{t_{\rm obs}}{1+z}. \quad (4)$$

We then fit the whole isotropic luminosity light-curve late phase with a decaying power-law function defined as:

$$L_{\rm iso}(t_{\rm rf}) = L_0\, {t_{\rm rf}}^{-\alpha}, \quad (5)$$

where α, the power-law index, is a positive number, and L_0 is the luminosity at an arbitrary time $t_{\rm rf} = t_0$ after the GRB trigger in the rest-frame of the source. All the power laws are shown in Figure 5(b). Figure 6(a) shows the distribution of the α indexes within the ES. Such a distribution follows a Gaussian behavior with a mean value of $\mu_\alpha = 1.48$ and a standard deviation of $\sigma_\alpha = 0.32$ follows. The LXRE luminosity light curves of the ES in the 0.3–10 keV rest-frame energy band are plotted in Figure 5(a), compared to the curves of the GS. Figure 5(a) shows that the power laws within the ES span around two orders of magnitude in luminosity. The spread of the LXRE light curves in the ES is better displayed by Figure 6(b), which shows the distribution within the ES of the LXRE integrated energies $E_{\rm LT}$ defined as:

$$E_{\rm LT} \equiv \int_{10^4\ {\rm s}}^{10^6\ {\rm s}} L_{\rm iso}(t_{\rm rf})\, dt_{\rm rf}. \quad (6)$$

We choose to represent the spread of the LXRE luminosity light curves with the late integrated energy $E_{\rm LT}$ at late times ($t_{\rm rf} = 10^4$–10^6 s) instead of the luminosity $L_{\rm iso}$ at a particular time for two reasons: (1) there is no evidence for a particular time in which to compute $L_{\rm iso}$ and (2) we want to have a measurement of the spread as independent as possible from the slopes, whose dispersion causes the mixing of part of the light curves over time (see Figure 5(b)). The integration time interval $t_{\rm rf} = 10^4$–10^6 reasonably contains most of the data in the late power-law behavior. In fact, the lower limit $t_{\rm rf} = 10^4$ s is basically the average of the initial time for our linear fits on the data (more precisely $t_{\rm rf}^{\rm start} = 9167.13$ s), while the upper limit $t_{\rm rf} = 10^6$ has been chosen because only 14% of the ES have X-ray data over such rest-frame time.

The solid red line in Figure 6(b) represents the Gaussian function that best fits the late integrated energies $E_{\rm LT}$ in logarithmic scale. Its mean value is $\mu_{{\rm Log}_{10}(E_{\rm LT})} = 51.40$, while its standard deviation is $\sigma_{{\rm Log}_{10}(E_{\rm LT})} = 0.47$.

The LXRE power-law spread, given roughly by $2\sigma_{{\rm Log}_{10}(E_{\rm LT})} = 0.94$, is larger in respect to the previous work of Pisani et al. (2013), which results as $2\sigma_{{\rm Log}_{10}(E_{\rm LT})} = 0.56$. This is clearly due to the significant growth of the number of BdHNe composing the ES (161) in respect to the ones of the GS (6).

Furthermore, Figures 6(c)–(d) show the scatter plots of the values of α and $E_{\rm LT}$, respectively, versus the values of the $E_{\rm iso}$ for all the sources of the ES. In both cases the correlation factors, $\rho = 0.20$ and $\rho = 0.37$, respectively, are low, confirming that there is no evidence for a correlation between the LXRE power-law behavior and the isotropic energy emitted by the source during the prompt radiation.

These results address a different aspect than the ones by Margutti et al. (2013). There, the authors, after correctly noticing the difficulties of the traditional afterglow model (Meszaros & Rees 1997; Sari et al. 1998), attempt to find a model-independent correlation between the X-ray light curve observed in both short and long GRBs with their prompt emission. In their work, Margutti et al. (2013) have considered the integrated X-ray emission over the entire light curve observed by XRT, following ~300 s after the GRB trigger both for short and long GRBs. Such an emission is clearly dominated by the contribution at $t_{\rm rf} < 10^4$ s, where a dependence from the $E_{\rm iso}$ is self-evident from the above Figures 2 and 3. Our approach instead solely applies to the BdHNe: (1) long GRBs, and (2) $E_{\rm iso} > 10^{52}$ erg. This restricts the possible sources in the Margutti et al. (2013) sample to 70 GRBs: in the present article, we consider a larger sample of 161 BdHNe. Moreover, (3) our temporal window starts at $t_{\rm rf} \gtrsim 10^4$ s. Under these three conditions, our result of the universal LXRE behavior has been found.

3. COLLIMATION

We here propose reducing the spread of the LXRE power-laws within the ES by introducing a collimation effect in the emission process. In fact, if the emission is not isotropic, Figures 5(a)–(b) should actually show overestimations of the intrinsic LXRE luminosities. By introducing a collimation effect, namely assuming that the LXREs are not emitted isotropically but within a double-cone region having half-opening angle θ, we can convert the isotropic $L_{\rm iso}(t_{\rm rf})$ to the intrinsic LXRE luminosity $L^{\rm intr}(t_{\rm rf})$ as:

$$L^{\rm intr}(t_{\rm rf}) = L_{\rm iso}(t_{\rm rf})\,(1-\cos\theta). \quad (7)$$

From Equation (7), an angle θ can be inferred for each source of the ES if an intrinsec universal LXRE light curve $L^{\rm intr}(t_{\rm rf})$ is assumed. For example, assuming an intrinsic standard luminosity $L_0^{\rm intr}$, at an arbitrary time $t_{\rm rf} = t_0$, Equation (7) becomes $L_0^{\rm intr} = L_0\,(1-\cos\theta)$, which, in principle, could be used to infer θ for each source. On the other hand, for the same reasons expressed in the previous section, we choose to estimate the angles θ using the LXRE integrated energy $E_{\rm LT}$ instead of the $L_{\rm iso}$ at a particular time. Therefore, we simply integrate Equation (7) in the rest-frame time interval 10^4–10^6 s:

$$\int_{10^4\ {\rm s}}^{10^6\ {\rm s}} L_{\rm intr}(t_{\rm rf})\, dt_{\rm rf} = \int_{10^4\ {\rm s}}^{10^6\ {\rm s}} L_{\rm iso}(t_{\rm rf})\,(1-\cos\theta)\, dt_{\rm rf}, \quad (8)$$

obtaining, consequentially

$$E_{\rm LT}^{\rm intr} = E_{\rm LT}\,(1-\cos\theta). \quad (9)$$

By assuming a universal $E_{\rm LT}^{\rm intr}$ for all BdHNe, it is possible to infer θ for each source of the ES. We assume GRB 050525A, having the lowest $E_{\rm LT}$ within the ES, as our unique "isotropic" source, namely, in which we can impose $E_{\rm LT}^{\rm intr} = E_{\rm LT}$, which automatically gives $\theta = 90°$, which means that the LXRE luminosity is emitted over all the isotropic sphere. On top of having the weakest LXRE over 11 years of *Swift*/XRT observations, GRB 050525A: (a) has been observed by Konus-WIND in the γ-rays (Golenetskii et al. 2005), then its $E_{\rm iso}$ estimate is reliable; (b) has a reliable late X-ray slope given by a complete *Swift*/XRT light curve (showing a late power-law behavior from 4000 to 7×10^5 s in the rest frame); (c) has an associated supernova (Della Valle et al. 2006a, 2006b). An instrumental selection effect cannot affect this choice since *Swift*/XRT can easily detect and follow X-ray emissions weaker than that of GRB 050525A. Some examples are the two X-ray luminosity light curves shown of GRB 060218 and GRB 101219B in Figure 8(a). Furthermore, in the case of a future observation of a BdHN

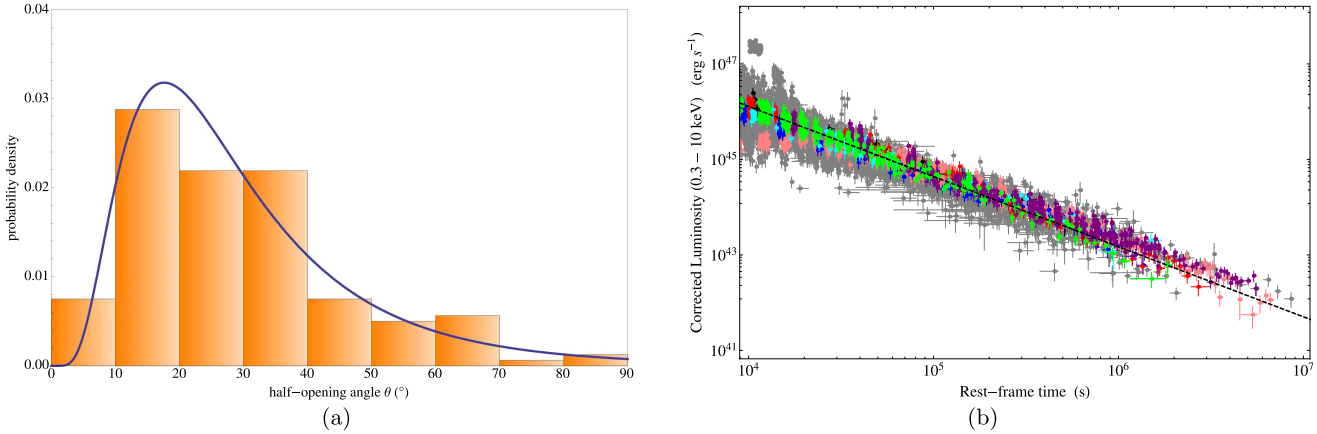

Figure 7. Left panel (a): probability distribution of the half-opening angle θ within the ES. The blue solid line represents a logarithmic normal distribution, which best fits the data. This distribution has a mode of $\mathrm{Mo}_\theta = 17.62°$, a mean of $\mu_\theta = 30.05°$, a median of $\mathrm{Me}_\theta = 25.15°$, and a standard deviation of $\sigma_\theta = 19.65°$. Right panel (b): corrected LXRE luminosity light curves of all 161 sources of the ES (gray) compared to the ones of the GS: GRB 060729 (pink), GRB 061007 (black), GRB 080913B (blue), GRB 090618 (green), GRB 091127 (red), and GRB 111228 (cyan), plus GRB 130427A (purple; Pisani et al. 2013; Ruffini et al. 2015). The black dotted line represents the universal LXRE power law, namely the linear fit of the late emission of GRB 050525A.

showing a E_{LT} weaker than the one of GRB 050525A, a renormalization of the angle distribution of Figure 7(a) down to lower angle values with respect to the new minimum one would be required, leaving the overall angle distribution unaltered. All of these facts make GRB 050525A a robust "isotropic" BdHN candidate. With $E_{\mathrm{LT}}^{\mathrm{intr}} = E_{\mathrm{LT}}^{050525A} = 2.43 \times 10^{50}$ now fixed, a half-opening angle θ is inferred for each source of the ES using Equation (9). The values of θ are listed in Table 2. Figure 7(a) shows the probability distribution of the half-opening angle θ within the ES. The blue solid line represents a logarithmic normal distribution, which best fits the data. This distribution has a mode of $\mathrm{Mo}_\theta = 17.62°$, a mean of $\mu_\theta = 30.05°$, a median of $\mathrm{Me}_\theta = 25.15°$, and a standard deviation of $\sigma_\theta = 19.65°$. Moreover, it is possible to verify that, by correcting the $L_{\mathrm{rf}}^{\mathrm{iso}}$ light curve of each ES source for its corresponding θ, an overlap of the LXRE luminosity light curves as good as the one seen in the GS by Pisani et al. (2013) shown in Figure 2 is obtained. Since the LXRE follows a power-law behavior, we can quantify the tightness of the LXREs overlap looking at the correlation coefficient ρ between all the luminosity light-curve data points of the ES sources in a log–log scale. Considering the data points of the LXRE power laws within the 10^4–10^6 s time interval (where we have defined E_{LT}), we obtain $\rho = -0.94$ for the GS, $\rho = -0.84$ for the ES before the collimation correction, and $\rho = -0.97$ after the correction. Therefore, the collimation correction not only reduces the spread of the LXREs within the ES, but makes the LXREs overlap even tighter than the one previously found in the GS.

Finally, in order to test the robustness of our results, we do the same analysis excluding, by the ES, the sources seen only by *Swift*/BAT or *HETE* and not by *Fermi*/GBM or Konus-WIND, under the hypothesis that their E_{iso} estimates are unreliable. The results obtained using this new sample called ES2, namely the typical value and the dispersion of α, E_{LT}, and θ are summarized in Table 1. There is no significant difference between the results obtained from the two samples. Therefore, we conclude that a possible wrong estimate of E_{iso} for the sources observed by only *Swift*/BAT or *HETE* and not by *Fermi*/GBM or Konus-WIND does not bias our results.

Table 1
Summary of the Results of This Work Obtained By the Complete ES Sample in Comparison with the Ones Arising Using the Sample ES2, Namely the ES Deprived By the Sources Seen by *Swift*/BAT or *HETE* Only

Sample	ES	ES2
Sources Number	161	102
α	1.48 ± 0.32	1.45 ± 0.24
$\mathrm{Log}_{10}(E_{\mathrm{LT}}/\mathrm{erg})$	51.40 ± 0.47	51.47 ± 0.48
θ (°)	30.05 ± 19.65	28.26 ± 17.85
θ mode (°)	17.62	17.08
θ median (°)	25.15	23.90

4. INFERENCES FOR THE UNDERSTANDING OF THE X-RAY AFTERGLOW STRUCTURE

In the last 25 years we have seen in the GRB community a dominance of the fireball model, which sees the GRB as a single astrophysical system, the "Collapsar," originating from an ultra-relativistic jetted emission described by the synchrotron/self-synchrotron Compton (SSC) and traditional afterglow models (see, e.g., Rees & Meszaros 1992; Woosley 1993; Piran 2005; Gehrels et al. 2009; Kumar & Zhang 2015, and references therein). Such methods have been systematically adopted to different types of GRBs like, for example, the short, hard GRB 090510 (Ackermann et al. 2010), the high energetic long GRB 130427A (Perley et al. 2014), the low energetic short GRB 051221A (Soderberg et al. 2006a), and the low energetic long GRB 060218 (Campana et al. 2006; Soderberg et al. 2006b), independently from the nature of their progenitors.

In the recent four years, substantial differences among seven distinct kinds of GRBs have been indicated, presenting different spectral and photometrical properties on different timescales (Ruffini et al. 2016). The discovery of several long GRBs showing multiple components and evidencing the presence of a precise sequence of different astrophysical processes during the GRB phenomenon (e.g., Izzo et al. 2012b; Penacchioni et al. 2012), led to the introduction of a novel paradigm expliciting the role of binary sources as progenitors of the long GRB-SN connection. This has led to the formulation of the IGC paradigm (Ruffini et al. 2001b, 2007,

Table 2
List of the the ES of BdHNe Considered in this Work

GRB	z	α	$E_{\rm LT}$[a]	θ (°)	$E_{\rm iso}$[b]	Instrument[c]	GCN
050315A	1.95	0.838	15.6	10.1	8.32	*Swift*	3099
050318A	1.44	1.74	0.442	63.3	3.70	*Swift*	3134
050319A	3.24	1.27	12.3	11.4	20.2	*Swift*	3119
050401A	2.9	1.59	3.82	20.6	92.0	KW	3179
050408A	1.24	1.14	2.19	27.2	10.8	*HETE*	3188
050505A	4.27	1.41	8.66	13.6	44.6	*Swift*	3364
050525A	0.606	1.47	0.243	90.0	2.31	KW	3474
050730A	3.97	2.42	1.74	30.7	42.8	*Swift*	3715
050802A	1.71	1.55	1.24	36.5	7.46	*Swift*	3737
050814A	5.3	2.23	2.90	23.6	26.8	*Swift*	3803
050820A	2.61	1.23	22.1	8.51	39.0	KW	3852
050922C	2.2	1.57	0.974	41.4	19.8	KW	4030
051109A	2.35	1.20	9.09	13.3	18.3	KW	4238
060108A	2.03	0.830	3.40	21.8	1.50	*Swift*	4445
060115A	3.53	1.58	2.23	27.0	19.0	*Swift*	4518
060124A	2.296	1.30	20.7	8.79	26.0	KW	4599
060202A	0.783	1.03	4.57	18.8	1.90	*Swift*	4635
060206A	4.05	1.44	28.8	7.45	3.90	*Swift*	4697
060210A	3.91	1.75	25.9	7.86	120.	*Swift*	4734
060418A	1.49	1.54	0.614	52.9	12.0	KW	4989
060502A	1.51	1.26	2.96	23.4	11.0	*Swift*	5053
060510B	4.9	1.54	3.39	21.8	66.0	*Swift*	5107
060512A	2.1	1.24	0.356	71.5	2.38	*Swift*	5124
060526A	3.21	2.27	1.36	34.7	5.40	*Swift*	5174
060605A	3.8	2.00	0.524	57.6	10.1	*Swift*	5231
060607A	3.082	3.04	0.481	60.4	34.0	*Swift*	5242
060707A	3.43	1.18	11.4	11.8	5.30	*Swift*	5289
060708A	1.92	1.21	1.22	36.8	2.20	*Swift*	5295
060714A	2.71	1.47	1.93	29.0	19.0	*Swift*	5334
060729A	0.54	1.31	3.36	21.9	1.60	*Swift*	5370
060814A	0.84	1.16	1.69	31.1	6.30	KW	5460
060906A	3.685	1.47	0.482	60.3	25.9	*Swift*	5534
061007A	1.261	1.68	0.477	60.6	88.0	KW	5722
061121A	1.314	1.50	3.75	20.7	27.0	KW	5837
061126A	1.159	1.30	3.06	23.0	8.10	*Swift*	5860
061222A	2.088	1.52	18.7	9.25	33.0	KW	5984
070110A	2.35	1.10	3.20	22.5	11.9	*Swift*	6007
070306A	1.5	1.58	8.22	14.0	15.5	*Swift*	6173
070318A	0.84	1.42	1.97	28.8	4.37	*Swift*	6212
070508A	0.82	1.60	1.08	39.1	7.57	KW	6403
070529A	2.5	1.22	1.79	30.2	31.9	*Swift*	6468
070802A	2.45	1.41	0.633	52.0	1.64	*Swift*	6699
071003A	1.6	1.75	1.61	31.9	35.8	KW	6849
080210A	2.64	1.38	1.26	36.2	11.8	*Swift*	7289
080310A	2.43	1.53	1.34	35.1	20.0	*Swift*	7402
080319B	0.94	1.59	1.99	28.6	122.	KW	7482
080319C	1.95	1.72	6.40	15.8	14.6	KW	7487
080605A	1.64	1.59	1.39	34.5	22.1	KW	7854
080607A	3.04	1.57	1.77	30.4	187.	KW	7862
080721A	2.6	1.62	8.93	13.4	132.	KW	7995
080804A	2.2	1.68	1.08	39.3	56.9	*Swift*	8067
080805A	1.51	1.07	1.21	36.9	9.96	*Swift*	8068
080810A	3.35	1.57	1.77	30.4	76.1	KW+Swift	8101
080905B	2.37	1.51	4.67	18.6	9.85	*Fermi*	8205
080916C	4.35	1.29	12.1	11.5	242.	*Fermi*	8278
080928A	1.69	1.69	0.564	55.3	4.93	*Fermi*	8316
081008A	1.97	1.80	0.596	53.7	9.34	*Swift*	8351
081028A	3.04	1.66	2.62	24.9	12.0	*Swift*	8428
081109A	0.98	1.32	1.07	39.4	1.87	*Fermi*	8505
081121A	2.51	1.51	5.77	16.7	24.9	*Fermi*	8546
081203A	2.1	2.00	0.446	63.0	35.1	*Swift*	8595
081221A	2.26	0.849	24.5	8.09	33.8	*Fermi*	8704
081222A	2.77	1.40	4.28	19.4	25.9	*Fermi*	8715
090102A	1.55	1.35	1.58	32.2	19.8	KW	8776

Table 2
(Continued)

GRB	z	α	$E_{\rm LT}$[a]	θ (°)	$E_{\rm iso}$[b]	Instrument[c]	GCN
090313A	3.38	2.72	10.4	12.4	13.1	*Swift*	8986
090328A	0.736	1.84	1.42	34.0	19.5	*Fermi*	9056
090418A	1.61	1.68	0.967	41.5	15.0	KW	9171
090423A	8.2	1.57	1.29	35.7	10.9	*Fermi*	9229
090424A	0.544	1.18	1.76	30.5	4.51	*Fermi*	9230
090516A	3.9	1.40	4.52	18.9	65.0	*Fermi*	9413
090618A	0.54	1.49	1.44	33.8	25.4	*Fermi*	9535
090715B	3.	1.18	4.08	19.9	22.1	KW	9679
090809A	2.74	1.57	0.727	48.3	4.98	*Swift*	9756
090812A	2.45	1.23	5.39	17.3	41.7	KW+*Swift*	9821
090902B	1.82	1.22	6.15	16.2	403.	*Fermi*	9866
090926A	2.11	1.50	5.29	17.4	217.	*Fermi*	9933
091003A	0.9	1.36	1.32	35.3	10.9	*Fermi*	9983
091020A	1.71	1.30	2.19	27.3	7.63	*Fermi*	10095
091029A	2.75	1.60	5.81	16.6	7.52	*Swift*	10103
091127A	0.49	1.32	1.36	34.9	1.79	*Fermi*	10204
091208B	1.06	1.09	1.15	38.0	2.03	*Fermi*	10266
100302A	4.81	0.812	5.67	16.8	5.24	*Swift*	10462
100425A	1.75	1.20	0.767	46.9	2.84	*Swift*	10685
100513A	4.77	1.44	3.74	20.8	25.7	*Swift*	10753
100621A	0.542	1.12	8.52	13.7	6.93	KW	10882
100814A	1.44	1.64	14.3	10.6	15.8	*Fermi*	11099
100901A	1.41	1.36	7.89	14.3	8.09	*Swift*	11169
100906A	1.73	1.87	1.32	35.3	22.5	*Fermi*	11248
110128A	2.339	1.16	0.620	52.6	3.60	*Fermi*	11628
110205A	2.22	1.59	0.913	42.8	41.0	KW	11659
110213A	1.46	1.81	2.33	26.4	7.00	*Fermi*	11727
110422A	1.77	1.24	6.03	16.3	62.0	KW	11971
110503A	1.613	1.36	2.45	25.7	19.0	KW	12008
110715A	0.82	1.69	7.33	14.8	5.60	KW	12166
110731A	2.83	1.22	6.31	16.0	42.0	*Fermi*	12221
110808A	1.348	1.33	0.588	54.1	6.10	*Swift*	12262
110918A	0.982	1.64	19.5	9.07	190.	KW	12362
111008A	4.9898	1.66	8.76	13.5	82.0	KW	12433
111123A	3.1516	1.55	2.82	24.0	70.0	*Swift*	12598
111209A	0.67	1.54	1.45	33.6	67.0	KW	12663
111228A	0.716	1.23	1.24	36.4	4.10	*Fermi*	12744
120119A	1.73	1.28	1.68	31.2	37.5	*Fermi*	12874
120326A	1.8	1.87	9.97	12.7	3.70	*Fermi*	13145
120327A	2.81	1.58	1.33	35.1	36.5	*Swift*	13137
120711A	1.41	1.58	18.1	9.40	166.	*Fermi*	13437
120712A	4.17	1.37	2.90	23.7	18.3	*Fermi*	13469
120909A	3.93	1.30	11.8	11.7	73.2	*Fermi*	13737
120922A	3.1	1.19	5.41	17.3	32.0	*Fermi*	13809
121024A	2.3	1.44	1.18	37.4	10.7	*Swift*	13899
121027A	1.77	1.28	15.8	10.1	6.55	*Swift*	13910
121128A	2.2	1.48	1.85	29.7	13.2	*Fermi*	14012
121217A	3	1.26	30.6	7.23	24.2	*Fermi*	14094
130418A	1.218	1.52	0.265	85.4	9.90	KW	14417
130420A	1.297	1.25	1.32	35.4	7.74	*Fermi*	14429
130427A	0.338	1.26	4.17	19.7	105.	*Fermi*	14473
130427B	2.78	1.85	0.275	83.4	5.04	*Swift*	14469
130505A	2.27	1.50	16.0	10.0	347.	KW	14575
130514A	3.6	1.56	5.16	17.7	52.4	KW+*Swift*	14702
130528A	1.25	1.02	2.03	28.3	4.40	*Fermi*	14729
130606A	5.91	1.91	1.24	36.4	28.3	KW	14808
130610A	2.092	1.47	0.472	61.0	6.99	*Fermi*	14858
130701A	1.155	1.20	0.639	51.7	2.60	KW	14958
130907A	1.238	1.68	7.02	15.1	304.	KW	15203
130925A	0.347	1.32	2.85	23.8	18.4	*Fermi*	15255
131030A	1.293	1.27	2.97	23.4	173.	KW	15413
131105A	1.686	1.24	1.75	30.6	34.7	*Fermi*	15455
131108A	2.4	1.72	0.932	42.3	73.0	*Fermi*	15477
131117A	4.042	1.31	0.816	45.4	1.02	*Swift*	15499

Table 2
(Continued)

GRB	z	α	$E_{\rm LT}$[a]	θ (°)	$E_{\rm iso}$[b]	Instrument[c]	GCN
131231A	0.642	1.44	3.39	21.8	22.2	*Fermi*	15644
140206A	2.74	1.43	13.5	10.9	35.9	*Fermi*	15796
140213A	1.2076	2.21	16.2	9.94	9.93	*Fermi*	15833
140226A	1.98	1.58	0.762	47.1	5.80	KW	15889
140304A	5.283	1.44	7.14	15.0	13.7	*Fermi*	15923
140311A	4.954	1.49	1.18	37.5	11.6	*Swift*	15962
140419A	3.956	1.84	9.32	13.1	186.	KW	16134
140423A	3.26	1.31	4.11	19.8	65.3	*Fermi*	16152
140506A	0.889	0.924	2.78	24.2	1.12	*Fermi*	16220
140508A	1.027	1.40	5.46	17.2	23.9	*Fermi*	16224
140509A	2.4	1.46	0.402	66.7	9.14	*Swift*	16240
140512A	0.725	1.62	2.22	27.1	7.76	*Fermi*	16262
140614A	4.233	1.24	2.00	28.5	7.30	*Swift*	16402
140620A	2.04	1.43	5.16	17.7	6.22	*Fermi*	16426
140629A	2.275	1.48	0.868	44.0	6.15	KW	16495
140703A	3.14	2.21	1.82	30.0	1.72	*Fermi*	16512
140907A	1.21	0.888	2.68	24.6	2.29	*Fermi*	16798
141026A	3.35	2.24	34.8	6.78	7.17	*Swift*	16960
141109A	2.993	1.31	7.85	14.3	5.05	KW	17055
141121A	1.47	1.67	6.56	15.6	14.6	KW	17108
141221A	1.452	1.18	0.970	41.5	1.94	*Fermi*	17216
150206A	2.087	1.28	10.1	12.6	151.	KW	17427
150314A	1.758	1.57	3.08	22.9	98.1	*Fermi*	17579
150403A	2.06	1.61	26.7	7.74	91.0	*Fermi*	17674
150514A	0.807	1.35	0.378	69.1	1.14	*Fermi*	17819
150821A	0.755	1.20	0.884	43.5	15.1	*Fermi*	18190
150910A	1.36	1.50	0.415	65.6	22.3	*Swift*	18268
151021A	2.33	1.47	2.69	24.6	211.	KW	18433
151027A	0.81	1.69	2.04	28.3	3.86	*Fermi*	18492
151027B	4.063	1.75	4.19	19.6	19.1	*Swift*	18514
151111A	3.5	1.29	0.871	43.9	5.13	*Fermi*	18582
151112A	4.1	1.54	3.31	22.1	12.4	*Swift*	18593
151215A	2.59	1.07	1.34	35.1	1.97	*Swift*	18699

Notes. It is composed by 161 sources spanning 11 years of *Swift*/XRT observation activity. In the table, we report important observational features: the redshift z, our estimates of the LXRE power-law slope α, the late-time energy $E_{\rm LT}$, the collimation half-opening angle θ, the isotropic energy $E_{\rm iso}$ of the GRB, the observing instrument in the γ-ray band, and the correspondent circular (GCN) from which we take the γ-ray spectral parameters in order to estimate the $E_{\rm iso}$ of the GRB source.
[a] In units of 10^{51} erg.
[b] In units of 10^{52} erg.
[c] "*Swift*" stands for *Swift*/BAT; "*Fermi*" stands for *Fermi*/GBM; "KW" stands for Konus-WIND.

2015; Izzo et al. 2012a; Rueda & Ruffini 2012; Fryer et al. 2014). Within the IGC paradigm, a tight binary system composed of a carbon–oxygen core ($\rm CO_{core}$) undergoing a supernova (SN) explosion in the presence of a binary NS companion has been suggested as the progenitor for long gamma-ray bursts. Different scenarios occur depending on the distance between the $\rm CO_{core}$ and the NS binary companion (Becerra et al. 2015). Correspondingly two different sub-classes of long bursts have been shown to exist (for details, see Ruffini et al. 2015, 2016). A first long burst sub-class occurs when the $\rm CO_{core}$–NS binary separation a is so large (typically $a > 10^{11}$ cm, see, e.g., Becerra et al. 2015) that the accretion of the SN ejecta onto the NS is not sufficient to have the NS reach its critical mass, $M_{\rm crit}$, for gravitational collapse to a BH to occur. The hypercritical accretion of the SN ejecta onto the NS binary companion occurs in this case at rates below 10^{-2} solar masses per second and is characterized by a large associated neutrino emission (Zel'dovich et al. 1972; Ruffini & Wilson 1973; Rueda & Ruffini 2012; Fryer et al. 2014). We refer to such systems as X-ray flashes (XRFs). A second long burst sub-class occurs when the $\rm CO_{core}$–NS binary is more tightly bound ($a < 10^{11}$ cm, see, e.g., Becerra et al. 2015). The larger accretion rate of the SN ejecta, e.g., 10^{-2}–10^{-1} solar masses per second, leads the companion NS to easily reach its critical mass $M_{\rm crit}$ (Rueda & Ruffini 2012; Fryer et al. 2014; Becerra et al. 2015), leading to the formation of a BH. We refer to such systems as binary-driven hypernovae (BdHNe, see, e.g., Ruffini et al. 2014c, 2015). A main observational feature, which allows us to differentiate BdHNe from XRFs is the isotropic γ-ray energy $E_{\rm iso}$ being larger than 10^{52} erg. Such a separation energy value is intimately linked to the binary separation a of the binary progenitor and the consequent birth or not of the BH (for details, see Ruffini et al. 2016).

Thanks to the XRT instrument on board the *Swift* satellite (Gehrels et al. 2004; Evans et al. 2007, 2010), we can compare and contrast the X-ray afterglow emissions of BdHNe and XRFs (see Figure 8). The typical X-ray afterglows of XRFs can be divided into two main parts: an initial bump with rapid decay, followed by an emerging slight decaying power law (see Figure 8). The typical X-ray afterglow light curve of BdHNe can be divided into three different parts: (1) an initial spike followed by an early steep power-law decay; (2) a plateau

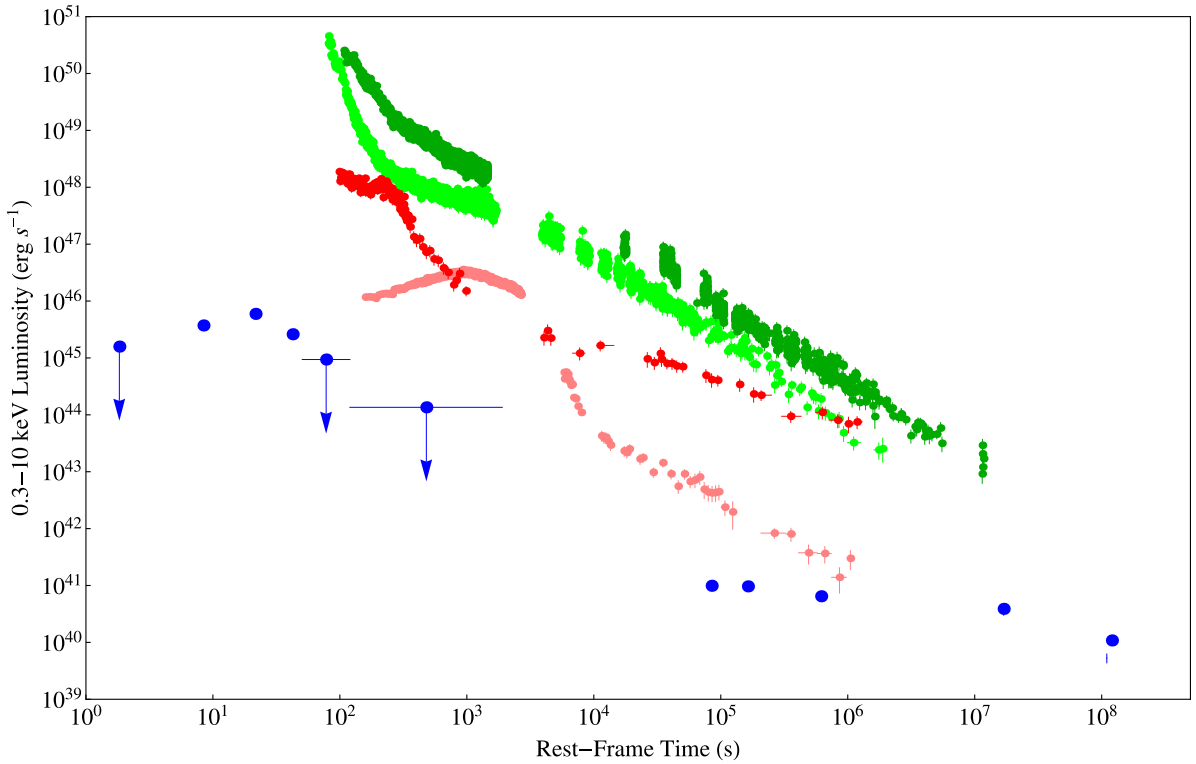

Figure 8. Comparison between rest-frame luminosity light curves of proto-typical BdHNe and XRFs sources. The BdHNe shown are GRB 130427A (dark green) and GRB 090618 (light green); while the XRF shown are GRB 101219B (red), GRB 060218 (pink), and GRB 980425 (blue).

phase; and (3) a late power-law decay, the LXRE, which is the presented in this work (Nousek et al. 2006; Ruffini et al. 2015). The treatment of the first parts of the X-ray afterglow of BdHNe, namely the spike, the initial steep decay, and the plateau phase, indeed fundamental within the BdHN picture, is beyond the scope of this article and it will be extensively shown in forthcoming works (R. Ruffini et al. 2016a, in preparation; R. Ruffini et al. 2016b, in preparation).

The universalities of the LXRE outlined in this article are then explained within the IGC paradigm, originating from the interaction of the GRB with the SN ejecta. The constancy of the late power-law luminosity in the rest frame is now explained in terms of the constancy in mass of the SN ejecta, which is standard in a BdHN (Rueda & Ruffini 2012; Fryer et al. 2014; Becerra et al. 2015).

It is appropriate to point out that no achromatic "Jet-break" effect has been observed in any of the 161 sources of our ES. We recall that the achromatic "Jet-break" effect is a consequence of relativistic jet pictures (Lorentz factor $\Gamma \sim 100$–200), in which a change of slope is expected in the late X-ray light curve (see e.g., Rees & Meszaros 1992; Woosley 1993; Piran 2005; Gehrels et al. 2009; Kumar & Zhang 2015, and references therein), which clearly does not apply in the case of the BdHN following the IGC model. In this scenario, a velocity of expansion $v \sim 0.8c$ (Lorentz factor $\Gamma \sim 2$) is found, indicating that the collimation of the SN ejecta originates in a mildly relativistic regime (Ruffini et al. 2014c, 2015). This cannot be related to the ultra-relativistic jet emission recalled above, considered in the early work of Frail et al. (2001) and continued all the way to the more recent results presented by Ghirlanda et al. (2013). These authors attempted to explain all GRBs as originating from a single object with an intrinsic energy approximately of 10^{50} erg (Frail et al. 2001) or 10^{48} erg (Ghirlanda et al. 2013): the different energetics and structures of all the GRBs were intended to be explained by the beaming effect with different ultra-relativistic Lorentz factors $\Gamma \sim 100$–200. Indeed, it is by now clear (see Ruffini et al. 2015, 2016) that at least seven different classes of GRBs exist, each with different progenitors, different energies, and different spectra. In no way can these distinct classes can be explained by a single common progenitor, using simply relativistic beaming effects.

5. CONCLUSIONS

In this work, we give new statistical evidence for the existence of a universal behavior for the LXREs of BdHNe, introducing the presence of a collimation effect in such emission, and presenting the common LXRE energy $E_{\rm LT}^{\rm intr} = E_{\rm LT}^{050525A} = 2.43 \times 10^{50}$ as a standard candle. We build an "enlarged sample" (ES) of 161 BdHNe, and focus on their LXREs and then we introduce a collimation effect. These analyses lead us to the following results.

(1) We find for the ES an increased variability in the decaying LXRE power-law behavior in respect to the result previously deduced by Pisani et al. (2013). The typical slope of the power-law characterizing the LXRE is $\alpha = 1.48 \pm 0.32$ (GS: $\alpha = 1.44 \pm 0.18$), while the late-time integrated luminosity between 10^4 and 10^6 s in the rest frame is $\mathrm{Log}_{10}(E_{\rm LT}/\mathrm{erg}) = 51.40 \pm 0.47$ (GS: $\mathrm{Log}_{10}(E_{\rm LT}/\mathrm{erg}) = 51.15 \pm 0.28$).

(2) The introduction of a collimation in the LXRE recovers a universal behavior. Assuming a double-cone shape for the LXRE region, we obtain a distribution of half-

opening angles peaking at $\theta = 17.62°$, with a mean value of 30.05°, and a standard deviation of 19.65°, see Figure 7(a).

(3) The application of the collimation effect to the LXREs of the ES indeed reduces the scattering of the power-law behavior found under the common assumption of isotropy; see Figures 5(a)–(b). The power-law scattering of the LXREs, after being corrected by the collimation factor, results in being even lower than the one found in the GS; see Figure 7(b).

The fact that these extreme conditions neither were conceived nor are explained within the traditional ultra-relativistic jetted SSC model (see, e.g., Rees & Meszaros 1992; Woosley 1993; Piran 2005; Gehrels et al. 2009; Kumar & Zhang 2015, and references therein), in view also of the clear success of the IGC paradigm in explaining the above features, comes as a clear support to a model for GRBs strongly influenced by the binary nature of their progenitors, involving a definite succession of selected astrophysical processes for a complete description of the BdHNe.

These intrinsic signatures in the LXREs of BdHNe, independent from the energetics of the GRB prompt emission, open the perspective for a standard candle up to $z \gtrsim 8$.

It is remarkable that the universal behavior occurs in the rest-frame time interval 10^4–10^6 s, which precisely corresponds to the temporal window of the early observations of Beppo-SAX at the time of the afterglow discovery (see Figure 1).

We thank both the editor and the referee for the fruitful correspondence that improved the presentation of our results. This work made use of data supplied by the UK Swift Science Data Center at the University of Leicester. M.K. and Y.A. are supported by the Erasmus Mundus Joint Doctorate Program by Grant Nunmbers 2013-1471 and 2014-0707, respectively, from the EACEA of the European Commission.

REFERENCES

Ackermann, M., Asano, K., Atwood, W. B., et al. 2010, ApJ, 716, 1178
Becerra, L., Cipolletta, F., Fryer, C. L., Rueda, J. A., & Ruffini, R. 2015, ApJ, 812, 100
Bloom, J. S., Frail, D. A., & Sari, R. 2001, AJ, 121, 2879
Boella, G., Butler, R. C., Perola, G. C., et al. 1997, A&AS, 122, 299
Campana, S., Mangano, V., Blustin, A. J., et al. 2006, Natur, 442, 1008
Costa, E., Feroci, M., Piro, L., et al. 1997a, IAUC, 6576, 1
Costa, E., Frontera, F., Heise, J., et al. 1997b, Natur, 387, 783
Della Valle, M., Malesani, D., Benetti, S., et al. 2006a, IAUC, 8696, 1
Della Valle, M., Malesani, D., Bloom, J. S., et al. 2006b, ApJL, 642, L103
de Pasquale, M., Piro, L., Gendre, B., et al. 2006, A&A, 455, 813
de Ugarte Postigo, A., Xu, D., Leloudas, G., et al. 2013, GCN Circ, 14646, 1
Dezalay, J.-P., Barat, C., Talon, R., et al. 1992, in AIP Conf. Ser. 265, Gamma-ray Bursts, ed. W. S. Paciesas & G. J. Fishman, 304
Evans, P. A., Beardmore, A. P., Page, K. L., et al. 2007, A&A, 469, 379
Evans, P. A., Willingale, R., Osborne, J. P., et al. 2010, A&A, 519, A102
Frail, D. A., Kulkarni, S. R., Sari, R., et al. 2001, ApJL, 562, L55
Frontera, F., Amati, L., Costa, E., et al. 2000, ApJSS, 127, 59
Frontera, F., Costa, E., Piro, L., et al. 1998, ApJL, 493, L67
Fryer, C. L., Rueda, J. A., & Ruffini, R. 2014, ApJL, 793, L36
Gehrels, N., Chincarini, G., Giommi, P., et al. 2004, ApJ, 611, 1005
Gehrels, N., Ramirez-Ruiz, E., & Fox, D. B. 2009, ARA&A, 47, 567
Ghirlanda, G., Ghisellini, G., Salvaterra, R., et al. 2013, MNRAS, 428, 1410
Golenetskii, S., Aptekar, R., Mazets, E., et al. 2005, GCN, 3474, 1
Izzo, L., Rueda, J. A., & Ruffini, R. 2012a, A&A, 548, L5
Izzo, L., Ruffini, R., Penacchioni, A. V., et al. 2012b, A&A, 543, A10
Klebesadel, R. W. 1992, in Gamma-Ray Bursts—Observations, Analyses and Theories, ed. C. Ho, R. I. Epstein, & E. E. Fenimore (Cambridge: Cambridge Univ. Press)
Kouveliotou, C., Meegan, C. A., Fishman, G. J., et al. 1993, ApJL, 413, L101
Kumar, P., & Zhang, B. 2015, PhR, 561, 1
Levan, A. J., Fruchter, A. S., Graham, J., et al. 2013, GCN Circ., 14686, 1
Margutti, R., Zaninoni, E., Bernardini, M. G., et al. 2013, MNRAS, 428, 729
Mazets, E. P., Golenetskii, S. V., Ilinskii, V. N., et al. 1981, Ap&SS, 80, 3
Meszaros, P., & Rees, M. J. 1997, ApJ, 476, 232
Nousek, J. A., Kouveliotou, C., Grupe, D., et al. 2006, ApJ, 642, 389
Penacchioni, A. V., Ruffini, R., Bianco, C. L., et al. 2013, A&A, 551, A133
Penacchioni, A. V., Ruffini, R., Izzo, L., et al. 2012, A&A, 538, A58
Perley, D. A., Cenko, S. B., Corsi, A., et al. 2014, ApJ, 781, 37
Piran, T. 2005, RvMP, 76, 1143
Pisani, G. B., Izzo, L., Ruffini, R., et al. 2013, A&A, 552, L5
Rees, M. J., & Meszaros, P. 1992, MNRAS, 258, 41
Rueda, J. A., & Ruffini, R. 2012, ApJL, 758, L7
Ruffini, R., Bernardini, M. G., Bianco, C. L., et al. 2007, ESA SP, 622, 561
Ruffini, R., Bianco, C. L., Chardonnet, P., Fraschetti, F., & Xue, S.-S. 2001a, ApJL, 555, L107
Ruffini, R., Bianco, C. L., Chardonnet, P., Fraschetti, F., & Xue, S.-S. 2001b, ApJL, 555, L113
Ruffini, R., Bianco, C. L., Chardonnet, P., Fraschetti, F., & Xue, S.-S. 2001c, ApJL, 555, L117
Ruffini, R., Bianco, C. L., Enderli, M., et al. 2013a, GCN Circ., 14526, 1
Ruffini, R., Bianco, C. L., Enderli, M., et al. 2013b, GCN Circ., 14888, 1
Ruffini, R., Bianco, C. L., Enderli, M., et al. 2013c, GCN Circ., 15576, 1
Ruffini, R., Bianco, C. L., Enderli, M., et al. 2014a, GCN Circ., 15707, 1
Ruffini, R., Izzo, L., Muccino, M., et al. 2014b, A&A, 569, A39
Ruffini, R., Muccino, M., Bianco, C. L., et al. 2014c, A&A, 565, L10
Ruffini, R., Rueda, J. A., Muccino, M., et al. 2016, ApJ, 832, 136
Ruffini, R., Wang, Y., Enderli, M., et al. 2015, ApJ, 798, 10
Ruffini, R., & Wilson, J. 1973, PhRvL, 31, 1362
Salvaterra, R., Della Valle, M., Campana, S., et al. 2009, Natur, 461, 1258
Sari, R., Piran, T., & Narayan, R. 1998, ApJL, 497, L17
Soderberg, A. M., Berger, E., Kasliwal, M., et al. 2006a, ApJ, 650, 261
Soderberg, A. M., Kulkarni, S. R., Nakar, E., et al. 2006b, Natur, 442, 1014
Tanvir, N. R., Fox, D. B., Levan, A. J., et al. 2009, Natur, 461, 1254
Tavani, M. 1998, ApJL, 497, L21
Woosley, S. E. 1993, ApJ, 405, 273
Zel'dovich, Y. B., Ivanova, L. N., & Nadezhin, D. K. 1972, SvA, 16, 209